NASA CR-165375
SKF AT81T014

DEVELOPMENT OF SMALL BORE, HIGH SPEED TAPERED ROLLER BEARING

By F. R. Morrison, S. S. Gassel, and R. L. Bovenkerk

SKF Technology Services
SKF Industries, Inc.

prepared for

NATIONAL AERONAUTICS AND SPACE ADMINISTRATION

NASA Lewis Research Center
Contract NAS3-20839

SKF TECHNOLOGY SERVICES
SKF INDUSTRIES, INC

1. Report No.	2. Government Accession No.	3. Recipient's Catalog No.
NASA CR-165375		

4. Title and Subtitle	5. Report Date
Development of Small Bore, High Speed Tapered Roller Bearing	June, 1981
	6. Performing Organization Code

7. Author(s)	8. Performing Organization Report No.
F. R. Morrison, S. J. Gassel and R. L. Bovenkerk	AT81T014
	10. Work Unit No.

9. Performing Organization Name and Address	11. Contract or Grant No.
SKF Technology Services SKF Industries, Inc. 1100 First Avenue King of Prussia PA 19406	NAS3-20839
	13. Type of Report and Period Covered Final May 1978 - June 1981

12. Sponsoring Agency Name and Address	14. Sponsoring Agency Code
National Aeronautics and Space Administration Lewis Research Center Cleveland OH 44135	

15. Supplementary Notes

16. Abstract

An analytical-experimental program was conducted to analytically evaluate the performance of four rolling bearing configurations for use on the input pinion shaft of a proposed commercial helicopter transmission, and to experimentally define the performance characteristics of a high speed tapered roller bearing operating under conditions comparable to those projected to exist at this input pinion shaft.

A tapered roller bearing shaft support configuration was developed for the gearbox using commercially available bearing designs. This configuration was optimized and subjected to an interactive thermo-mechanical systems analysis. These results were subsequently compared to those achieved from three other proposed bearing configurations. This effort demonstrated that the proposed tapered roller bearing design offered advantages in both performance and system simplification compared to typical bearing configurations.

An experimental evaluation defined the performance characteristics of that tapered roller bearing selected as the primary load supporting element on the analytically defined pinion shaft support system. This was a commercially available M88000 series bearing modified for high speed operation. This activity established that automotive pinion quality tapered roller bearings are capable of reliable operation under load and speed conditions in excess of those anticipated in the helicopter transmission. There were some indications, however, that the elastohydrodynamic lubricant films existing under those conditions are inadequate.

It was concluded that tapered roller bearings are primary candidates for use on input pinion shafts in helicopter transmissions. The introduction of these bearings into this application can produce benefits in the areas of system performance and hardware simplification.

17. Key Words (Suggested by Author(s))	18. Distribution Statement
Tapered Roller Bearings Helicopter Transmission Bearings High Speed Bearing System Analysis High Speed Bearing Tests	Publicly Available (No restrictions on provision to domestic or foreign requestors)

19. Security Classif. (of this report)	20. Security Classif. (of this page)	21. No. of Pages	22. Price*
Unclassified	Unclassified		

* For sale by the National Technical Information Service, Springfield, Virginia 22161

Foreword

This report presents the results of an analytical-experimental development study conducted by SKF Technology Services, a division of SKF Industries, Inc., located in King of Prussia, PA 19406 for the National Aeronautics and Space Administration, Lewis Research Laboratory, Cleveland, Ohio, 44135 under contract NAS3-20839. The work was completed under the technical direction of the NASA Project Manager, Mr. Richard J. Parker, Bearing, Gearing and Transmission Section, Structures and Mechanical Technologies Division.

TABLE OF CONTENTS

TABLE OF CONTENTS - CONTINUED

Summary

The combined analytical-experimental program described in this report had two primary objectives. These were;

(1) To analytically evaluate and compare the performance of a number of rolling bearing configurations to be used to support the input pinion shaft in a proposed commercial helicopter transmission design; and

(2) To experimentally define the performance characteristics of a high speed tapered roller bearing operating under conditions comparable to those analytically projected to exist at this input pinion shaft.

Analytically, a tapered roller bearing shaft support configuration was developed for the gearbox application by selecting commercially available bearing designs. This configuration was optimized for a number of parametric variations and the resulting design was subjected to an interactive thermo-mechanical systems analysis. These results were subsequently compared to those achieved from another proposed design, consisting of a thrust carrying cylindrical roller bearing preloaded against two angular contact ball bearings, and a typical current bearing configuration, a standard cylindrical roller bearing and a preloaded stack of three angular contact ball bearings.

The analytical effort demonstrated that both proposed alternate designs offer advantages in both performance and system simplification when compared to the current bearing configuration. While the configuration containing the thrust carrying cylindrical roller bearing as a preload bearing, appears to offer the best approach, the lack of experience with this novel design precludes the recommendation of that configuration for use in the transmission without conducting additional experimental evaluations.

An experimental series was completed to evaluate commercially available M88000 series tapered roller bearings modified for high speed operation. This bearing had been selected as the primary load supporting element on the analytically defined tapered bearing pinion shaft support system. The experimental activity established that automotive pinion quality tapered roller bearings are capable of reliable operation under load and speed conditions in excess of those anticipated in the helicopter transmission. This good performance was repeatably noted in a number of short duration performance tests and over an extended period of more than 30 hours in a long term test run. There

were some indications, however, that the elastohydrodynamic lubricant films generated in the bearings under those conditions are inadequate to allow these bearings to achieve their full endurance potential in the application.

On the basis of this program, it would be concluded that tapered roller bearings are primary candidates for use on input pinion shafts in helicopter transmissions. The introduction of these bearings into this application can produce benefits in the areas of system performance and hardware simplification.

1. Introduction

1.1 Background

During the last decade a significant amount of effort has been expended on the development of advanced power generation and transmission systems for helicopters. Much of this activity has been funded by the government and has been military in nature since the armed forces represented the single primary user of helicopter systems. For the most part commercial helicopters produced during this period have been copies or simple adaptations of the existing military hardware.

However, this trend is now changing. Near the end of 1979, an FAA spokesman stated that "the helicopter is the fastest growing segment of aviation today" [1].* A significant portion of this growth is apparent in the commercial sector and this activity is expected to show continued expansion in the years to come. This rapid expansion creates a continued need for power generation and transmission system development and alters, to some degree, the focus of these efforts.

The primary emphasis of the military programs conducted to date has been the achievement of increased performance, reduced vulnerability to ballistic impact, and increased survivability once ballistic damage has been sustained. The emphasis in commercial development is expected to center on increased safety, improved weight carrying capacity, and increased operating efficiency. While some aspects of these goals are common to both areas, others are either unimportant or even mutually exclusive.

The development of more advanced power transmission systems is basic to both areas of activity. Gearboxes which can operate at higher input speeds and can simultaneously transmit higher power levels are needed to meet many of the stated goals. Concurrently, it would be desired that these systems would also offer reduced weight, improved reliability, cost less to manufacture, and be easier to maintain.

The input pinion shaft assembly of the main helicopter transmission is seen as one area where gains are achievable in all these areas. Typically such shafts have been supported on stacks of multiple angular contact bearings or using combined ball and cylindrical roller bearing sets. In these cases, the multiplicity of bearing assemblies creates problems in assuring the proper degree of load sharing among the bearings and in

*Numbers in brackets refer to References listed in Section 9.

reliably providing adequate lubrication and cooling to all of the assemblies. Solutions to these problems usually added even more complexity to the hardware. The replacement of these multiple bearing units with a single bearing assembly capable of supporting large combined loads at high speeds would be a major step in improving the reliability and maintainability of the transmission. Simultaneously, this substitution would provide weight reductions and reduced manufacturing costs.

The transmission development activity funded by the military is now culminating in three major programs sponsored by the U.S. Army Aviation Research and Development Command (AVRADCOM) to design and construct three different state of the art transmissions [2, 3, 4]. All three of these programs incorporate major changes in the input pinion shaft support system. One program is considering the use of two high speed tapered roller bearings, including an experimental outer ring flanged version, on this shaft to support the gear assembly [2]; the second is incorporating an experimental thrust carrying cylindrical roller bearing in place of the multiple bearing assembly [3, 5]; and the third incorporates integral bearing races on the pinion shaft itself [4]. Experience, to date, with the two single bearing designs has been favorable in these programs. However, their ultimate acceptability in military systems can be severely limited by an apparent decrease in survivability of these bearings exposed to small arms fire.

The need for lost lubrication survivability still exists in helicopters designed purely for commercial applications as a safety consideration relating to lubrication system failures. However, these requirements need not be as extensive as those now being applied to military aircraft where hostile territory and mission responsiveness are major considerations. It is known that these single bearing units can operate reliably and provide the enumerated advantages over existing shaft support systems when adequate lubrication is provided and projected methods now exist to achieve a degree of lost lubrication survivability. Thus these bearing designs are primary candidates for incorporation into helicopter transmissions in the commercial sector.

1.2 Program Objectives

In support of the potential growth in the commercial helicopter field and to encourage the technical independence of commercial design principles, the Lewis Research Laboratory of NASA initiated a program to design, build and experimentally evaluate an advanced transmission system for a projected commercial helicopter. As a portion of that effort, SKF Technology Services was awarded a contract for the analytical and experimental.

evaluation of alternative input pinion shaft bearing supports. The specific objectives of the modified contract, Number NAS3-20839, are iterated below.

Analytically, a number of distinct specific activities were to be completed. These were;

Bearing Selection and Design of Modifications for High Speed:

A computerized analytical study was to be completed using existing computer codes, on four existing commercial tapered-roller bearing designs in a size range consistent with the specified transmission design. Each bearing design was to be evaluated on the basis of bearing stiffness and deflection, heat generation rate, roller end/flange loading and stress levels, and bearing fatigue life. Roller end radius was varied in the analysis to determine the benefit of this modification. Operating conditions for this analysis were as follows: loads as determined for the most heavily loaded bearing from the system analysis; a shaft speed of 3766 rad/s (35,963 rpm); a maximum bearing temperature of 422K (300°F) and lubrication provided with a MIL-L-23699 synthetic fluid.

The two (2) most promising designs were selected and specifications prepared for modification of bearing components to be compatible with the high-speed operating conditions. The calculated B_{10} fatigue life of the most heavily loaded bearing at 60% of the nominal load was specified as not less than 2500 hours. This nominal load was defined as the maximum load on the most heavily loaded bearing. The projected modifications included (a) removal of the cone small end flange, (b) the use of a machined steel, silver plated, cone-land riding cage, (c) the addition of lubricant supply holes from the cone bore to the undercut located at the large end flange and from the cone bore to the small end cage riding land, (d) improvement of the cone flange surface finish and (e) the alteration of roller end profile.

Preliminary Shaft-Bearing Design Evaluated:

This analysis was performed to obtain a recommendation for a preliminary design of a shaft and tapered-roller bearing system to support the high-speed input pinion of the advanced helicopter transmission. The effort included the consideration of both a straddle arrangement where the bevel pinion is located axially between the two tapered-roller bearings and a cantilevered

arrangement where the pinion is outboard of the two tapered-roller bearings. The resulting design also included recommendations for preloads and fits for use at the maximum torque condition. Once again the design size limitations of the transmission were specified and limits were placed on the allowable deflections and misalignment which could exist at the gear.

Preliminary designs were to be presented in both straddle and cantilevered arrangements and the advantages and disadvantages of each were to be delineated and discussed.

Final Definition of Input Pinion Support System:

This was a continuation of the previous activity where different sizes of precision toleranced tapered roller bearings were to be selected for each end of the shaft to support the input pinion in a straddle arrangement within the defined space limitations of the transmission design. An overall computer analysis of the selected bearing arrangement was to be completed including a thermal analysis accounting for the thermal and mechanical interactions of the pinion in its environment. The analysis also considered preload and fit variations to obtain optimum performance of the bearings. The resulting deflections and inclination of the pinion and the bearing fatigue lives were specified as output parameters of the effort.

Analysis of Alternative Shaft Support Systems:

An analysis was to be completed on alternate design shaft and bearing systems comprising four arrangements of ball and/or cylindrical roller bearings. These were defined as two straddle systems with a three element angular contact ball bearing stack and a cylindrical roller bearing, using different sized bearings, and two arrangements with two element angular contact ball bearing stack with a thrust carrying cylindrical roller bearing providing the preload in both straddle and cantilever configurations.

The extent of the analysis was similar to the other preliminary analysis and included lubricant and traction effects in the bearings. Again the analysis considered preload, fit and lubricant flow rate variations to obtain optimum performance of the bearings. Deflections and inclination of the pinion and bearing fatigue life were to be determined using operating conditions identical to those used in previous analysis.

The latter configuration was also subjected to steady state thermal analysis to consider the coupled thermomechanical system including the pinion and its mechanical environment.

The experimental activities contained in this program consisted of the following:

Fabrication of Test Bearings:

The two sizes of commercial tapered roller bearings selected in the analytical effort were procured and modified according to the specifications developed in that same analysis. In addition, a lot of precision tolerance bearings of one design was procured and the bearings were modified.

Test Facility Preparation:

An existing test fixture was modified to be capable of the simultaneous testing of two test bearings in the opposed position. Maximum operating conditions for the test system were specified as 110% of the transmission design speed and 150% of the transmission design loads. The test system was also required to have sufficient instrumentation to define applied load levels, bearing operating temperature, lubricant supply and scavenge temperatures, shaft speed, and cage rotational speed.

Bearing Performance Tests:

A series of step speed performance test runs were to be completed under a variety of loading and lubrication conditions. The primary objective of these tests was to determine the capability of the two bearing designs to survive the applied range of operating conditions. In addition, values of various operating parameters were recorded to allow an evaluation of the primary performance indicators of the bearings, e.g. heat generation rate, temperature rise, etc., under each set of conditions. The condition of the bearings were examined after each test using optical and scanning electron microscopy to define the residual conditions of the contact surfaces.

Extended Duration Test:

One 50 hour extended duration test run was to be completed at maximum design operating conditions to establish the long term operating characteristics of the selected bearing. A major portion

of the evaluation would be the definition of the post test condition of the contact surfaces using optical and scanning electron microscopy.

Detailed discussions of the conduct and results of these activities are contained in the subsequent chapters of this report.

2. Design and System Analysis

A number of specific analytical tasks were included in this combined analytical-experimental program. These tasks included: (1) the selection of tapered roller bearings to be used in the program and the definition of the modifications to be made to those bearings; (2) the comparative evaluation of taper supported pinion shaft configurations considering straddle and cantilever mounting of the gear; (3) the evaluation of alternative pinion shaft support configurations considering ball and cylindrical roller bearing systems and a thrust carrying cylindrical roller bearing system; and (4) the evaluation of a pinion shaft supported on non symmetrical tapered roller bearings. The latter two items (3, 4) included a detailed thermal evaluation of the selected pinion configurations. Each of these individual analytical tasks is described in some detail in the following subsections.

2.1 Bearing Selection and Design of Modifications

Prior to the initiation of this program, it was established that the tapered roller bearing to be used in this pinion application should meet the following requirements;

(1) Be from an existing tapered roller bearing product line;

(2) Have a bore diameter between 25 and 35 mm (0.984 and 1.378 inches);

(3) Have an outer diameter less than 63.5 mm (2.5 inches);

(4) Provide a minimum calculated L_{10} life of 2500 hours with an operating speed of 3770 rad/s (36,000 rpm) under loads equal to 60% of the maximum generated by the gear; and

(5) Provide sufficient shaft stiffness to limit deflections at the gear to less than 25 μm (0.001 inch) and limit the inclination of the pinion to less than 1.74 mrad (0.1°) under the maximum gear load.

The design of the spiral bevel input pinion gear to be used on this shaft had been established as shown in Table 1.

TABLE 1

Spiral Bevel Pinion Gear Design Definition

Number of Teeth	12
Pitch Diameter*	44 mm (1.733 in.)
Face Width	17.3 mm (0.68 in.)
Pressure Angle	0.35 rad (20°)
Spiral Angle (left hand)*	0.52 rad (30°)
Pitch Angle	1.310 rad (75.07°)
Bevel Gear Ratio	3.75
Rotational Direction	Driving Clockwise
Pinion Speed	3766 rad/s (35,963 rpm)
Pinion Torque at Maximum Power, i.e. 397 kW (533 HP)	105 N.m (933 in. lbf)

*These values were altered partially through the program as a result of analytical work concurrently performed by NASA. The corrected values were:

Pitch Diameter	46.78mm
Spiral Angle	Ranging from 0.52 to 0.61 rad

Four standard design tapered roller bearings were selected from the catalog which appeared to meet most or all of the specifications. These were the M88048/M88010, the L14130/L14274, the LM67048/LM67010, and the L68149/L68110. The major design features of these four bearings are listed in Table 2. As can be seen, the selected designs included relatively large variations in internal geometry, i.e. taper angle, roller number, roller diameter and included angle and roller end flange geometry.

A preliminary analysis was then conducted considering only individual components, not a shaft system, to compare the characteristics of the bearings and to select two for further consideration. First, the loads generated at the spiral bevel pinion were calculated using those data from Table 1. In this way, the nominal thrust load applied to the shaft was approximated as 8.4 kN (853 lbf). For the calculations which followed it was assumed that the generated radial load was always 60% of the axial load, or 5.0 kN (512 lbf) at the nominal level, and applied load levels of 0.6, 0.75, 1.0 and 1.5 times nominal were considered.

These initial comparative evaluations were completed using the computer program TABACY to calculate the L_{10} fatigue life and the lubricant film thickness generated at the flange for each individual bearing design. These two parameters were selected as the evaluation criteria since life was a specified design constraint and scuffing or smearing at the flange roller end contact was a likely mode of failure. The other operating conditions for these runs were established as follows; shaft speed 3770 rad/s, average operating temperature 422 K (300°F), and circulating MIL-L-23699 lubrication. The results of these calculations are shown in Table 3.

The selection of the two bearing designs to be used in this program was completed considering that the four candidate bearings consisted of two distinct subsets. The LM67000 and L68000 series bearings contain small diameter, relatively light rollers. This is a marked advantage for a high speed bearing, but the small roller size also limits the potential fatigue life of the assembly. On the other hand, the L14000 and M88000 series have large rollers yielding significantly greater life potential. However, the outer diameter of these bearings exceeds the specified limit for the application.

TABLE 2

Comparison of Bearing Design Parameters

	MB8048/MB8010	L14130/L14274	LM67048/LM67010	L68149/L68110
Envelope Dimensions:				
Bore Diameter; mm (inches)	33.3 (1.313)	33.3 (1.313)	31.8 (1.250)	35 (1.378)
Outer Diameter; mm (inches)	68.3 (2.688)	69 (2.717)	59.1 (2.328)	59.1 (2.328)
Width; mm (inches)	22.2 (0.875)	19.8 (0.781)	15.9 (0.625)	15.9 (0.625)
Internal Geometry:				
Cone Angle; mRad (Degree)	263 (15.1)	187 (10.7)	204 (11.7)	216 (12.38)
Flange Angle, Deviation from Square; mRad (Degree)	8.7 (0.5)	7.7 (0.44)	9.6 (0.55)	7.0 (0.40)
Number of Rollers	19	17	19	23
Included Roller Angle; mRad (Degree)	85 (4.9)	62 (3.58)	64 (3.67)	54 (3.12)
Roller Large End Diameter; mm (inches)	7.95 (0.313)	7.8 (0.306)	6.3 (0.257)	5.6 (0.22)
Roller Length; mm (inches)	16.3 (0.643)	13.4 (0.527)	10.7 (0.423)	10.8 (0.426)
Roller End Radius; mm (inches)	91.9 (3.618)	125 (4.916)	102 (4.017)	103 (4.056)
Roller Crown:				
Type	Full	Full	Full	Full
Radius; mm (inches)	12,700 (500)	12,700 (500)	12,700 (500)	12,700 (500)
Basic Load Rating; kN (lbf)	49 (11,000)	40.5 (9150)	30 (6700)	29 (6550)

From Table 3, it appears that the calculated lives of the former pair of bearings is insufficient for the application since calculated values less than 2500 hours were noted at 60% nominal load. However, TABACY calculates life using the basic Lundberg Palmgren formulation without considering the life adjustment factors included in the more recent AFBMA formulations [6]. It is reasonable to assume at this time that the helicopter transmission application will demand bearings manufactured from at least vacuum melted material if not Vim Var M50 tool steel. It is not unrealistic therefore to consider the use of an a_2 material life adjustment factors ranging in value from 3 to 5. At the speeds and operating temperatures noted, Λ values greater than 1.3 are anticipated producing a_3 application life adjustment factors of 1.0 and greater. Thus utilizing the most recent life calculation techniques, all of the bearing designs achieve the calculated L_{10} life specified for the application. This being the case, the LM67048/LM67010 was selected for use in the program since it provided the greatest life of the low roller mass designs with no reduction in the thickness of lubricant film generated at the flange.

The significant increase in fatigue life potential offered by the high roller mass designs produced the desire to consider one of these variations. It was reasoned that the design features which produced these life increases could probably be incorporated into a bearing meeting the size limitations of the gearbox. Furthermore, it was considered that this preliminary effort ought to consider a broad range of design features to allow the further optimization of subsequent high speed tapered roller bearing designs for life, performance and size. The M88000 bearing was selected as the second bearing for this project since it has the greatest life potential of the four candidate designs.

Attention was then turned to the establishment of the design modifications to be incorporated into these standard bearings. The first parameter to be evaluated was the roller end sphere radius. A comparative analytical study was conducted using the computer program TABACY on the M88000 design geometry to establish the effects of varying roller end radii on the values of flange contact stress, heat generation rate, lubricant film thickness, and location of the contact zone. These results are shown in Table 4 and indicate that the thickness of the lubricant film layer decreases with decreasing sphere radii. Concurrently, substantial increases in contact stress level and heat generation rate are also experienced with small radius values. On this basis it appears that large sphere end radii are most desirable.

TABLE 3

Comparative Study of Alternate Taper Series

Series Bearing Number	% Nominal Load	Axial Load/ Radial Load [kN (lbs.)]	L_{10} Life [Hrs.]	Film Thickness At the Flange [μm (μin.)]
L68000	60	5.0/3.0(512/307)	1270	0.33 (13)
	75	6.3/3.8(640/384)	494	0.33 (13)
	100	8.4/5.0(853/512)	148	0.30 (12)
	150	12.6/7.6(1280/768)	27	0.30 (12)
LM67000	60	5.0/3.0(512/307)	1611	0.33 (13)
	75	6.3/3.8(640/384)	602	0.33 (13)
	100	8.4/5.0(853/512)	168	0.30 (12)
	150	12.6/7.6(1280/768)	29	0.30 (12)
L14000	60	5.0/3.0(512/307)	4743	0.38 (15)
	75	6.3/3.8(640/384)	1884	0.38 (15)
	100	8.4/5.0(853/512)	525	0.35 (14)
	150	12.6/7.6(1280/768)	88	0.35 (14)
M88000	60	5.0/3.0(512/307)	-	- -
	75	6.3/3.8(640/384)	-	- -
	100	8.4/5.0(853/512)	3405	0.38 (15)
	150	12.6/7.6(1280/768)	616	0.35 (14)

TABLE 4

Effects of Variation of Roller End Sphere Radius

Rs (mm)	% Apex Distance	h (μm)	Pmax (MPa)	Vs (m/s)	U (m/s)	S* (mm)	a (mm)	b (mm)
68.94	75	0.44	329	23.8	42.5	2.37	0.87	0.37
73.53	80	0.46	298	21.4	43.4	2.53	0.98	0.36
79.20	86	0.49	259	18.5	44.4	2.73	1.18	0.35
89.36	97	0.56	165	13.3	46.3	3.08	2.46	0.26
91.90	100	0.71	46	12.0	46.8	3.17	29.8	0.08

Bearing Type: M88000
Shaft Speed: 3744 rad/s
Flange Contact Load: 222N
Lubricant: MIL-L-23699
Operating Temperature: 422K

Rs - Roller End Sphere Radius
h - Film Thickness Developed at Flange Contact
Pmax - Maximum Hertz Stress
Vs - Sliding Velocity
U - Rolling Velocity
S* - Perpendicular Distance From Roller Center Line to Flange Contact
a - Hertz Contact Semi-Major Axis
b - Hertz Contact Semi-Minor Axis

It had, however, been previously reported [7] that an optimum film thickness is experienced on the flange of a tapered roller bearing when the roller end radius is 80% of the apex distance. This trend did not exist in the current results. Further study established that the previous calculations had been conducted using the Archard-Cowking lubricant film model [8] which was derived for circular contacts. The computer program TABACY incorporates the modification of this model proposed by Cheng [9] to account for the ellipticity of the contact. Since elliptical contacts areas are calculated to exist on the flange, the current film thickness calculations were considered to be more realistic.

It can also be noted that the location of the flange contact moves higher on the flange as the radius is decreased. In a tapered roller bearing of this size range, the usable flange contact zone is quite narrow, approximately 0.76 mm (0.030 in.). Thus it becomes extremely difficult to insure that the contact remains totally on the flange at all possible extremes of the tolerance ranges. Experimental experience has illustrated that overruning the top edge of the flange is usually catastrophic since the corner tends to remove all of the protective lubricant film. Overrunning the lower corner does produce undesirable stress concentrations, but does not create similar critical performance characteristics. Thus contact location is a decisive factor and it is desirable to bias the contact towards the low side of the flange.

Considering all factors, it was decided that the normally specified sphere end radius, which is ~93% of the apex distance, was the best selection for these bearings yielding low contact stress, low heat generation rate, low contact point, and the maximum obtainable film thickness.

The next factor to be considered was the size and number of the lubricant supply holes into the large end cone undercut. Calculations quickly demonstrate that centrifugal forces can pump extremely large volumes of oil through even very small radial supply holes. The size of the holes is therefore defined by that which can be practically achieved rather than that size necessary to insure delivery of a specified quantity of lubricant. In this case, the maximum size of the hole is also limited by the confines of the undercut and the necessity of not relieving or otherwise destroying the integrity of the roller path surface. With this in mind, the actual hole into the undercut was limited to 0.8 mm (0.030 in.) diameter. However, to aid the drilling process and to limit the deflection of the small drill as it progressed through the thickness of the cone, the holes were first partially drilled to a depth of 75-80% with a 1.6 mm (0.062 in.) diameter. The final cut was subsequently made from the bottom of this hole to the undercut with the smaller drill.

Again, the number of holes to be used is not critical considering the volume of lubricant to be provided, but this factor is very decisive in assuring the adequate distribution of the flow over the entire flange area. A previous experimental study conducted on large bearings defined the number of lubricant holes necessary for adequate lubrication of the flange as a function of flange velocity [7]. These guidelines would indicate that a minimum of 24 holes would be needed in this bearing which has a tangential flange velocity of 106 m/s (21,000 fpm) at the maximum speed. However, other testing completed on high speed taper roller bearings of a size similar to that used in this effort had indicated that successful operation could be achieved at flange speeds up to 152 m/s (30,000 fpm) with as few as 6 lubricant supply holes [10]. That same test series had graphically illustrated that these holes can be initiation points for cracks which could produce catastrophic ring fractures. It was desirable to minimize the number of holes and yet achieve sufficient flange lubrication for reliable long term operation. Accordingly, the number of holes was established at a compromise value of nine. Later during the experimental portion of the program, this number was increased to eighteen in an attempt to eliminate the roller end-flange failures which were being experienced. However, as other possibly more directly related factors were also varied simultaneously, there is no direct evidence that this change was decisive in the subsequent success achieved in the test effort.

Numerous cage designs have been employed successfully in past high speed taper roller bearing test programs. These range from a silver plated version of the standard stamped steel cage [7] through a number of varieties of stamped and machined retainers, up to a unique silver plated, machined steel "Z" cage [11]. Typical considerations for high speed bearings require the use of land riding cages due to the dynamic variations produced with roll body centered retainers. This eliminated consideration of a stamped configuration. The silver plated machined steel cage used in previous programs [10,12] had performed extremely well. This basic design was therefore scaled for use in the current program.

The remaining modification features were determined on the basis of good bearing design practice. These modifications were then incorporated in the standard series bearings to produce the M88000 VAC and LM67000 VAC designs described in Section 3.

2.2 Preliminary Shaft-Bearing System Analysis

The objective of this analytical effort was to recommend preliminary designs of shaft high speed tapered roller bearing systems to support the high speed input pinion in the proposed helicopter transmission. This was accomplished by completing a series of computer analyses considering existing tapered-roller bearing systems selected in the preceding analysis (Section 2.1) mounted both in a straddle arrangement, where the pinion gear is located between the bearings, and a cantilever arrangement, where the pinion is outboard of the two bearings.

The analyses were completed using an existing load support system software package, SHABERTH, which is described in [13]. This program performs thermo-mechanical analyses of arbitrarily configured rolling-element bearing - shaft systems. The software is structured by nesting computation loops which address ever increasing levels of detail in system characterization. The present investigation used the first two levels of sophistication which are described below;

LEVEL 0 - Elastic Contact Forces are calculated. No lubrication or friction effects are considered.

LEVEL 1 - Elastic Contact Forces are calculated. Lubrication and friction effects are considered using an isothermal model and epicyclic assumptions to estimate rolling element and cage speeds. An interacting thermal analysis is optional in this level, but was not employed in these preliminary analyses. Later analyses (Sections 2.3 and 2.4) did employ this option.

Once again a successful system was defined as one which would meet the design constraints delineated in Section 2.1, i.e. $L_{10} \geq$ 2500 hours at 60% the nominal gear load (NGL), gear deflections $\leq$ 25 μm (0.001 in.) at 100% NGL, and gear rotation $\leq$ 1.74 mrad (0.1°) at 100% NGL. Concurrently, shaft length restrictions were imposed by the transmission configuration. For the straddle configuration, the distance between the front face of the preload bearing cone and the load application point of the pinion was not to exceed 27.2 mm (1.07 inch). In the cantilevered configuration the same dimension was not to exceed 77.5 mm (3.05 inch).

Initial system analyses were completed on the M88000 and the LM67000 series tapered roller bearings selected in Section 2.1, evaluating system life as a function of applied load and shaft wall thickness. At that time, it became obvious that even considering the life adjustment factor for Vim Var M50 material, i.e. $a_2 = 5$ [14], the LM67000 bearing did not provide adequate rating lives. The continued studies considering the effects of preload, shaft-cone interference fits, bearing spacing and misalignment were completed only on the M88000 bearing. The effects of these variations on load distributions and bearing rating lives, including simulation of bearing and shaft elastic deformations, were evaluated for both support geometries. This analysis has previously been documented in detail [15] which is attached as Appendix 1.

Concurrently, some additional effort was expended under SKF support to detail the performance of the pinion designs over a range of shaft rotational speeds. Lubrication and friction effects were included at that time. Particular attention was directed to local as well as global heat generation rates (HGR) to provide design information for proper lubrication of the bearings. This work was described in [16] which is attached as Appendix 2.

In summarizing the results of this work, it is noted that neither of these commercial bearings provided a completely satisfactory design with respect to the original constraints on bearing rating life and available housing space. The M88000 series bearing, the larger of the two designs, was judged to be the best suited candidate since it afforded acceptable bearing rating life. However, it violated the housing space limitations. The smaller LM67000 series bearing did not demonstrate acceptable bearing life under the specified operating conditions.

The results itemized below correspond to analyses which were carried out using pairs of M88000 series tapered roller bearings. Executions at Level 0 were done under the following operating conditions; shaft speed = 3744 rad/s (1.2×10^6 DN), nominal gear load vector (P_x, P_y, P_z) = (-3.8, 1.2, -4.0 KN) varied from 60%-100% NGL, bearing material = Vim Var M50 tool steel, preload range = 0.0 to 222.4 N, shaft and housing fit range = line-on-line to 0.01 mm tight, shaft wall thickness = 10% to 100%, temperature = 423 K. Executions at Level 1 include a range of speeds = 1040 to 6240 rad/s (0.33 to 2.0×10^6 DN), lubricant = MIL-L-23699 (estimated bearing flow rate = 1.5 ℓ/min. (0.4 gpm).

Results at Level 0

- A comparison of the bearing load distributions for the straddle and cantilever designs demonstrates that the straddle more equally distributes both radial and axial loads. This factor has a significant effect on bearing rating life. Analyses demonstrated an increase in L_{10} life of 25% for the straddle arrangement compared to the cantilever for identically sized arrangements.

- Calculation of the deformations at the point of load application showed the straddle enjoyed a significant advantage over the cantilever at all load levels. Consideration of alternate designs with reduced bearing spacing demonstrated that radial deflection decreases could be achieved.

- The influence of preload on bearing life performance illustrated a marked increase in life over a substantial preload range for the bearing not opposing the applied thrust. Use of a smaller bearing in its place represented a potential means to conserve design mass and volume. This was exploited in later analyses (Section 2.3). The L_{10} life for the thrust carrying (life-limiting) bearing decreased monotonically with increased preload.

Results at Level 1 (Isothermal

- Resulting L_{10} lives for both straddle and cantilever designs illustrated that the proposed lubricant scheme precipitated reduced performance at the specified operating temperature. Life adjustment factors less than 0.6 were computed at the roller-race contacts at all shaft speeds because of thin films caused by low operational lubricant viscosities (and insufficient replenishment layer thickness). Film Parameter Ratios, Λ, ranged from 0.56 - 1.74 for these contacts over the specified speed range.

- The current analysis was performed without the benefit of an interacting thermal analysis which couples the load support system with its thermal environment. The sensitivity of the design performance to preload, coupled with the potential for large thermal gradients and high heat generation rates predicted by analysis, indicated that the interactions of bearing and system generated heat sources could have a significant effect on system life.

2.3 Optimization of Taper Support Straddle Design

These analyses were conducted using the best shaft configuration, straddle mounting of the gear, and the most satisfactory load support bearing, the M88000, as defined in previous analyses (Section 2.2). A complete systems study, including variations in the size of the preload bearing, the value of applied preload, bearing center to center distances, shaft-cone fits, and lubricant flow rates, was conducted to select the best shaft bearing design for the application. The runs were completed using either a LM11700 or LM67000 series tapered roller bearing at the side opposite the axial load direction, i.e. the preload bearing. The details of these analyses are contained in Appendix 3 and the results are summarized below.

The analyses were again completed using the load support system analysis software SHABERTH. The executions carried out at Level 0 were done under the following conditions; shaft speed = 3744 rad/s, shaft wall thickness = 50%, shaft-cone fits = line-to-line, temperature = 373K. Gear loads were specified at 60 or 100% of the nominal applied gear load. Preloads ranged from 0-0.2 KN (0-50 lbs.). In each configuration, both bearing centers were held at 38.4 mm from the point of load application. The M88000 was employed as the primary load carrying bearing since it was known to be adequate.

The executions at Level 1 (isothermal) used the LM11700 bearing in the preload position Preloads and gear loads were maintained at 0.2 KN and 60% NGL, respectively. The lubricant was Santotrac 50. Bearing center-center distance was varied from 38.4 to 76.8 mm. Computer runs at Level 1 with the thermal option activated also explored a range of shaft fits, line-to-line to 0.01 mm tight, and lubricant flow rates, 0.76-3.4 ℓ/min. (0.2-0.9 gpm).

Results at Level 0

- The life limiting bearing switches from the load carrying (M88000) to the preload position and the system L_{10} life increases with the introduction of either the LM67000 or LM11700 series bearing. The reduction in contact angles from 20° in the M88000 to 15.37° and 10.8° in the LM67000 and LM11700, respectively, enables a substantial reduction in the internally generated axial load. This reduced load on the load carrying bearing produces the increased system L_{10} life.

- The effect of preload on the L_{10} life of each bearing is reversed when the LM11700 bearing is employed. The reversal in effect exists since the fully-loaded roller complement in the M88000 bearing becomes partially unloaded when the LM11700 is employed. The life then increases with preload since increased load results in the load being carried by more of the rollers.

- No significant change in the magnitude of the gear deflections was exhibited by varying bearing type.

Results at Level 1 (Isothermal)

- The addition of lubrication and friction effects to the analysis produces a decrease in the lives of both bearings, i.e. equal to a loss of 600 hours in the critical LM11700 bearing. These losses were attributed to to starvation effects at the minimal lubricant flow rate assumed for these test cases. It was anticipated that the trend would reverse in future thermal evaluations conducted with larger lubricant flows, given that the bearing temperatures would remain close to the current operating values of 373 K (100°C).

- An increase in bearing separation increases the estimated fatigue lives of both bearings. For the critical LM11700 bearing, the life varies from 1200 hours at a distance of 38.4 mm to 7200 hours at 76.8 mm. The design constraint that the bearings have a 2500 hours L_{10} life at 60% nominal applied gear load dictated a minimum bearing centerline-to-centerline distance of 45 mm. Previous calculations established that gear deflections are maintained within the specified levels using separations as

large as 76.8 mm. Therefore, the thermal analyses were initiated at a specified separation of 55 mm as a compromise to minimize mass and maintain acceptable L_{10} life.

Results at Level 1 (Thermal Option Activated)

- The limiting system L_{10} life, that of the LM11700 bearing, for a separation of 55 mm, a line-to-line fit, minimal preload (44.48 N) and large lubricant flow rate 3.4 ℓ/min. (0.9 gpm) was 2300 hours or 92% of the required design life of 2500 hours. The L_{10} life decreased to 1588 hours, 63% of the required value, at a flow rate of 1.5 ℓ/min. (0.4 gpm).

- Subsequent simulations in which the bearing centerline-to-centerline distance was increased from 55 mm to 65 mm, showed adequate system life. The increase is caused by decreased reaction loads at the life limiting LM11700 bearing. All simulations at 60% NGL and 3.4 ℓ/min. flow rate achieved 2500 hours life, regardless of the fit. The preload was set at 44.5 N for all executions.

- Relative location of the gear with respect to the bearings has a significant impact on limiting L_{10} life. Movement of the gear center 10 mm closer to the location of the load carrying bearing, M88000, increased the L_{10} life of the preload bearing, LM11700, from 3779 hours to 5192 hours, considering the same total bearing separation of 65 mm and identical operating conditions.

- Reduction of lubricant flow rate from 3.4 ℓ/min. to 1.5 ℓ/min. for the previous test cases reduced the limiting life from 5192 hours to 1694 hours. Increase in shaft-cone fits from line-to-line to 0.01 mm tight reduced the life of the preload bearing from 5192 hours to 2501 hours.

- All executions at 100% NGL showed gear deflection and rotations were well within the prescribed constraints.

2.4 Analysis of Alternative Shaft Support Configurations

This phase of the analytical activity evaluated the customary designs for the input pinion support system for comparison with the tapered support systems. Four specific configurations were evaluated each employing a combination of angular contact ball bearings and cylindrical roller bearings. The first two configurations were straddle arrangements using either a 205 or 303 size cylindrical roller bearing on one end of the shaft and three 205 size angular contact ball bearings on the other end. The angular contact bearings were arranged with two in the primary axial load direction and one preloaded against the pair. The cylindrical bearing only carries radial load.

The second two configurations employed straddle or cantilever configurations with a novel thrust carrying cylindrical (TCC) roller bearing and two 205 angular contact bearings. Both angular contact bearings were in the primary axial load direction with the preload applied by the cylindrical bearing. However, while transmitting power through the gearbox, the cylindrical would again only see an applied load in the radial direction and the axial preload would be relieved.

The details and results of these analyses are presented in Appendix 4 and summarized below. The operating conditions used in the analysis were analogous to those employed in previous efforts with the tapered roller bearing systems (Section 2.3). One exception was that preloads on the ball and thrust carrying cylindrical bearings were specified at 890 N and 445 N, respectively. Shaft fits also ranged over twice the previously specified values, i.e. up to 0.02 mm tight, and temperature was selected at 423 K for Level 0 and Level 1 (isothermal) runs.

Results at Level 0

- The L_{10} lives for both conventional designs and one other design were adequate. The design employing a cantilever geometry with the thrust carrying cylindrical, exhibited poor L_{10} life. Misalignment due to excessive deflections produced an L_{10} life of only 70 hours in the cylindrical bearing.

- Gear deformations at 100% NGL for the three designs with acceptable life were also acceptable. Radial and axial deflection for the cantilever TCC configuration exceeded the allowable limit (0.025 mm).

- The conventional design using a 303 size cylindrical roller bearing offered better system L_{10} life over the second version. This configuration and the straddle TCC configuration were selected for further study at Level 1 (isothermal).

Results at Level 1 (Isothermal)

- A significant reduction, >2 to 1, in fatigue life, was demonstrated compared with the Level 0 results, i.e. no lubrication and friction effects. This decrease is attributed to the low a_3 lubrication related life adjustment factors, 0.56, associated with a small elastohydrodynamic film. The latter is due to low lubricant viscosity at the specified operating temperature of 423 K (150°C). Lubricant temperatures in the application were expected to be significantly lower, ~373 K, so that life reductions smaller than those predicted here are anticipated.

- Interference shaft-cone fits caused a redistribution of the load vector; hence the bearing fatigue lives were seen to vary with fits. Limiting L_{10} lives ranged from 1632 hours to 2290 hours for fits of 0.00 mm to 0.02 mm in the conventional design, and from 2157 hours to 3115 hours in the TCC design.

- The fits tend to stiffen the system by eliminating the operating clearance in the cylindrical bearings. As such, the deformations are smaller than previously computed in the Level 0 runs, and within the prescribed limits.

- The relative L_{10} life performance slightly favored the TCC design. Also, this configuration employs 3 instead of 4 bearings and thus weighs less. This configuration was selected for further study at Level 1 with the thermal option activated.

Results at Level 1 (Thermal Option Activated)

- The design TCC configuration exhibits adequate minimum L_{10} life over the specified range of fits, preloads and lubricant flow rates, except for the heavier shaft fit

case (0.04 mm). At fits of 0.02 mm or less, greater than 2800 hours L_{10} life was found for the largest specified preload (890 N) at flow rates as small as 0.76 ℓ/min.

- Deflections/rotations at the gear mesh were well within acceptable limits at 100% NGL.

3. Test Bearings

The test bearings used in the experimental program were obtained by the modification of existing standard commercial tapered roller bearings. The basic size of the bearings to be used and the values of the modified parameters had been selected in the early analytical effort described in Section 2.1.

The bearings utilized in this effort were the M88048/010 and the LM67048/010 sizes which are standard domestic automotive bearing designs. These units were transformed into high speed bearing designs through a series of modifications identified through past experimental programs. The modifications consisted of the following:

(1) The removal of the small end cone flange to form a land riding surface for the cage, and allow the use of a machined cage in the assembly.

(2) The drilling of nine equally spaced holes of 0.89 mm (0.035 in.) diameter through this land to deliver lubrication directly to the cage-land interface.

(3) The addition of a large chamfer at the large end bore corner of the cone to create a lubricant reservoir between the ring and shaft.

(4) The drilling of nine equally spaced holes from the chamfer surface into the large end flange undercut to supply lubricant to the flange roller end surfaces. The minimum diameter of the breakout of the hole into the undercut bottom was specified as 0.80 mm (0.030 in.).

(5) The replacement of the pressed steel roller riding cage with a machined silver plated steel cage. This component was supported on the O.D. of the large flange and on the land created at the small cone end.

The machined cage has a thicker web dimension than the normally used roller riding stamped cage. Thus to accomodate this change, it was necessary to reduce the number of rollers from 19 to 16 in the M88000 bearing and from 19 to 17 in the LM67000 bearing.

(6) The polishing of the flange surface and roller ends to produce surface roughness values $\leq$ 0.13 µm AA (5×10^{-6} in.) and improve the sphere end profile of the rollers.

The resulting bearing designs were designated as M88000 VAC and LM67000 VAC and the basic features of these bearings are illustrated in the Customer Drawings included as Figures 1 and 2.

Standard production M88000 and LM67000 bearings were purchased from Tyson Tapered Roller Bearing Division of SKF Industries, Inc. These were then modified to the VAC designs in the Special Bearing Fabrication Shop maintained by SKF Technology Services, and the quality of the finished parts was verified against the specified parameter ranges in the Metrology Laboratory. Six finished bearings of each size were prepared. Later in the program after a number of failures had been experienced with the original bearings, a second 6 bearing lot of the M88000 VAC design was prepared. At this time, the number of oil supply holes into the large end undercut was increased from 9 to 18 in an attempt to provide better lubrication to the flange roller end interface. This design variation is designated M88000 VAC-1.

Partially through the program, it was ascertained that SKF Kugellager Fabriken, GmbH of West Germany was commercially manufacturing increased precision tapered roller bearings for specific automotive pinion applications. An M88000 size bearing was included in that product line designated as ASIK M88048/2/H/KM010/2. A comparison of the product specifications illustrated that these bearings were of the same basic design as the standard M88000, but the running tolerances, e.g. roundness, concentricity and squareness/parallelism, and the surface roughness tolerances had been tightened. Also closer controls were applied to the roller end and flange profiles. All of these attributes are desirable for a high speed bearing so SKF decided to evaluate these units after the conclusion of the sponsored program for comparison with the domestic bearings. Accordingly, a sample of these bearings was procured to be modified to the high speed design using SKF funds. Once again eighteen lubricant supply holes were added at the large end. However, the small end holes were deleted from this variation since lubricant was no longer supplied to this location in the test rig. Furthermore, measurement data established that the profiles and surface roughness levels existing on the roller end and flange surfaces

Figure 1

Customer Definition Drawing of M88000 VAC Bearing

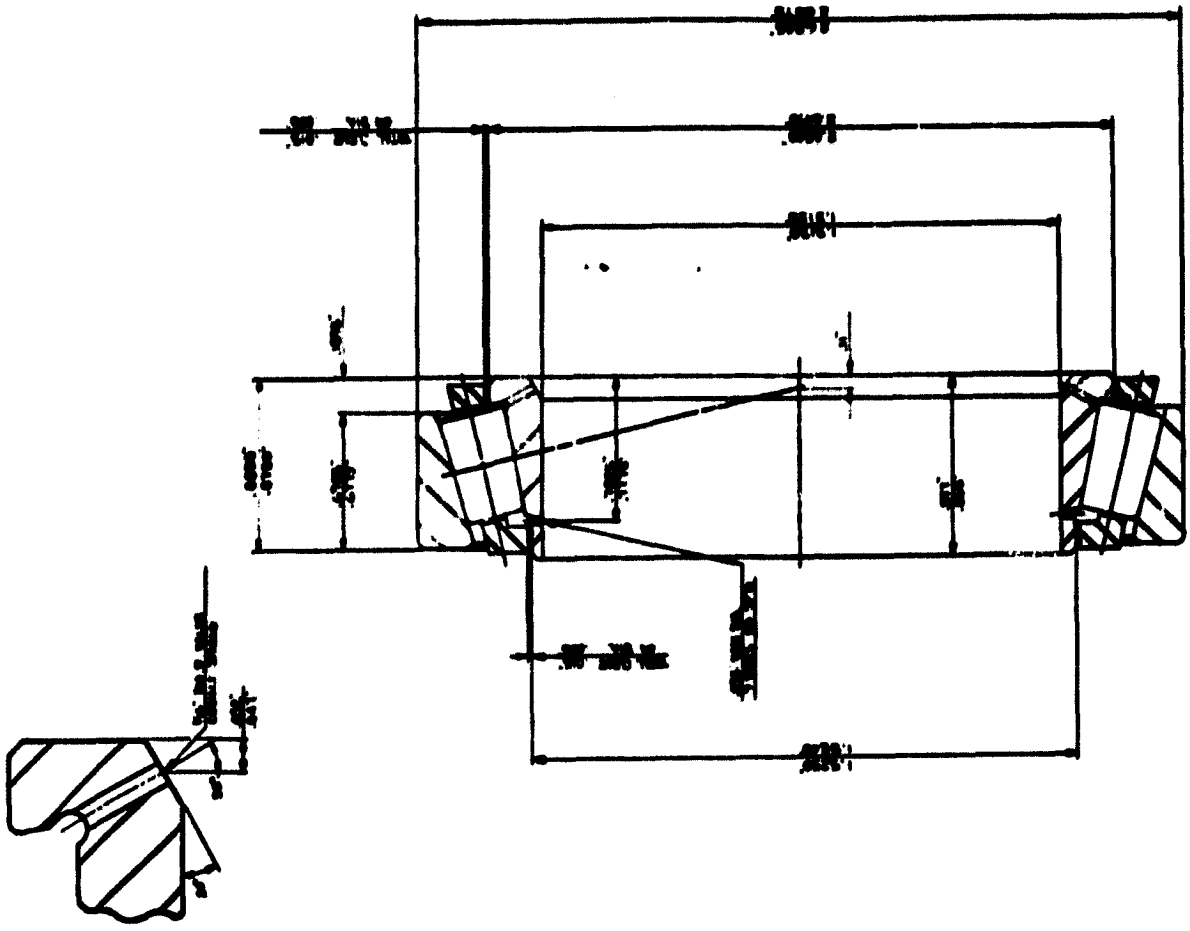

BEARING DATA	SKF
	M 88000 VAC
	M 88000 VAC
	CLASS 0
	16
	250° F
	.818"
CUP INCLUDED ANGLE	40° 0' 0"
BASIC RATING 500 RPM — BRR	8x10 LBS
BTR	2450 LBS
R	LOT

1. CUP, CONE & ROLLERS TO BE MADE FROM AISI 8620 STEEL CASE HARDNESS R 58-62
2. CAGE TO BE MADE FROM AISI 8615 ONE PIECE MACHINED & BONDED INNER LAND RIDING, SERVICABLE
3. CAGE TO BE SILVER PLATED ALL OVER PER AMS 2412 THICKNESS PER SURFACE TO BE .001"—.002" UNLESS SHOWN ARE AFTER PLATING.
4. CAGE TO BE 100% FLUORESCENT PENETRANT INSP (4709908)
5. SURFACE ROUGHNESS:

CONE ROLLER TRACK	8 AA
CUP ROLLER TRACK	8 AA
ROLLER BODY	8 AA
ROLLER SPHERICAL END	8 AA
RACE RIBBING LAND	16 AA
CAGE RIBBING LAND	40 AA
CONE RIB FACE	8 AA

Figure 2

Customer Definition Drawing of LM67000 VAC Bearing

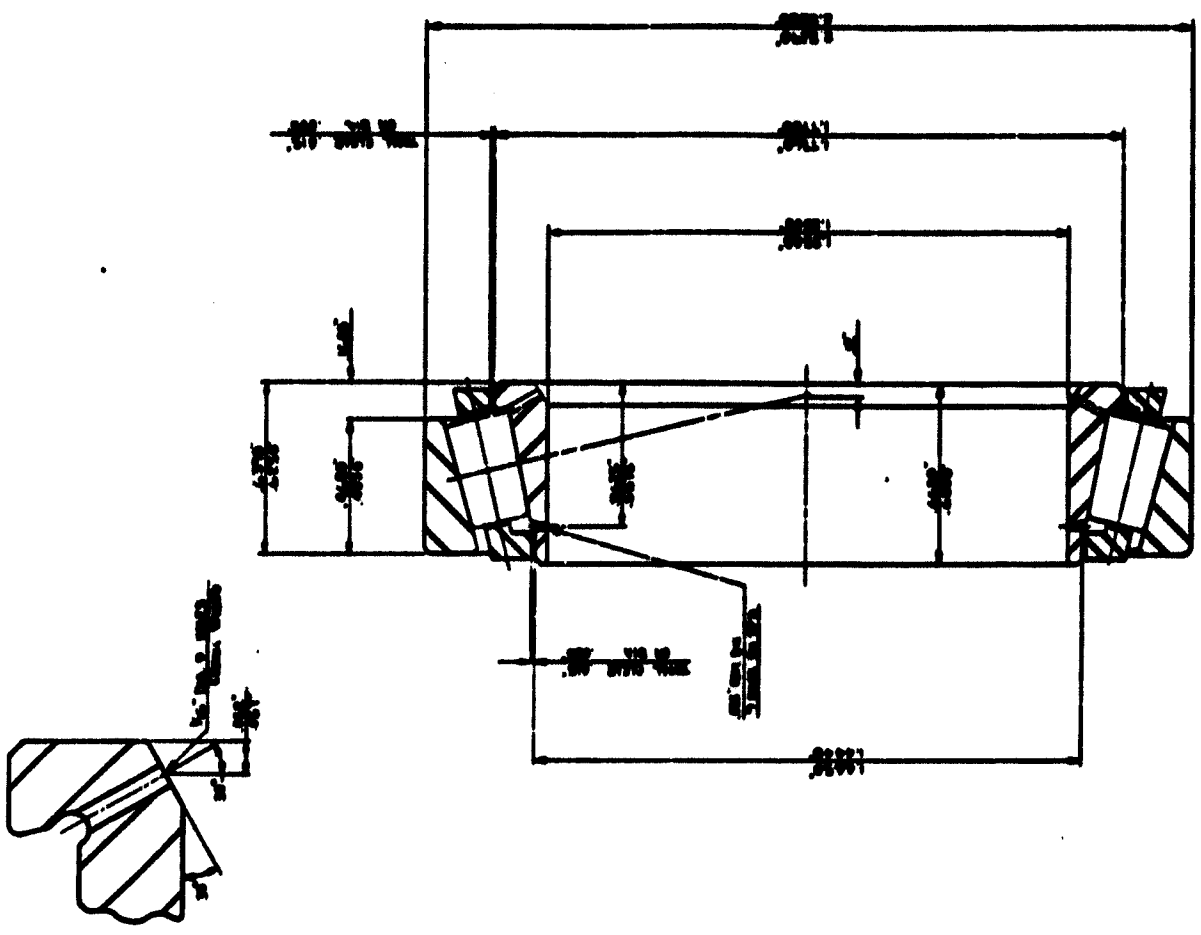

ORIGINAL PAGE IS
OF POOR QUALITY

of the purchased parts was in agreement with the requirements of the M88000 VAC design. These surfaces were thus not polished but left in the as received condition. New cages were not made for these assemblies; rather it was intended to utilize existing cages from the previous test lot. This design variation is designated M88000 VAC-2.

When it became obvious that the original domestic bearings would not operate under the intended conditions, these four modified bearings were supplied to the program. Following the successful performance of those bearings, seven additional assemblies were modified to the VAC-2 design. To conserve funds at that point, these seven bearings were also fitted with previously tested machined steel cages which had been stripped and replated with silver. Five of these bearings were then used in the experimental effort and two were delivered to NASA for future use.

4. Test Facility

To achieve the objectives of the experimental portion of the program, a test system was required which could test two small tapered roller bearings at a variety of speeds up to 4188 rad/s (40,000 rpm) under various combinations of radial and thrust loads. This basic capability was achieved through the combination of two existing test systems and the fabrication of specific hardware for these test bearings.

An existing extreme environments test facility provided the fundamental services for the test rig. The drive train included a 50 HP direct current variable speed motor powered via a motor generator set, and a belt driven gearbox speed increaser. The gearbox has an 8:1 speed ratio which when coupled with the drive pulley ratio of 3.65:1 provides variable test speeds up to 4710 rad/s (45,000 rpm). The facility also supplied a 94.6 liter (25 gallon) self contained circulating oil system for the test lubricant. This system included the thermally insulated sump, thermostatically controlled electric oil heaters, water cooled heat exchanger with a thermostatically regulated water flow rate, a full flow 25 μm filter, a supply pump and a return oil scavenge pump.

The existing angular contact ball bearing test fixture was removed from the precision base, and replaced with the arbor support housing and casting from an existing R2 type high speed bearing endurance tester. This assembly provided the precision test shaft bearing support surfaces required for a high speed shaft. In addition, a dead weight loading arm/fulcrum assembly is designed into this unit providing the mechanism for the application of radial loads.

The specific test hardware for this program was designed to interface with this composite test system as schematically illustrated in Figure 3. The test arbor is mounted horizontally in a pair of preloaded angular contact bearings at one end to fix the location of the shaft, and a cylindrical roller bearing at the other to react the externally applied radial load. Precision high speed bearings were employed in all of these shaft support locations. The test arbor was driven at one end through a flexible quill to the gearbox limiting the transmission of vibrations and parasitic forces to the test assembly.

Figure 3

Schematic Layout of High Speed
Tapered Bearing Tester

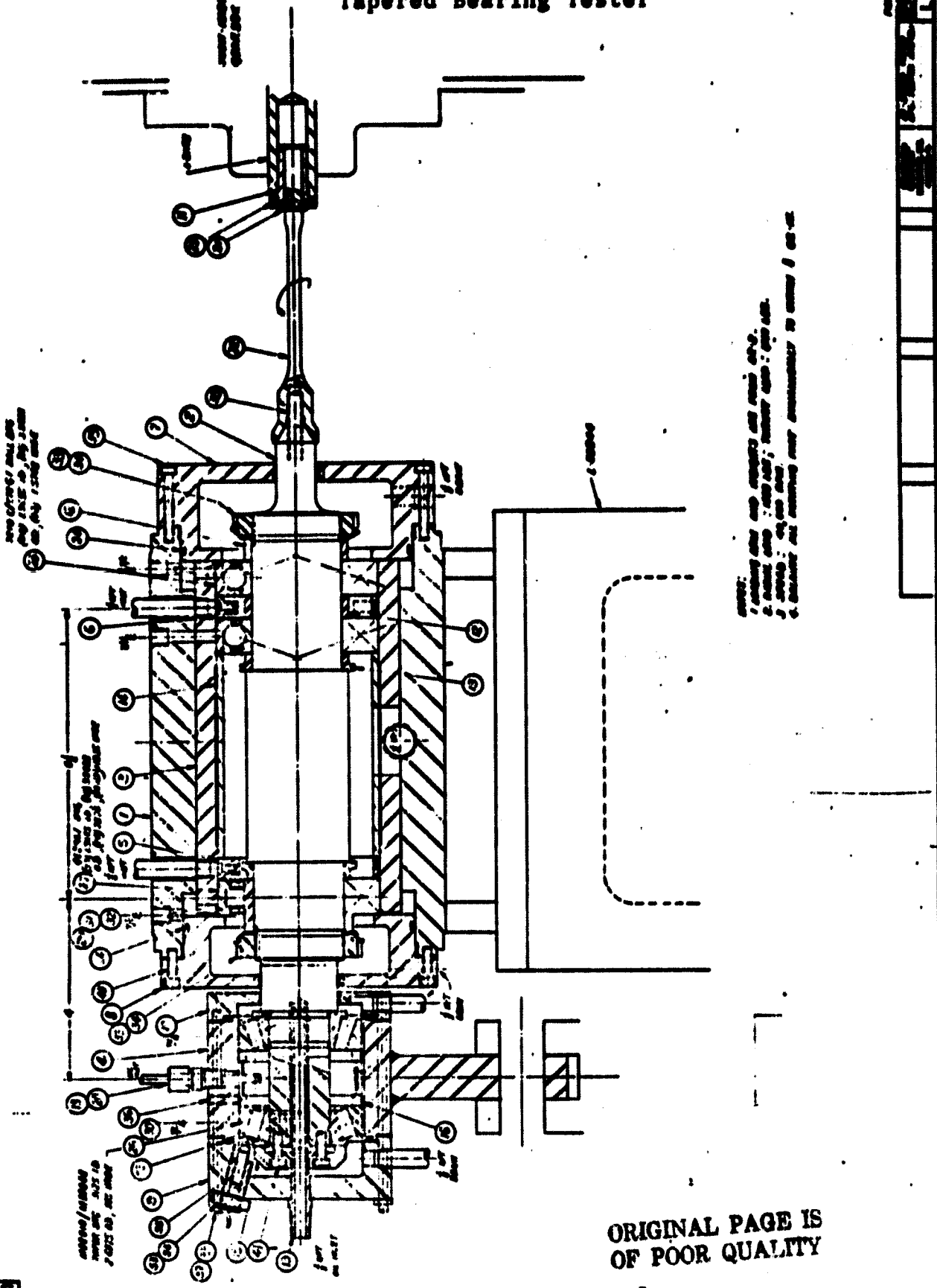

ORIGINAL PAGE IS
OF POOR QUALITY

The two tapered roller test bearings were mounted on the far end of the shaft in a separate housing. Radial load was applied to both bearings through a load link attached to the dead weight system. Axial load was internally generated by adjusting the location of the cone of the outboard bearing. The magnitude of this load was monitored with a strain gage transducer on the spacer between the cups of the two bearings.

Two methods were employed to deliver lubricating fluid to the test bearings. Three double sided jets were located between the bearings to deliver lubricant into the small end. The natural pumping action of the tapered bearing would then transport the fluid through the bearing and out the large end. Simultaneously, however, the centrifugal forces move the lubricant flow radially outward against the cup races. Thus lubricant supplied in this manner will not lubricate or cool the critical flange/roller end sliding contacts. To deliver lubricant to these areas, a tube was placed inside the hollow test shaft with radial supply holes located to deliver lubricant at the large and small ends of both test bearings. Centrifugal forces would then pump this fluid through holes in the shaft and bearing cones to deliver lubricant directly to the flange roller end interface and small end cage riding interface. A flow meter was used on the input to both supplies so the total flow provided through each system could be monitored.

Thermocouples were provided on the outer diameter of each test bearing to measure the bearing operating temperatures. Lubricant input and output temperatures were also measured with thermocouples.

Initially, a magnetic probe was mounted near the pitch diameter of the outboard bearing and connected to a frequency counter to allow the measurement of cage speed. Due to the thickness and closed configuration of the large end cage rail, the roller ends were not visible to this probe. Relatively large indentations were required in the cage rail to trigger the counting signal. This process was soon discontinued due to concern over the potential loss of dynamic balance created in the altered cage.

Photographs of the final test system are shown in Figure 4.

Figure 4

Photographic Views of High Speed Tapered Bearing Tester

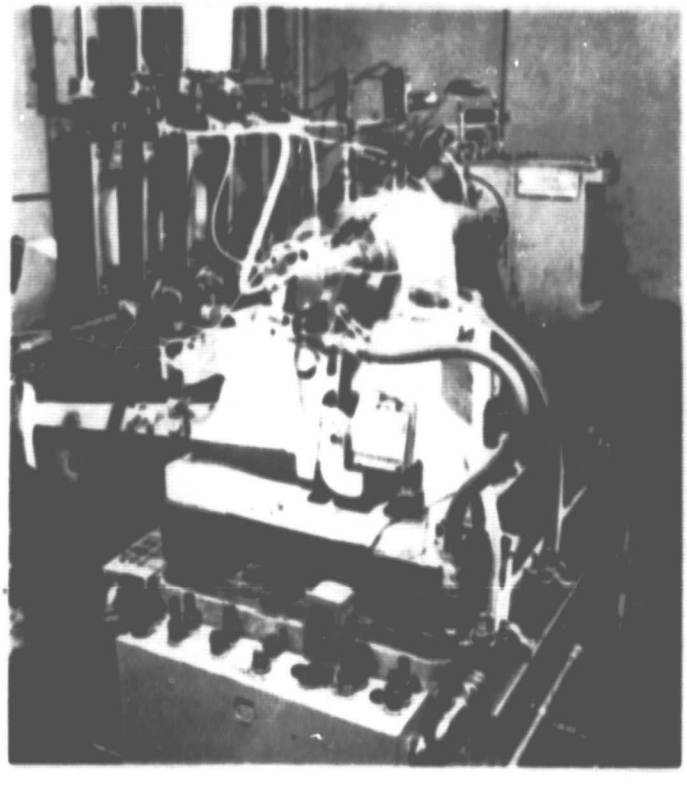

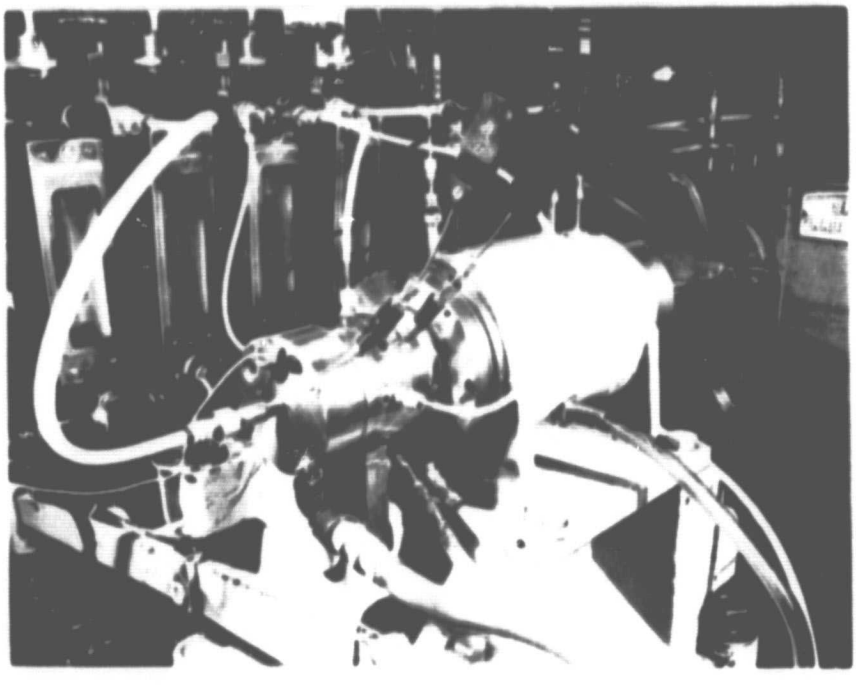

5. Experimental Evaluations

The original concept for the experimental portion of the program was quite simple; each bearing design was to be performance tested under five load levels; the lubrication requirements of each bearing design were to be established via a series of flow variation studies; and the best of the two designs was to be subjected to an extended duration test sequence.

The actual experimental activity followed a significantly different scenario. Testing was initiated on the M88000 VAC design as planned. However, due to complications created by deficiencies in lubricant distribution and by geometrical inaccuracies in the original bearings, the initial test sequence was protracted. Finally, increased precision M88000 bearings were procured from an European SKF source, modified to the VAC design and subjected to performance tests at three load levels and an extended duration test procedure. Due to time and funding limitations, testing of the LM67000 VAC bearings was not undertaken.

The basic test procedures that were employed in the conduct of these test sequences are described in the subsequent paragraphs. Also, the results achieved in each of the test sequences are described herein and the actual test data collected are included in Appendix 5. For the purposes of discussion, the test activity has been subdivided into four related groupings; these are (1) the checkout and preliminary test sequences, (2) performance tests on the original domestically manufactured bearings, (3) performance tests on the imported increased precision bearings, and (4) the extended duration test sequence.

5.1 General Test Procedures

The basic procedure utilized for the conduct of a high speed tapered roller bearing performance test included the following steps. As the rig was being assembled, the position of the outboard test bearing cone was adjusted to produce an axial preload on the bearings. The magnitude of the preload was estimated as that load level thought to produce the desired axial loading component at the elevated rig operating temperatures. Concurrently, calibrated weights were added to the hanger at the end of the load arm to produce the desired radial load component.

Prior to startup of the test system, the electrical heaters in the lubricant sump were activated. After approximately 30

minutes when the lubricant had reached its specified temperature level, the supply and scavenge pumps were activated to circulate the hot lubricant through the test unit. This process was continued for an additional 30 minutes to allow the rig components to stabilize at an intermediate temperature level prior to initiation of the test run. The value of the lubricant supply temperature was selected to be representative of that seen in helicopter transmission service. Early in the program, the level was set at 388K (240°F) which is near the high end of the typical service range. Later this value was reduced to 366K (200°F), the lower limit of the service range, to improve the EHD film conditions in the bearings.

Operation of the test system was then initiated at low speed and slowly accelerated to 523 rad/s (5000 rpm). Testing was maintained at that speed for a minimum of 30 minutes to allow thermal stability to be achieved. Test data would then be recorded and the speed would be increased to the next level where the process would be repeated. In general, the speed increments employed were equal to 523 rad/s (5000 rpm). Early tests conducted before personnel were totally familiar with the test system utilized speed increase increments of smaller value and longer running periods were often experienced at each level. Later when it was known that problems often occurred at speeds between 3141 and 4188 rad/s (30,000 to 40,000 rpm), increments of 262 rad/s (2500 rpm) were regularly employed after reaching this critical region.

The performance tests were conducted totally under manual control and all data was manually recorded from a variety of test instruments. During these periods, operators were instructed to shutdown the test immediately if (a) a rapid thermal increase was noted on any monitored point in the absence of a speed increase, (b) a change in rig sound level or pitch was noted, or (c) in the presence of any other unexplained incident. Testing in each series was terminated after accumulating 30 minutes of operation at the maximum speed condition, 4188 rad/s (40,000 rpm) or with a bearing failure.

The procedure for the extended duration runs was similar to that used in the functional testing. The rig was assembled and preheated prior to startup as previously described. However, after initiating one of these runs, the test speed would be gradually increased manually so that 3141 rad/s (30,000 rpm) would be achieved after approximately one hour. Fifteen minutes of operation would then be accumulated at that level

and at 3665 rad/s (35,000 rpm) before the test speed would be increased to the maximum condition.

After 15 to 20 minutes of uneventual operation at 4188 rad/s, the control of the test system would be transferred to the computerized test control system. Subsequently, the computer would check the value of each operating temperature and the axial load at a rate approximating once every two seconds, and compare the measured value against established limits. An excursion in the level of any of these points would cause the test to be automatically shutdown by the computer. Since the runs were only conducted during the day, test personnel would also periodically check the rig and test area for any other occurrence which might affect test operation.

The loading conditions to be used in the test runs were originally designated as 60, 100 and 150% of nominal. In this context, the nominal load was defined as that load developed on the most heavily loaded bearing on the pinion shaft with the gear operating at the stated maximum conditions. These load levels, calculated as a portion of the systems analysis, are given in Table 5. It should be noted that these values were calculated at an early stage using a shaft supported on two equally sized bearings and without considering many of the thermal mechanical system interactions. As a result, the loads used in the test program are significantly higher than those calculated to exist in the optimized tapered bearing support system discussed in Section 2.3 which uses a smaller bearing in the preload position and minimizes the magnitude of the internally generated system thrust load.

5.2 Checkout and Preliminary Test Runs

Prior to the initiation of any of the planned tests, the test rig was assembled with standard production M88048/M88010 bearings. This process was completed to achieve four specific objectives; (1) to check the test rig hardware and verify the assembly of the test unit, (2) to develop assembly and disassembly procedures to be utilized with the test bearings, (3) to allow the evaluation and calibration of the test subsystems e.g. lubrication supply and scavenge loops, thrust load application and monitoring, etc. and (4) to verify the operational ability of the system at low speeds.

During this process, it was noted that the axial load application method was lacking in precision. Even with hydraulic pressure applied beneath the outboard cone to relieve the heavy interference fit, the ring would not move smoothly under the pressure of the jacking screws. This created a situation where the preload varied stepwise rather than being totally variable. Furthermore, due to the nature of the loading mechanism, the magnitude of the applied load varied with temperature and was not adjustable during periods of running. While these latter points had been foreseen, the problem encountered with the load adjustment now made it impractical to temporarily suspend testing to reset the load

TABLE 5

Definition of Test Load Levels

	Load/Bearing			
	Radial		Axial	
Classification	N	lbf	N	lbf
60% Nominal	1913	430	5106	1148
Nominal	3216	723	7041	1583
150% Nominal	4844	1089	9448	2124

level. It was considered undesirable to reduce the shaft/bearing fit to alleviate the adjustment problem since this would increase the risk of cone spinning at high speeds. Considering that the load variations to be experienced would have only minor impact on the objectives of the program, it was decided to proceed without altering the test rig design.

All other checkouts and calibrations were successfully completed. The test system was operated for significant periods of time at speeds up to 1047 rad/s (10,000 rpm) to familiarize test personnel with system behavior. Speeds were limited to that level by concerns about the performance limitations of the unmodified checkout bearings. At the conclusion of these runs, the rig was declared to be operational.

Testing was then initiated on the preliminary performance test runs which are summarized in Table 6. In the interests of time, the first test run was conducted using cages which had not been dynamically balanced. For these early tests, the total lubricant flow to the two test bearings was set at approximately 0.95ℓ/min. (0.25 gpm). This flow was thought to be evenly divided between the two test bearings at a flow rate comparable to that which might be used in helicopter transmission service. This flow was provided from two distinct sources; half was delivered through jets directly into the small ends of the bearings, and half was injected into the hollow test shaft where it would be centrifugally pumped through four sets of holes into the large and small ends of each test bearing.

This first step speed run, being conducted at a 60% load level, was terminated after 50 minutes of operation at a speed of 2094 rad/s (20,000 rpm) by an increase in system torque. An examination of the test bearings disclosed a 120° arc of wear on the large cage bore with a matching wear pattern accompanied by transferred silver on the large land of the bearing that had been mounted in the outboard test position. This bearing also showed a minor amount of roller end/flange distress. The inboard bearing showed no evidence of damage.

Since the damage noted was relatively minor, the cage bore and land surfaces of bearing #1 were repolished. The same bearings were then remounted on the rig with their positions reversed. Run 2 also achieved a maximum speed of 2094 rad/s before operation was again terminated by a torque increase. This

TABLE 6

Summary of Preliminary Performance Test Runs

Run Number	Loading Condition	Bearing Type	Test Bearing Numbers Inboard	Outboard	Maximum Speed Achieved (rad/s)	Time at Max. Speed (Min.)	Total Lubricant Flow/Brg. (ℓ/min.)	Result
1	60%	New VAC (Unbalanced Cages)	2	1	2094	50	0. 47	Outboard Brg. (#1) Failed Cage-Land Wear
2	60%	Used VAC (Unbalanced Cages)	1 (repolished)	2	2094	20	0. 47	Outboard Brg. (#2) Failed Roll End/Flange Smearing
-	Rig Modified to Improve Outboard Lubrication							
3	60%	New VAC	4	3	2617	-	0.66	Outboard Brg. (#3) Failed Roll End/Flange Smearing
4	Pure Thrust	Used VAC	4	1	2617	35	0.66	Outboard Brg. (#1) Failed Roll End/Flange Smearing
-	Performed Lubricant Distribution Tests; Modified Rig							

time bearing #2 had suffered severe roller end/flange distress, e.g. wear, smearing and heat discoloration. The condition of the inboard bearing, damaged in the original test run, was essentially unchanged.

The premature failure of two bearings in the outboard location, coupled with the seemingly successful operation of the inboard bearing, indicated that adequate lubricant flow was not being provided to the outboard flange supply reservoir. In an attempt to correct this situation, two alterations were made to the test hardware. A cross cut was made on the inside end of the load cap to provide channels to deliver the lubricant directly into the flange supply reservoir. Also the internal profile of the load cap was altered to feed all of the lubricant entering that cavity into the flange supply reservoir. These alterations are noted in Figure 5.

Run 3 was then conducted at 60% load with new test bearings and using an increased lubricant flow rate, 0.66 ℓ/min. (0.175 gpm) per bearing. These bearings now totally conformed to the M88000 VAC design containing cages balanced to the specified limit of 3 gm cm (0.042 in ounces). This test proceeded to a maximum speed of 2617 rad/s (25,000 rpm) where operation was promptly terminated by a torque increase. Once again the outboard bearing had suffered a roller end/flange failure, while the inboard assembly showed no signs of deterioration.

While it appeared that a lubricant distribution problem still existed, it was not immediately obvious why this should be the case or how it could be corrected. The possibility that misalignments produced by shaft deflections were adversely affecting the operation of the outboard bearing was also considered. To insure that this was not the case, it was decided to conduct a test run under pure thrust load. This test run utilized used bearings numbers 1 and 4 which had survived the previous tests. The axial load was set at 6.7 kN (1500 lbf) and step speed testing was initiated. After 35 minutes of operation at 2617 rad/s (25,000 rpm) the outboard bearing suffered a roller end/flange failure. It was now established that the lubricant being supplied through the hollow shaft was not adequately distributed between the two test bearings.

It was then considered necessary to directly measure the individual flow rates through each of the four shaft supply routes, i. e. through the cones of each test bearing at the large and small ends. Since this could not be done within the normal test arrangement, a four chamber collection box with a drain in each chamber was designed to mount over the shaft with the cones in place. This box allowed the direct measurement of the individual lubricant flow rates and also the observation of the flow process via a viewing port. A series of tests were then conducted to establish the lubricant flow balance as a function of test speed. The data collected during these tests are also contained in Appendix 5.

Initial tests were conducted at a total flow rate of 0.49 ℓ/min. (0.13 gpm) with an elevated supply temperature of 343 K. These established that the flows through these four routes were relatively well balanced at low speeds. However, as the speed was increased, the flow through the outboard bearing flange supply holes decreased until at 2617 rad/s (25,000 rpm), it was essentially zero. It was postulated that the problem was created by the large volumes of air and fluid pumped by the shaft holes at high speed. This pumping efficiency could create a low pressure area at the inboard end of the shaft forcing the migration of oil from the outboard supply areas to the inboard areas. It was, however, not apparent whether this redistribution occurred inside of the supply tube, whether oil moved along the O.D. of the tube, or whether both situations occurred. An "O" ring was placed around the supply tube between the outboard bearing large end and small end supply holes, i.e. near the end of the shaft, and the distribution tests were repeated to determine the effects on the flow balances. It was noted that the flow through the outboard supply was improved by this device although the rate still decreased with increasing speed. This indicated that flow variations were produced inside the tube and some lubricant migration also occurred along the exterior of the tube. Both of these situations would need to be corrected in order to balance the flows.

For the next test run, the 3 sets of inboard holes in the lubricant supply tube were blocked forcing all of the flow into the area feeding the outboard bearing flange. A Teflon flinger, shaped to closely conform to the chamfer at the shaft end, was located on the supply tube to prevent migration on the tube outer surface. Tests were run up to 30,000 rpm and little or no lubricant was collected from the three inboard cavities which indicated that the flinger effectively sealed this flow path. This flinger configuration is also illustrated in Figure 5.

A series of runs was then initiated to establish the proper sizes for the sets of inboard holes to produce a balanced flow situation at high speeds. When the first holes were added to the inboard end of the supply tube, i.e. below the inboard bearing flange feed holes in the shaft, it was noted that lubricant was pumped out of all three remaining shaft locations, e.g. at the inboard flange and at the small end of both cones. Since it was impractical to attempt to segregate these three supply routes and since the flows were rather equitably divided, it appeared that two sets of holes would suffice. The flow rate measurements verified the adequacy of this simplification at speeds up to 3141 rad/s (30,000 rpm) where the cylindrical load bearing supporting the test shaft suffered a skidding failure as a result of its unloaded condition. The bearing was replaced, but further attempts to exceed operating speeds of 2617 rad/s for periods sufficient to obtain flow data were terminated by dynamic instabilities. It was decided at that point to continue the performance test series using that hole pattern which had produced balanced flows at 2617 rad/s, i.e. 2 outboard and 2 inboard holes all of 2.3 mm (0.089 in.) diameter, and using the Teflon flinger on the oil supply tube at the shaft end.

5.3 Domestic Bearing Performance Tests

Testing was then resumed as summarized in Table 7. Run 5 was conducted at "light" loads, i.e. 890 N (200 lbf) radial and 3560 N (800 lbf) axial. The one remaining previously tested bearing, number 4, was used along with one new bearing. Once again the lubricant flow rate was increased to 0.95 ℓ/min. (0.25 gpm) per bearing. After 45 minutes of operation at 3351 rad/s (32,500 rpm), the inboard bearing suffered a roller end/flange failure. This bearing had been running slightly hotter throughout the run, so it was assumed that the flow balance was now slightly biased towards the outboard end. One of the holes in the inner most set was thus increased in diameter one drill size, i.e. to 2.5 mm (0.100 inch) diameter.

Run 6 was also conducted under light loads using one used and one new bearing. This time both bearings failed after running for 5 minutes at 4188 rad/s (40,000 rpm). While the damage to the inboard bearing was somewhat greater, it was considered that (a) the flows were now adequately balanced and (b) the flange roller end interfaces required a larger lubricant flow for reliable operation. At this time, the number of lubricant supply holes through the bearings at the flange undercut was increased from nine to eighteen to allow an increased flow rate and an improved radial distribution of the flow to this critical area.

TABLE 7

Summary of Domestic Bearing Performance Tests

Run Number	Loading Condition	Bearing Type	Test Bearing Numbers Inboard	Outboard	Maximum Speed Achieved (rad/s)	Time at Max. Speed (Min.)	Total Lubricant Flow/Brg. (ℓ/min.)	Result
5	"Light"	Used/New VAC	4	5	3351	45	0.95	Inboard Brg. (#4) Failed Roll End/Flange Smearing
6	"Light"	New/Used VAC	6	5	4188	5	0.93	Both Brgs. Failed Roll End/Flange Smearing Inboard Worse
7	"Light"	New VAC-1 (18 Oil Holes)	8	7	3665	30	1.56	Inboard Brg. (#8) Failed Roll End/Flange Smearing
-	Performed Lubricant Distribution Tests; Modified Rig							
8	"Light"	New VAC-1	9	10	3665	10	2.3	Outboard Brg. (#10) Failed Cage Failure
9	60%	Used VAC-1	9	7	3141	60	1.9	Inboard Brg. (#9) Failed Roll End/Flange Smearing Unusual Loading Patterns

Test run 7 utilized two new bearings with the increased number of holes, i.e. M88000 VAC-1, and the lubricant supply rate was increased to 1.56 ℓ/min (0.41 gpm) per bearing by increasing the flow through both sources. This run, also conducted under light loads, was terminated by the failure of the inboard bearing after 30 minutes of operation at 3665 rad/s (35,000 rpm).

Testing was temporarily suspended at that point to allow a comprehensive review of the results achieved. In addition, the M88000 VAC design was analytically compared to a similarly sized experimental tapered roller bearing which had run successfully at speeds up to 8378 rad/s (80,000 rpm) under light loads [10], and a special thrust carrying cylindrical roller bearing which supported extremely high loads at 2250 rad/s (21,500 rpm) [5]. These studies indicated that the values of the critical flange roller end parameters, i.e. sliding speeds, stress levels, heat generation rates, etc., in the M88000 VAC bearing at maximum operating conditions were not significantly different than those successfully achieved in the previous test programs. It was concluded that if the flange roller end contacts could be adequately lubricated, the current bearing would operate at the targeted conditions.

Before running any more performance tests, it was considered necessary to affirm the flow balances in the speed range between 3665 and 4168 rad/s where the failures were being experienced. To allow operation at these high speeds without an externally applied load, the cylindrical roller bearing supporting the arbor was replaced with an angular contact ball bearing. This latter bearing was preloaded against the duplex pair at the other end of the shaft by a preformed washer spring. Unfortunately, the selection of this replacement bearing was limited by the existing rig envelope and by the stock of commercially available precision bearings. The only precision ball bearing available in this size contained a phenolic cage which fills the majority of the volume between the rings. This design coupled with the design of the shaft support hardware made it impossible to reliably lubricate and cool this bearing at speeds in excess of 3141 rad/s (30,000 rpm). Again it was undesirable to alter the basic design of the system since the cylindrical roller bearing would need to be reincorporated to finish the tapered roller bearing test series. Maximum test speeds were once again limited for the lubricant distribution runs.

While extensive running could not be accumulated in the high speed ranges, the brief runs achieved did illustrate the existance of a severe flow distribution problem. As illustrated in Figure 5, the holes in the supply tube were aligned with holes in the shaft to deliver lubricant to the large end of each test bearing. It was noted that at the higher speeds, a large amount of the lubricant intended for the flange of the inboard bearing was actually being diverted further outboard and pumped through the holes at the small end of the two cones. While the sharing of this supply had existed at lower speeds, the distribution had been fairly reasonable for the experimental objectives. However, at these higher speeds the amount of lubricant being supplied to the flange had been drastically reduced. This occurrence explained the most recent failures at the flange roller end interface of the inboard bearing.

A dual approach was selected to rectify this recurring problem. First, it was decided to simplify the overall flow distribution problem by eliminating the through race lubricant supply to the small end of the bearings. This could be accomplished without risk to the test effort since jets already existed to supply lubricant to this location. All effects of this supply route were eliminated by using a supply tube with only two delivery locations and by plugging the existing holes through the test shaft. The second change was the relocation of the inboard delivery location in the supply tube. In lieu of supplying the lubricant radially under the location of the inboard shaft holes, the lubricant was injected axially onto the end of the hollow recess inside the shaft. It was reasoned that the lubricant would then be forced to migrate outwards to the shaft holes where it would be pumped into the bearing at the desired location. These modifications are also noted on Figure 5.

Following the completion of the hardware modifications, flow balance tests were completed with the results shown in Figure 6 . At a total through shaft flow rate of 1.13 ℓ/min. (0.3 gpm), the average rate utilized in the previous tests, the flows were balanced to within 11% at the worst case. When the total flow rate was increased to 1.89 ℓ/min. (0.5 gpm), a value projected for use in future tests, the balance was significantly worse at the low end of the speed range, but converged to a 13% variation at the high end, i.e. 3141 rad/s (30,000 rpm). While this variation was greater than one would intuitively desire, it did seem to provide adequately balanced lubrication for testing purposes. Additionally, it did not appear from the illustrated trends that operation at higher speeds would severely alter the existing flow balance. This configuration was accepted for use in the continuation of the performance test series.

Figure 5

Diagram of Modifications to Flange Lubricant Supply System

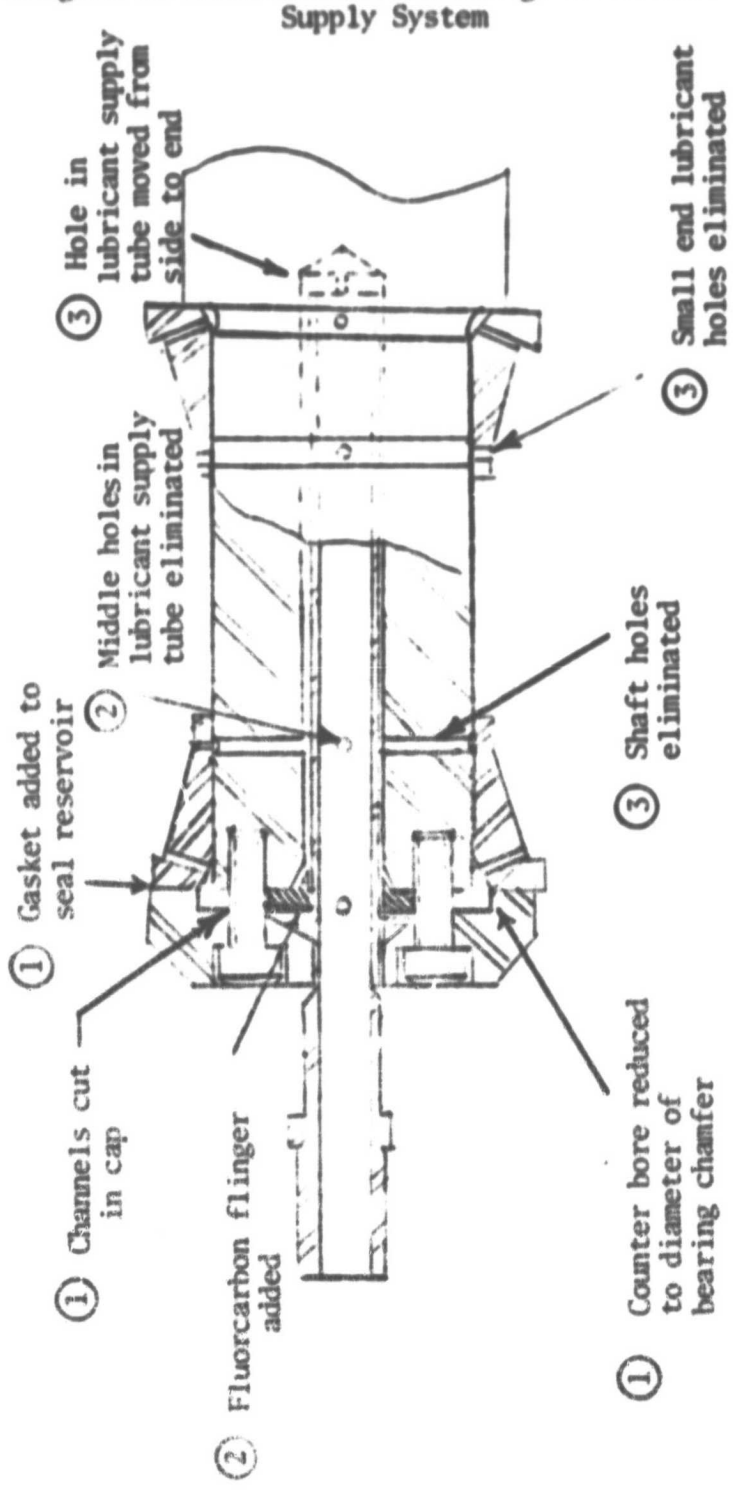

Note: Circled Numbers Denote Sequence of Modifications

AT81T014

FIGURE 6
DISTRIBUTION OF THROUGH RACE LUBRICANT FLOWS IN FINAL SYSTEM CONFIGURATION

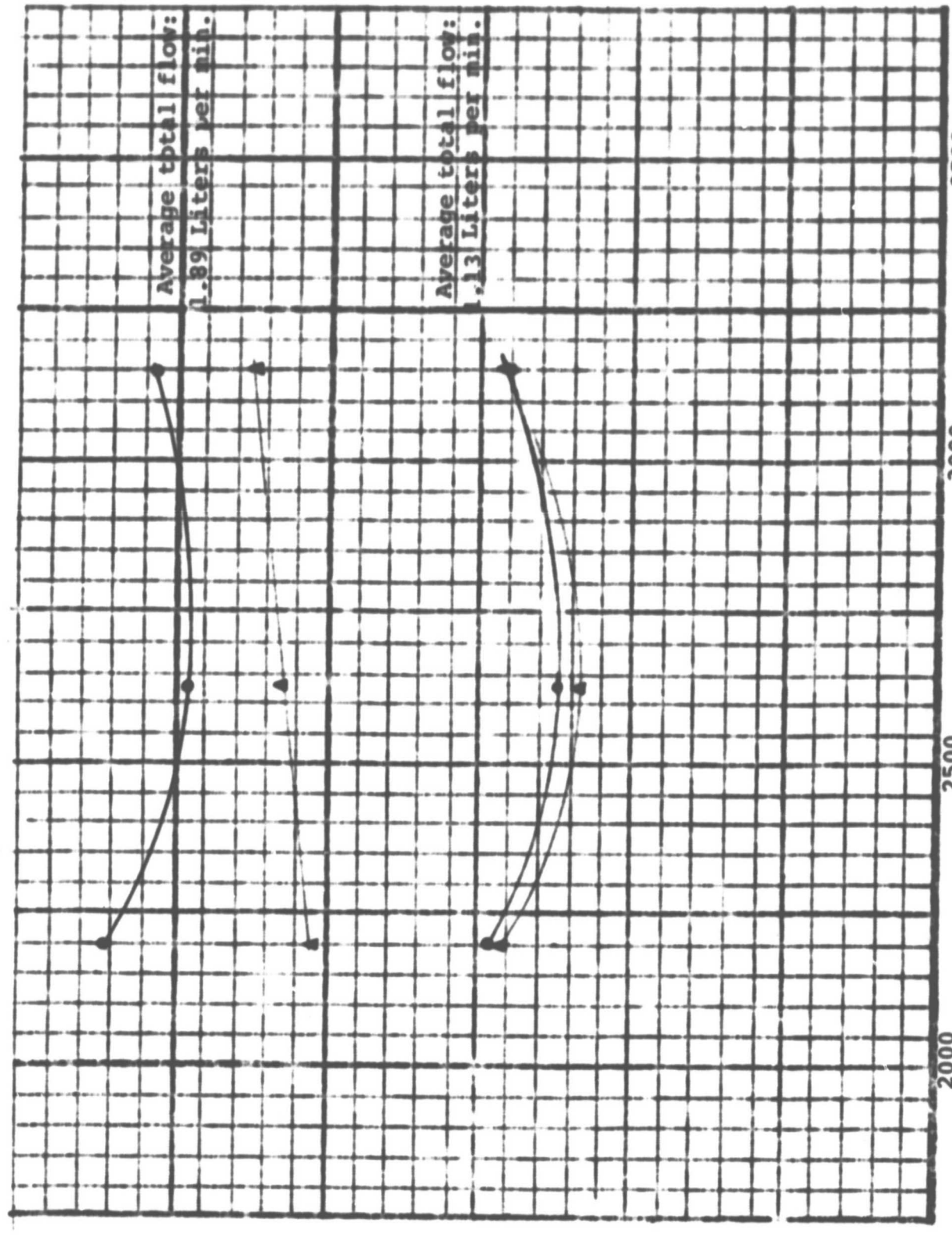

ORIGINAL PAGE IS
OF POOR QUALITY

Testing was resumed using two new VAC-1 bearings at light loads, 871 N (196 lbf) radial and 3247 N (730 lbf) axial. Since the completion of test 7, larger drain holes had been added to the test hardware and the scavenge system had been improved to allow the use of increased lubricant flow rates. For this test run, the lubricant supply was increased to 1.1 ℓ/min. (0.3 gpm) through each source, i.e. jets and through shaft, for each test bearing. Testing proceeded to 3665 rad/s (35,000 rpm) without incident. At that level, fluctuations were noted in the generated audible noise level as well as in the apparent magnitude of the axial load. After 10 minutes of operation, the cage in the outboard bearing failed. This was the first time that a cage failure had been experienced in the program. Given the condition of the retainer, one missing rib and three others severely cracked, it was suspected that this might have resulted from a material or heat treatment deficiency. However, this could not be verified by metallurgical analysis.

The test system was again reassembeld using two used VAC-1 bearings that had remained in satisfactory condition. Testing was conducted at the 60% load using lubricant flow rates of 0.8 ℓ/min. (0.2 gpm) through the jets and 1.1 ℓ/min (0.3 gpm) through the shaft for each test bearing. This time the inboard bearing suffered a flange roller end failure after 60 minutes of operation at 3141 rad/s (30,000 rpm). Photographs of the failure mode, which is typical of that experienced in the early tests, are shown in Figure 7. However, it can also be seen that the race contact patterns on this bearing were not centered and were distorted. This condition would not be expected to occur considering the applied loading conditions.

The results of the testing conducted up to this time strongly suggested that the tolerance ranges utilized for commercial automotive wheel bearings were not sufficient to sustain continued high speed operation. Testing was thus suspended on the domestic commercial bearings.

5.4 Imported Bearing Performance Tests

Sometime earlier it had been discovered that the German SKF company manufactured a line of increased precision tapered roller bearings for automotive pinion applications. Since the M88000 series was included in this line, a sample had been obtained and modified to the VAC-1 design. The experimental evaluation of these M88000 VAC-2 bearings was now undertaken as summarized in Table 8.

Figure 7

Typical Failure Mode as Seen on Test Bearing #9

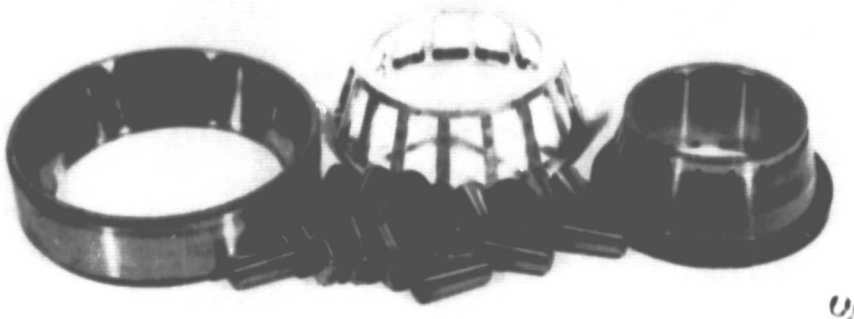

Overall View of Bearing: Severe Heat Discoloration
and Smearing on Roll Ends and Flange
(Note Offset Load Pattern on Cup and Cone Races)

Smeared Roller Ends

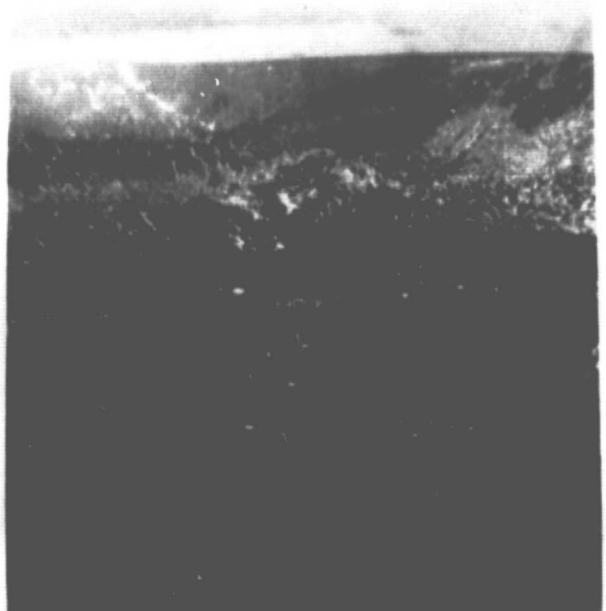

Heavily Smeared Flange Surface

TABLE 8

Summary of Imported Bearing Performance Tests

Run Number	Loading Condition	Bearing Type	Bearing Numbers Inboard	Bearing Numbers Outboard	Max. Speed Achieved (Rad/s)	Time at Max. Speed (Min.)	Total Lubricant Flow/Brg. (ℓ/min.)	Result
10	60%	New VAC-2	12	11	4188	30	3.0	Test Completed
11	100%	New VAC-2	14	13	4188	75	3.2	Test Completed
12	150%	New VAC-2	16	15	3403	15	3.2	Inboard Brg. (#16) Failed Roll/End Flange Smearing
13	150%	New-Used VAC-2	17	15	3141	15	3.2	Terminated After Check of Scavenge Flow Balance
-	Switched Lubricants to Santotrac 50							
14	100%	Used VAC-2	17	15	4188	60	3.2	Test Completed

Run 10 was completed at the 60% load level using the first two new VAC-2 bearings. MIL-L-23699 lubricant was originally supplied to each bearing at a rate of 0.8 ℓ/min. (0.2 gpm) through the jets and 1.1 ℓ/min. (0.3 gpm) through the shaft. During the run, the former flow rate was increased to 1.1 ℓ/min. (0.3 gpm) and the latter to 1.9 ℓ/min. (0.5 gpm) to minimize bearing operating temperatures and provide maximum lubricant films on the critical surfaces. Step speed testing continued until 30 minutes of operation were successfully accumulated at 4188 rad/s (40,000 rpm). During the conduct of this test sequence, it was obvious that the noise and vibration levels generated by these bearings were much improved over that of the previous test lot. Post test examination of the bearing components established that all of the contact surfaces remained in excellent condition. In fact, it was difficult to discern any visible signs of contact even using magnifications as great as 30X. The post test condition of one of these bearings is illustrated in Figure 8.

Run 11 was subsequently run under 100% load conditions using two new VAC-2 bearings. Initially, lubricant flows were maintained at the levels used in Run 10 and then slightly increased during the test to 3.2 ℓ/min. (0.85 gpm) per bearing. Again the maximum speed of 4188 rad/s was successfully achieved in two separate test sequences and a total of 75 minutes of operation were accumulated at that level. Once again the bearing components remained in excellent shape as illustrated in the photographs contained in Figure 9.

Run 12 was completed using two new VAC-2 bearings under the 150% loading conditions. These bearings, as well as all of the remaining bearings used in the program, contained used cages which had been stripped and replated with silver. Lubricant flow rates were maintained at previously utilized levels. This time the inboard bearing suffered a flange roller end failure after 15 minutes of operation at 3403 rad/s (32,500 rpm). The condition of this bearing is shown in Figure 10.

Throughout Run 12 this inboard bearing had been running slightly hotter, ~4°C, than the outboard bearing. While this difference is not highly significant, it and the failure occurrence again raised doubts about the flow balance through the shaft. It is recalled from the data shown in Figure 6 that there was an apparent relationship between total flow rate and flow balance. Since the last flow balancing process, the total shaft flow rate had been increased from 1.9 ℓ/min. to 3.8 ℓ/min. to minimize bearing operating temperatures.

Figure 8

Post Test Condition of Test Bearing #11 Run For 30 Minutes at 60% Load and 4188 rad/s

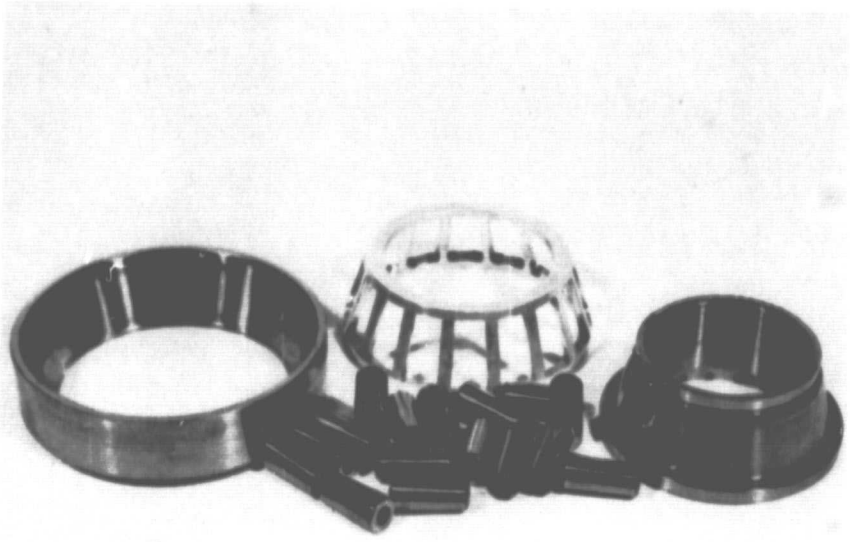

Overall View of Bearing

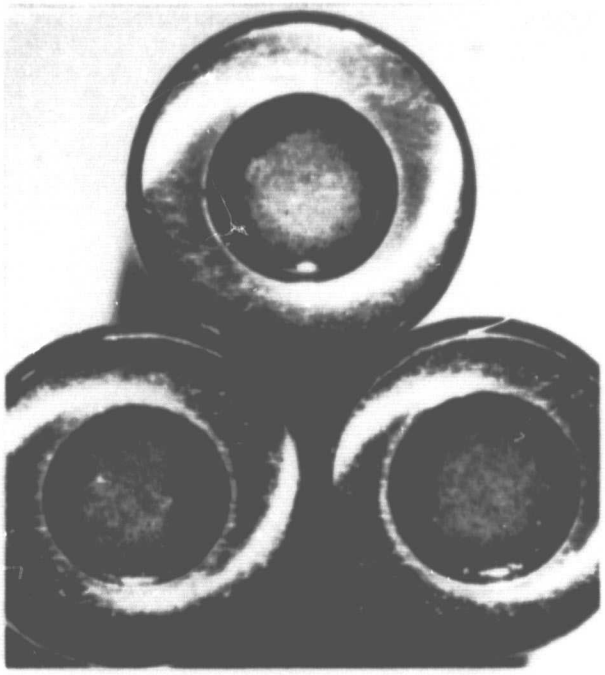

Typical Roll End Contacts

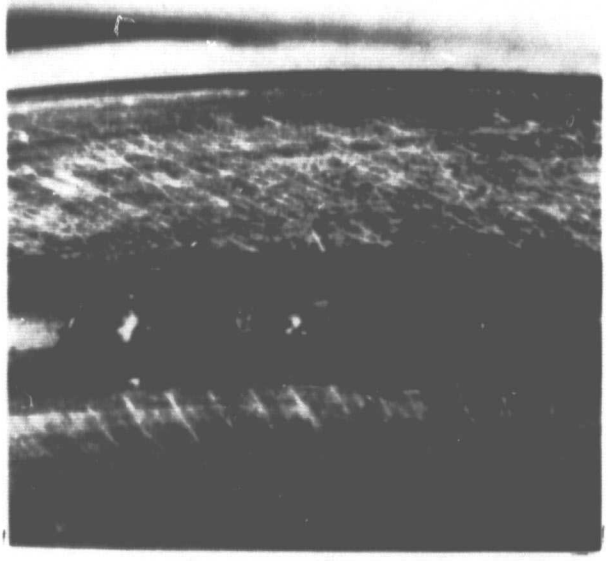

Flange Contacts

Figure 9

Post Test Condition of Test Bearing #13 Run for 75 Minutes at 100% Load and 4188 rad/s

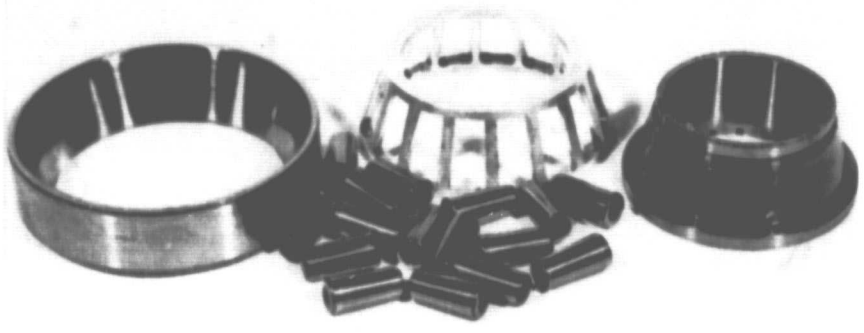

Overall View of Bearing

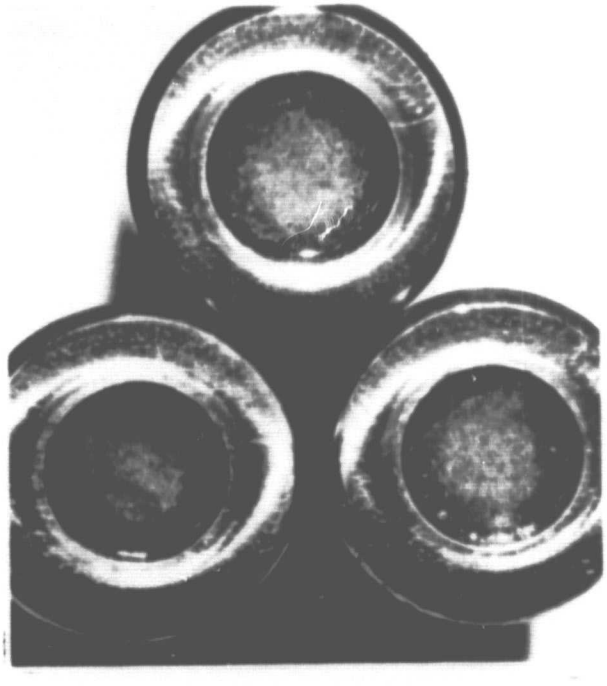

Typical Roll End Contacts

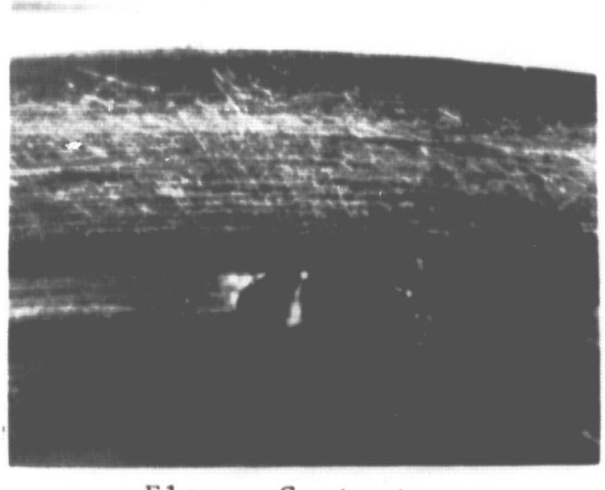

Flange Contact

Figure 10

Failure of Test Bearing #16 Run for 15 Minutes
at 150% Load and 3403 rad/s

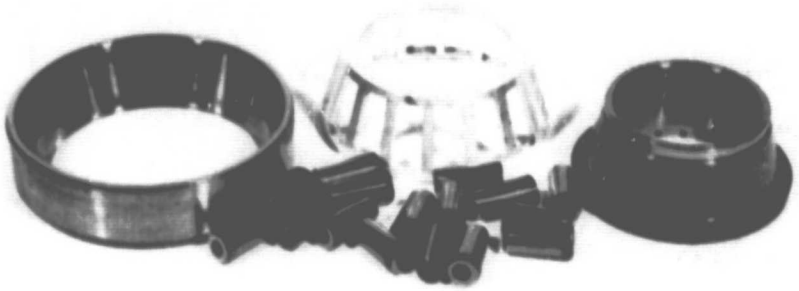

Overall View of Bearing

Smeared Roll End Contacts

Smeared Flange Contact

A rough check on the existing balance was obtained by monitoring the scavenge rates from both ends of the test chamber. The rig was reassembled with one new and one used VAC-2 bearings and the step speed test was repeated using the conditions of Run 12. Fifteen minutes of successful operation were achieved at a speed of 3141 rad/s (30,000 rpm) while the flow balance measurements were made. These checks illustrated that most of the increased flow was going to the outboard bearing while the flow rate to the inboard bearing had remained essentially unchanged. The hole at the end of the tube was again slightly increased in size to improve the flow distribution.

Before a total flow balance could be achieved, a technical redirection changed the test lubricant from MIL-L-23699 synthetic turbine engine lubricant to Santotrac 50, a synthetic fluid developed for its traction capabilities. After cleaning out the lubrication system and changing the fluids, a step speed test was repeated at the 100% load condition to evaluate the new test lubricant. Run 14 was conducted using the bearings that had been on the rig for Run 13 and previously established lubricant flow rates. Once again 60 minutes of successful operation were achieved at maximum speed, 4188 rad/s, without difficulty and the bearings remained in excellent condition. The measurement of scavenge flows indicated that a significant flow imbalance still existed at the maximum speed condition with the outboard bearing receiving approximately twice as much lubricant as the inboard bearing. However, given the overall success of the two runs conducted at the 100% load level and considering the existing time constraints on the program, it was decided to overlook this problem, and to proceed with the long term test run.

5.5 Extended Duration Test Runs

The extended duration test sequence was conducted with the objective of achieving 50 hours of operation at the maximum speed level of 4188 rad/s (40,000 rpm) under a 100% nominal load, i.e. 3.2 kN (723 lbf) radial and 6.6 kN (1483 lbf) axial per bearing. Lubricant flow rates were maintained as before, i.e. average rate per bearing of 1.1 ℓ/min. (0.3 gpm) delivered through the jets and 2.2 ℓ/min. (0.6 gpm) supplied through the shaft. This test utilized those bearings previously tested in Runs 13 and 14 while the outboard bearing had additionally been used in Run 12.

The test was composed of a series of day long runs conducted following the procedure outlined in Section 5.1. The running time accumulated prior to reaching the maximum test conditions was not considered as a portion of the actual test.

A summary of the seven completed test sequences is shown in Table 9 while the data collected are contained in Appendix C.

The initial test hours were accumulated without incident. Then on the second day, after approximately 6 hours of running time had been accumulated, testing was interrupted by a load bearing failure. After repairing the shaft and replacing the cylindrical bearing, testing was resumed. A check of the operating parameters after test resumption indicated that there had been no significant change from those existing prior to the failure. Testing was therefore allowed to continue. No further incidents were experienced for an additional 23 hours. At that time, problems with the computer monitoring system precipitated a number of unexplained rig shutdowns. This problem was subsequently corrected and testing was again resumed in a normal fashion. After approximately 2 more hours of uneventful operation, the line supplying lubricant to the inside of the shaft, i.e. to the flange roller end interfaces of the test bearings, failed. Although the test control computer shut the power off to the rig as soon as the cup temperatures increased, the thermal lag in the bearing systems and the tester inertia resulted in the two test bearings being damaged. A total operating time of 31.1 hours had been accumulated prior to the failure.

The post test inspection of the bearings found evidence of severe wear, smearing, and heat discoloration on the roller end flange contact surfaces of the outboard bearing. This damage had subsequently precipitated a failure of the cage and the ultimate destruction of the bearing components. The inboard bearing was not damaged to the same degree; the flanges and roller ends showed evidence of slight smearing and wear, but the contacts had not yet turned blue. The conditions of both bearings are illustrated in Figures 11 and 12.

In addition, the visual examination of the inboard bearing cone disclosed a pattern of short cross groove marks at approximately the center of the race surface. Higher magnification study of these indications conducted using the scanning electron microscope established that these were skid marks, most likely produced at the time of failure. An SEM photomicrograph of one

TABLE 9

Summary of Extended Duration Test Runs

Bearings: Used VAC-2 (#17 and 15)
Lubricant: Santotrac 50
Load: 100% (3.2 kN Radial, 6.6 kN Axial)
Speed: 4188 Rad/s

Run #	Lubricant Flow/Brg. (ℓ/Min.)	Lubricant Supply Temp. (K)	Outer Ring Operating Temp. (K)		Running Time (Hrs.)	
			Inboard	Outboard	This Run	Total
E1	3.3	-	-	-	4.9	4.9
E2					1.3	6.2
	Load Bearing Failure; Arbor Repaired					
E3	3.3	371	405	395	5.5	11.7
E4	3.3	365	401	395	6.0	17.7
E5	3.3	359	398	394	6.0	23.7
E6	3.3	369	407	404	6.2	29.9
E7	3.3	365	398	393	1.2	31.1
	Through Shaft Lubricant Supply Line Failed Outboard Brg. (#15) Seized					

Figure 11

Failed Test Bearing #15 After 31 Hours of Operation at 100% Load and 4188 rad/s

Overall View of Bearing

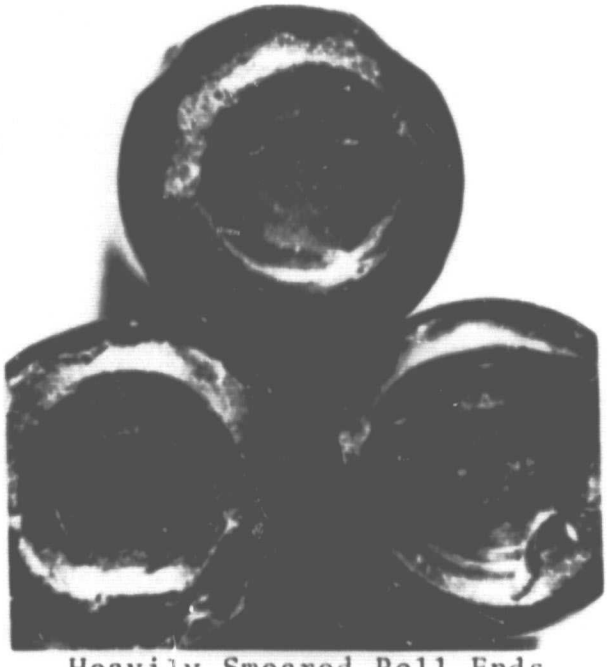

Heavily Smeared Roll Ends

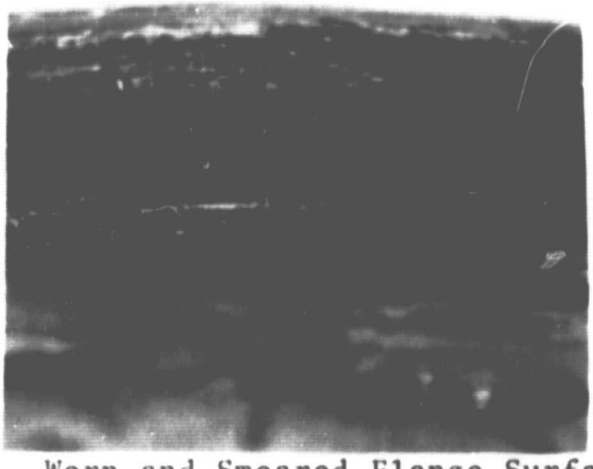

Worn and Smeared Flange Surface

Figure 12 AT81T014

Failed Test Bearing #17 After 31 Hours of Operation
at 100% Load and 4188 rad/s

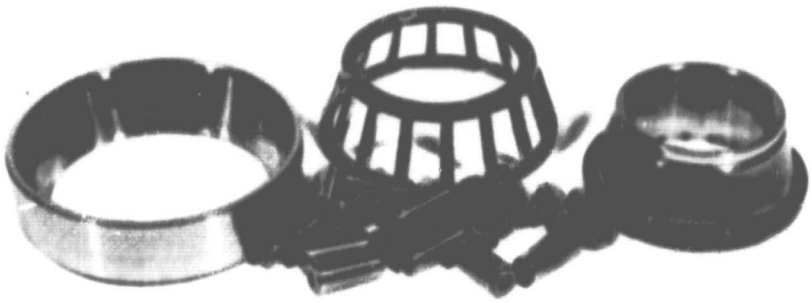

Overall View of Bearing

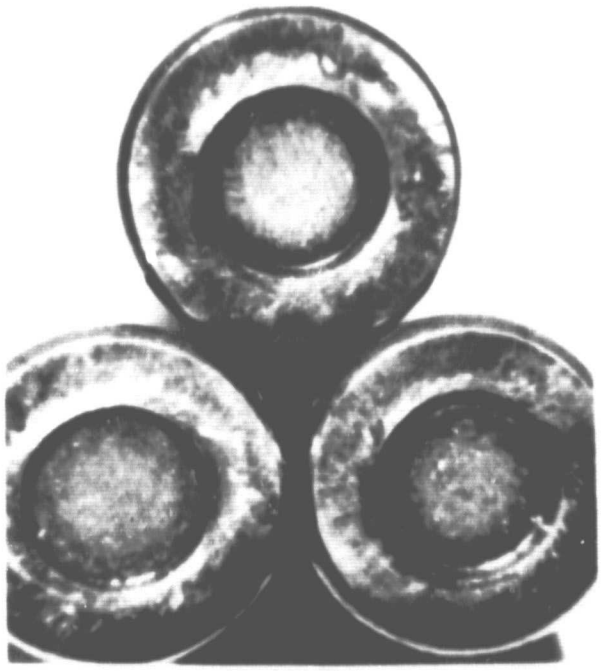

Lightly Smeared Roll Ends

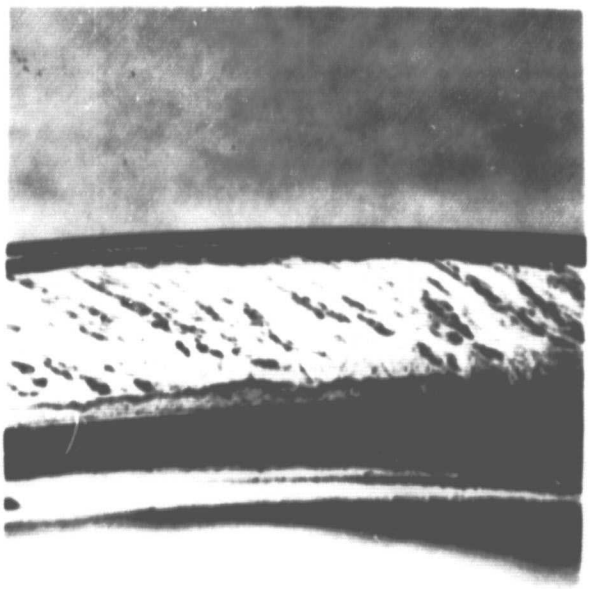

Smeared Flange Surface

of these marks is contained in Figure 13. It was also noted during this examination that the cone race had a frosted appearance which is normally associated with the existence of an inadequate lubrication condition. SEM examination of the surface subsequently confirmed that the race was covered with an extensive pattern of microspalling as would be expected if the lubricant film had been inadequate. A photomicrograph of this condition is also shown in Figure 13. The experimental program was terminated at this point.

Figure 13

Scanning Electron Photomicrographs of Features Seen on Test Bearing #17

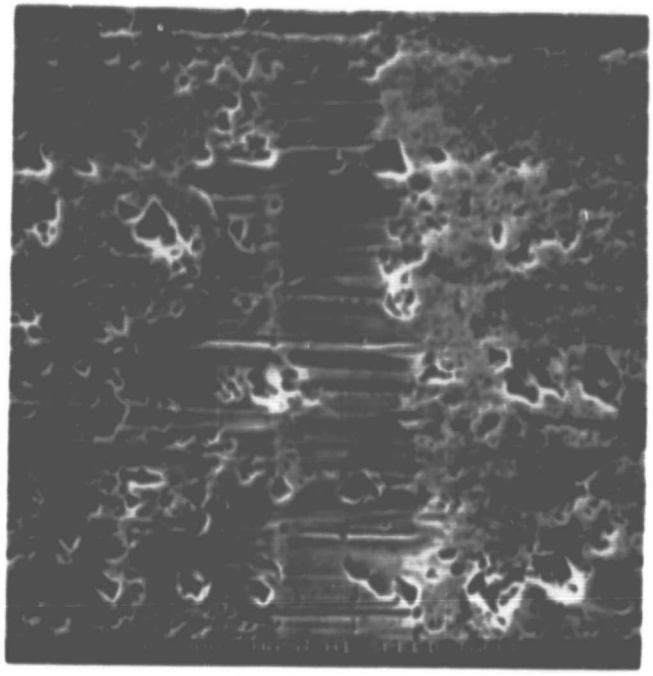

Skid Mark on Cone Race (1000X)

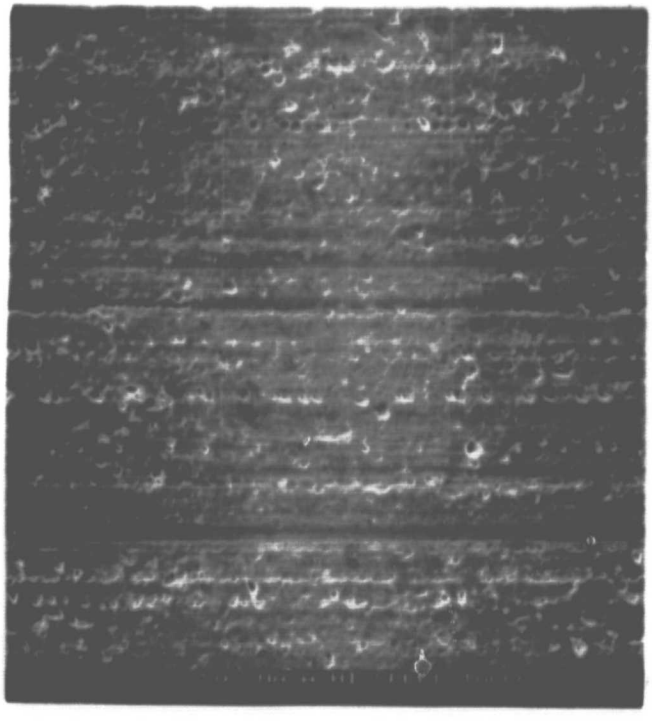

Microspalling Patterns on Cone Race (250X)

6. Discussion of Results

6.1 Primary Analytical Results

The preliminary load support system analyses which used pairs of commercially available bearings; the M88000 and LM67000 series, demonstrated that neither bearing type provided a completely satisfactory design with respect to the constraints on bearing rating life and available housing space. The M88000 series bearing, the larger of the two, was judged to be the best suited candidate since it afforded acceptable bearing rating life, although it was too large for the available space.

The first effort to define an optimal shaft configuration using a pair of M88000 series tapered roller bearings revealed that straddle arrangements are preferable to cantilever arrangements. The straddle configuration consistantly yielded larger L_{10} lives for the same system mass.

Additionally it was noted that the capacity, and therefore the size, of the bearing not opposing the applied thrust load could be reduced. The L_{10} life of this bearing exceeds the accepted value, 2500 hours at 60% NGL, with the proper adjustment of the preload.

The subsequent analytical effort, directed at selecting an optimum straddle design, used an M88000 bearing to carry the applied thrust load and a smaller taper for preload purposes. Two (2) bearing types, LM11700 and LM67000, were considered for this location with the former being selected through parametric studies. This shaft configuration was found to perform within the design constraints, provided that a higher than specified lubricant flow rate is supplied to the small LM11700 bearing to enable sufficient heat removal. A value of 3.4 ℓ/min. (0.9 gpm) is recommended. Also it is necessary to maintain sufficient bearing spacing and a value of 65 mm (bearing center-center) is suggested.

The final portion of the analytical activity evaluated more customary designs for the input pinion support system. These arrangements employed a cylindrical roller bearing at one end of the shaft and a stack of angular contact ball bearings at the other. Four specific configurations were evaluated.

Ultimately an optimal candidate; a straddle arrangement with a thrust carrying cylindrical bearing opposed by a pair of angular contact ball bearings, was selected. This configuration was analyzed to quantify the effects of preload, fits, lubricant flow rate load distribution and percent gear load on bearing fatigue lives and gear deformations. It was concluded that for the prescribed load and speed conditions, wherein the thrust carrying capability of the cylindrical roller bearing is used primarily to carry preload, the design exceeds the specified criteria for the application. It is, in fact, slightly superior to the optimal tapered bearing design considering system L_{10} life and gear deflections.

6.2 Primary Experimental Results

The test results demonstrated that the special pinion quality tapered roller bearings which have been modified for high speed operation, can run successfully for extended periods of time at the maximum design conditions of an input pinion shaft for a proposed helicopter transmission. The M88000 VAC-2 bearing repeatably achieved stable operation at speeds of 4188 rad/s (40,000 rpm), a DN level of 1.3×10^6, under loads originally calculated to be 100% of the gear load generated on the most heavily loaded bearing at maximum torque conditions, a bearing C/P level of 6. A total of 33.35 hours of operation were accumulated under these conditions without difficulty prior to the ultimate failure of the bearings. This failure was caused by the fracture of a lubricant supply line, and does not detract from the successful performance of the bearings.

One of the objectives of this effort had been to sustain operation at an overload condition equal to 150% of the generated gear loads. The one attempt which was made to reach these conditions produced a bearing failure. However, it is known that the rate at which lubricant was supplied to the critical roller end flange contacts of the failed bearing, was less than desired during that test run. With an adequate flow of lubricant, this bearing might well have survived without damage as did the companion bearing.

Moreover, it can be noted that the actual test loads utilized in these sequences were excessive when viewed from a practical standpoint. The test load levels were established during an early analytical phase which utilized a symmetrical shaft support system. A substantial portion of the bearing loads seen on a shaft supported by two tapered roller bearings, is internally generated. The use of two M88000 bearings on the pinion shaft results in large internal thrust levels producing relatively high

bearing loads for specified gear loading levels. Subsequent analytical work conducted on a more optimal shaft support system employing a smaller, reduced angle bearing on the end opposite the gear generated thrust direction, produced significantly lower bearing load levels. For example, the equivalent radial load, i.e. that load used for life calculations as defined by Industry Method [17], for the most heavily loaded bearing in the latter case at the 100% gear loading condition, is only 65% of the 100% test level. Assuming that this same trend would exist at the 150% level, it can be seen that the test loads designated as 100% are comparable to those which would most likely exist at the 150% torque condition in a practical transmission. Thus, it is reasonable to consider that the M88000 VAC-2 bearing meets all of the stated performance requirements of the application.

The other major bearing design parameter was fatigue life. The experimental program provides no information as to the ability of the M88000 VAC-2 bearing to achieve this specification since life data were not accumulated in this effort.

Concurrently, the test activity also demonstrated the limitations of the standard tapered roller bearings which are manufactured for current automotive applications. Even when modified to incorporate high speed bearing features, these M88000 VAC and VAC-1 bearings repeatably failed to achieve speeds in excess of 3141 rad/s (30,000 rpm), a DN level of 1.0×10^6, under loads at the 60% level, a bearing C/P of 8. This poor performance was often related to inadequate lubrication, but the trend continued even when lubricant supply rates were used that later yielded successful operation with the pinion quality bearings. In addition, the operation of these bearings at high speeds, i.e. in excess of 2094 rad/s, was accompanied by relatively high noise and vibration levels. The combination of all these factors leads to the conclusion that the overall quality level of these bearings is not sufficient to allow their use in high speed applications.

The data collected during the performance test runs using MIL-L-23699 lubrication were evaluated to determine the effects of operating conditions on performance parameters. Figures 14 and 15 illustrate the variations produced in the temperature differential existing between the lubricant supply and bearing operating temperatures as speed and load are varied. The changes in temperature produced with increasing speed, Figure 14, seem to show a tendency to level off between the speeds of 1000 and 2250 rad/s. While the existence of this band might imply an inherent

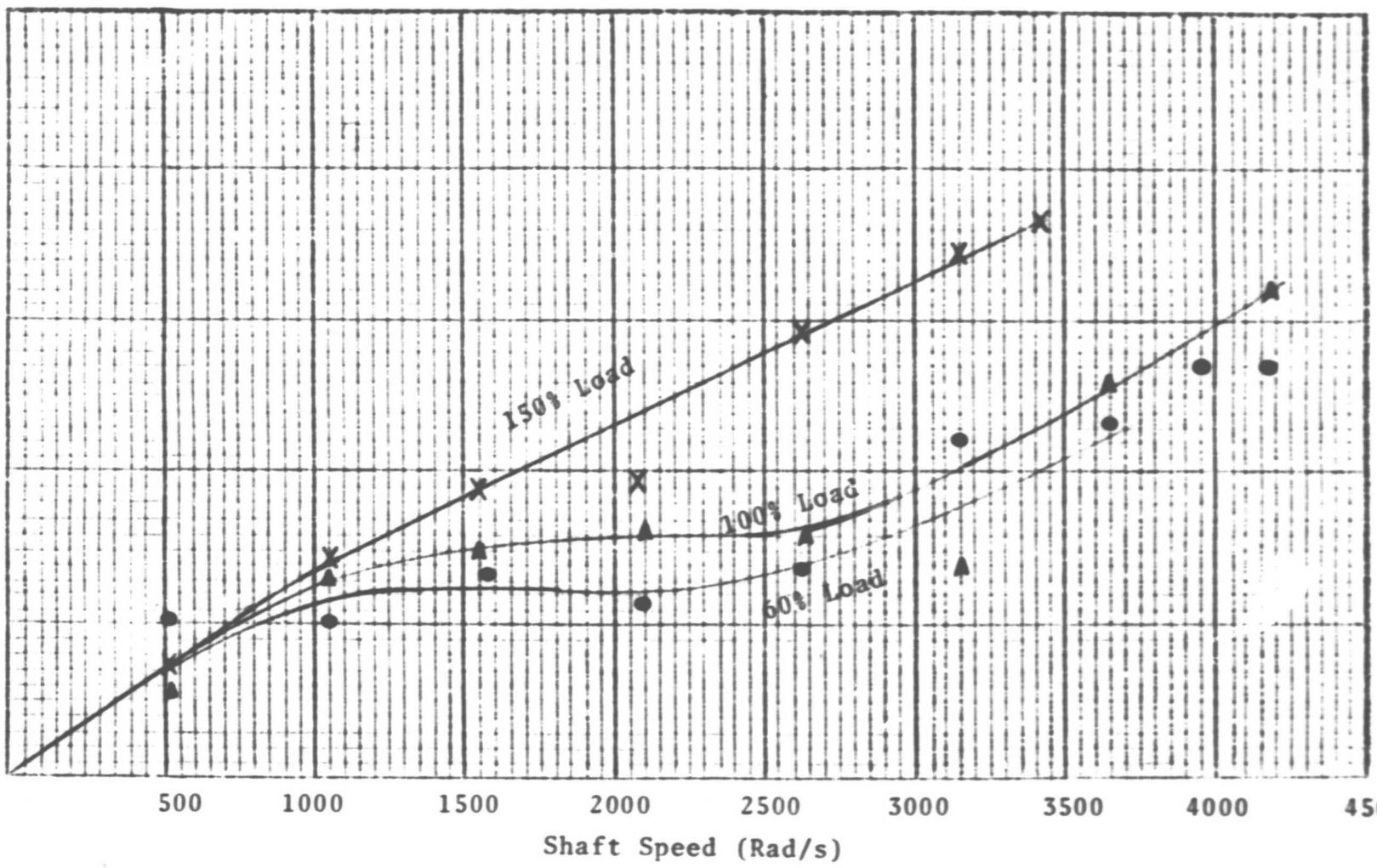

Figure 14

Bearing Operating Temperature Rise
As a Function of Speed

AT81T014

Lubricant-Mil-L-23699
Flow/Brg.-3.2 ℓ/min.
Supply Temp.-370K

Figure 15

AT81T014

Bearing Operating Temperature Rise
As a Function of Applied Load

thermal stability of the assembly at those conditions, the increases experienced above that range are not excessive enough to be of concern. The temperature changes produced by varying load, Figure 15, illustrate a significant increase between the 100% and 150% loading levels. These data would imply that the latter load level is somewhat excessive for the bearing in question operating at these high speeds.

The data from the same runs were also used to approximate the bearing heat generation rates. These calculations only considered the heat rejected into the lubricant and were completed using the following formula:

$$Q = M\ Cp\ \Delta T$$

where

Q = Heat Absorbed by Lubricant

M = Lubricant Mass Flow Rate

Cp = Specific Heat of the Lubricant, and

ΔT = Change in Lubricant Temperature passing through the Test System

The results of the calculations are shown in Figures 16 and 17 as functions of both speed and applied load. The trends illustrated are essentially identical to those seen in the operating temperature data. Once again, a major increase is noted between the 100 and 150% loading conditions. This increase further establishes that the experimental 150% load level is excessive for these bearings. Again it should be recalled that the test loads used are significantly greater than the loads calculated for the optimal tapered bearing shaft configurations. Thus this result does not alter the projection that the M88000 bearing will perform at a 50% overload condition in the application.

During some of the early test runs measurements were taken to determine cage rotational speed. Figure 18 shows a graph of cage speed as a function of shaft speed at test speeds up to 2617 rad/s (25,000 rpm). These data indicate that the ratio between speeds is relatively constant at a value approximately 0.433 over the entire range. The sensitivity of the measuring apparatus was attenuated by speed effects and the silver plating on the cage. As a result at high speeds, the signal level was not sufficient to reliably accumulate cage rotational speed data. Increased signal strength could have been achieved by removing the silver plate from the discontinuities in the cage face and enlarging them. However, this approach was rejected since there was concern about biasing the dynamic balance of the cage. Also

AT81T014

Figure 16

Bearing Heat Generation Rate as a Function of Speed

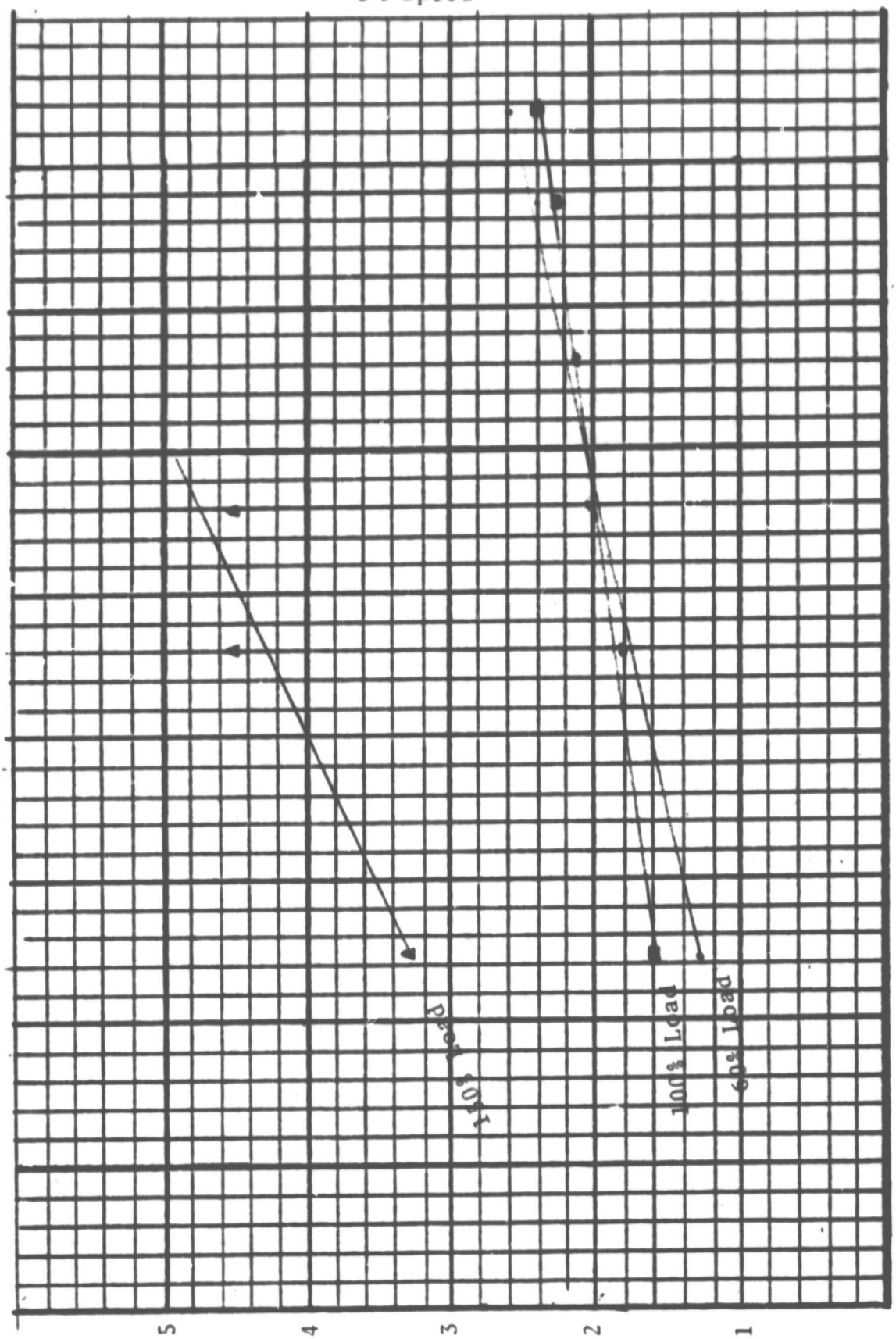

it was known from other tests conducted with larger tapered roller bearings at speeds up to 2.4 x 10^6 DN [18], that the ratio of cage to shaft speeds had remained consistant to within 1%. It would be expected that the same trend would exist in these tests. These measurements were thus discontinued.

A comparison of bearing performance characteristics was also made considering the effects of the two lubricants, i.e. Mil-L-23699 and Santotrac 50. Figure 19 compares the bearing operating temperature rise for the step speed runs made with each lubricant under 100% load. This illustrates that at speeds in excess of 2500 rad/s bearing operating temperatures are somewhat higher with the traction fluid. The maximum variation noted was a 17% increase experienced at the maximum operating speed of 4188 rad/s. The experimental heat generation rates for these runs are shown in Figure 20. These curves illustrate that below speeds of 3500 rad/s (33,700 rpm) the traction fluid produces a lower heat generation rate than does the Mil-L-23699 lubricant. However, above that speed the trend reverses and the heat generation rate achieved with the traction fluid appears to increase quite rapidly. At the maximum speed condition the difference in these two values is 25% of the lower value.

At the conclusion of the extended duration run, it was observed that the race surface of the inboard cone contained a visible degree of lubrication distress. This was comprised of an extensive pattern of microspalling, visible only using the SEM, that produced the classical "frosted" appearance during optical examination. The existance of this condition would be expected to precipitate premature spalling failures in the application not allowing the full fatigue potential of the bearings to be realized. The calculated EHD film parameters, Λ, at the inner ring-roller contacts for this application are only 1.3 at 60% load and 1.0 at 100% load. These are definitely in the range, i.e. $\Lambda < 2$, where lubrication distress would be expected to occur. It would thus seem obvious that if the specified fatigue life of the shaft support bearings is to be realized, the viscosity of the lubricating fluid must be increased, the operating temperature of the transmission must be reduced or a combination of the two achieved to provide a more satisfactory lubricating condition.

Figure 17

AT81T014

Bearing Heat Generation Rate as A Function of Load

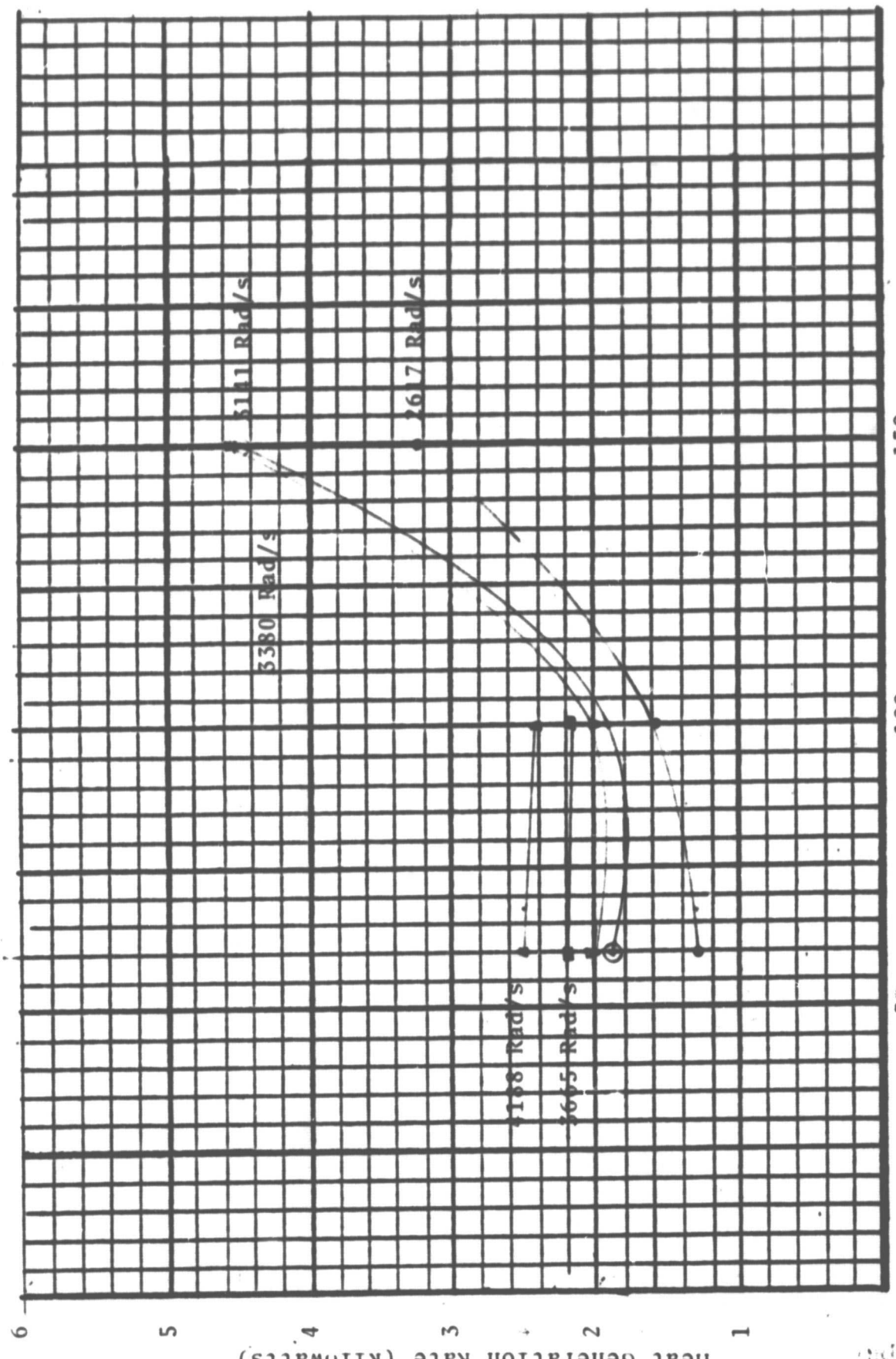

Figure 18

Bearing Cage Speed as a Function of Shaft Speed

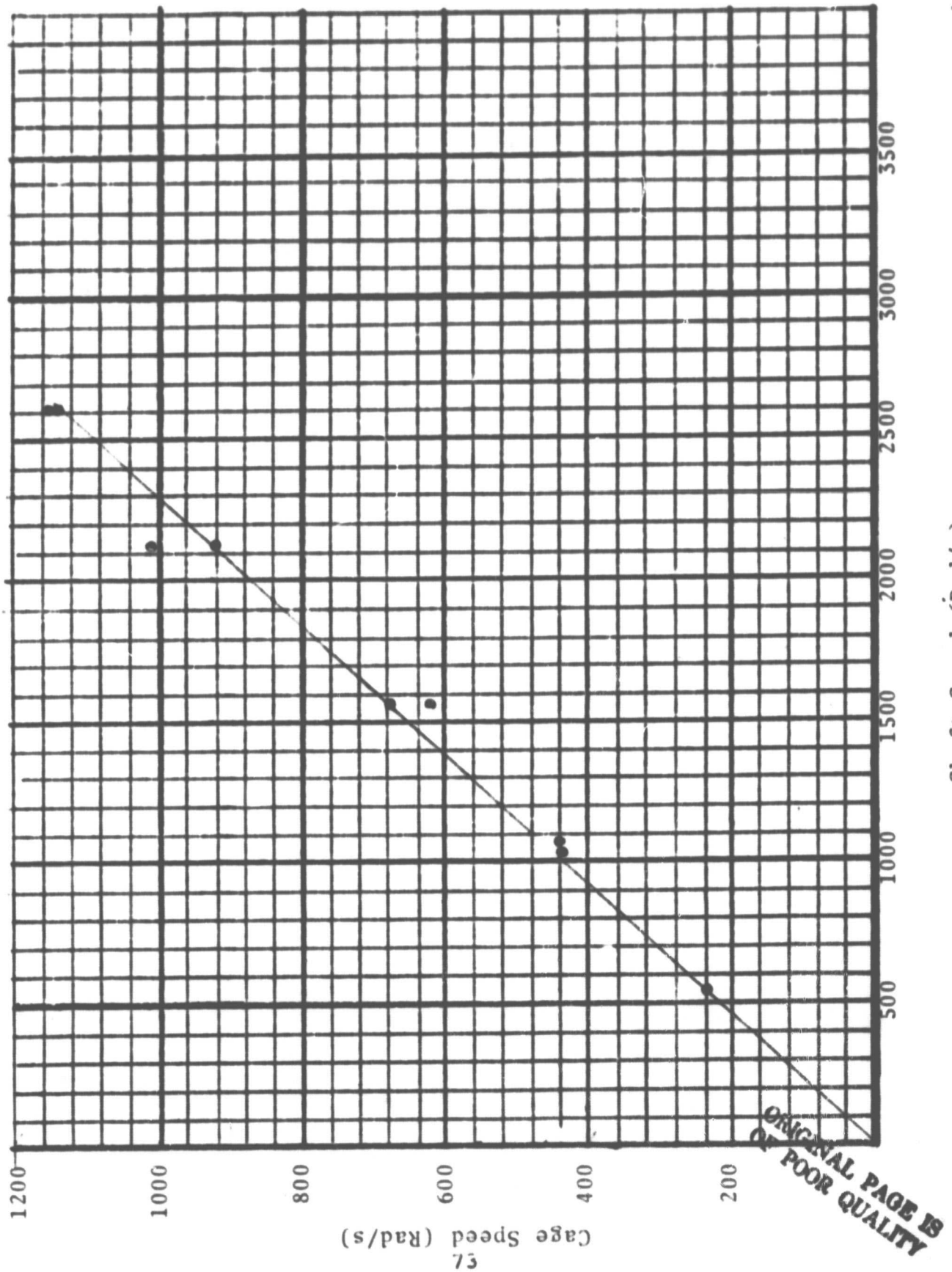

AT81T014

Figure 19

Bearing Operating Temperature Rise With Two Lubricant Types

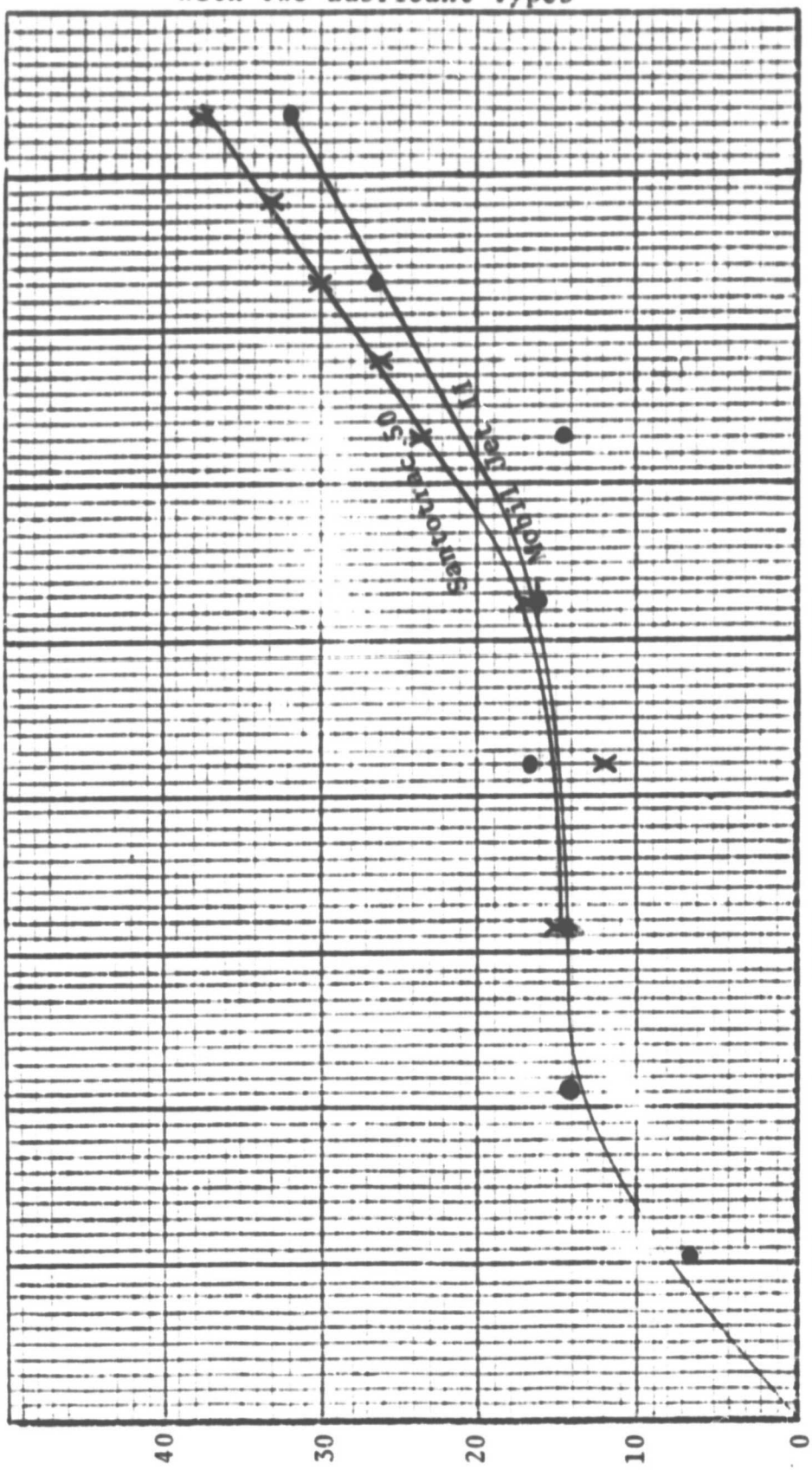

Figure 20

AT81T014

Bearing Heat Generation Rates With
Different Lubricants

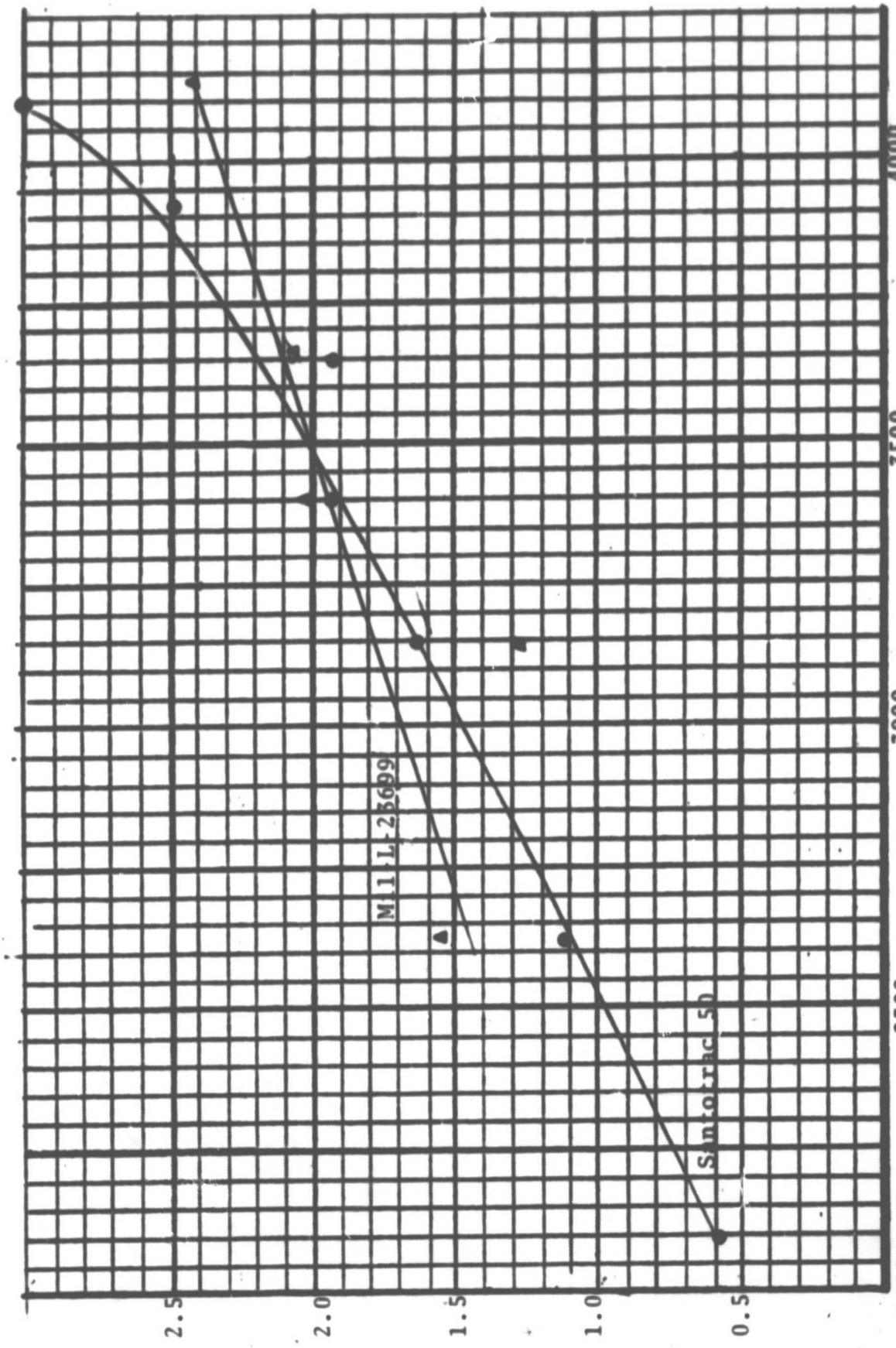

7. Conclusions

1. Thermomechanical system analyses have demonstrated that simplified support systems employing tapered roller bearings can be successfully used on the spiral bevel input pinion shaft of a proposed commercial helicopter transmission. Due to a reduction in the number of components required, these alternative bearing configurations offer potential for reductions in system cost and weight as well as improvements in system reliability and maintainability.

2. The optimized tapered roller bearing shaft support system utilizes a straddle configuration with a M88000 series bearing in the load carrying position and an LM117000 series bearing in the preload position. Theoretically, this configuration exceeds the design requirements for bearing life and shaft stiffness established for the application. However, these results were achieved by altering some of the original transmission design constraints; namely by increasing the allowable outer diameter of the load carrying bearing, extending the length of the pinion shaft, and increasing the lubricant flow requirements to the bearings.

3. Experimental results demonstrated that an automotive pinion quality M88000 tapered roller bearing modified for high speed operation can successfully operate under the maximum load and speed conditions anticipated in the transmission. Furthermore, it is probable that this good performance was achieved under loads equivalent to a 150% overload condition using the optimized tapered bearing shaft configuration.

4. Successful long term operation was also achieved with the same tapered roller bearing at maximum design conditions for an extended test period in excess of 30 hours. This result establishes the long term performance potential of the bearing although it is insufficient to insure that the fatigue potential of the bearing can be realized.

5. The experimental evidence supports the theoretical concern about the inadequacy of the elastohydrodynamic lubricant films in the bearing. Extensive microspalling, probably caused by inadequate lubrication, was noted on the race surfaces at the conclusion of the extended

duration test. This condition would be expected to precipitate the premature spalling failure of the bearing rings if uncorrected.

6. Theoretically, the shaft support configuration incorporating the thrust carrying cylindrical roller bearing as a preload bearing offers performance advantages over the optimized tapered roller bearing system in this application. However, this is a three bearing system rather than the two bearing configuration provided with the tapered roller bearings. Furthermore, more experimental experience is required with this novel bearing design before it could be recommended for use in this helicopter transmission.

8. Recommendations

Both the analytical and experimental portions of this program have indicated that tapered roller bearings have the basic capabilities required for use on the input pinion shaft of the proposed helicopter transmission. The use of these bearings offers a number of advantages over current systems, i.e. reduced cost and weight, improved maintainability, etc. so it would be recommended that the further development of this shaft support system be pursued.

There are a number of activities currently seen as necessary in this continued development process. The first is the continued optimization of the tapered shaft design. It was not possible to address all of the potential dimensional variations in the analysis completed in this program. Concurrently, it was also indicated that parameters other than those examined could have a dramatic effect on overall system performance. For example, it was seen that varying the distance between the gear and the primary load carrying bearing even when holding the bearing spacing constant, would produce changes in the performance of the straddle configuration. The optimization of this and other variations should be addressed in further analytical evaluations.

In addition, the current project demonstrated that two potential lubricant related problem areas exist. The first of these is achieving sufficient lubricant flow rates directed to the proper areas, i.e. races and flange, to provide the necessary cooling of the bearing components. Secondly, it is seen that the lubricant film thicknesses generated within the bearings are inadequate for the reliable protection of the contact surfaces. These factors should be studied in a combined analytical-experimental effort aimed at optimizing the lubricant flow parameters and achieving satisfactory fluid films in the bearings.

Once these investigations have been successfully completed, the results can be utilized to construct an optimal tapered roller bearing supported input pinion shaft system. This assembly should then be subjected to a series of experimental evaluations in a full scale transmission to verify the performance of the bearings in the actual application.

The analytical results also established the potential of a thrust carrying cylindrical roller bearing for use in this helicopter transmission. A thrust carrying cylindrical roller bearing offers advantages in high speed applications since the magnitude of the flange loads are not affected by the magnitude of the applied radial loads or the magnitude of the centrifugal forces as they are in a tapered roller bearing. While this program only considered the thrust carrying cylindrical as a

preload bearing not carrying axial load at operating conditions, past work has demonstrated, both analytically and experimentally, that this novel bearing design can be employed as the primary load carrying bearing on the input pinion shaft of a current generation helicopter transmission [5]. It would be recommended, therefore, that this design be analytically evaluated in the load carrying position on the current input pinion shaft. If the results of this preliminary evaluation are again positive, a combined analytical-experimental program should be undertaken to optimize the shaft support system, and to verify the performance of the bearing under anticipated transmission operating conditions in a test stand environment.

9. References

1. Ferris, H., "Safety Considerations for Helicopter Drive Systems of the 1980's" American Helicopter Society, Preprint HPS-11, November, 1979.

2. Lenski, J. W. Jr., and Mack, J. C., "Drive System Development for the 1980's" American Helicopter Society, Preprint HPS-9, November, 1979.

3. FitzGerald, P. C. and Gardner, G. F., "Advanced Transmission Component Development and Test Program", American Helicopter Society, Preprint HPS-8, November, 1979.

4. Battles, R. A., "Development of Helicopter Transmission Components for the 1980's" American Helicopter Society, Preprint HPS-10, November,1979.

5. Morrison, F. R., Pirvics, J. and Crecelius, W. J., "A Functional Evaluation of a Thrust Carrying Cylindrical Roller Bearing Design", ASME Transactions, Journal of Lubrication Technology, Vol. 101, No. 2, April, 1979, pp 164-169.

6. ANSI/AFBMA Standard 11-1978, "Load Ratings and Fatigue Life for Roller Bearings", 1978.

7. Lemanski, A. J., Lenski, J. W., Jr., Drago, R. J., "Design Fabrication, Test and Evaluation of Spiral Bevel Support Bearings (Tapered Roller), USAAMRDL Technical Report 73-16, Eustis Directorate, U. S. Army Air Mobility Research and Development Laboratory, June, 1973 AD769064.

8. Archard, J. F. and Cowking, E. W., "Elastohydrodynamic Lubrication at Point Contacts", Paper 3, Proc. of Inst. of Mech. Eng., Vol. 180, 1965-1966, pp 47-56.

9. Cheng, H. S., "A Numerical Solution of Elastohydrodynamic Film Thickness in an Elliptical Contact", Journal of Lubrication Technology, ASME Trans., Vol. 92, No. 1, January, 1970, pp 155-162.

10. Connors, T. F., and Morrison, F. R., "Feasibility of Tapered Roller Bearings for Main-Shaft Engine Applications," USAAMRDL Technical Report 73-46, Eustis Directorate, U.S. Army Air Mobility Research and Development Laboratory, August, 1973.

11. Orvos, P. S., and Dressler, G. J., "Tapered Roller Bearing Development for Aircraft Turbine Engines", AFAPL-TR-79-2007, U. S. Air Force Aero Propulsion Laboratory, Wright Patterson Air Force Base, March, 1979.

12. Rosenlieb, J. W., Martinie, H. M., Maurer, R. E., "Feasibility of Induction Skin Hardened Tapered Roller Bearings for Engine Main Shaft and Transmission Pinion Applications," USAAMRDL Technical Report 74-90, Eustis Directorate, U. S. Army Air Mobility Research and Development Laboratory, July, 1974.

13. Crecelius, W. J., and Pirvics, J., "SHABERTH, A Computer Program for the Analysis of the Steady State and Transient Thermal Performance of Shaft Bearing Systems," AFAPL-TR-76-90, U. S. Air Force Aero Propulsion Laboratory, Wright Patterson Air Force Base, October, 1976.

14. Morrison, F. R., McCool, J. I., and Ninos, N. J., "M50 Steel Bearing Material Factors for Rolling Element Life Calculations - Phase II", AVRADCOM TR79-48, U. S. Army Aviation Research and Development Command, August, 1979.

15. Gassel, S. S., "Development of Small Bore, High Speed Tapered Roller Bearing; Task I - Bearing-Shaft System Analysis", SKF Report AL79P001, National Aeronautics and Space Administration, Lewis Research Laboratories, Contract NAS3-20839, January, 1979.

16. Gassel, S. S. and Pirvics, J., "Load Support System Analysis; High Speed Input Pinion Configuration", ASME Transactions, Journal of Lubrication Technology, Vol. 102, No. 1, January, 1980, pp 97-106.

17. Tyson Tapered Roller Bearing Catalog, SKF Industries, Inc. Philadelphia PA, 1978.

18. Parker, R. J., Pinel, S. I. and Signer, H. R., "Performance of Computer Optimized Tapered Roller Bearings to 2.4 Million DN". ASME Transactions, Journal of Lubrication Technology, Vol. 103, No. 1, January 1981, pp 13-20.

APPENDIX 1
BEARING-SHAFT SYSTEM ANALYSIS

RESEARCH REPORT
DEVELOPMENT OF A SMALL BORE, HIGH SPEED TAPERED ROLLER BEARING
TASK I - BEARING-SHAFT SYSTEM ANALYSIS

JANUARY 1979

Stuart S. Gassel

Contract No. NAS3-20839

SKF Report No. AL79P001

Submitted to:

NASA LEWIS RESEARCH CENTER
21000 BROOKPARK ROAD
CLEVELAND, OH 44135

Submitted by:

SKF INDUSTRIES, INC.
TECHNOLOGY SERVICES DIVISION
1100 FIRST AVENUE
KING OF PRUSSIA, PA 19406

TABLE OF CONTENTS

LIST OF TABLES

LIST OF FIGURES

DEVELOPMENT OF A SMALL BORE, HIGH SPEED TAPERED ROLLER BEARING

BEARING-SHAFT SYSTEM ANALYSIS

INTRODUCTION

Advances in helicopter transmission design are obtained by the successful maximization of power transmitted through hardware of minimum volume and mass. As the volume of the design envelope decreases, higher speeds and loads are imposed on components of the system. With the higher power densities processed by material volumes of lower mass content, reliable and predictable performance of components within the system becomes crucial.

Several modules in existing transmissions, the planetary reduction set and the input pinion for example, have to be redesigned to achieve performance advances for the complete system. The most critical is the input pinion which serves as the first link between the high speed power plant input and the low speed mast rotor output.

Input pinions have been designed customarily as load support systems where a shaft is supported by a series of rolling element bearings which in turn straddle a central gear. Typically, a cylindrical rolling element bearing is located at one end of the shaft and a stack of angular contact ball bearings supports the other. These designs take advantage of the high, line contact load carrying capacity of the cylindrical roller bearing and the axial displacement control of the ball bearing stack.

The advanced transmission system requirements noted above have promoted investigation of alternate load support configurations [1]. Specifically, use of the tapered rolling element bearing has seen increased attention. This is due to this bearing's ability to support larger loads for a given design envelope and mass penalty. Several investigations have revealed the potential present if careful attention is devoted to design cooling and lubrication at the higher speeds desired [2,3,8-11].

The material which follows describes the design/analysis methodology and results obtained in developing an input pinion supported by high speed small bore tapered-roller bearings. The report documents efforts expended at evaluating the relative merits of designs where the gear of the shaft is supported in both straddle and cantilever configurations. The role played by this effort is seen by more detailed examination of the complementary analytic-experimental scope of the complete program. The specific tasks were:

I. Bearing-Shaft System Analysis
II. Bearing Design Analysis
III. Test Bearing Preparation
IV. Test Facility Preparation
V-A. Step Speed, Load Spectrum Tests
V-B. Lubrication Optimization Tests
V-C. Repeatability Verification Tests
V-D. Testing of Second Bearing Design
V-E. Extended Duration Test
VI. Definition of Second Generation Bearing Design

The analytic portion of the program (Task I) evaluated the performance of and recommended preliminary designs for a support system, consisting of a shaft and two tapered-roller bearings. These results were used in conjunction with those from the analytic study performed in Task II to select the best candidates

from two "off-the-shelf" bearing designs. These bearings were then modified to provide aircraft type tapered-roller bearings for use in the subsequent test phases (Task V). The analyses executed will help define critical parameters for the computer evaluations of the second generation custom bearing design (Task VI).

SHABERTH [4], a computer program designed to perform thermo-mechanical analyses of arbitrarily configured bearing-shaft systems, was employed to analyze competing design concepts.

The effects of preload, interference fits, shaft wall thickness, bearing spacing and type as well as position of the pinion gear were explored. System rigidity and bearing rating lives including the detailed simulation of bearing and shaft elastic deformations were evaluated for both support geometries. The results were used to specify preliminary designs for a straddle and cantilever support configuration.

PRELIMINARY DESIGNS

The recommended designs for the straddle and cantilever configurations are shown schematically in Figures 1 and 2, respectively. The system performance characteristics for a line-to-line condition at zero preload and 60% of the applied gear load are also tabulated. Suggested values for the interference fits between the inner ring and shaft and the outer ring and housing are .01 mm and 0.mm, respectively. Preloads at these fits should not exceed 43.1 N and 33.1 N for the straddle and cantilever designs to allow adequate bearing life. These two basic designs were optimized for bearing rating life with specified constraints on pinion gear axial and radial deflection (<.0254 mm), pinion inclination (<.1°), and geometric design volume.

Analysis revealed that it was possible to lower design weight and geometric volume by reducing shaft length and still maintain acceptable bearing lifespans. Alternate designs and associated performance characteristics were explored and are detailed in the discussion of results. Their shorter bearing lives prevent recommendation.

DESCRIPTION OF ANALYSES

The stragegy employed to determine particular support system designs is defined by Figure 3. Computational details are provided in Appendices (A-E).

The particular parameters which were varied to design/analyze these systems are shown in Figures 4 and 5. Note, all individual load support designs use pairs of the same bearing types. The number of computer runs was minimized by requiring shaft wall thicknesses to be fixed at either 10% or 100% (solid) of the diameter extent. Design performance was found to be insensitive even to such large variations in wall thickness. Preloads were varied from 0-218.8 N to represent existing bearing design practice. A light interference fit between the shaft and inner ring (.01mm) was selected to ensure adequate bearing rating life.

All analyses were performed at a shaft speed of 36,000 rpm and at the specified maximum bearing temperature of 150°C. Shaft length restrictions were maintained as follows. In the straddle arrangement, the cone back face of the preload bearing does not extend more than 27.18 mm beyond the point of load application on the pinion. This violates the specified shaft length constraints. However, analysis demonstrates that a viable straddle design requires relaxation of this requirement for the off-the-shelf bearings selected. In the cantilevered arrangement the cone front face of the preload bearing does not extend more than 77.47 mm beyond the point of load application on the pinion. The gear face width was held at a value of 17.27 mm. In addition, minimum values for roller crown radii were used and the housing was considered to be rigid to provide further conservatism with respect to bearing rating life predictions. Finally, all materials were modelled as steel (Young's modulus $E = 2.04\ (10)^5\ N/mm^2$, Poisson's ratio $v = .3$, weight density = $7.87\ (10)^{-5}\ N/mm^3$) and a bearing material life factor of 5 was used considering that M50 tool steel would be required in the application.

DISCUSSION OF RESULTS

Results from the series of computer runs which were carried out to select the preliminary load support designs and define the respective systems' performance characteristics are provided in Tables 1-8 and Figures 6-9.

In Table 1 radial/axial bearing load ratios (N/N) and bearing rating lives (hours) for various wall thicknesses and specified percents of the gear loads in the straddle (s) and cantilever (c) geometries at zero preload are presented for designs using the M88000 series bearings. Table 2 provides similar results for identically arranged designs using the LM67000 series bearings. Note that the bearings were mounted back to back for the straddle designs and front to front for the cantilever designs (see Figures 1 and 2). These orientations provided superior performance for the specified loading condition. Only results for these orientations are presented, although test cases were completed considering the alternate mounting arrangements.

The larger bearing (M88000 series) exceeds the allowable housing space, and the width of the bearing precludes satisfying the specified shaft length restrictions. However, it affords acceptable bearing lifespans for either the cantilever or straddle design when the system is subjected to 60% of the gear load. The LM67000 series bearing does not meet the life requirements for the design configurations that were studied. As noted, the shaft wall thickness has a small effect on bearing life performance. This is due to the short, stocky nature of the shafts and the associated small deformations.

Tabulation of results for the deflection and rotation of the pinion gear at the point of load application for these same systems are presented in Tables 3 and 4. It is pointed out that the SHABERTH shaft deflection model considers transverse shear deformation as a secondary effect. This assumption is justified in Appendix D.

Since the support designs using the LM67000 series bearing did not provide adequate bearing rating lives for this application, only the M88000 series was used to evaluate the effects of preload and interference fits. The load ratios and rating lives at various preloads for the preliminary designs shown in Figures 1 and 2 are given in Tables 5a and 6a. A solid shaft was used for the straddle design since this provided conservative bearing rating life predictions. Load and life predictions at the specified interference fits are listed in Tables 5b and 6b. Plots of the bearing rating life vs. preload are given in Figures 6 and 7. Pinion gear deflections and rotations are presented in Tables 7 and 8.

It is interesting to note that for each design one bearing has a dramatic increase in life with increase in preload before eventually plunging to failure, while the life of the companion bearing decays monotonically. This behavior is associated with the number of rollers sharing the load. In Figure 8 the roller loads are plotted for the straddle design at zero (N) and 78.3 (N) preload, respectively. The preload forces more rollers to carry the gear loads so that initially there is an increase in life. As the preload continues to increase the roller loads become life-limiting. The analogous effect is shown in Figure 9 for the cantilever geometry. This behavior could possibly be exploited by specifying use of the smaller bearing (LM67000) in place of the bearing that experiences increased life.

Alternate bearing-shaft system configurations were considered to obtain weight optimization. The effects of changing bearing spacing and adjusting the pinion location relative to the bearings were also evaluated. Referring to Figures 4 and 5, the specific geometries considered are defined along with the system load, life and deflection responses in Tables 9-11.

Closer bearing spacings and/or shorter span lengths (lighter systems) degraded bearing rating life for both the straddle and cantilever geometries. This was particularly noticeable for the alternate cantilever designs (cases 1 and 2) where the overhang increased but the overall length was held fixed.

The straddle design with the asymmetric pinion gear location (case 3) also demonstrated decreased life. This was expected since the applied gear loads are distributed less equally between the bearings. Finally, comparing case 1 (straddle) with the original cantilever design it is noted that the straddle configuration provides greater bearing rating life than the cantilever geometry for identically sized arrangements and is therefore considered a superior design.

CONCLUSIONS AND RECOMMENDATIONS

A series of computer analyses have been carried out to explore competing design concepts of a shaft and existing tapered-roller bearing system to support the high-speed input pinion of an advanced commercial helicopter transmission. The results were used to specify preliminary designs for both a straddle arrangement where the pinion gear is located between the bearings and a cantilever arrangement where the pinion is outboard of the two bearings.

The analyses demonstrated that the straddle geometry provides improved bearing rating life compared to the cantilever geometry for identically size arrangements. The symmetry of this configuration helps distribute the radially applied gear load equally to the bearings as opposed to one bearing carrying the entire load. The straddle is therefore considered a preferable design.

The load support system analyses were based on the selection of two commercially available bearings. Neither bearing type was found to provide a completely satisfactory design with respect to the constraints on bearing rating life and available housing space.

C-2

The M88000 series bearing (larger) was judged to be the best suited condidate since it afforded acceptable bearing rating life, although it violates the housing space requirement. The LM67000 series bearing did not demonstrate acceptable bearing rating life for the designs that were evaluated so that the effects of preload as well as alternate geometric configurations which use this bearing type were not explored at this time.

The following alternatives are recommended for consideration to obtain a design that better meets the prescribed size and performance constraints:

1. Modify the design of the M88000 series to create an outer envelope which fits within the specified housing space.

2. Evaluate alternate support designs which employ, both, the M88000 (modified) and LM67000 bearing types. Due to the significant increase in life of one of the M88000 bearings for a range of preloads, a viable design should be possible by replacing that bearing with one from the smaller LM67000 series.

3. If the loss in system life created by the modification suggested in Step 1 creates an unsuitable design, relax the housing space requirement and evaluate designs which use both the M88000 and LM67000 bearing types.

4. The current analysis was performed without the benefit of a thermal analysis which couples the load support system with its thermal environment. The sensitivity of the design performance to preload indicates the merits of a future examination which takes proper account of interacting bearing and system generated heat sources.

REFERENCES

1. Morrison, F. R., et al, "A Functional Evaluation of a Thrust Carrying Cylindrical Roller Bearing Design," ASME Paper No. 78Lub28.

2. Parker, R. J. and Signer, H. R., "Lubrication of High Speed Large Bore Tapered-Roller Bearings," ASME Paper 77Lub13.

3. Taha, M. M. A., et al, "The Rigidity and Performance of a Helicopter Gearbox With a Cantilevered Housing and Two Taper Roller Bearings," ASME Publication 77-DET-103.

4. Crecelius, W. J., Research Report User's Manual for SKF Computer Program, "SHABERTH, for the Steady State and Transient Thermal Analysis of Shaft Bearing Systems Including Ball, Cylindrical and Tapered Roller Bearings," SKF Report No. AL77P015, developed under U.S. Army Contract DAAD05-75-C-0747.

5. Przemieniecki, J. S., Theory of Matrix Structural Analysis, McGraw-Hill, Inc., New York, 1968.

6. SKF Engineering Data, SKF Industries, Inc., Philadelphia, PA, 1973, page 31.

7. Roark, R. J. and Young, W. C., Formulas for Stress and Strain, Fifth Edition, McGraw-Hill, Inc., 1975, page 185.

8. Crecelius, W. J., and Milke, D. R., "Dynamic and Thermal Analysis of High Speed Tapered Roller Bearings Under Combined Loading," NASA Report CR-121207, National Aeronautics and Space Administration, Lewis Research Center, March 1973.

9. Lemanski, A. J., Lenski, J. W., Jr., Drago, R. J., "Design Fabrication, Test and Evaluation of Spiral Bevel Support Bearings (Tapered Roller), USAAMRDL Technical Report 73-16, Eustis Directorate, U.S. Army Air Mobility Research and Development Laboratory, June, 1973 AD769064.

10. Connors, T. F., and Morrison, F. R., "Feasibility of Tapered Roller Bearings for Main-Shaft Engine Applications," USAAMRDL Technical Report 73-46, Eustis Directorate, U. S. Army Air Mobility Research and Development Laboratory, August, 1973.

11. Cornish, R. F., et al, "Design Development and Testing of High Speed Tapered Roller Bearings for Turbine Engines," AFAPL-TR-75-26, U.S. Air Force Aero Propulsion Laboratory, Wright-Patterson Air Force Base, July, 1975.

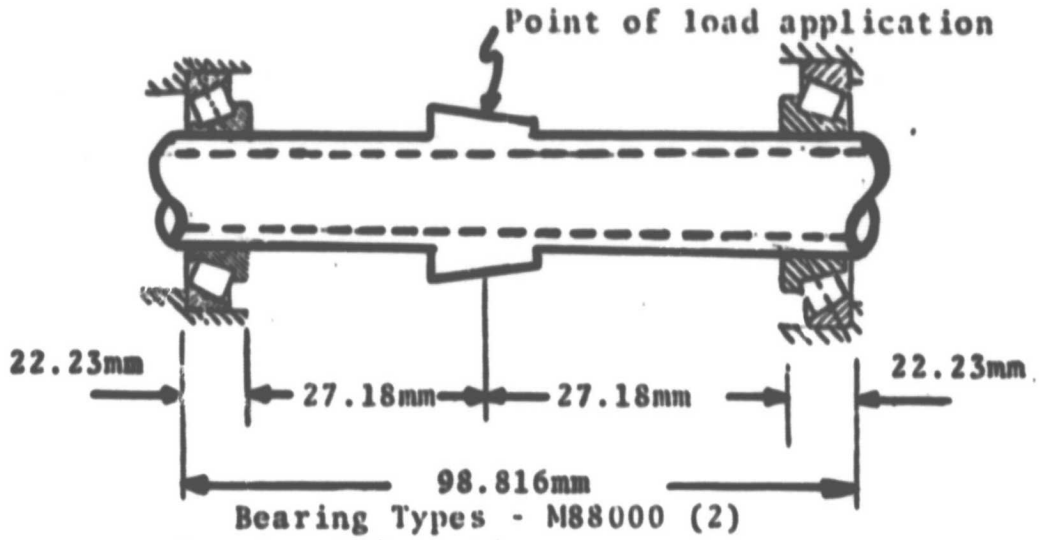

Bearing Types - M88000 (2)
Bearing Orientation - Back to Back

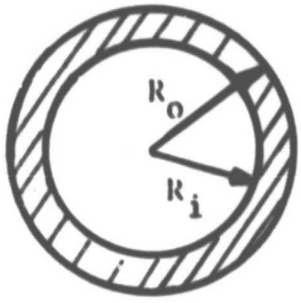

Shaft Section

R_o = 16.67 mm
R_i = 15.00 mm

Performance Characteristics at Zero Preload With 10% Wall Thickness and 60% of Gear Load - Fits = Line-to-Line

$|F_r/F_a|$ L (N/N) = 1917/5106

$|F_r/F_a|$ R (N/N) = 1481/2789

L_{10}^{L} (hrs) = 4434

L_{10}^{R} (hrs) = 9153

δ_a (mm) = .0178

δr (mm) = .00432

γ_v (deg) = .0011

γ_h (deg) = .0041

L, R = Left, Right
a, r = axial, radial
v, h = vertical, horizontal

Figure 1: Preliminary Support System Design - Straddle Geometry

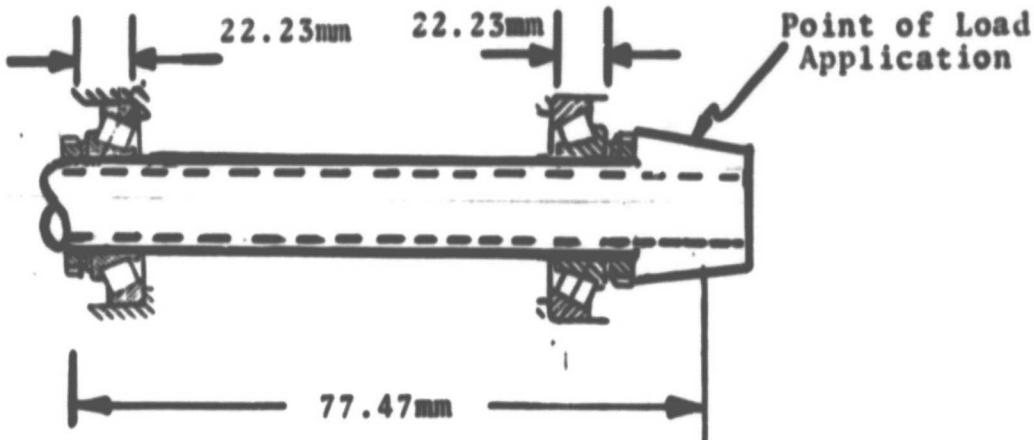

Bearing Types - M88000 (2)
Bearing Orientation -Front to Front

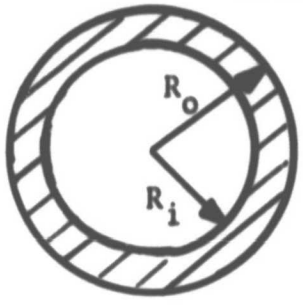

Shaft Section

R_o = 16.67 mm

R_i = 15.00 mm

Performance Characteristics at Zero Preload With 10% Wall Thickness and 60% of Gear Load-Fits=Line-to-Line

$|F_r/F_a|$ L (N/N) = 805/2522

$|F_r/F_a|$ R (N/N) = 3429/4817

L_{10}^{L} (hrs) = 3388

L_{10}^{R} (hrs) = 3669

δ_a (mm) = .017

δ_r (mm) = .011

γ_v (deg) = .021

γ_h (deg) = .014

Figure 2: Preliminary Support System Design - Cantilever Geometry

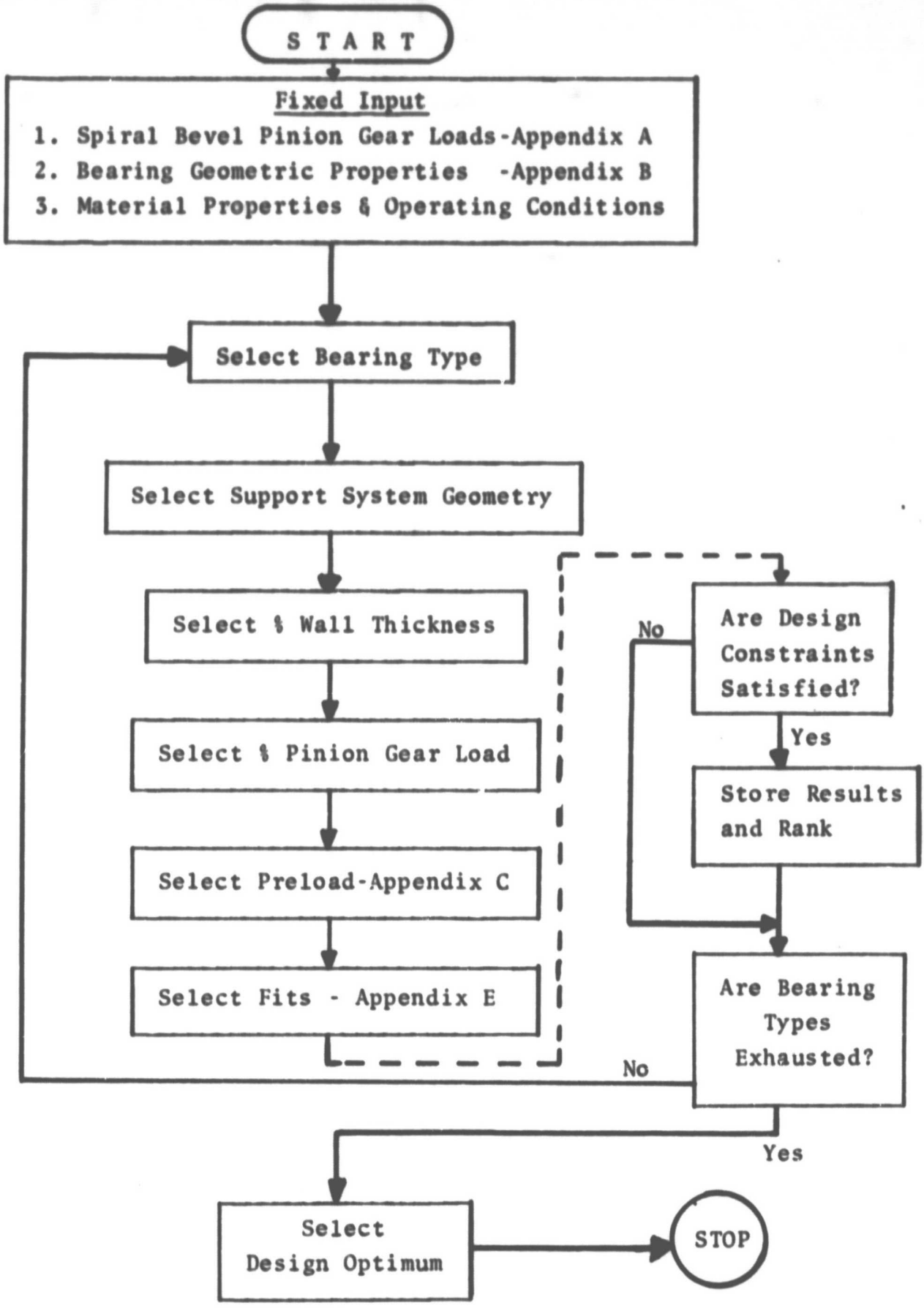

Figure 3: Flowchart of Design-Analysis Strategy for Support System

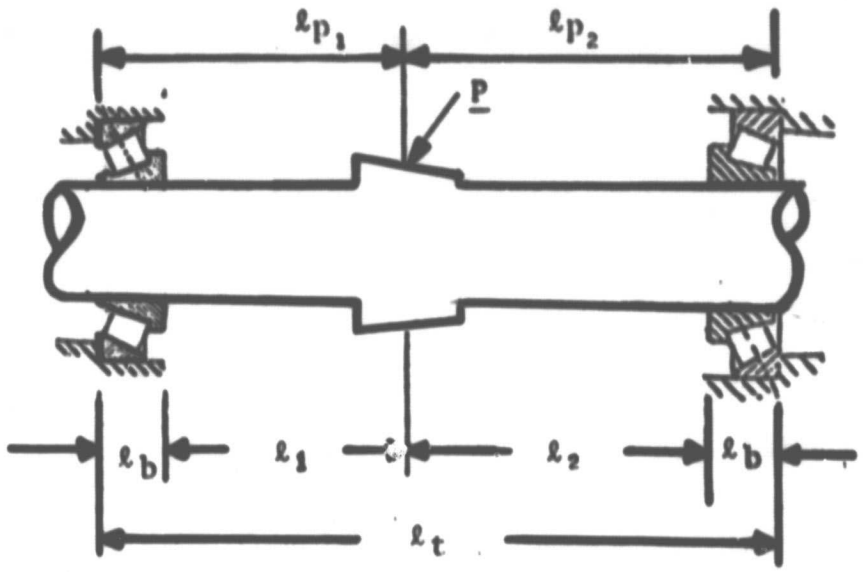

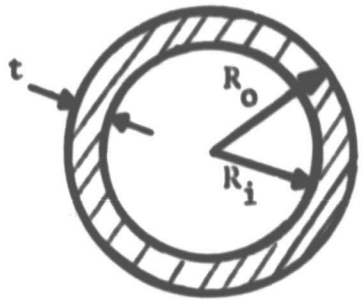

Shaft Section

Nomenclature

$\underline{P}$	=	Pinion gear load vector
ℓ_b	=	Bearing width
ℓ_1, ℓ_2	=	Distance from cone front face of preload bearing to point of load application
ℓ_{p_1}	=	Location of pinion gear ($\ell_i = \ell_{p_i}$, i=1,2 if bearings mounted back to back)
ℓ_t	=	Total length of support system
R_o, R_i	=	Outer, inner shaft radii
t	=	$R_o - R_i$ = wall thickness

Figure 4: Parameters Defining Geometry of the Straddle Design

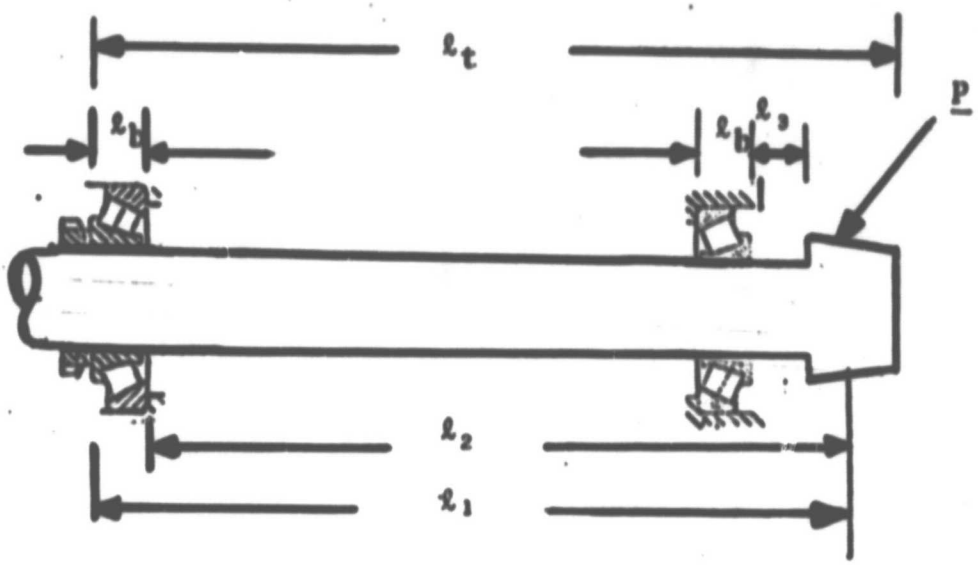

Shaft Section

Nomenclature

ℓ_2 = (replaces) ℓ_1 for bearings oriented front to front

All other parameters defined as per Figure 4.

Figure 5: Parameters Defining Geometry of Cantilever Design

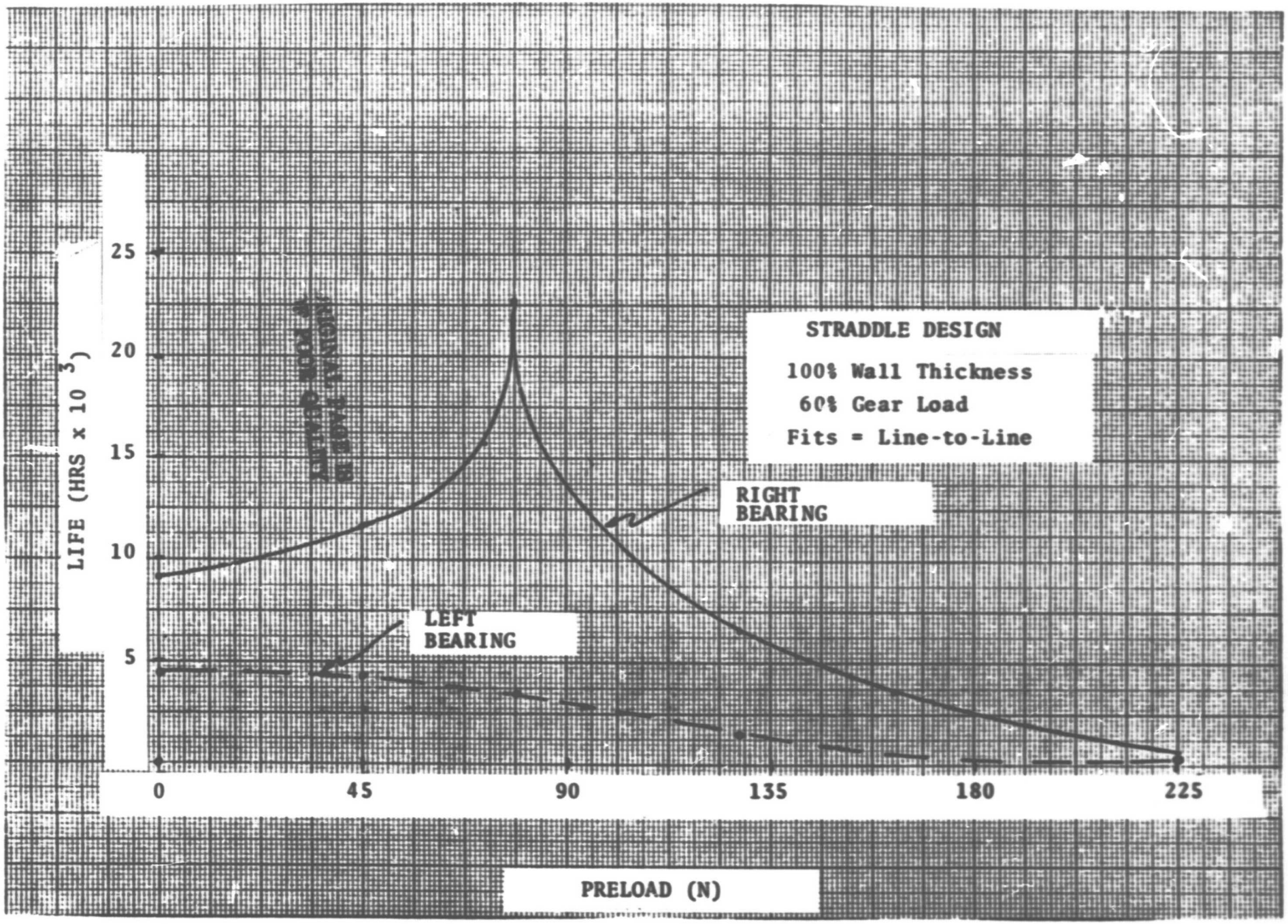

Figure 6: Bearing Rating Life vs. Preload - Straddle

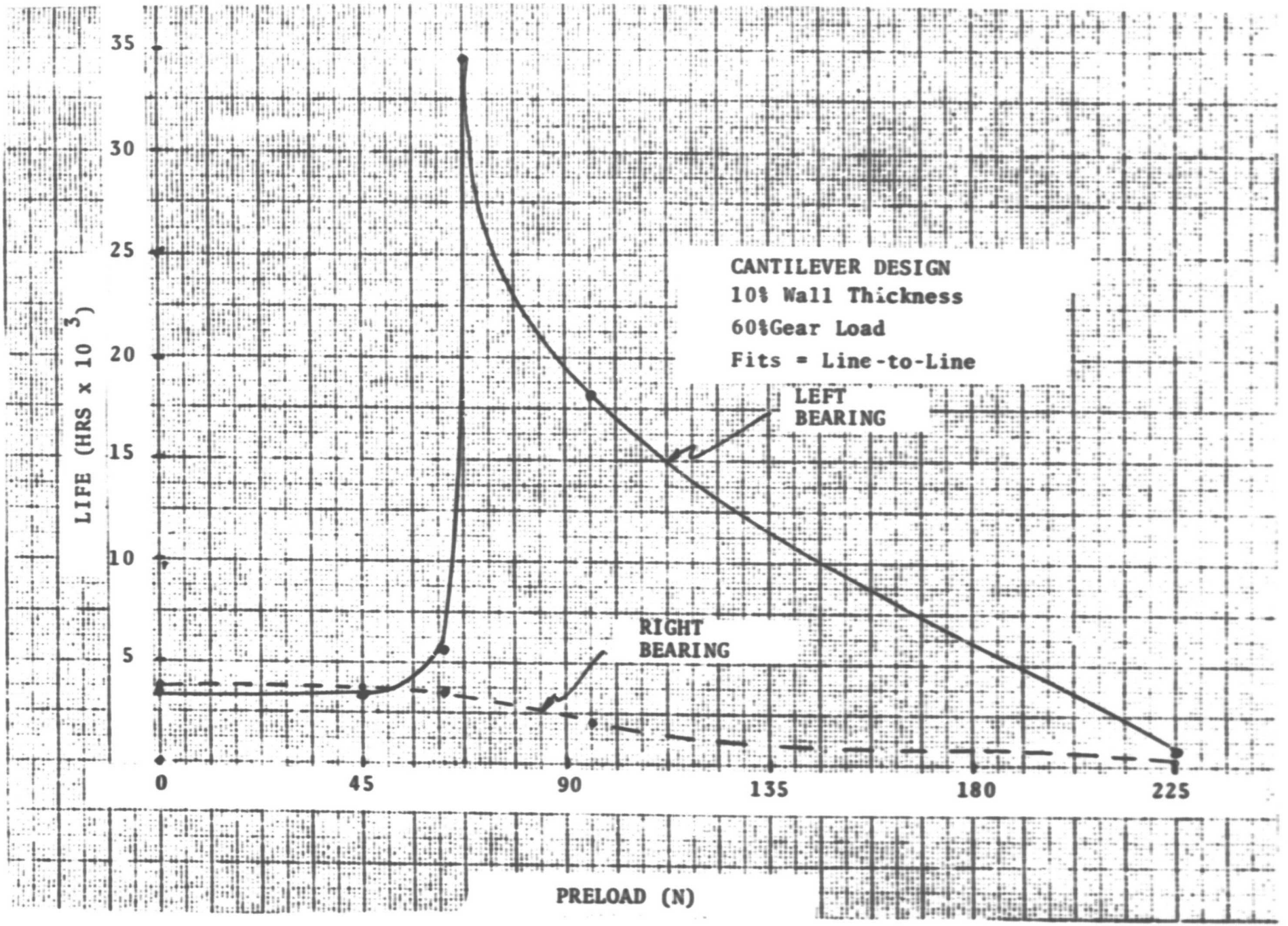

Figure 7: Bearing Rating Life vs. Preload - Cantilever

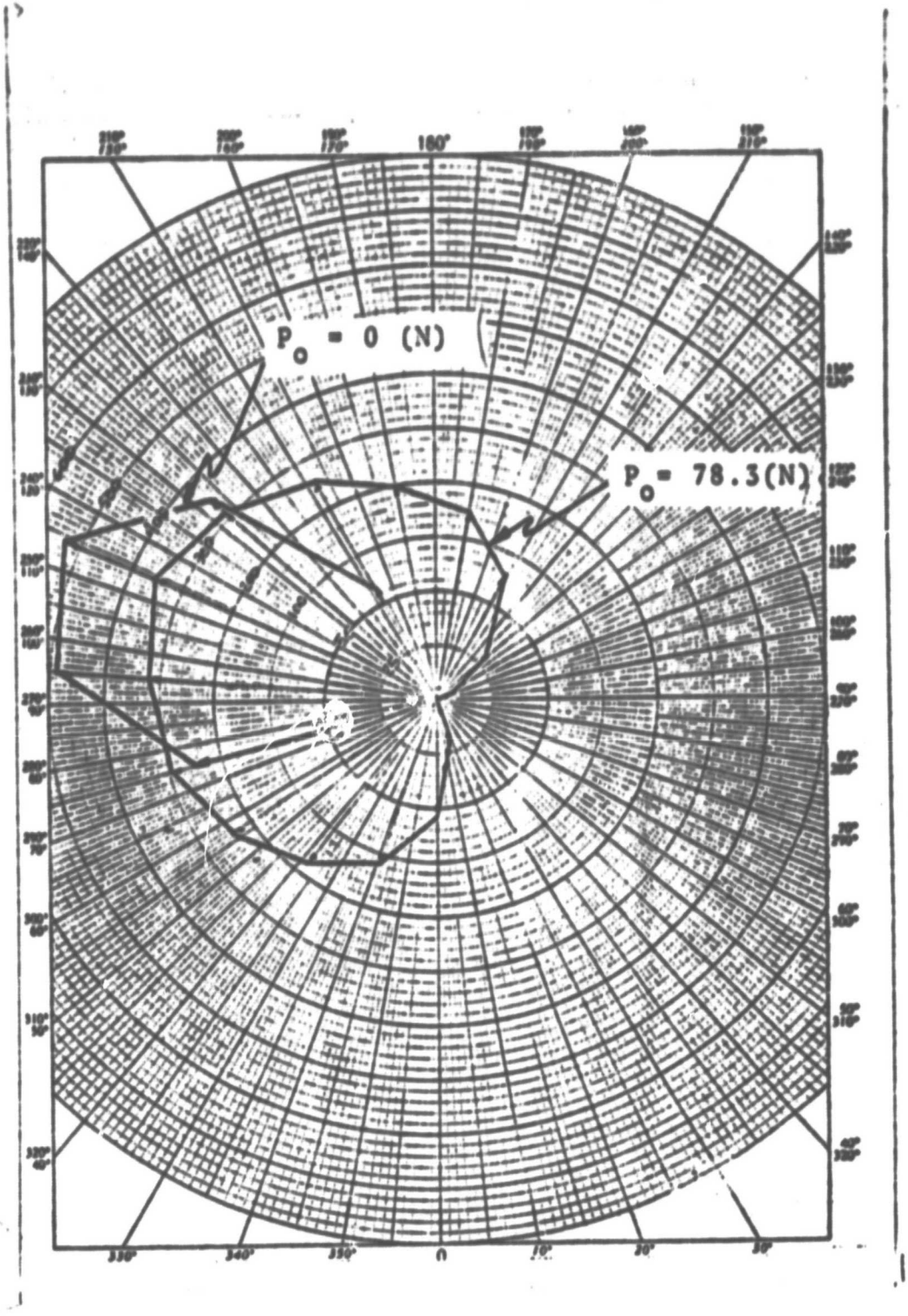

Figure 8: Roller Load Distributions (Newtons) at 0 (N) & 78.28 (N) Preload-Straddle

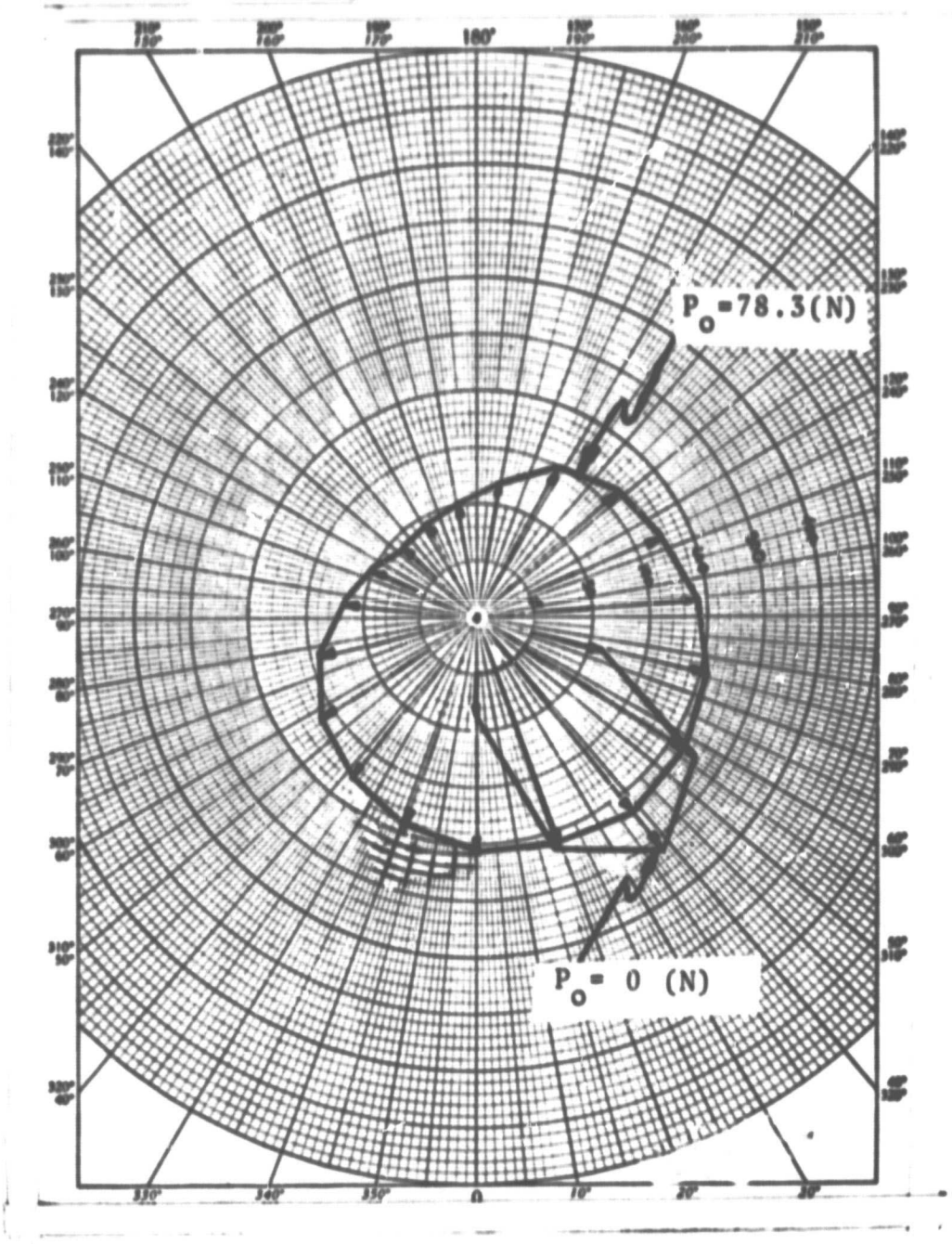

Figure 9: Roller Load Distributions (Newtons) at 0 (N) & 78.28 (N) Preload for 10% Wall Thickness, 60% Gear Load and Fits = Line-to-Line - Cantilever

Table 1: Load Ratios and Life Predictions - M88000 Series
Fits = Line-to-Line and Preload = 0

Geom.	%W.T.*	%G.L.*	$\lvert F_R/F_A \rvert L$* (N/N)	$\lvert F_R/F_A \rvert R$* (N/N)	L_{10}^{L} (hrs)	L_{10}^{R} (hrs)
S	100	100	3216/7041	2451/3171	1190	3186
S	100	60	1917/5106	1481/2789	4417	9070
S	10	100	3216/7041	2446/3171	1190	3281
S	10	60	1917/5106	1481/2789	4434	9153
C	100	100	1348/2736	5720/6600	1414	931
C	100	60	823/2526	3447/4848	3448	3626
C	10	100	1308/2718	5689/6587	1386	956
C	10	60	805/2522	3429/4817	3388	3669

Table 2: Load Ratio and Life Predictions - LM67000 Series
Fits = Line-to-Line and Preload = 0

Geom.	%W.T.	%G.L.	$\lvert F_R/F_A \rvert L$ (N/N)	$\lvert F_R/F_A \rvert R$ (N/N)	L_{10}^{L} (hrs)	L_{10}^{R} (hrs)
S	100	100	3220/5364	2513/1495	172	737
S	100	60	1926/3523	1517/1197	756	2806
S	10	100	3234/5364	2507/1495	172	742
S	10	60	1926/3518	1517/1197	755	2734
C	100	100	1326/1137	5653/5008	366	146
C	100	60	801/983	3403/3309	1184	648
C	10	100	1294/1130	5636/5000	357	146
C	10	60	792/983	3394/3300	1172	655

* W.T. = Wall Thickness
G.L. = Gear Load
L = Left
R = Right

Table 3: Deflections & Rotations of Pinion Gear - M88000 Series
Fits = Line-to-Line and Preload = 0

Geom.	%W.T.	%G.L.	δ_r^* (mm)	δ_a^* (mm)	γ_v^* (deg)	γ_h^* (deg)
S	100	100	.0048	.02286	.00148	.0043
S	100	60	.00305	.01780	.00094	.0026
S	10	100	.00686	.02286	.00183	.0063
S	10	60	.00432	.01778	.0011	.0041
C	100	100	.01194	.02108	.0197	.0107
C	100	60	.00838	.01702	.013	.0067
C	10	100	.01651	.02108	.033	.022
C	10	60	.01092	.01702	.021	.014

Table 4: Deflections & Rotations of Pinion Gear - LM67000 Series
Fits = Line-to-Line and Preload = 0

Geom.	%W.T.	%G.L.	δ_r (mm)	δ_a (mm)	γ_v (deg)	γ_h (deg)
S	100	100	.0051	.0381	.0022	.0054
S	100	60	.00331	.0279	.0015	.0036
S	10	100	.00762	.0381	.0025	.0079
S	10	60	.004826	.0330	.0016	.0051
C	100	100	.011176	.0356	.0206	.013
C	100	60	.007569	.02692	.0134	.0082
C	10	100	.016256	.0356	.036	.028
C	10	60	.010668	.02692	.0227	.017

---

r,a = radial, axial

v,h = vertical, horizontal

Table 5a: Load Ratio and Life Predictions at Various Preloads for Line-to-Line Condition at 100% Wall Thickness and 60% Gear Load - Straddle

Preload (N)	$\lvert F_R/F_A \rvert_L$ (N/N)	$\lvert F_R/F_A \rvert_R$ (N/N)	L_{10}^{L} (hrs)	L_{10}^{R} (hrs)
0	1917/5106	1481/2789	4417	9070
.44	1913/5111	1482/2790	4415	9071
43.10	1901/5165	1518/2847	4232	11450
50.30	1899/5182	1521/2860	4184	11490
55.60	1899/5204	1526/2882	4125	13210
62.27	1895/5234	1527/2916	4030	13510
71.178	1894/5300	1529/2975	3860	15760
78.28	1893/5431	1528/3104	3534	22970
125.90	1891/6988	1528/4670	1423	6555
218.80	1884/11220	1522/8898	262	612

Table 5b: Load Ratios and Life Predictions at Various Preloads and Interference Fit of .01 mm for 10% Wall Thickness and 60% Gear Load - Straddle

Preload (N)	$\lvert F_R/F_A \rvert_L$ (N/N)	$\lvert F_R/F_A \rvert_R$ (N/N)	L_{10}^{L} (hrs)	L_{10}^{R} (hrs)
0	1912/5148	1503/2826	4310	28945
43.1*	1905/6332	1518/4008	2600	15885
78.3	1899/7299	1531/4973	1205	5219

*Values computed by linear interpolation.

Table 6a: Load Ratio and Life Predictions at Various Preloads for Line-to-Line Condition at 10% Wall Thickness and 60% Gear Load - Cantilever

Preload (N)	$\lvert F_R/F_A \rvert_L$ (N/N)	$\lvert F_R/F_A \rvert_R$ (N/N)	L_{10}^{L} (hrs)	L_{10}^{R} (hrs)
0	805/2522	3429/4817	3388	3669
.44	807/2522	3432/4842	3389	3668
4.44	809/2524	3433/4842	3392	3658
43.10	839/2563	3449/4881	3466	3549
50.30	841/2575	3450/4893	3513	3521
62.27	843/2657	3452/4975	5570	3345
78.28	841/3091	3449/5418	34550	2596
95.60	839/3682	3447/6003	18110	1900
125.90	835/4698	3442/7019	7113	1158
146.80	827/5847	3438/8168	3053	705
166.80	822/6665	3436/8987	1823	514
186.80	821/7544	3429/9868	1151	378
218.80	814/8936	3425/11260	618	243

Table 6b: Load Ratio and Life Predictions at Various Preloads and Interference Fit of .01 mm for 10% Wall Thickness and 60% Gear Load - Cantilever

Preload (N)	$\lvert F_R/F_A \rvert_L$ (N/N)	$\lvert F_R/F_A \rvert_R$ (N/N)	L_{10}^{L} (hrs)	L_{10}^{R} (hrs)
0	824/2552	3446/4876	75528	3600
43.1*	831/3915	3444/6237	36971	2172
78.3	837/5028	3442/7350	5481	998

*Values computed by linear interpolation.

Table 7: Deflections and Rotations of Gear at Various Preloads for 100% Wall Thickness and 60% Gear Load
Fits = Line-to-Line - Straddle

Preload (N)	δ_r (mm)	δ_a (mm)	γ_v (deg)	γ_h (deg)
0	.00305	.01778	.00094	.0026
43.10	.002972	.00838	.00072	.0021
50.20	.002972	.007366	.00071	.00208
55.60	.0029693	.00635	.00070	.00203
62.27	.0029566	.005518	.00069	.00198
71.17	.0029185	.0046936	.00069	.00193
78.28	.0028829	.004064	.00068	.00187
125.90	.0024206	.003124	.00031	.00167
218.80	.0020193	.002438	.000117	.001496

Table 8: Deflections and Rotations of Gear at Various Preloads for 10% Wall Thickness and 60% Gear Load
Fits = Line-to-Line - Cantilever

Preload (N)	δ_r (mm)	δ_a (mm)	γ_v (deg)	γ_h (deg)
0	.0109200	.0170180	.02100	.01400
0.44	.0108710	.0164592	.02097	.01375
4.44	.0108710	.0155960	.02091	.01370
43.10	.0106680	.0068326	.02030	.01350
50.20	.0106450	.0058928	.02028	.01347
62.27	.0105160	.0041910	.02000	.01335
78.28	.0099060	.0035814	.01925	.01306
95.60	.0093472	.0032715	.01845	.01278
125.90	.0086868	.0029464	.01760	.01243
146.80	.0082040	.0027432	.01700	.01220
166.80	.0080010	.0025908	.01660	.01209
186.80	.0077978	.0024994	.01640	.01197
218.80	.0075692	.0002352	.01600	.01186

Table 9a: Geometry of Alternate Straddle Designs

Case No.	ℓ_1 (mm)	ℓ_2 (mm)	ℓ_t (mm)
Original	27.18	27.18	98.816
1	20.823	20.823	86.106
2	18.156	18.156	80.772
3	8.636	45.974	98.816
4	15.240	15.240	74.94

$$\ell_b = 22.23 \text{ mm}$$

$$\ell_{p_1} = \ell_1 + \ell_b$$

$$\ell_{p_2} = \ell_2 + \ell_b$$

Table 9b: Geometry of Alternate Cantilever Designs

Case No.	ℓ_1 (mm)	ℓ_2 (mm)	ℓ_3 (mm)	ℓ_t (mm)
Original	77.47	55.24	0.	86.106
1	77.47	55.24	5.334	86.106
2	77.47	55.24	24.384	86.106
3	72.136	49.906	0.	80.772
4	69.38	47.15	0.	78.016
5	66.77	44.54	0.	75.406

$$\ell_b = 22.23 \text{ mm}$$

Table 10a: Alternate Straddle Designs-Load Ratios & Rating Lives at 60% of Gear Load & 100% Wall Thickness Fits = Line-to-Line and Preload = 0

Case No.	$\lvert F_R/F_A \rvert_L$ (N/N)	$\lvert F_R/F_A \rvert_R$ (N/N)	L_{10}^{L} (hrs)	L_{10}^{R} (hrs)
Original	1917/5106	1486/2789	4417	9070
1	2069/5131	1527/2808	4224	8905
2	2157/5142	1561/2820	4116	7704
3	2749/4859	854/2540	4262	9679
4	2280/5165	1620/2844	3955	7349

Table 10b: Alternate Cantilever Designs-Load Ratios & Rating Lives at 60% of Gear Load & 10% Wall Thickness Fits = Line-to-Line and Preload = 0

Case No.	$\lvert F_R/F_A \rvert_L$ (N/N)	$\lvert F_R/F_A \rvert_R$ (N/N)	L_{10}^{L} (hrs)	L_{10}^{R} (hrs)
Original	805/2522	3429/4839	3388	3669
1	1030/2611	3741/4931	3115	3182
2	2580/3225	5422/5555	1767	1517
3	886/2554	3483/4875	3260	3545
4	929/2571	3509/4893	3194	3485
5	975/2589	3537/4910	3125	3422

Table 11a: Alternate Straddle Designs-Deflections & Rotations of Pinion Gear at 60% of Gear Load & 100% Wall Thickness With Fits = Line-to-Line and Preload = 0

Case No.	δ_r (mm)	δ_a (mm)	γ_v (deg)	γ_h (deg)
Original	.00305	.0178	.00094	.0026
1	.0025	.0180	.00122	.00296
2	.0023724	.0180	.0014	.00316
3	.002874	.017018	.00183	.0029
4	.002245	.01796	.00126	.0032

Table 11b: Alternate Cantilever Designs-Deflections & Rotations of Pinion Gear at 60% of Gear Load & 10% Wall Thickness With Fits = Line-to-Line and Preload = 0

Case No.	δ_r (mm)	δ_a (mm)	γ_v (deg)	γ_h (deg)
Original	.010922	.017018	.021	.014
1	.016000	.016700	.029	.01576
2	.04826	.017272	.067	.021
3	.011176	.016764	.0215	.0136
4	.011274	.01668	.0217	.01358
5	.011480	.01672	.0221	.01363

APPENDIX A

CALCULATION OF FORCE COMPONENTS ON SPIRAL BEVEL PINION GEAR

The procedure for computing the loads acting on the spiral bevel pinion gear was taken from Reference 6. General expressions for the tangential, axial and radial load on the left hand gear driving clockwise are given below (See also Figure A-1).

$$K_t = \frac{T_p}{r_p}$$

$$K_a = \frac{K_t}{\cos\psi} \quad (\tan\phi \sin\gamma_p + \sin\phi \cos\gamma_p)$$

$$K_r = \frac{K_t}{\cos\psi} \quad (\tan\phi \cos\gamma_p - \sin\phi \sin\gamma_p)$$

where

T_p = pinion torque = 105,410 N-mm

r_p = pitch radius = 22.01 mm

ϕ = pressure angle = 20°

ψ_p = spiral angle = 35°* (gives maximum loads)

γ = pitch angle = 15.22°

Substitution of these values gives

$$K_t = \frac{105,410}{22.0091} = 4789.2 \text{ N}$$

$$K_a = \frac{4789.2}{20.8026} \quad [(.364)(.263)+(.574)(.965)] = 3796.8 \text{ N}$$

$$K_r = \frac{4789.2}{20.8026} \quad [(.364)(.965)-(.574)(.263)] = 1172.5 \text{ N}$$

---

* The spiral angle ranges from 30° - 35°.

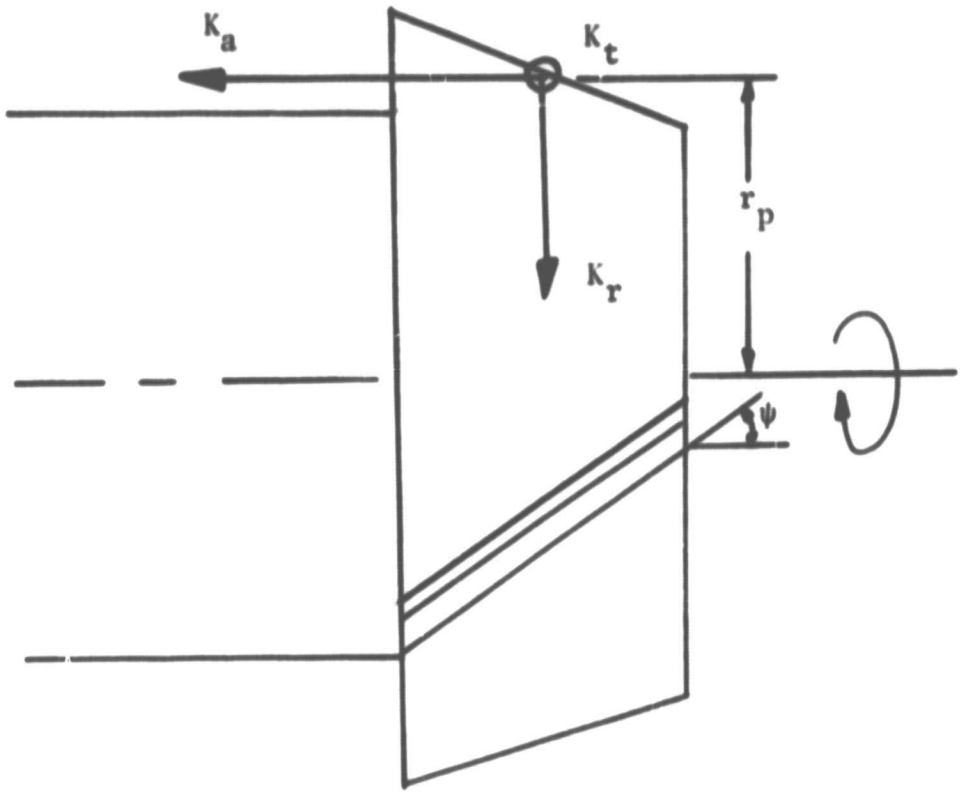

Figure A-1: Tooth Forces on Spiral Bevel Gear

APPENDIX B
BEARING GEOMETRIC PROPERTIES

The geometric properties for the bearings were computed from drawings of the assemblies, inner rings and rollers. The numerical values for the geometric parameters used in the analyses are tabulated below (Table B-1) while the nomenclature is defined with Figure B-1.

Table B-1: Bearing Geometric Parameters

Parameter	M88000 Series	LM67000 Series
α	20°	15.37°
β	15.05°	11.7°
θ	15.55°	12.25°
2ε	4.95°	3.67°
R_s	87.38 mm	102.00 mm
R_c	4500.88 mm	2049.78 mm
ℓ_w	16.32 mm	10.75 mm
ℓ_a	15.80 mm	10.26 mm
D_w	7.94 mm	6.53 mm
D_b	33.34 mm	31.75 mm
B	22.23 mm	15.88 mm

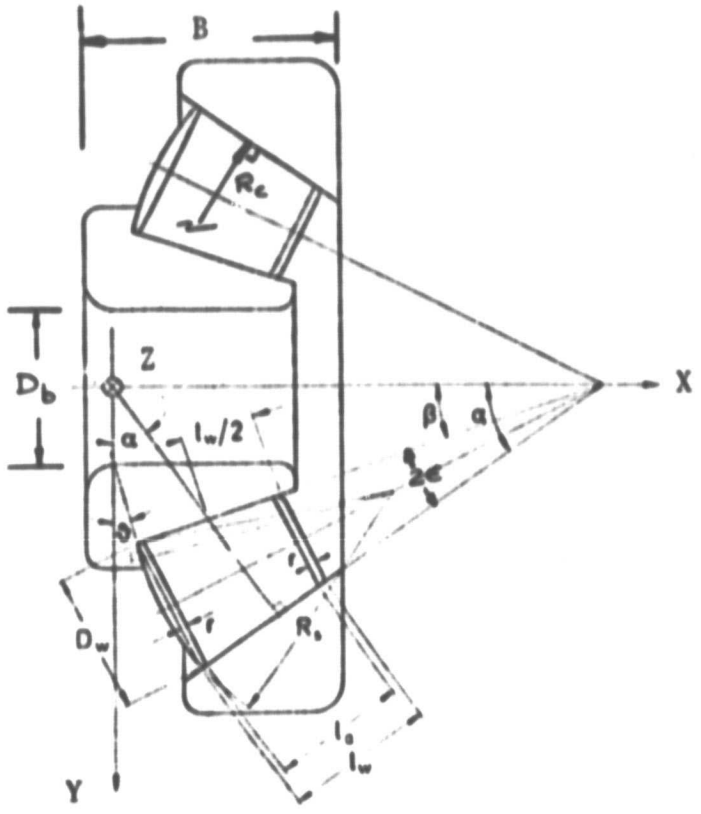

Figure B-1: Tapered Roller Bearing with Characteristic Geometrical Dimensions

APPENDIX C

PRELOAD CALIBRATION

In SHABERTH, axial preloads are imposed by selection of a negative initial deformation (axial play) parameter. An equivalent preload was computed using the procedure described below.

The system external loads were removed and the rotational speed set to zero. An axial play (compression) was selected and the support system analyzed to evaluate bearing axial loads on the inner rings. This provided a point on the load-deflection curve. The process was repeated until the entire calibration curve (Figure C-1) was obtained. At this point the displacement corresponding to a given preload could be extracted from the curve.

Since only the M88000 series was found to be suitable for this application, a calibration was done for this bearing type alone. The range in axial displacement was 0-.03 mm corresponding to a range of 0-333.6 N. The sequence of axial play values selected and the associated bearing thrust loads computed are shown in Table C-1.

Table C-1: Axial Play vs. Preload - Calibration Data

Axial Compression (mm x 10^4)	Preload (N)
0.000	0.000
10.000	43.199
20.000	125.999
30.000	219.002
40.000	333.000

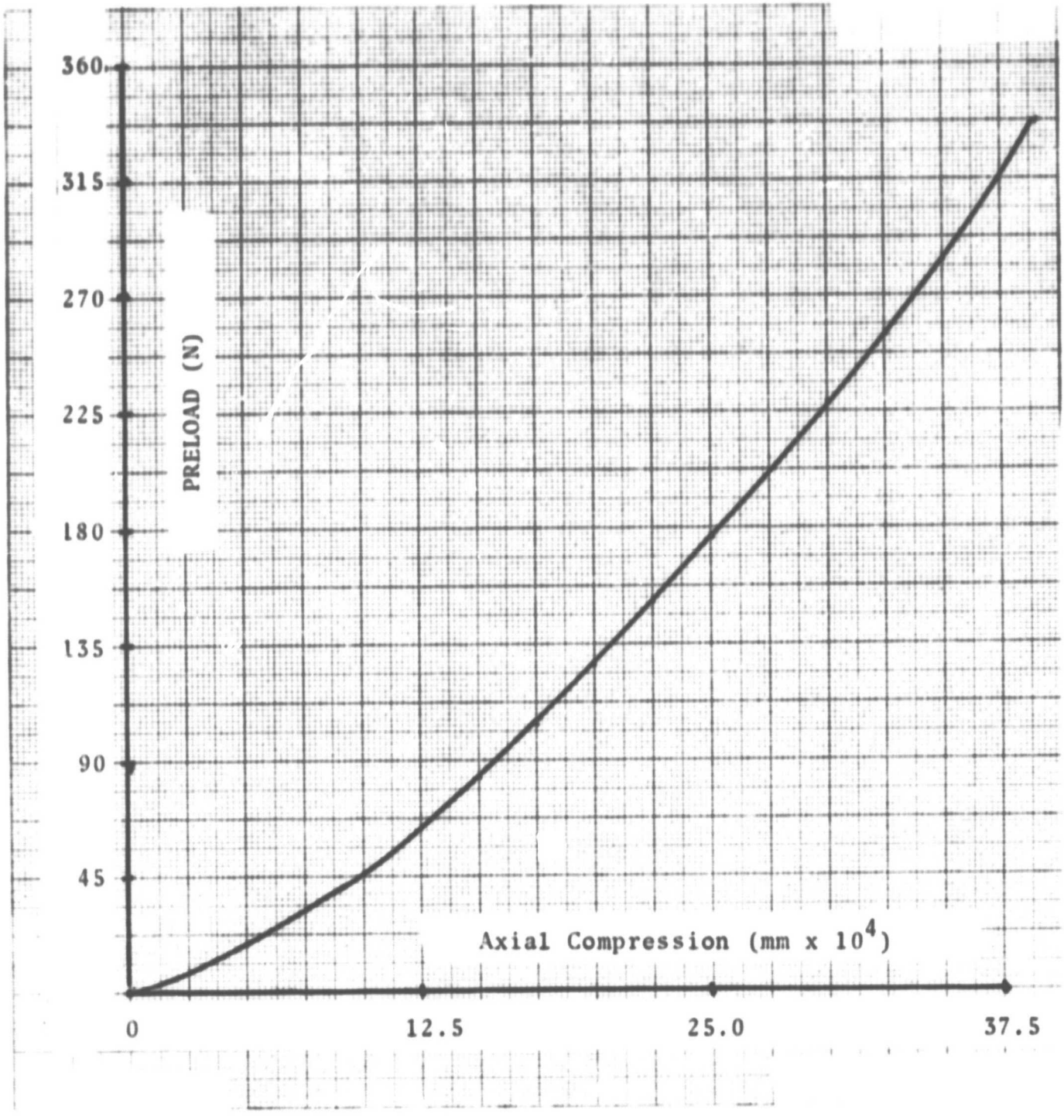

Figure C-1: Preload Calibration Curve

APPENDIX D
EFFECT OF TRANSVERSE SHEAR DEFORMATION ON PINION GEAR DEFLECTION

An estimate of the increase in the pinion gear radial deflection due to the influence of transverse shear deformation was obtained for the straddle designs by comparing the deflections, with and without shear effects, under the load using the model shown in Figure D-1. A similar comparison was not made for the cantilever designs since any additional deflection at the point of load application would be a multiple of the extremely small relative displacement between the gear mid-section and the adjacent bearing.

The deflection δ_s, including shear deformation, for the simply-supported beam of Figure D-1 was derived from References 5 and 7 as

$$\delta_s = \frac{P L^3}{48 EI} (1 + \phi) \quad \text{(mm)}$$

where

- E = Young's Modulus (N/mm^2)
- I = Inertia of Section (mm^4)
- $\phi = 24(1+\nu) \frac{A}{A_s} (\frac{r}{L})^2$ = shear coefficient
- $L=2\ell$ = Span length (mm)
- A = Cross sectional area (mm^2)
- A_s = Shear area = .5A (mm^2)
- r = Radius of gyration (mm)

Numerical values for these parameters were computed for a 10% wall thickness. Note that half the minimum span length and mean pinion radius were used to compute ϕ to make the estimate of the increase in deflection conservative.

For $2\ell = 80.772$ mm and $R_o = 21.996$ mm

$r/2\ell = 9.32/50.8 = .184$

and

$\phi = 2.1.$

Let δ = deflection without shear ($\phi=0$).

Then,

$$\frac{\delta_s}{\delta} = (1 + 2.1) = 3.1$$

As previously noted, this amplification is not large enough to violate the imposed limits on pinion gear deformation.

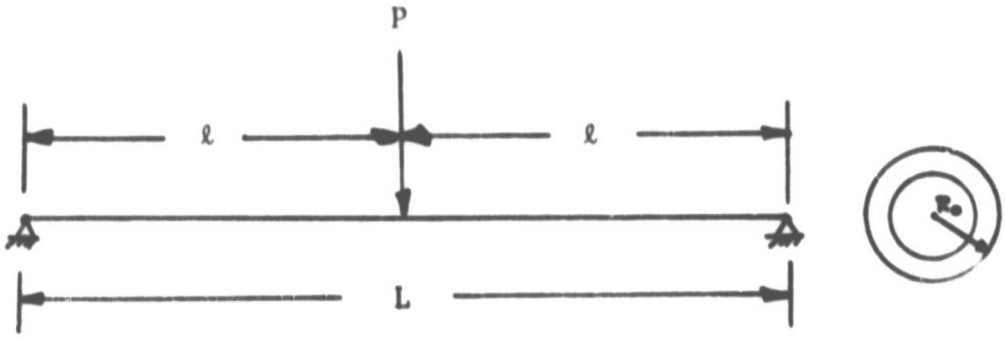

Figure D-1: Simply-supported Beam Model

APPENDIX E

FIT ANALYSIS - DESCRIPTION OF ANALYTIC MODEL

To accurately analyze the performance of a bearing, its operating clearance must be known. In SHABERTH* an analysis was developed to account for the effect of initial and operating shaft and housing fits.

The bearing rings are treated as thick walled circular cylinders of constant wall thickness subjected to the action of uniformly distributed internal and external pressure. Mean values for the inner/outer diameter and wall thicknesses of both rings were specified to accommodate the tapered geometry.

The external pressure arises in the case of the outer ring from a press fit into the bearing housing. The internal pressure on the outer ring arises from the discrete rolling element loads which are regarded as uniform internal pressure acting on the outer ring. Similarly for the inner ring the press fit on the shaft provides a uniform internal pressure and the rolling element loads are regarded as a uniform external pressure. Figure E-1 shows the idealized sections used in the analysis and their numerical values are given in Table E-1.

The parameters W_S and W_H are effective widths of the shaft and housing cylindrical sections. These were taken as twice the inner (W_I) and outer (W_O) ring widths, respectively. The inner diameter of the inner ring was set at 33.34 mm and the outer diameter of the shaft at 33.35 mm to provide a .01 mm (light) interference fit. Zero clearance was specified between the outer ring and housing since the bearing "grows" into a tight fit from centrifugal expansion.

---

*See Technical Report AFAPL-TR-76-90, October, 1976.

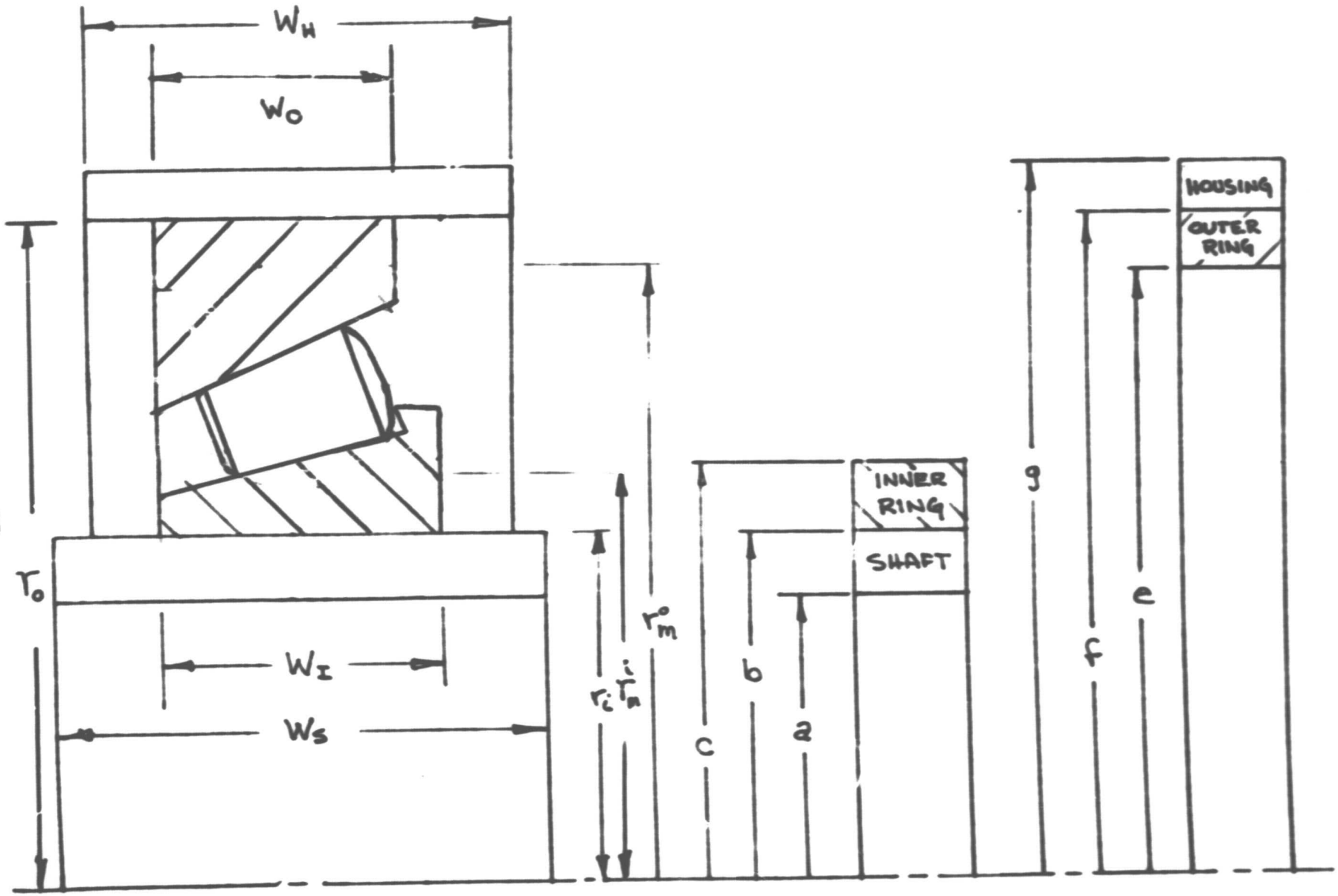

Figure E-1: Fit Analysis-Bearing Assembly Equivalent Sections

Table E-1: Fit Analysis - Model Parameters and Dimensions

Parameter	Numerical Value (mm)
a = Shaft Inner Radius	15.00
b = Shaft Outer Radius	16.675
c = Inner Ring Outer Radius	25.30
r_i = Inner Ring Inner Radius	16.67
r_m^i = Inner Ring Mean Radius	20.1
e = Outer Ring Inner Radius	25.37
r_o = Outer Ring Outer Radius	34.13
r_m^o = Outer Ring Mean Radius	29.75
f = Housing Inner Radius	34.13
g = Housing Outer Radius	42.67
W_I = Inner Ring Width	22.22
W_O = Outer Ring Width	17.46
W_S = Shaft Effective Width	44.44
W_H = Housing Effective Width	34.92

APPENDIX 2
LOAD SUPPORT SYSTEM ANALYSIS
HIGH SPEED INPUT PINION CONFIGURATION

LOAD SUPPORT SYSTEM ANALYSIS
HIGH SPEED INPUT PINION CONFIGURATION

BY

S. S. GASSEL

J. PIRVICS

DECEMBER 1979

SKF REPORT NO. AL79P039

SKF INDUSTRIES, INC.
TECHNOLOGY SERVICES DIVISION
1100 FIRST AVENUE
KING OF PRUSSIA, PA 19406

The material presented is based upon work performed at SKF Industries under NASA Contract No. NAS3-20839. This paper was presented at the joint ASME/ASLE Lubrication Conference, Dayton, Ohio, October 16-18, 1979, and has been published in the ASME Journal of Lubrication Technology, Vol. 102, No. 1, January 1980, pp 97-106.

LOAD SUPPORT SYSTEM ANALYSIS
HIGH SPEED INPUT PINION CONFIGURATION

by

S. S. Gassel
J. Pirvics

ABSTRACT

Structural assemblies which transmit power, helicopter gearboxes for example, require accurate evaluation of load and displacement distributions to ensure system design optimization. Particular performance parameters which depend on detailed understanding of the distributions are operating life and rigidity. The coupling complexity of system components; gears, shafts, bearings and the housing itself, prevents meaningful evaluation of performance from the study of isolated components. The entire load support system has to be examined in its interacting entirety.

In this paper a theoretical study has been made to determine the performance of a load support system, consisting of a shaft and two tapered roller bearings for the high-speed input pinion of an advanced helicopter transmission. SHABERTH, a computer program designed to perform thermo-mechanical analyses of arbitrarily configured rolling element bearing-shaft systems, was employed to analyze, both, a straddle arrangement where the spiral bevel pinion gear is located axially between the two bearings, and a cantilevered arrangement where the pinion is outboard of the bearings.

The effects of preload, shaft wall thickness, bearing spacing and misalignment of bearing races were examined. Their influence on load distributions and bearing rating lives including simulation of bearing and shaft elastic deformations were evaluated for both support geometries. Additional effort was expended to detail the performance of the pinion designs over a range of shaft rotational speeds. Lubrication and friction effects were included. Particular attention was directed to local as well as global heat generation rates (HGR) to provide design information for proper lubrication of the bearings.

The results provide guidance for improved design of transmissions and the load vector control within them. In particular, the relative merits of the straddle versus the cantilever design have been exposed so that their individual characteristics may be exploited to increase system survivability.

INTRODUCTION

Advances in helicopter transmission design are obtained by the successful maximization of power transmitted through hardware of minimum volume and mass. As the volume of the design envelope decreases, higher speeds and loads are imposed on components of the system. With the higher power densities processed by material volumes of lower mass content, reliable and predictable performance of components within the system becomes crucial.

Several modules in existing transmissions, the planetary reduction set and the input pinion for example, have to be redesigned to achieve performance advances for the complete system. The most critical is the input pinion which serves as the first link between the high speed power plant input and the low speed mast rotor output.

Input pinions have been customarily designed as load support systems where a shaft is supported by a series of rolling element bearings which in turn straddle a central gear. Typically, a cylindrical roller bearing is located at one end of the shaft and a stack of angular contact ball bearings supports the other [1]. These designs take advantage of the high, line contact radial load carrying capacity of the cylindrical roller bearing and the axial displacement control and thrust load capacity of the ball bearing stack.

The advanced transmission system requirements noted above have promoted investigation of alternate load support configurations [2]. Specifically, use of the tapered roller bearing has seen increased attention. This is due to this

bearing's ability to support large combined loads for a given design envelope and mass. Several investigations have revealed the potential present if careful attention is devoted to cooling design and lubrication at the higher speeds desired [3-6].

These and other studies, notably [7,8], have also revealed the requirement for computerized simulation of the complete load support system which evolves. The simulation is complex due to the cross coupling of effects experienced by individual components with the surrounding hardware. The imposed constraints on space and mass for example, affect load support stiffness and thus require accurate accounting for the resulting load and displacement vector distribution at the gear mesh. Failure to do so results in unacceptable power loss, accelerated wear and elevated temperature operation of the system.

The material which follows describes the analysis and resulting data obtained in developing design prototypes for an input pinion supported by high speed small bore ($2.0 \times (10)^6$DN) range tapered roller bearings. The paper documents efforts expended at evaluating the relative merits of designs where the gear of the shaft is supported in both straddle and cantilever configurations.

Each design configuration offers distinct advantages. The symmetric straddle arrangement enhances bearing life by providing a more equal distribution of the gear load among the support bearings. However, two-sided access to the supported gear imposes a design penalty by increasing housing volume and mass. The cantilever geometry provides an easily positioned, free, gear

mesh point, but reduces bearing life for a given design volume and mass.

SHABERTH [10], a computer program created to perform thermo-mechanical analyses of arbitrarily configured rolling element bearing-shaft systems, was employed to analyze competing design concepts. The program was exercised at a level which considers the elastic contact forces to explore the effects of preload, shaft wall thickness, interference fits and bearing spacing, as well as position of the pinion gear on performance. A sequence of code executions over a spectrum of the applied gear loads was implemented. The data obtained was used to evaluate system rigidity, bearing load distribution and bearing rating life for both support geometries. These results parallel the analyses performed by Taha, et al, [8] for the cantilever case.

This effort was further extended by executing the code at the next higher level which activates the simulation of a lubricant and includes traction effects. A range of shaft rotational speeds was considered. This allowed quantification of such parameters as EHD film thickness and lubricant life adjustment factors in terms of shaft operating speed. Particular attention was directed to the heat generation rates at various component locations (e.g. flanges and raceways) to provide design guidance for lubrication systems.

THEORY

SHABERTH has been written to describe the detailed thermodynamic equilibrium of a load support system consisting of a shaft and rolling element bearings. Examples of bearing-shaft configurations addressed in this study are shown schematically for a straddle and cantilever geometry in Figure 1 and Figure 2. Along with the variations of parameters considered, positive directions for forces/moments and displacements/rotations are defined. These are representative of load support systems found in helicopter-type input pinion assemblies.

The general loading is expressed as an applied force and moment vector combination. The formulation allows a variable cross-section, flexible shaft which can be solid or hollow. With the tapered roller option activated individual bearing performance is detailed by simulation with concentrated contact elastohydrodynamic traction models. Further detail is present in the computation of film starvation effects.

The shaft, bearings and lubricant, characterized by individual material properties, interact with their environment so that thermal and inertial effects are taken into account. Bearing dimension changes for example, reflect the influence of external and bearing generated time dependent heat sources.

SHABERTH is structured by nesting computation loops which address ever increasing levels of detail in system characterization. The present investigation used the first two levels of sophistication of the four possible.

Level 0 - Elastic Contact Forces are calculated. No lubrication or friction effects are considered.

Level 1 - Elastic Contact Forces are calculated. Lubrication and friction effects are considered using epicyclic assumptions to estimate rolling element and cage speeds.

BEARING CLEARANCE ANALYSIS

The change in bearing diametral clearance is computed according to the generalized equation set.

$$\Delta DCL = f\{(Fits)_m, t_i, \Omega_m, (Q_r)_m\}, \qquad (1)$$

m = 1,2 for inner and outer rings, respectively

i = 1,2,3,4,5 for shaft, inner ring, outer ring, housing and rolling element, respectively

where: ΔDCL is the change in bearing diametral clearance.

Fits are the cold mounted shaft and housing fits

t_i are the component temperatures

Ω_m refers to the ring rotational speeds

Q_r refers to the radial component of the rolling element-race normal force

In general, the clearance analysis accounts for the following effects:

1. Temperature changes and gradients.
2. Initial and operating shaft and housing fits.
3. Rotation induced, ring radial growth.
4. Radial components of the rolling element-raceway normal loads.

The bearing rings are treated as thick walled circular cylinders of constant wall thickness subjected to the action of uniformly distributed internal and external pressure.

The external pressure arises in the case of the outer ring from a press fit into the bearing housing. The internal pressure on the outer ring is due to discrete rolling element loads which are represented as equivalent to a uniformly distributed internal pressure of finite extent acting on the outer ring. Similarly, for the inner ring the press fit on the shaft provides a uniform internal pressure and the rolling element loads are regarded as a uniform finite sector external pressure.

SHAFT-BEARING ANALYSIS

The shaft-bearing system load equilibrium scheme calculates bearing inner ring positions relative to those of the outer ring. The external loading applied to the shaft is balanced by rolling element loads which develop at the bearing inner ring at a defined thermo-mechanical state.

The deflection characteristics of the shaft are calculated one plane at a time. The differential equation for the deflection curve of the shaft, in the XY plane, is taken to be

$$\frac{d^2Y}{dX^2} = - \frac{M(X)}{EI(X)} \qquad (2)$$

where M = moment

E = modulus of elasticity

I = moment of inertia

The coordinates X and Y and typical loading condition are shown in Figure 3 .

The formulation considers the shaft to be axially rigid. Therefore, pinion gear axial displacements at the shaft centerline equal bearing axial displacements. Transverse shear deformation is considered to be a second order effect.

The bearings may take force and/or moment loads and they may be initially displaced (δ_{yo},γ_{zo}), Figure 4. The reaction forces and moments on the shaft from the bearings are calculated as functions of bearing deflections. The bearing deflections can be looked upon as shaft support displacements, (δ_y, γ_z).

The shaft reaction at any location i is calculated as the shaft reaction, F_{oi}, at i when all additional displacements of the shaft supports are zero, plus the additional reactions at i caused by all additional displacements, or bearing deflections:

$$F_i = F_{oi} + \sum_{j=1}^{N_b} \frac{\partial F_i}{\partial \gamma_{zj}} \gamma_{zj} + \sum_{j=1}^{N_b} \frac{\partial F_i}{\partial \delta_{yj}} \delta_{yj}, \quad N_b = \text{no. of bearings} \qquad (3)$$

BEARING INNER RING EQUILIBRIUM

The bearing inner ring equilibrium solution is obtained by solving the system:

$$\{F_b\}_i - \{F_s\}_i = 0 \qquad i = 1,2...N_b \qquad (4)$$

for N_b bearings.

WHERE:

$\{F_b\}_i$ denotes a vector of the i-th bearing loads and moments resulting from rolling element/race forces and moments.

$\{\vec{F_s}\}_i$ denotes a similar vector of loads, exerted on the inner ring by the shaft.

The variables in this system of equations are the bearing inner ring deflections $\{\Delta_b\}$ and the shaft displacements $\{\Delta\}$ at all bearing locations. The bearing loads may be expressed as a function of the inner ring deflections.

$$\{F_b\} = \{F_b \quad (\Delta_b)\} \tag{5}$$

The deflection $\{\Delta_b\}$ of a bearing is described by two radial, two angular and one axial deflection, δ_y, δ_z, γ_y, γ_z and δ_x respectively. The axial deflection, δ_x is assumed to be the same for all bearings on a shaft. Positive displacements and rotations are in the positive directions of the bearing and rolling element coordinate axes shown in Figure 5.

The system of equations represented in Eq. (4) is solved with a Newton-Raphson iterative scheme for a quasidynamic equilibrium state.

The latter stipulates that the true dynamic equilibrium terms, containing first derivatives of the rolling element rotational speed vectors and the second derivatives of rolling element position vectors with respect to time, are replaced by numerical expressions which are position rather than time dependent.

ROLLING ELEMENT EQUILIBRIUM EQUATIONS

The equations which define rolling element quasi-dynamic force equilibrium take the form:

$$\sum_m \left[\int_{-a_m}^{a_m} (\{Q\}_m + \{f\}_m) \cdot dt + \{F\}_m \right] + \{F\} = 0 \qquad (6)$$

WHERE:

m — 1,2, 3 refers to the outer raceway, inner raceway and cage.

$\{Q\}_m$ — is the vector normal load per unit length of the contact.

$\{f\}_m$ — is the vector of friction force per unit length of the contact. This force arises from asperity friction and lubricant shear.

$\{F\}$ — is the vector of flange contact, inertia and drag forces.

t — is a coordinate along the contact perpendicular to the direction of rolling (usually the major axis).

a_m — is half the contact length.

$\{F\}_m$ — is the vector sum of the hydrodynamic forces acting on the rolling element at the m-th contact.

Rolling element moment equilibrium is defined by:

$$\sum_m \left[\int_{-a_m}^{a_m} \{r\}_m \times (\{Q\}_m + \{f\}_m) \cdot \{dt\} \right] + \{r\}_m \times \{F\}_m + \{M\}_I = 0 \qquad (7)$$

$\{Q\}_m$, $\{f\}_m$, $\{F\}_m$, $\{a\}_m$, and t are defined above, $\{M\}_I$ is a vector of inertia and flange-induced moments.

$\{r\}_m$ is a vector from the rolling element center to the point of contact.

The solution to the equation sets described above generates the necessary data to calculate bearing heat generation rates and fatigue life.

In the frictionless elastic solution $\{F\}_m$ and $\{f\}_m = 0$. Additionally, the only rolling element inertia terms considered in the frictionless solution are centrifugal force and gyroscopic moments. For each roller, the radial and axial force equilibrium and the tilting moment about the z_R axis are solved.

The friction solution determines roller quasi-dynamic equilibrium for five degrees of freedom. The rolling-element variables in this solution are x_1, y_1, γ_t, W_r and W_o.

WHERE:

x_1 is the rolling element axial position

y_1 is the rolling element radial position relative to the outer race.

γ_t is the roller tilt angle about the Z_R axis

W_r is the rolling element rotational speed about the x_R axis

W_o is the rolling element orbital speed.

BEARING FATIGUE LIFE CALCULATIONS

Within SHABERTH, roller bearing raceway fatigue life is calculated using the methods introduced by Lundberg-Palmgren [11]. The life thus calculated is modified by multiplicative factors which account for material and lubrication effects.

To account for non-symmetrical load distributions across a line contact, the roller and raceways are thought as being comprised of a number of sliced discs. Raceway and roller L_{10} fatigue life, in millions of revolutions at a given slice is expressed by:

$$L_{10mk} = \left(\frac{Q_{cmk}}{Q_{emk}}\right)^4 \tag{8}$$

Q_{cmk} is the dynamic capacity of a raceway and roller slice contact pair, defined as the load for which the slice will have a 90 percent assurance of surviving 1 million revolutions. Index m refers to raceway, k refers to slice, n is the index of the last slice, from [11]

$$Q_{cmk} = \frac{49500\ \lambda\{D_k(1\pm\gamma_k)^{1.074}\Delta\ell_{mk}^{0.778}(\gamma_k)^{0.222}}{\{Z(1\pm\gamma_k)\}^{0.25}} \tag{9}$$

m = 1,2 (outer,inner)
λ = 0.61, k=1 or k=n
λ = 1.0 , k=2 →n-1
D_k = slice diameter

$$\gamma_k = \frac{D_k \cos\alpha}{d_{mk}}$$

$\Delta\ell_{m,k}$ = slice width
Z = no. of rollers
d_{mk} = slice pitch dia.
α = contact angle

The upper sign is used for the outer race. the lower sign refers to the inner race. Q_{emk} is the equivalent load for the slice.

$$Q_{emk} = \frac{1}{Z}\left(\sum_{j=1}^{Z} Q_{mkj}^{\varepsilon}\right)^{1/\varepsilon} \tag{10}$$

Q_{mkj} is the individual roller contact load on the k-th slice and $\epsilon = 4.0$ or $\epsilon = 4.5$ depending, respectively, upon whether the applied load rotates or is stationary with respect to the raceway in question.

The L_{10} life of a raceway is given by

$$L_{10m} = a_2 a_3 a_3^* \left\{ \sum_{k=1}^{n} L_{10mk}^{-e} \right\}^{-1/e} \tag{11}$$

where e is the Weibull slope exponent, here taken to be 9/8 for roller bearings.

a_2 is a life improvement factor to account for improved materials.

a_3 is a life improvement factor to account for full film lubrication.

a_3^* is a life adjustment factor which is less than 1 when full film lubrication is not obtained.

The L_{10} life of the bearing considering both raceways is:

$$L_{10} = \left\{ \sum_{m=1}^{2} (L_{10m})^{-e} \right\}^{-1/e} \tag{12}$$

In [12] the form of a reduction factor accounting for the effect of surface asperity interaction was deduced and its parameters were set to best fit to a large body of rolling contact life test data.

As employed in program SHABERTH, the reduction factor (a_3^*) for tenth percentile life L_{10} is calculated as follows:

$$a_3^* = \left[1 + \frac{\psi^2 (h/\sigma)}{\psi(1.5)}\right]^{-1/e} \tag{13}$$

where:

$$\psi(h/\sigma) = \frac{\phi^2(h/\sigma)}{1 - \Phi(h/\sigma)}$$

$\phi(\cdot)$ = density function of standard normal distribution

$\Phi(\cdot)$ = cumulative distribution function of standard normal distribution

$h/\sigma = \Lambda$ = ratio of plateau film thickness to surface roughness for most heavily loaded roller

LUBRICANT FILM THICKNESS

The elastohydrodynamic (EHD) film thickness, h, at each contact is computed as the product of the film thickness predicted by the Archard-Cowking [13] (point contact) Dowson-Higginson [14] (line contact) formulas and two reduction factors ϕ_t and ϕ_s. The factors ϕ_t and ϕ_s account respectively for the reduction in film thickness due to heating in the contact inlet and the decrease in film due to lubricant starvation, i.e., due to the finiteness of the distance between the contact zone and the inlet oil meniscus. In equation form,

$$h = \phi_t \cdot \phi_s \cdot \{h_{\substack{A.C. \\ D.H.}}\} \qquad (14)$$

The Archard-Cowking and Dowson-Higginson film thickness formulas takes the following forms, respectively

$$h_{A.C.} = 2.04 \left[1+\frac{2R_x}{3R_y}\right]^{-0.93} (v\eta V)^{0.74} R^{0.407} (Q/E')^{-.074}$$

$$h_{D.H.} = 1.6.R_x \cdot (vE')^{0.6} \cdot \left(\frac{\eta V}{2E'R_x}\right)^{0.7} / \left(\frac{q}{E'R_x}\right)^{0.13} \qquad (15)$$

R_x, R_y = effective radii of curvature parallel and transverse to the rolling direction

$R = [R_x^{-1} + R_y^{-1}]^{-1}$

v = pressure viscosity coefficient

V = lubricant entrainment velocity

q = maximum load per unit length

Q = load

$E' = 2\left[\frac{1-\nu_1^2}{E_1} + \frac{1-\nu_2^2}{E_2}\right]^{-1}$

η = absolute viscosity

E_1, E_2 = Young's modulus for the contacting bodies

ν_1, ν_2 = Poisson's ratio for the contacting bodies

DESCRIPTION OF ANALYSES

The analyses were implemented in two phases. SHABERTH software was initially applied to the "original" straddle and cantilever pinion designs whose dimensions are given in Tables 1 and 2. The tabultated parameters, along with Figure 1 and Figure 2, specify the geometries of the original designs. These configurations resulted from an analytic study documented in reference [9]. The direct objective for that effort was to create a 400 kw load support system operating at 36,000 rpm and 150°C, whose bearing L_{10} life expectency was 2500 operating hours at 60% of the applied gear load. The load vector (P_x,P_y,P_z)= (-3800,1200,-4800) Newtons defines the nominal gear load vector used in the following material.

A detailed description of the support bearing geometry is given in Figure 5. Note that pairs of these bearings were used for all analyses. Materials were modelled as M-50 tool steel (Young's modulus=$2.04(10)^5 N/mm^2$, Poisson's ratio = .3, weight density=$7.87(10)^{-5} N/mm^3$, Bearing material life factor=5).

A sequence of computations was made at 60, 75, 100 and 150 percent of the nominal applied gear load to quantify design performance over a load spectrum. Conditions of zero preload and line-to-line fits were used , while shaft wall thicknesses of 10% and 100% of the diameter were considered to explore the potential for reduction in mass.

The effects of changing bearing spacing and adjusting pinion location relative to the bearings were also evaluated to minimize assembly mass while maximizing bearing life.

The first phase analyses were completed by investigating the effects of preload and interference fits on the load distributions, bearing rating lives and pinion gear deformations. Preloads were varied from 0.0 to 218.8N to represent existing bearing design practice. The interference fits between the shaft and inner ring (cone), and outer ring (cup) and housing were selected to be 0.01 mm and 0.0 mm, respectively.

In the second phase of the analysis, SHABERTH was executed at Level 1 to evaluate the performance of the original pinion geometries and observe bearing heat generation rates, internal load distribution among rolling elements, centrifugal effects, and film thickness within concentrated contacts over a range of operating speeds (10,000-60,000 rpm) (0.33-2.0 x 10^6DN).

Later on, reference is made to program input defining the roughness of the contacting surfaces and lubricant properties. Center line average (CLA) roughness at the outer race, inner race, roller and flange were selected to be 0.12, 0.14, 0.08 and 0.08μm. RMS asperity slopes were taken as 2°. The lubricant was a MIL-L-23699 oil.

Heat generation rates due to friction at the roller-flange and roller-raceway contacts were computed. Bearing load ratios, rating lives and normal contact loads at the flange and raceways were developed as functions of speed. Finally, EHD film thicknesses and the portion of the contact loads carried by asperities at the flange and raceway contacts were determined.

DISCUSSION OF RESULTS

Results from the phase one series of computer runs are provided in Figures 1-14. Shaft speed and temperature were maintained at 36,000 RPM and 150°C, respectively. Note also that the bearings were mounted back-to-back for the straddle designs and front-to-front for the cantilever designs (see Figures 1 & 2). These orientations provided superior performance within the confines of the design space envelope for the specified loading condition. Only results for these orientations are presented, although test cases were completed considering the reversed mounting arrangements.

Original Pinion Configurations

It is significant to understand the distribution of the gear load vector among the support bearings in order to optimize the life of the design. In particular, it is of interest to flag catastrophic failures such as galling. Such failures could occur due to overstressing of material attributed to unexpectedly large loads. A series of curves providing various bearing load ratios as a function of the applied gear load are presented in Figure 6 to provide design guidance for the particular configurations under investigation.

Specifically, graphs of bearing load ratios (radial/axial for each bearing of a particular design and axial/axial for each design) for various percentages of the gear load are presented for the original straddle and cantilever geometries. These data are for conditions of zero preload, 100% wall thickness (solid shaft) and line-to-line fits.

Comparison of the load ratios for both designs demonstrates that the straddle configuration distributes both radial and axial loads more equally. The axial load ratios (left/right) for the straddle vary from approximately 1.8 to 2.6 with gear load ranging (60-150) percent of the nominal applied load. Cantilever ratios (right/left) are approximately

1.9 to 2.9 over the same load range. The (left/right) bearing radial load ratios, not shown in Figure 6, were computed to be 1.3 and 2.4 for the straddle and cantilever, respectively, over the entire range of gear loads.

The tapered rolling element bearing's coupling of radial and axial loads is seen to produce an axial load equilibrium distribution which significantly amplifies the applied thrust gear load for the bearing opposing the axial gear load. Using the axial load ratios given in Figure 6 and considering axial equilibrium, the thrust carried by the left bearing of the straddle is computed to be 2.25 times the applied thrust at 60% of the nominal gear load. This reduces to 1.63 times the applied thrust at the 150% load level. The corresponding factors for the right bearing of the cantilever design are 2.1 and 1.53 at the 60% and 150% load levels, respectively. As the gear load increases, the bearing carries more of the applied load as radial load.

Radial/axial load ratios increase markedly over the specified load range for both designs highlighting the system's nonlinear character. The lightly loaded (right) bearing for the straddle shows an 83% increase. This ratio more than doubles for the left bearing of the cantilever.

L_{10} lives are presented as a function of gear load for both geometries in Figure 7. Each configuration shows, as expected, continuously decreasing life with increasing gear load. Bearing life for the life-limiting right bearing of the cantilever decreased 91% from 3448 hrs. for the gear load range of (60-150) percent of nominal. The straddle design demonstrates approximately 30% greater limiting bearing rating life at all load levels. In the cantilever design, the life-limiting bearing location switches shaft position

at an applied load level between 60% and 75% of nominal. The magnification of the applied thrust load imposed on the left bearing reaches a maximum (110%) at the minimum applied load (Figure 6), explaining its shorter lifespan at the 60% load level.

The preceding cases were also run using a hollow shaft (10% wall thickness). The large variation in wall thickness was found to have a small (<5%) effect on the load distributions and bearing life performance. This is due to the short, stocky nature of the shaft and the associated small deformations. A significant shaft weight savings is obtained by taking advantage of this result. The availability of a hollow shaft provides inner race lubrication design flexibility.

Deformations at the point of load application are compared for the cantilever and straddle designs in Figure 8. Ratios (straddle/cantilever) of displacements and rotations show the straddle enjoys a significant advantage, except for the axial displacements, which are approximately the same magnitude. Ratios of radial displacements range from 0.37 at 60% nominal load to 0.54 at 150% nominal load. Pinion rotations (γ_h, γ_v) vary from (0.25, 0.05) to (0.4, 0.09), respectively, over the given load spectrum.

In Figure 9, the effect of shaft wall thickness on the deformation of the pinion is evaluated for both designs at the 60% and 100% load levels. Ratios (100%/10% wall thickness) of displacement and rotations are insensitive to these shifts in load for both designs.

Horizontal rotations for the straddle exhibit the maximum percent change (~8%). The cantilever rotations are affected more by changes in shaft wall thickness than those of the straddle. At 60% nominal load, the horizontal rotation ratios are .47 and .63, respectively, for the cantilever and straddle. This trend reverses for the radial displacement ratios.

Alternate Configurations

Alternate bearing-shaft configurations were considered. The effects of changing bearing spacing and adjusting the pinion location relative to the bearings were evaluated. Referring to Figure 1 and Figure 2, the specific geometries considered are defined in Table 1 and Table 2. Shaft wall thicknesses of 10%, line-to-line fits and a 60% load level were employed to develop these data.

Closer bearing spacings and/or shorter span lengths degraded bearing rating life for both the straddle and cantilever geometries. Limiting bearing rating life for alternate cantilever designs (cases 1 and 2) decreased by 8% and 48%, respectively, from the original design life of 3388 hrs. In these designs, the overhang increased but the overall length was held fixed. The straddle design with the asymmetric pinion gear location (case 3) demonstrated a decrease in life of 4% from the original design value of 4434 hrs. This was expected, since the applied gear loads are distributed less equally among the support bearings.

Limiting bearing rating life versus percent decrease in bearing spacing is displayed in Figure 10 for the straddle (cases = 0, 1, 2, 4) and cantilever (cases = 0, 3, 4, 5) designs. These alternates were obtained by reducing shaft length between the bearings. A 44% decrease in bearing spacing is seen to reduce bearing life by approximately 11% for the straddle and 8% for the cantilever. Comparing the straddle (cases=1,2) and cantilever (cases=0,3), respectively, it is noted that the straddle configuration provides greater limiting bearing rating life (~25%) than the cantilever geometry for identically sized arrangements.

Radial displacement versus percent decrease in bearing spacing is presented in Figure 11 for these same designs. Cantilever deflection increases 7% for the corresponding 44% decrease in spacing. A similar result was reported in [8] for cantilever designs with short spans, where bearing deflection controls pinion motion. An opposite trend is displayed for the straddle where the shaft, stiffened by a decrease in length, dictates pinion deflection. Straddle radial deflection decreases 27% for a 44% decrease in bearing spacing. Since the gear deflection in the cantilever design is controlled by the bearing deflection, this explains why the cantilever radial displacement was less sensitive than the straddle to shaft wall thickness (Figure 9).

Preload and Fits

The influence of preload and interference fits on bearing life performance is illustrated in Figure 12 and Figure 13 for the original straddle and cantilever designs. These graphs of bearing rating life versus preload with 0.0 mm (line-to-line) and 0.01 mm interference fits are for a preload range (0.0 - 218.3) N. Shaft wall thicknesses are 10% for the straddle and cantilever configurations. Gear loads are 60% of the nominal applied load.

It is interesting to note that, for each design with a line-to-line fit condition, the bearing not opposing the applied thrust has a dramatic increase in life with increase in preload before the life decays. The life of the companion bearing decreases monotonically. The straddle shows a 153% increase in life over the preload range (0-78) N. The corresponding increase for the cantilever is 920%.

A similar effect was documented by Taha, et al, [8] for a cantilever geometry. The behavior is associated with the number of rollers sharing the load. In Figure 14, roller loads are plotted for the straddle at preloads of 0.0 N and 78.0 N, respectively. The 78.0 N preload forces 15 of the 19 rollers to carry the gear load, as opposed to 5 rollers at zero preload, so that initially there is an increase in life. As the preload continues to increase above 78 N the roller loads become life-limiting. This phenomenon could possibly be exploited to reduce design mass and volume requirements by specifying use of a smaller bearing in place of the bearing that experiences increased life. At the interference fit of 0.01 mm, all the rollers are loaded. Therefore, the bearing life decreases with increasing preload.

Lubrication and Friction Effects

The remaining computation results detail the effects of lubrication and friction on the performance of the pinion. These data evolved using the original straddle and cantilever designs with 10% wall thickness and a 60% gear load level. The interference fits between the cone and shaft was 0.01 mm. A constant operating temperature of 150°C was specified, since this represents an upper limit. Preload was set at 43.1 N.

In Figure 15, radial/axial bearing load ratios are given for the left bearing of the straddle and right bearing of the cantilever as functions of speed. The torque on the pinion was constant. Since all rollers are loaded, the centrifugal forces on the rollers do not affect the resultant radial load. However, the axial load increases producing approximately 56% reductions in the load ratios for the straddle and cantilever designs over the speed range (10,000-60,000 RPM) (0.33-2.0 x 10^6 DN).

L_{10} lives for these bearings are displayed in Figure 16. Comparison with previous results demonstrated a marked decrease in life, more than 50% , at the 36,000 rpm operating speed. Life adjustment factors (a_3^* in Eq. (13)) were computed to be less than 0.5 and account for this result. This indicates a failure to generate an adequate separating elastohydrodynamic film. Causes for an inadequate EHD film are: (1) a drastic reduction in lubricant viscosity from 28 centistokes at 37.8°C to 2.6 centistokes at the specified operating temperature of 150°C, (2) insufficient replenishment layer thickness (i.e., starved contact).

It is noted that most of the decrease in life up to 36,000 rpm shown in Figure 16 is simply the conversion from life in revolutions to life in hours. However, the knowledge of life in hours is more significant for this particular application since it is the survival time of the helicopter which is of interest.

The rate at which energy is dissipated as heat (HGR) by the bearings is tabulated as a function of speed in Figure 17 for the straddle design. The sum of the bearing losses ranges from 1.1% to 4.7% of the total power transmitted by the pinion over the speed spectrum.

The distribution of power loss within the bearing complement is illustrated graphically in Figure 17. Percentages of bearing total HGR produced at the outer ring, inner ring and flange contacts are presented as functions of speed for both bearings of the straddle. Cantilever results were virtually identical, where the roles of the left and right bearings are reversed.

The primary heat generation contribution comes, as expected, from the flange contact. The majority of the remaining heat is generated at the raceways. Flange contacts account for approximately 55% of bearing HGR at all speeds. Inner ring HGR's vary from 15% to 5% over the speed range (10,000-60,000 rpm). Rolling element drag, cage-roller and cage-land interactions are the remaining sources of power loss. These results indicate the potential for sharp thermal gradients within the bearings.

EHD film thicknesses at the outer ring, inner ring and flange contacts are shown in Figure 18 as functions of speed. These data correspond to the maximum loaded roller of the left bearing of the straddle. Analogous results were obtained from studies of the cantilever arrangement.

Film thicknesses at both raceways increase approximately 200% over the entire speed range. The increase at the outer race is due to increased lubricant entrainment velocity counteracting a reduction caused by increased contact load. This trade-off is characterized analytically in Eq. (15). The flange film thickness increases 43% for the speed range (10,000-36,000rpm). Above this speed, increasing contact force due to the centrifugal effects causes a slight reduction (13%) in the film at 60,000 rpm.

Note that at the lower rotational speeds (20,000 rpm), the EHD film thicknesses are about the same magnitudes as the input values for CLA surface roughnesses. This observation, together with the symptom of low life adjustment factors, expresses the inability of the lubricant to produce an adequate separating film. The percent of load carried by the asperities (Figure 20) at the contacts quantifies this problem further.

Graphs of normal loads as a function of rotational speed at these contacts are shown in Figure 19. At 60,000 rpm, the load at the inner race decreases by 7.3% from the value 820 N at 10,000 rpm. For this speed range, the loads at the outer race and flange increase by 100% and 400%, respectively.

As a complement to Figure 18 and Figure 19, the fraction of total contact load carried by the asperities versus speed is presented in Figure 20. The SHABERTH asperity contact model is based on the work of Tallian [15]. At 10,000 rpm, the asperities carry nearly all the load at the flange and approximately 70% at the races. This reduces to 50%, 20% and 8%, for the flange, inner race and outer race, respectively, at 60,000 RPM. Typically, the load borne by elastic deformation of asperities is a small percentage (<5%) of the total, the remaining load being carried by the EHD film.

It is noted once again, that this analysis was made for a constant operating temperature of 150°C. Thus, for safe operation of this bearing in this range of speed and load conditions, some lower temperature must be maintained and more lubricant supplied to the various contacts.

SUMMARY AND CONCLUSIONS

An analysis and series of computerized computations were carried out to explore competing prototype design concepts of a shaft and (.33-2.0 x 10^6 DN) tapered-roller bearing system to support the input pinion of an advanced commercial helicopter transmission. The results were used to evaluate designs for, both, a straddle arrangement where the pinion gear is located between the bearings, and a cantilever arrangement where the pinion is outboard of the two bearings.

Effects of varying parameters including applied gear load, preload, wall thickness, interference fits, bearing spacing and pinion gear location on system rigidity, load distribution and bearing rating life were explored.

A comparison of the bearing load distributions for these designs demonstrated that the straddle more equally distributes both radial and axial loads. This impacted bearing rating life, wherein the straddle exhibited superior performance. Analyses of alternate designs reiterated this conclusion by demonstrating increased L_{10} life (25%) for the straddle compared to the cantilever for identically sized arrangements.

Deformations at the point of load application were also monitored. The straddle enjoyed a significant advantage over the cantilever at all load levels. As in [8], consideration of alternate cantilever designs with reduced bearing spacing, demonstrated the existence of an optimum spacing with respect to pinion deflection. This same effect was not exhibited by the straddle. Radial deflection decreased with decreasing bearing spacing.

The influence of preload on bearing life performance illustrated a marked increase in life over a substantial preload range for the bearing not opposing the applied thrust. Use of a smaller bearing in its place represnets a potential means to conserve design mass and volume. The L_{10} life for the thrust carrying (life-limiting) bearing decreased monotonically with increased preload.

Effort was expended to detail the performance of these designs over a range of shaft rotational speeds with lubrication and friction effects included.

Resulting L_{10} lives for both designs illustrated that the proposed lubricant scheme precipitated reduced performance at the specified operating temperature. Life adjustment factors less than 0.6 were computed at the roller-race contacts at all shaft speeds because of thin films caused by low operational lubricant viscosities (and insufficient replenishment layer thickness). Ratios (Λ) ranged from 0.56 - 1.74 for these contacts over the speed range (10,000 - 60,000 rpm).

The current analysis was performed without the benefit of an interacting thermal analysis which couples the load support system with its thermal environment. The sensitivity of the design performance to preload, coupled with the potential for large thermal gradients and high heat generation rates predicted by analysis, indicates the merits of a future examination which takes proper account of interacting bearing and system generated heat sources.

ACKNOWLEDGEMENT

The authors thank NASA Lewis Research Center, Cleveland, Ohio, for their permission to publish this work, portions of which were carried out under Contract No. NAS3-20839. A debt of gratitude is acknowledged to Mr. R. J. Parker of NASA Lewis Research Center as well as our colleagues at SKF Industries for their helpful discussions and constructive criticisms. Particular thanks are extended to Messrs. F. R. Morrison, M. A. Ragen and R. J. Kleckner.

REFERENCES

1. Thompson, W. S. and Pirvics, J., "Methodology for Performance Prediction of a Helicopter Transmission Under Oil Starvation," to appear in, The Proceedings of the 1978 JTCG/AS Third Biennial Aircraft Survivability Simposium.

2. Morrison, F. R., et al, "A Functional Evaluation of a Thrust Carrying Cylindrical Roller Bearing Design," ASME Paper No. 78Lub28.

3. Connors, T. F. and Morrison, F. R., "Feasibility of Tapered Roller Bearing for Main-Shaft Engine Applications," USAAMRDL Technical Report 73-46, Eustis Directorate, U.S. Army Air Mobility Research and Development Laboratory, August 1973.

4. Parker, R. J. and Signer, H. R., "Lubrication of High Speed, Large Bore Tapered-Roller Bearings," ASME Journal of Lub. Tech., Vol. No.1, 1979, p.31

5. Lemanski, A. J., Lenski, J. W., Jr., Drago, R. J., "Design Fabrication, Test and Evaluation of Spiral Bevel Support Bearings (Tapered Roller)," USAAMRDL Technical Report 73-16, Eustis Directorate, U.S. Army Air Mobility Research and Development Laboratory, June 1973, AD769064.

6. Cornish, R. F., et al, "Design Development and Testing of High Speed Tapered Roller Bearings for Turbine Engines," AFAPL-TR-75-26, U.S. Air Force Aero Propulsion Laboratory, Wright-Patterson Air Force Base, July 1975.

7. Andreason, S., "Load Distribution in a Taper Roller Bearing Arrangement Considering Misalignment," Tribology (London), Vol. 6, No. 3, June 1973, pp. 84-92.

8. Taha, M. M. A., et al, "The Rigidity and Performance of a Helicopter Gearbox With a Cantilevered Housing and Two Taper Roller Bearings," ASME Publication 77-DET-103.

9. Gassel, S. S., "Development of a Small Bore, High Speed Tapered Roller Bearing, Task I - Bearing-Shaft Analysis," SKF Report No. AL79P004, January 1979.

10. Crecelius, W. J., Research Report User's Manual for SKF Computer Program, "SHABERTH, for the Steady State and Transient Thermal Analysis of Shaft Bearing Systems Including Ball, Cylindrical and Tapered Roller Bearings," SKF Report No. AL77P015, developed under U.S. Army Contract DAAD05-75-C-0747.

11. Lundberg, G. and Palmgren, A., "Dynamic Capacity of Rolling Bearings," Engineering Series 1, Proceedings of the Royal Swedish Academy of Engineering, Vol. 2, No. 4, 1952.

12. McCool, J. I., et al, "Interim Technical Report on Influence of Elastohydrodynamic Lubrication on the LIfe and Operation of Turbine Engine Ball Bearings," SKF Report No. AL73P014, submitted to AFAPL and NAPTC under AF Contract No. F33615-72-C-1467, Navy MIPR No. M62376-3-000007, October 1973.

13. Archard, J. and Cowking, E., "Elastohydrodynamic Lubrication at a Point Contact," Proc. Inst. Mech. Eng., Vol. 180, Part 3B, 1965-1966, pp. 47-56.

14. Dowson, D. and Higginson, G., "Theory of Roller Bearing Lubrication and Deformation," Proc. Inst. Mech. Engr., London, Vol. 177, 1963, pp. 58-69.

15. Tallian, T. E., "The Theory of Partial Elastohydrodynamic Contacts," Wear, 21 (1972) pp. 49-101.

LIST OF TABLES

Table 1: Geometry of Alternate Straddle Designs

Case No.	L_1 (mm)	L_2 (mm)	L_t (mm)
Original	27.18	27.18	98.816
1	20.823	20.823	86.106
2	18.156	18.156	80.772
3	8.636	45.974	98.816
4	15.240	15.240	74.94

L_b = 22.23 mm

R_o = 16.67 mm

R_i = 15.00 mm

Table 2: Geometry of Alternate Cantilever Designs

Case No.	L_1 (mm)	L_2 (mm)	L_3 (mm)	L_t (mm)
Original	77.47	55.24	0.	86.106
1	77.47	55.24	5.334	86.106
2	77.47	55.24	24.384	86.106
3	72.136	49.906	0.	80.772
4	69.38	47.15	0.	78.016
5	66.77	44.54	0.	75.406

LIST OF FIGURES

LIST OF FIGURES (CONTINUED)

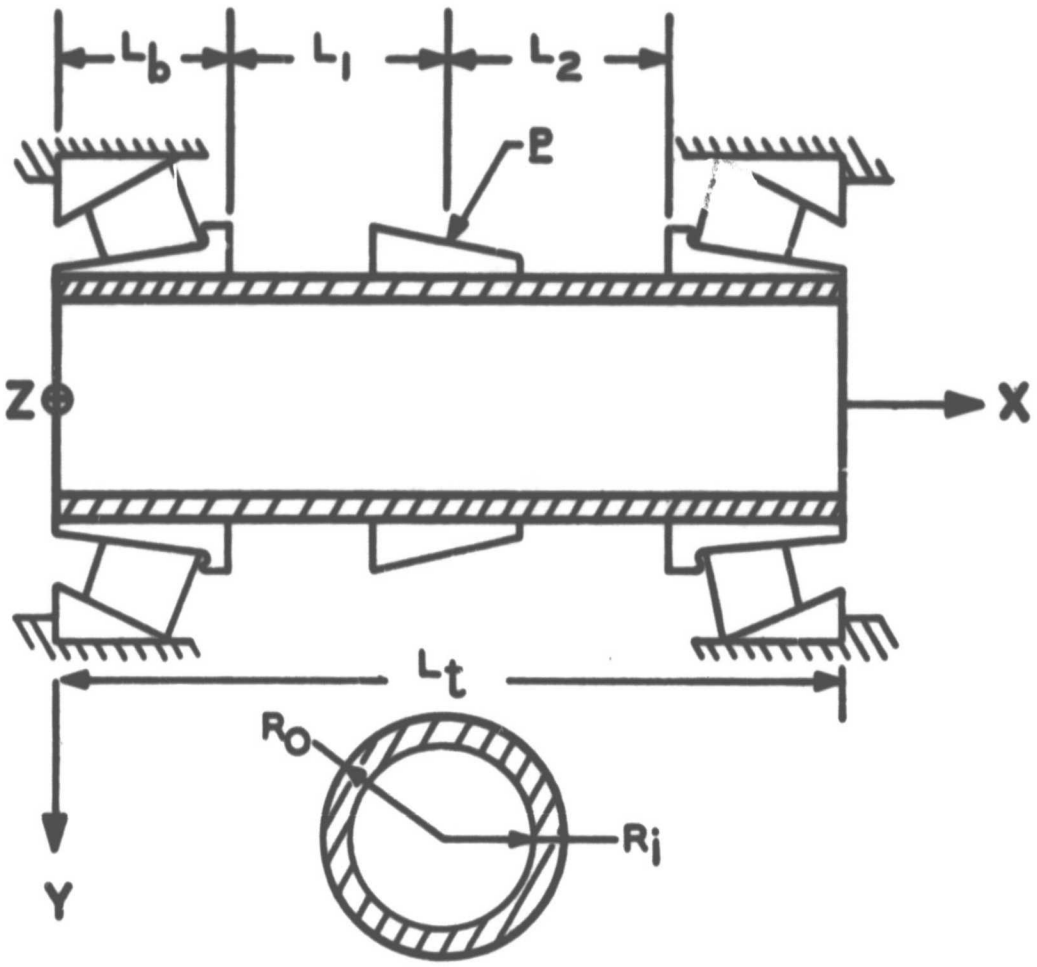

SHAFT SECTION

NOMENCLATURE

- $\underline{P}$ = PINION GEAR LOAD VECTOR
- L_b = BEARING WIDTH
- L_1, L_2 = DISTANCE FROM CONE BACK FACE OF BEARING TO POINT OF LOAD APPLICATION
- L_t = TOTAL LENGTH OF SUPPORT SYSTEM
- R_o, R_i = OUTER, INNER SHAFT RADII

SIGN CONVENTION

POSITIVE FORCES, MOMENTS, DISPLACEMENTS AND ROTATIONS ARE IN POSITIVE DIRECTIONS OF X, Y, Z AXES

FIGURE NO.1 GEOMETRY OF STRADDLE PINION

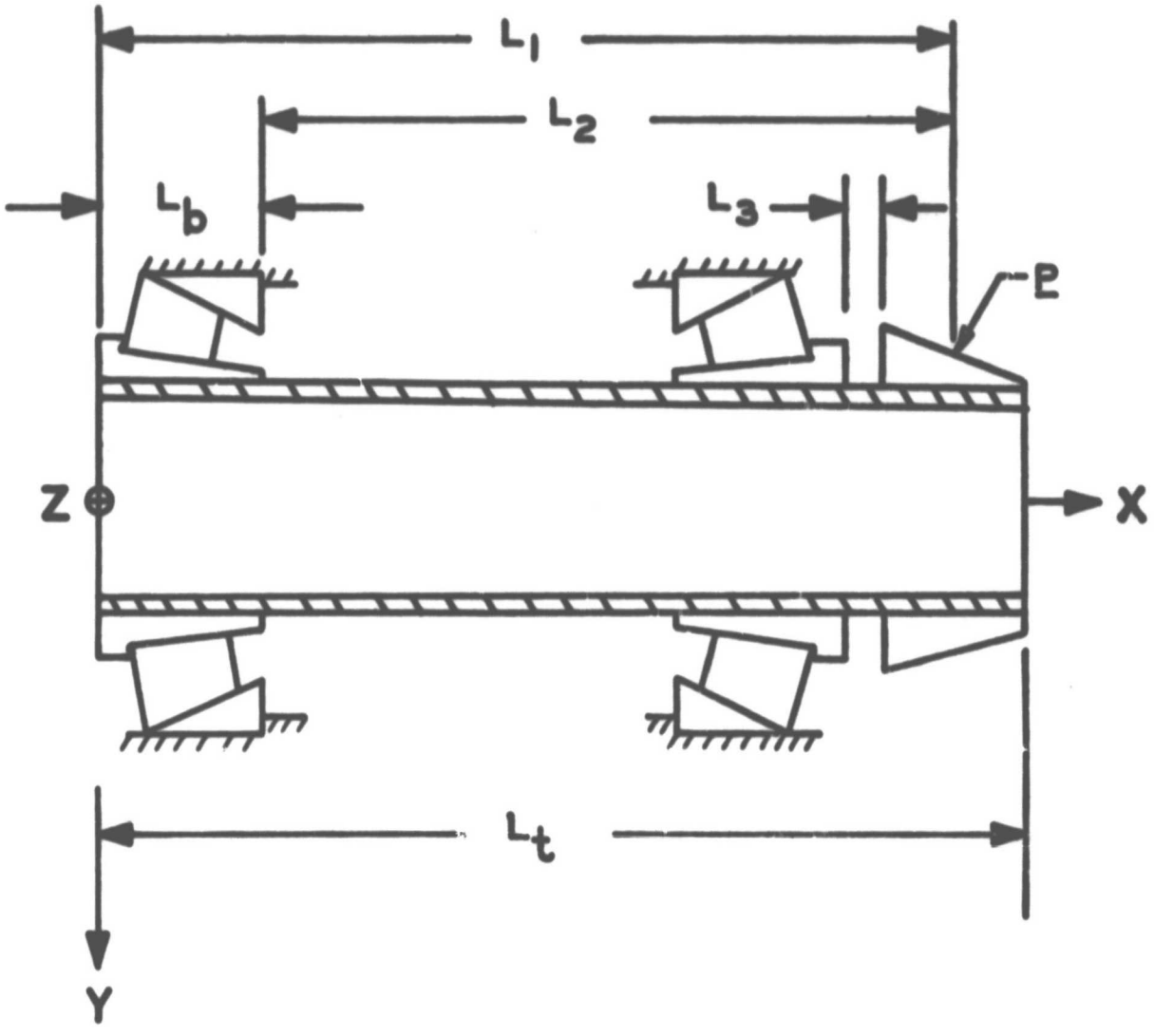

NOMENCLATURE

L_2 = (REPLACES) L_1 FOR BEARINGS ORIENTED BACK TO BACK.

ALL OTHER PARAMETERS DEFINED AS PER FIQURE 1.

FIGURE NO. 2 GEOMETRY OF CANTILEVER PINION

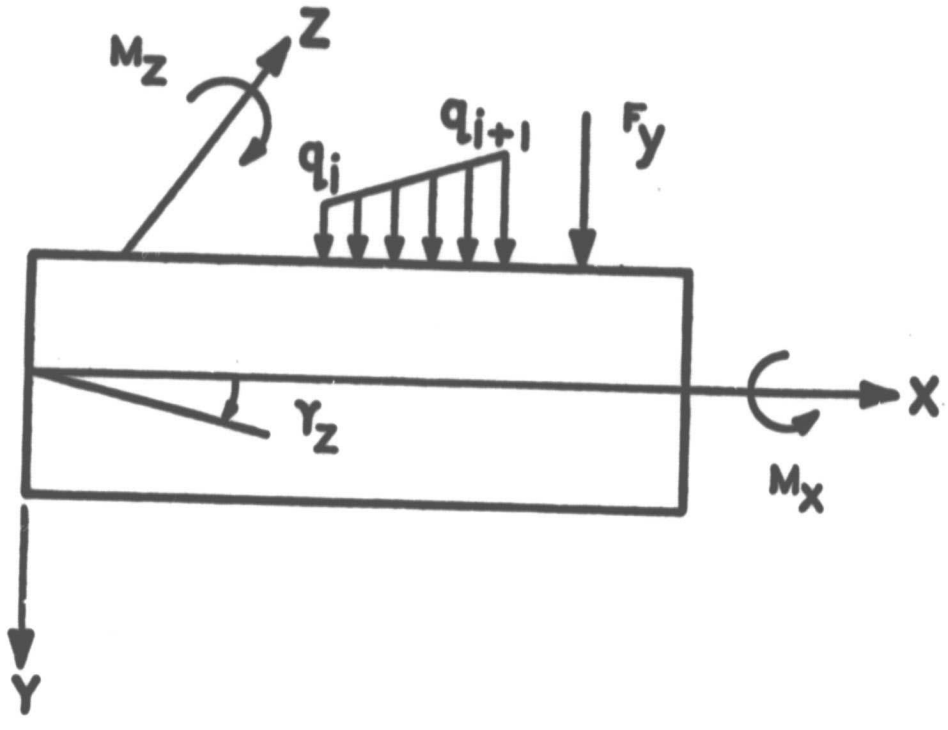

FIGURE NO. 3 SHAFT CORRDINATE SYSTEM AND SHAFT BEARING

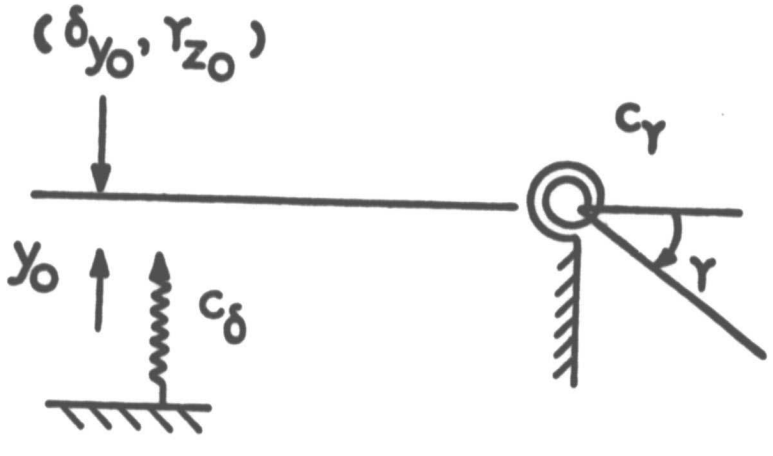

FIGURE NO. 4 SCHEMATIC-SHAFT SUPPORTS

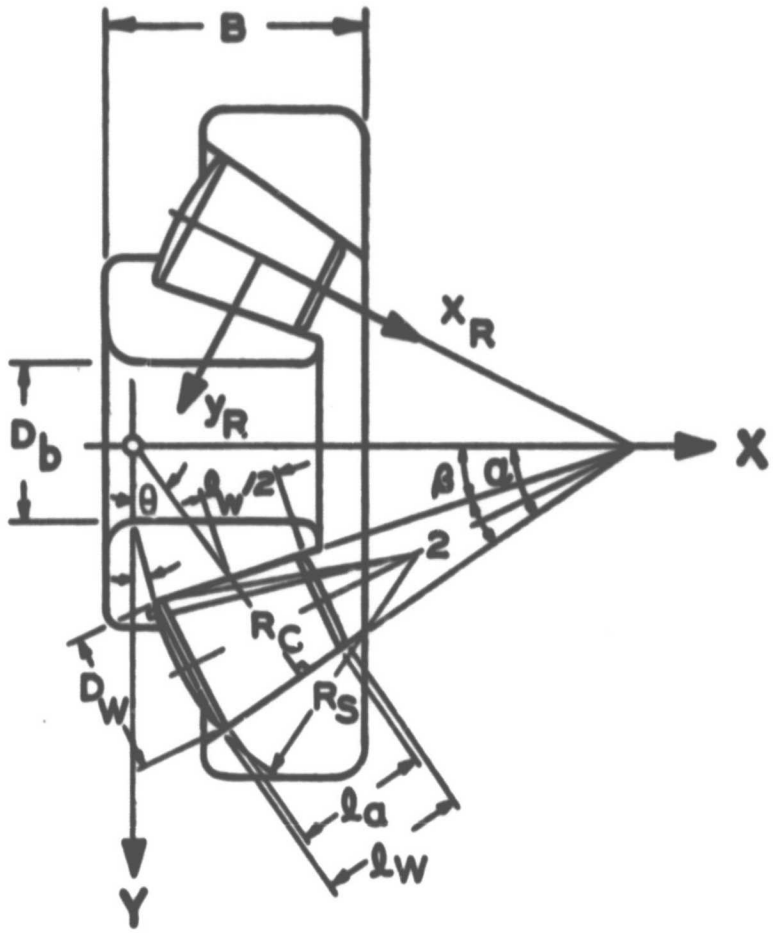

PARAMETER	
α	20°
β	15.05°
θ	15.55°
2ε	4.95°
R_S	87.38 MM
R_C	4500.88 MM
ℓ_w	16.32 MM
ℓ_a	15.80 MM
D_W	7.94 MM
D_b	33.34 MM
B	22.23 MM

FIGURE NO. 5 TAPERED ROLLER BEARING CHARACTERISTIC GEOMETRICAL DIMENSIONS

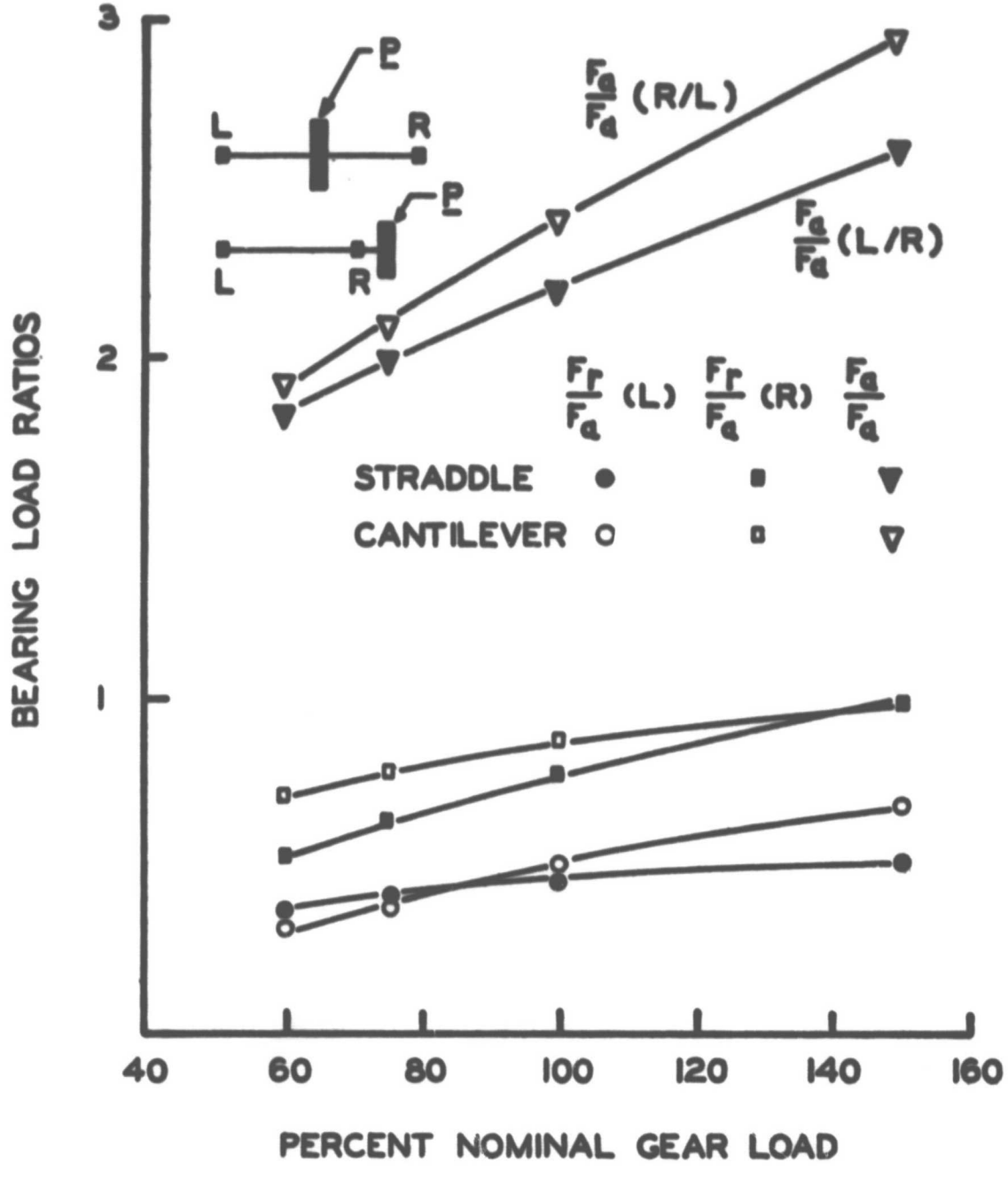

FIGURE NO. 6 BEARING LOAD RATIOS VERSUS PERCENT NOMINAL GEAR LOAD FOR ORIGINAL DESIGNS

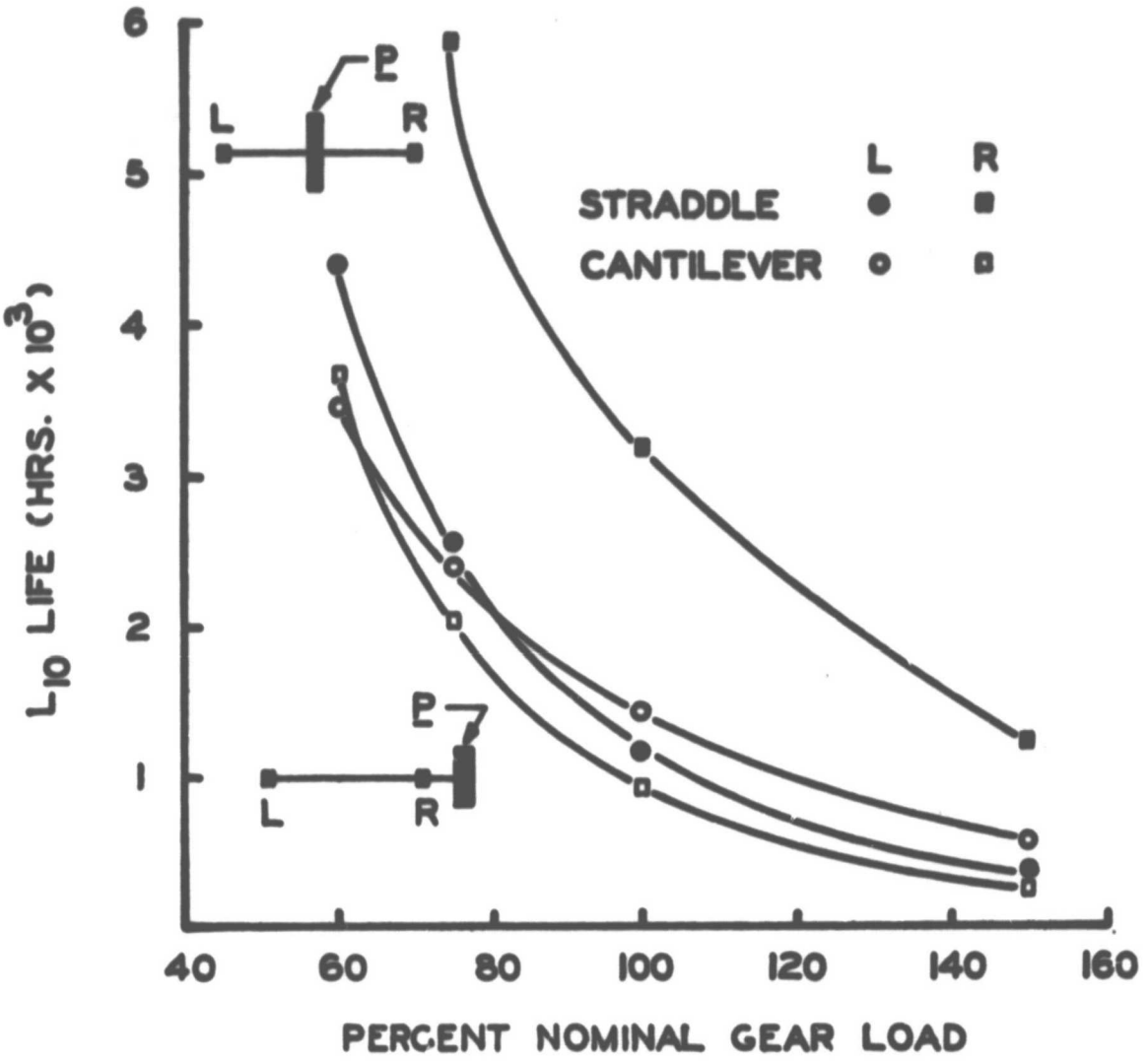

FIGURE NO. 7 L_{10} LIFE VERSUS PERCENT NOMINAL GEAR LOAD FOR ORIGINAL DESIGNS

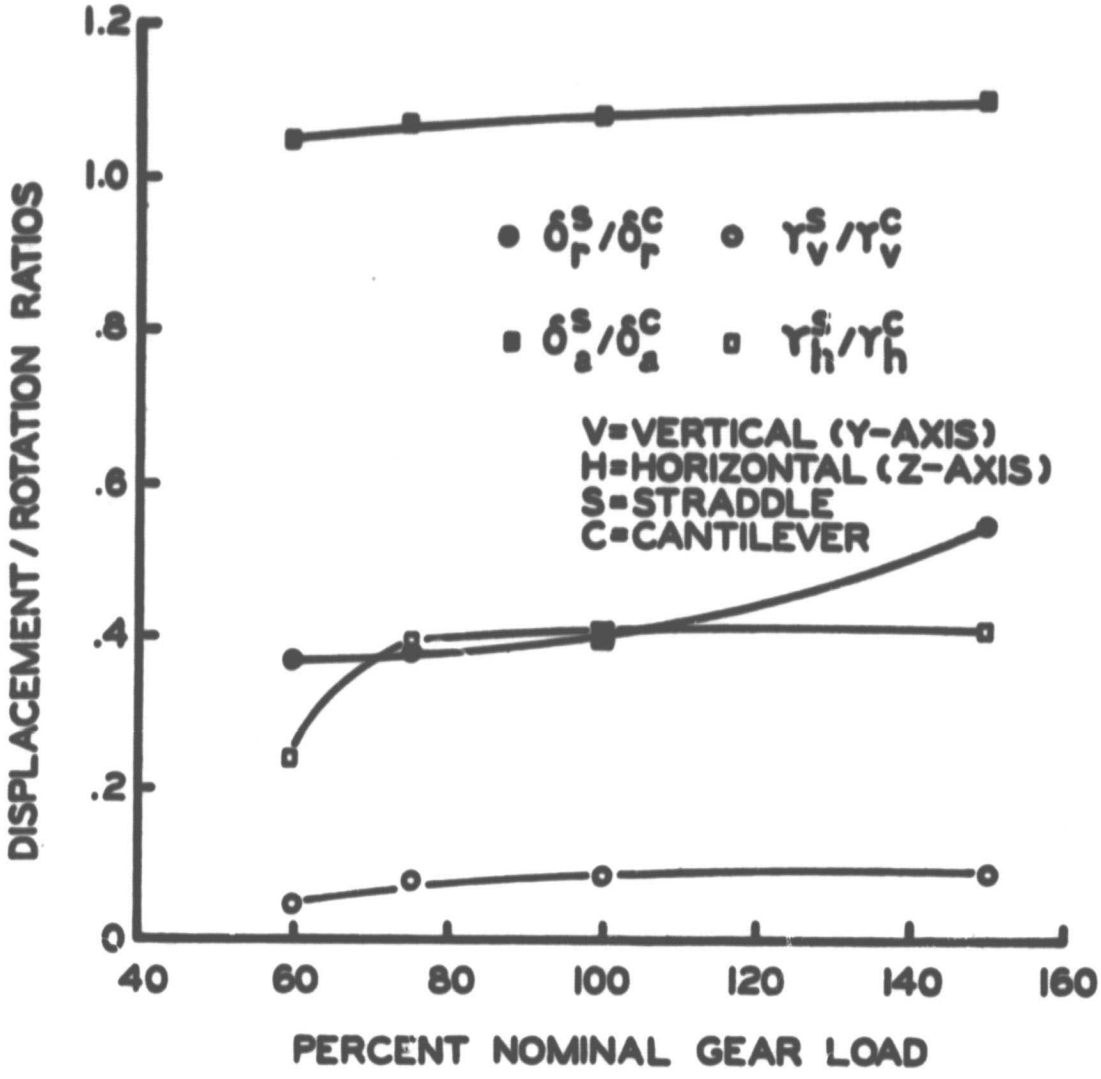

FIGURE NO. 8 DISPLACEMENT AND ROTATION RATIOS (S/C) AT POINT OF LOAD APPLICATION VERSUS PERCENT NOMINAL GEAR LOAD FOR ORIGINAL DESIGNS

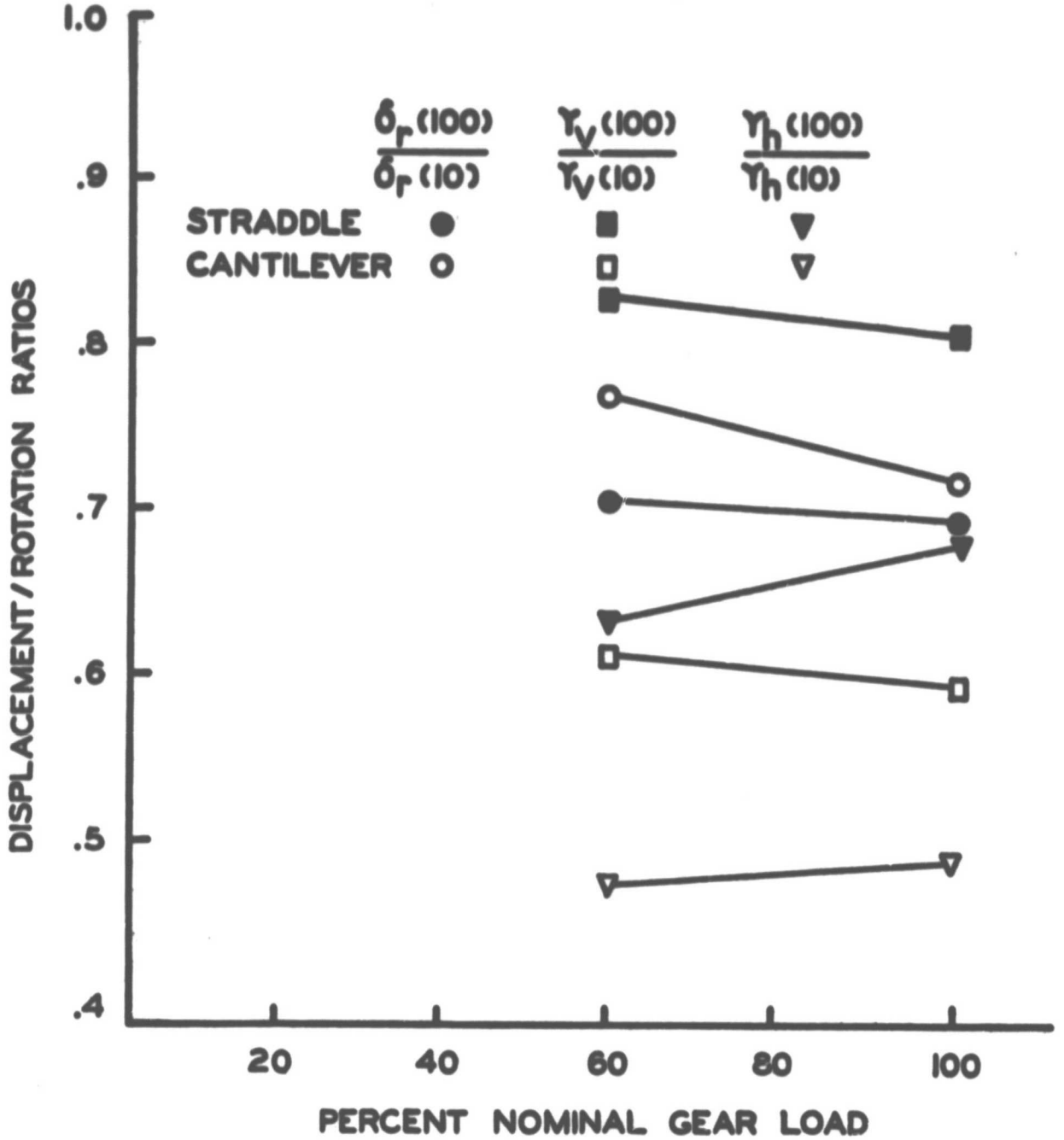

FIGURE NO. 9 DISPLACEMENT AND ROTATION RATIOS (100% WALL THICKNESS/10% WALL THICKNESS) AT THE POINT OF LOAD APPLICATION FOR THE ORIGINAL STRADDLE AND CANTILEVER DESIGNS VERSUS PERCENT NOMINAL GEAR LOAD

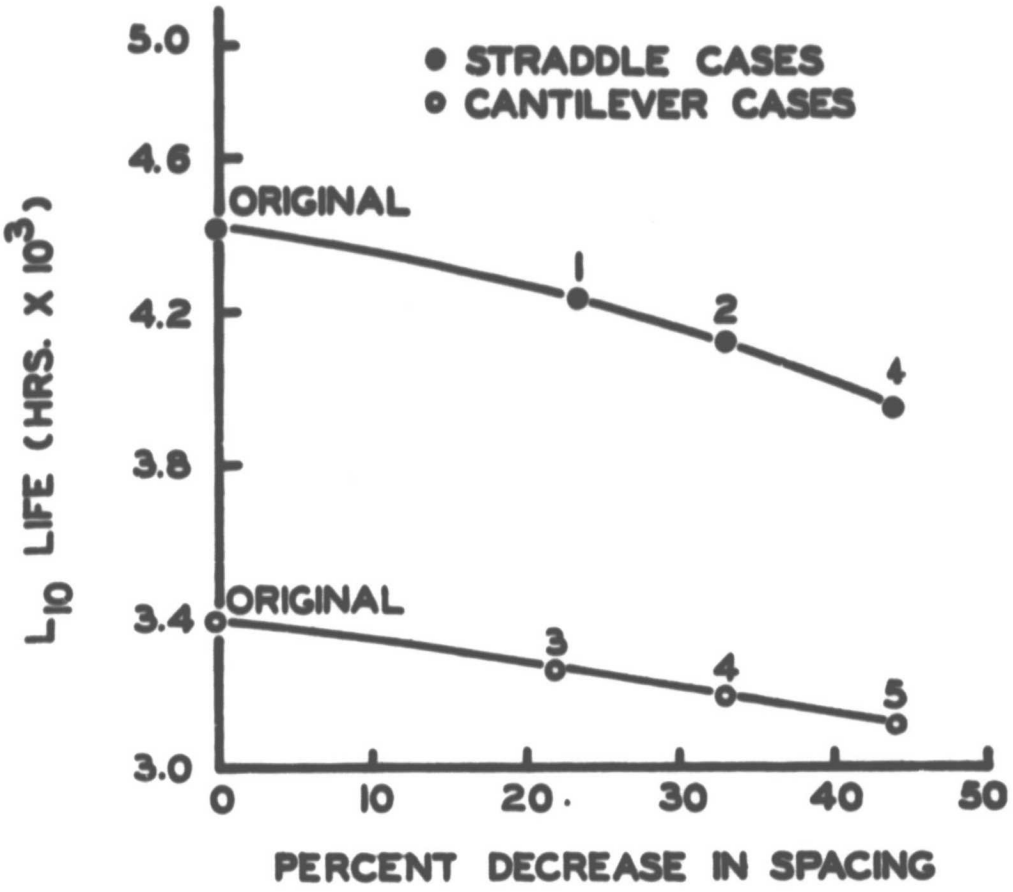

FIGURE NO. 10 LIMITING BEARING RATING LIFE VERSUS PERCENT DECREASE IN BEARING SPACING

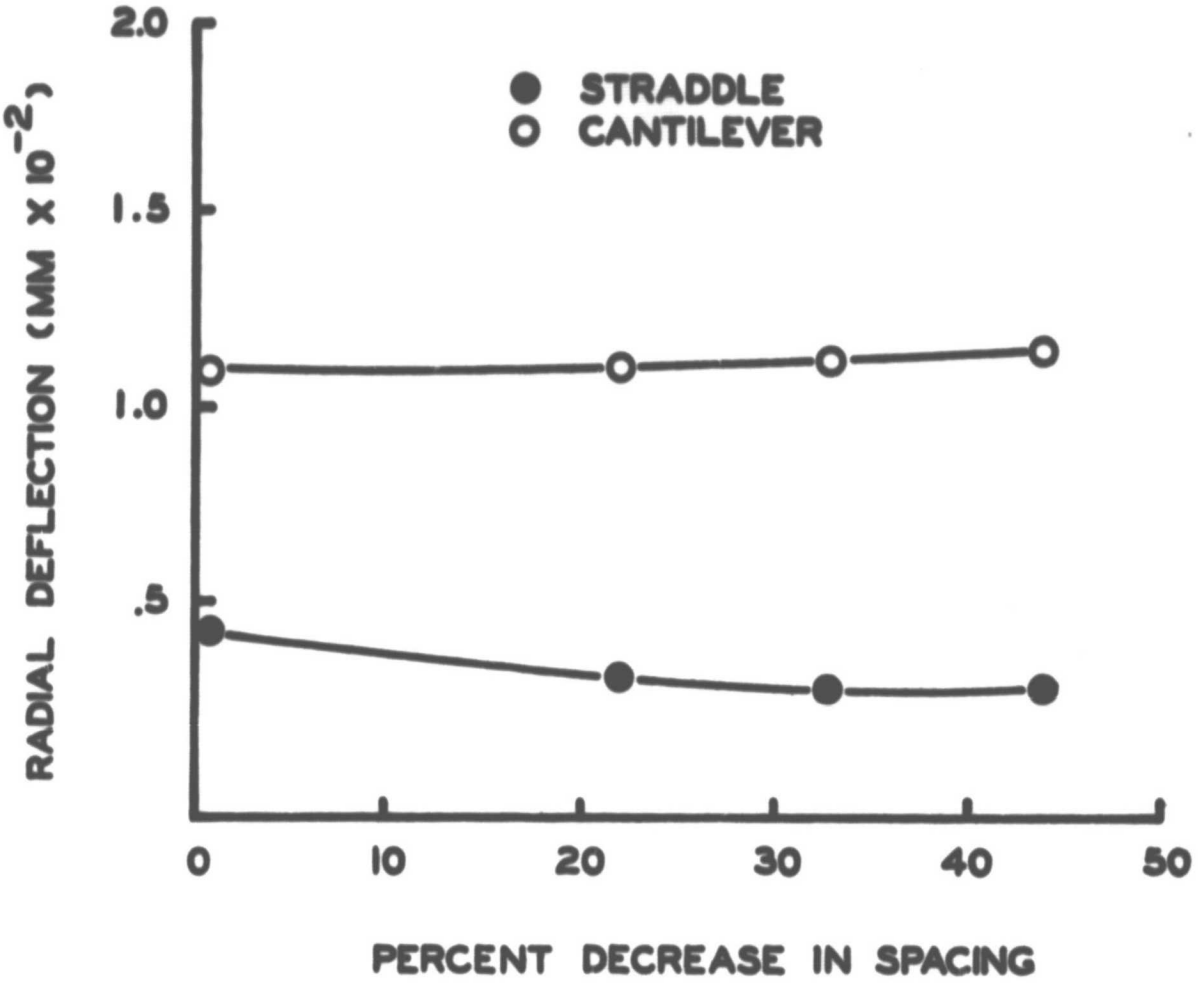

FIGURE NO. 11 RADIAL DEFLECTIONS AT THE POINT OF LOAD APPLICATION VERSUS PERCENT DECREASE IN BEARING SPACING

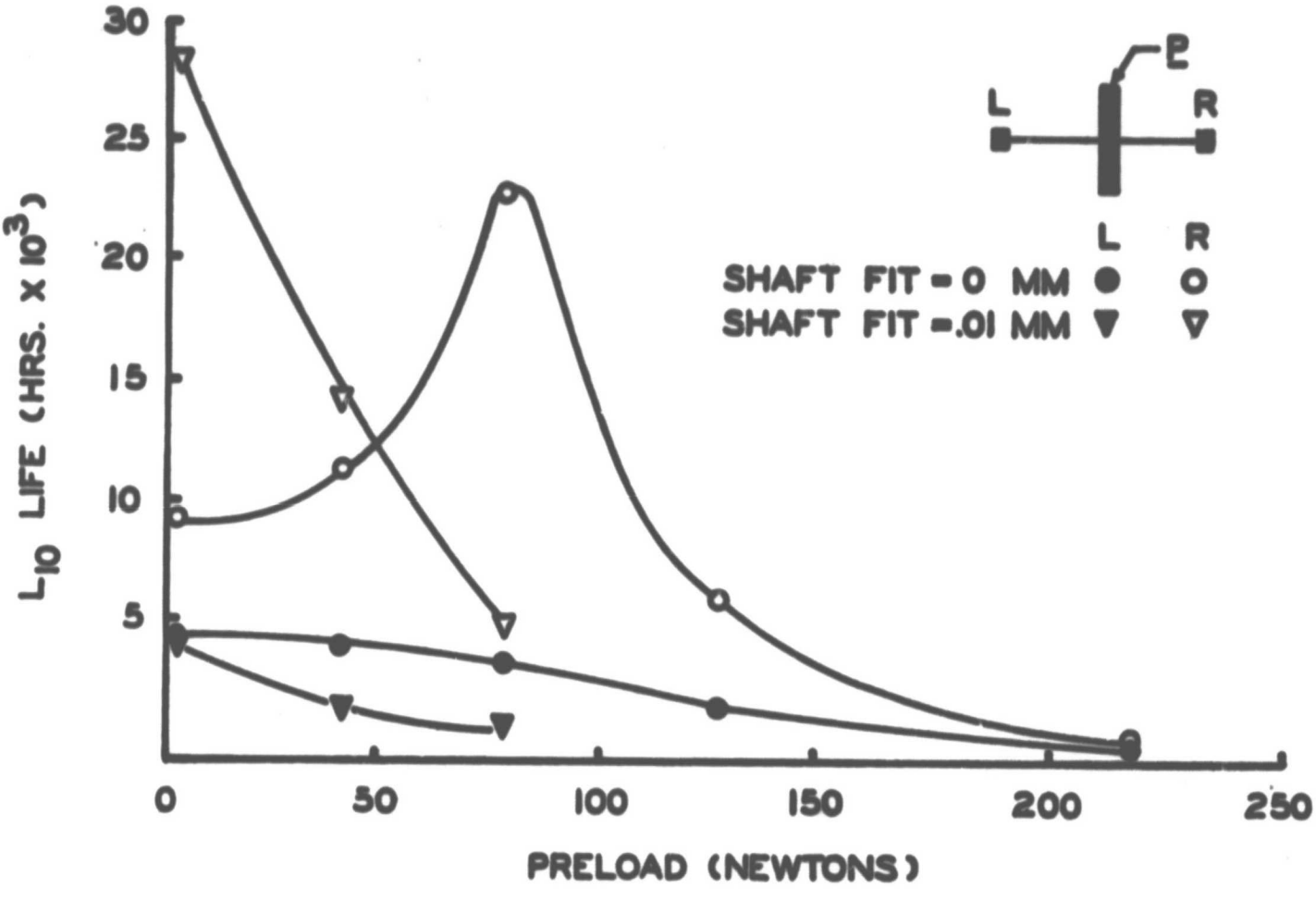

FIGURE NO. 12 BEARING RATING LIFE VERSUS PRELOAD FOR SHAFT INTERFERENCE FITS OF 0. MM AND .01 MM - ORIGINAL STRADDLE

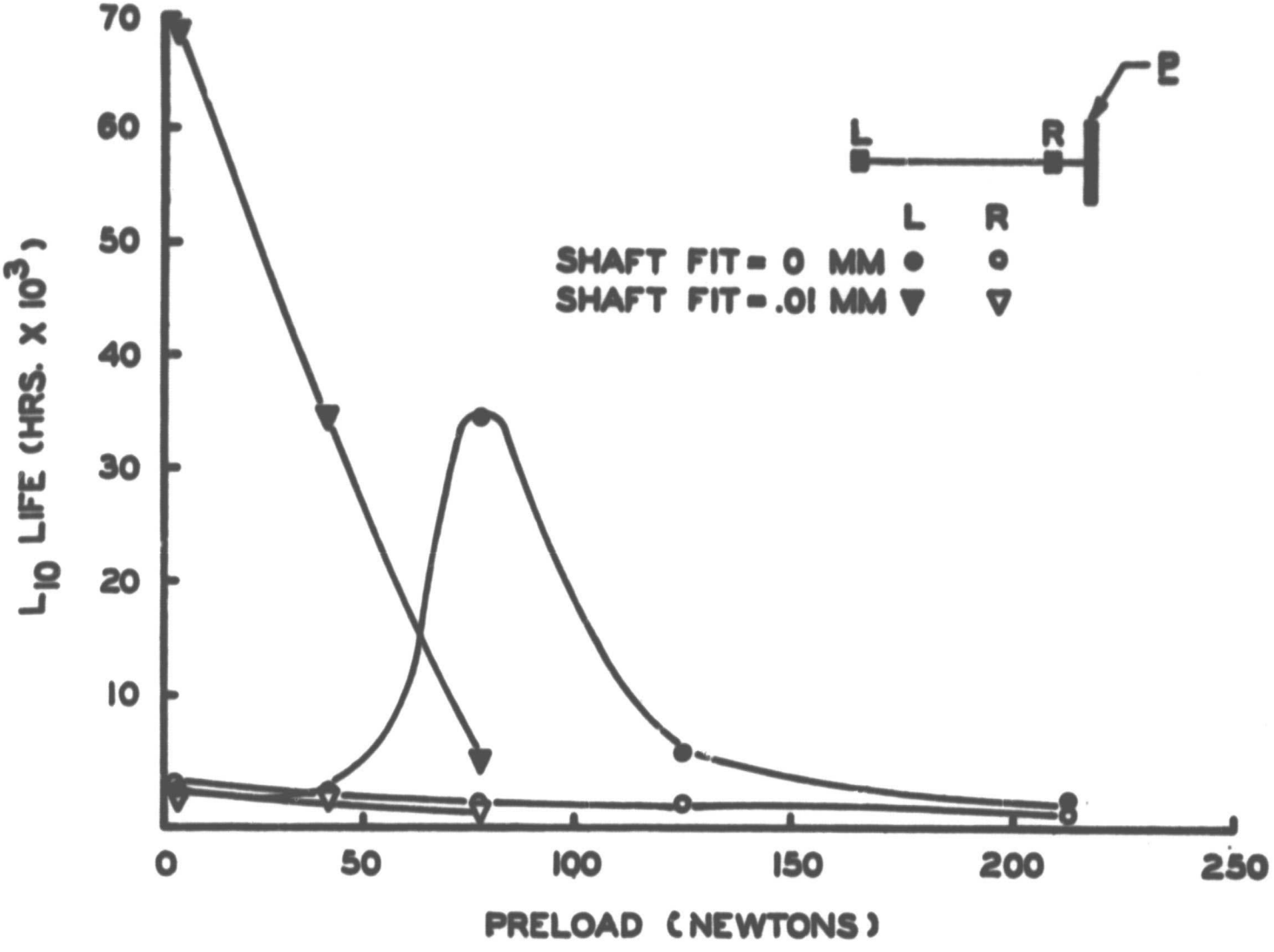

FIGURE NO. 13 BEARING RATING LIFE VERSUS PRELOAD FOR SHAFT INTERFERENCE FITS OF 0. MM AND .01 MM - ORIGINAL CANTILEVER

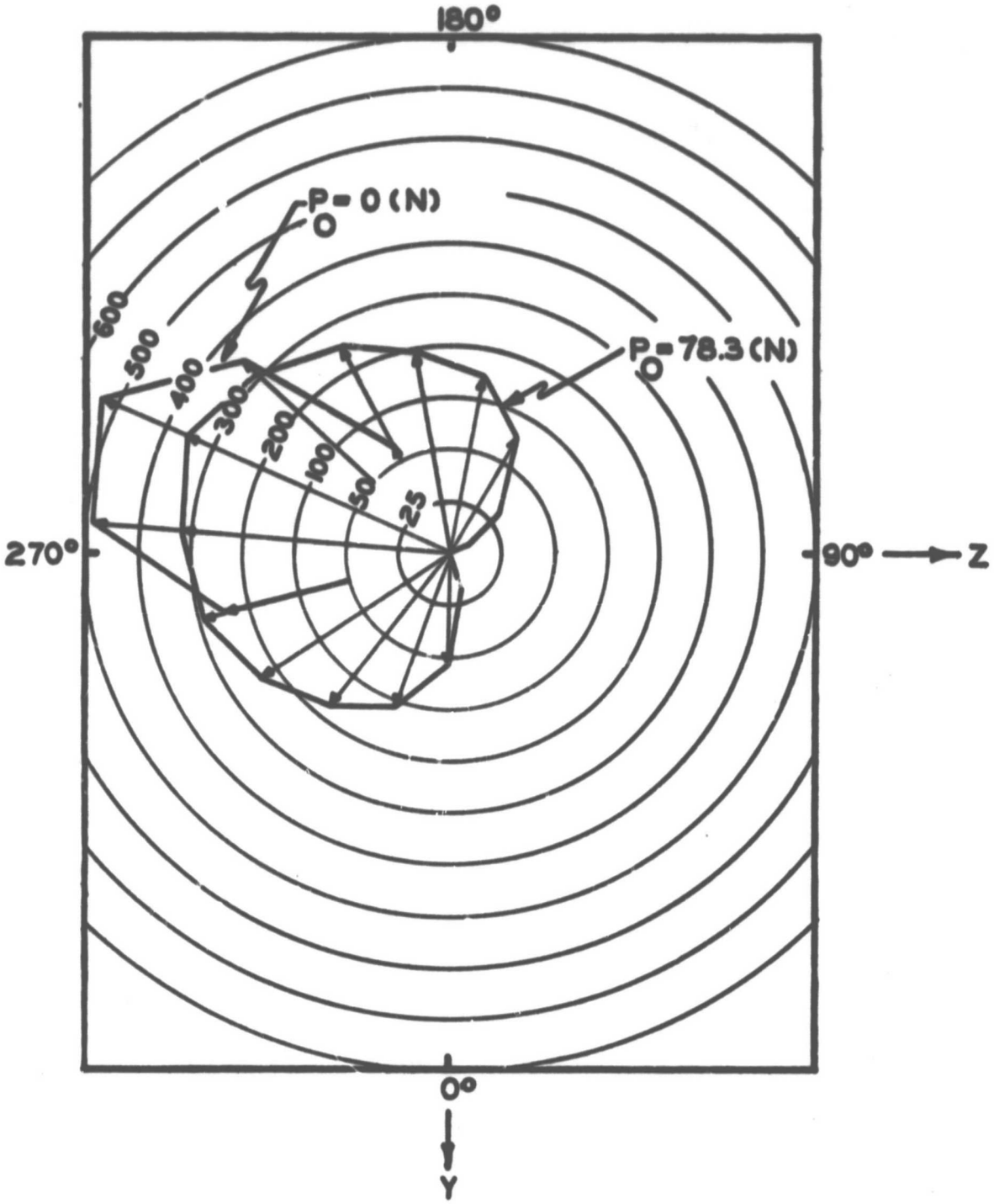

FIGURE NO. 14 ROLLER LOAD DISTRIBUTIONS (NEWTONS) AT (O) N & 78.28 (N) PRELOAD FOR 100% WALL THICKNESS, 60% GEAR LOAD AND FITS = LINE-TO-LINE - STRADDLE

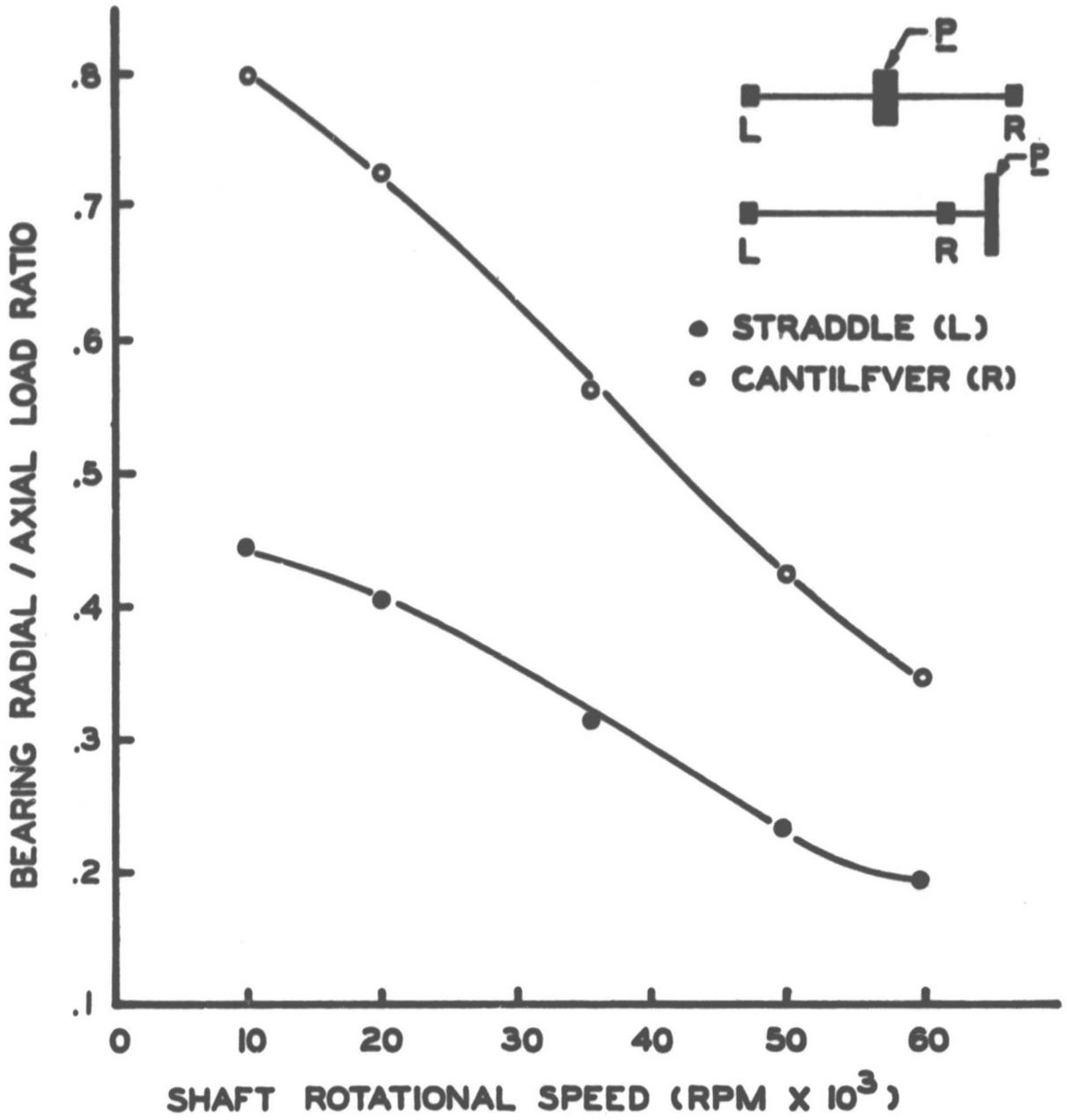

FIGURE NO. 15 RADIAL/AXIAL LOAD RATIO VERSUS SHAFT SPEED - ORIGINAL DESIGNS

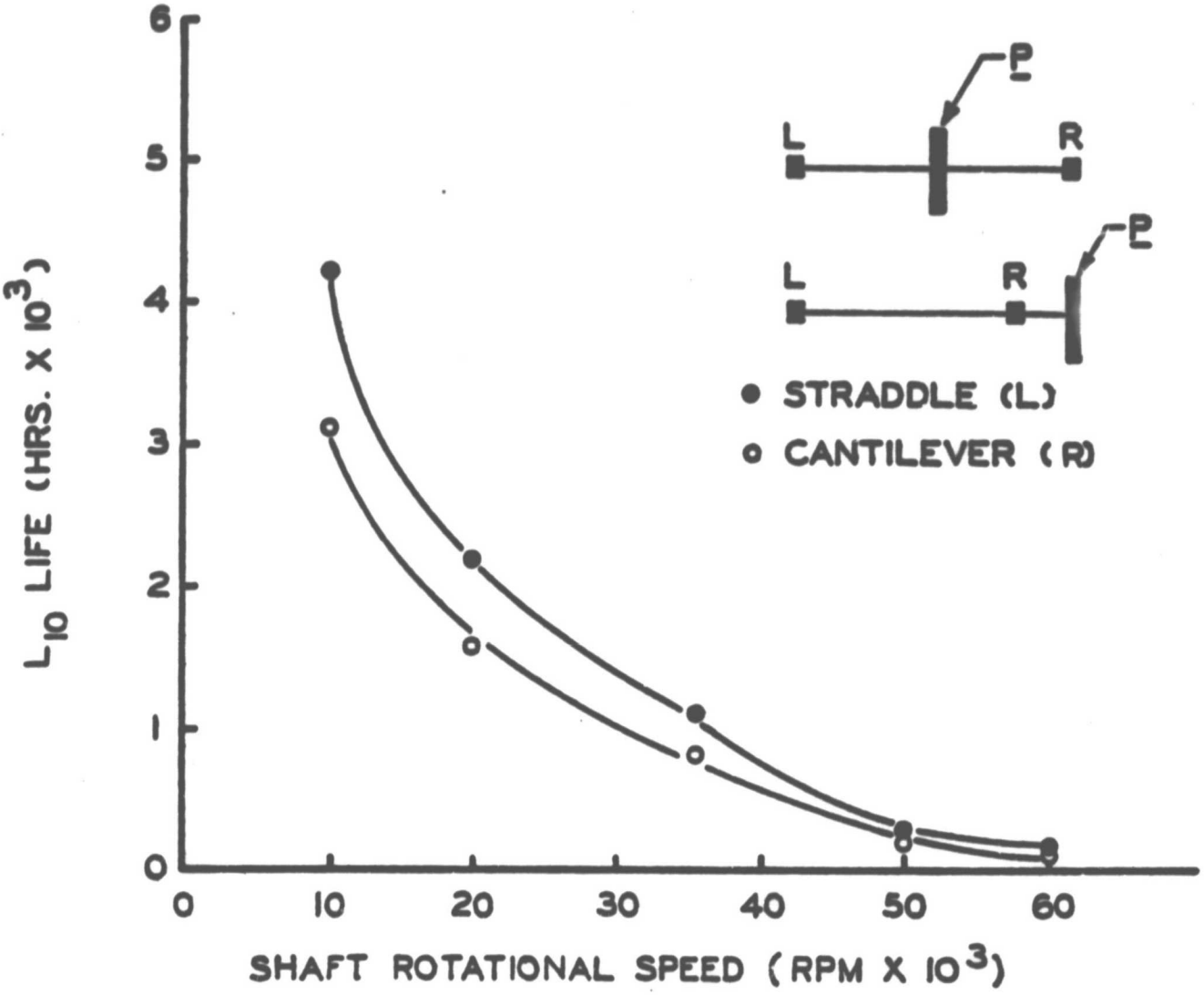

FIGURE NO. 16 LIMITING BEARING RATING LIFE WITH FRICTION AND LUBRICATION EFFECTS VERSUS SHAFT SPEED - ORIGINAL DESIGNS

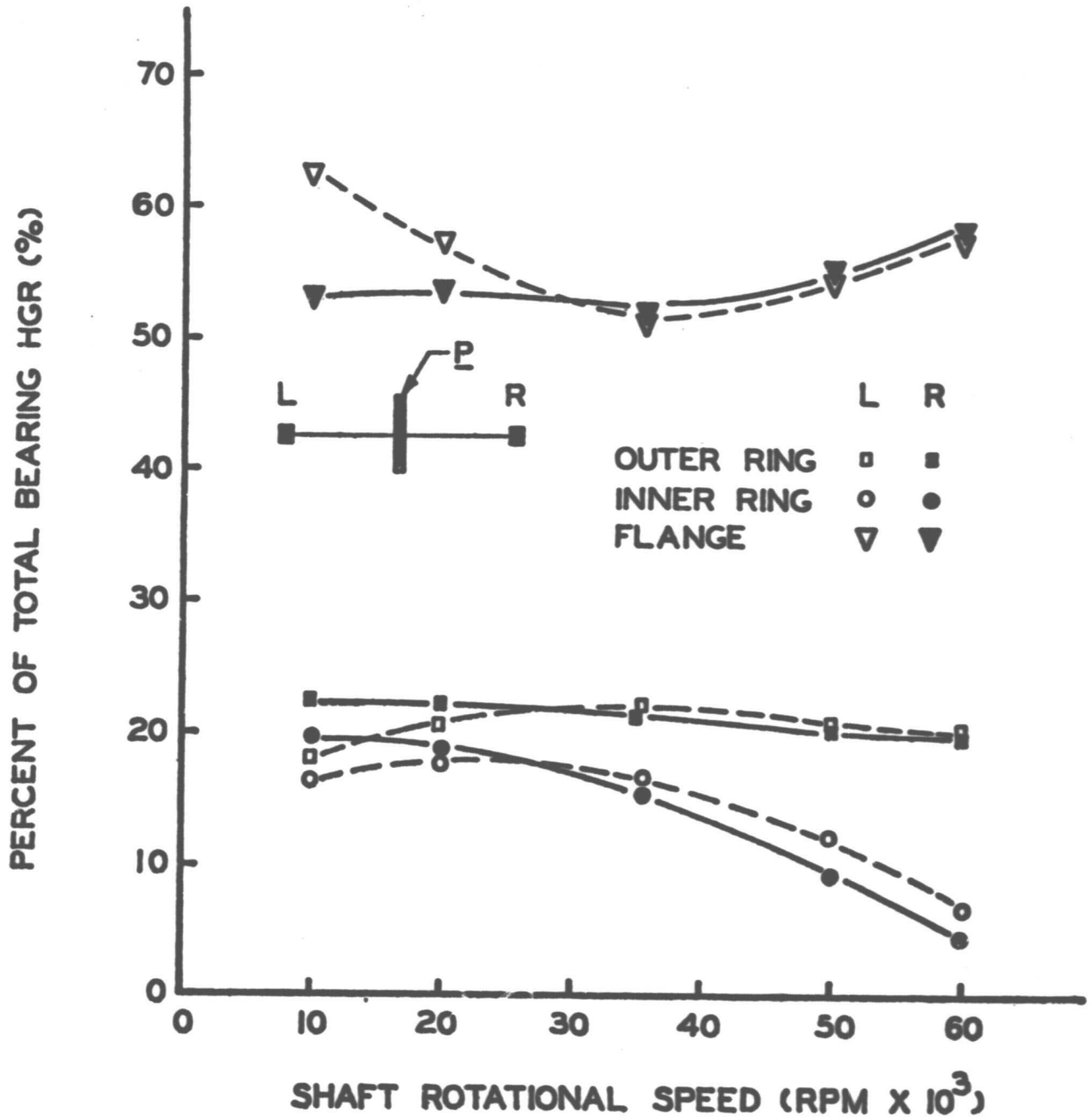

HGR (WATTS)		SHAFT SPEED
L	R	RPM X10³
772	469	10
2107	1579	20
5737	4829	36
10950	9952	50
16010	14810	60

FIGURE NO. 17 LOCAL DISTRIBUTION OF BEARING HGR'S VERSUS SHAFT ROTATIONAL SPEED - ORIGINAL STRADDLE

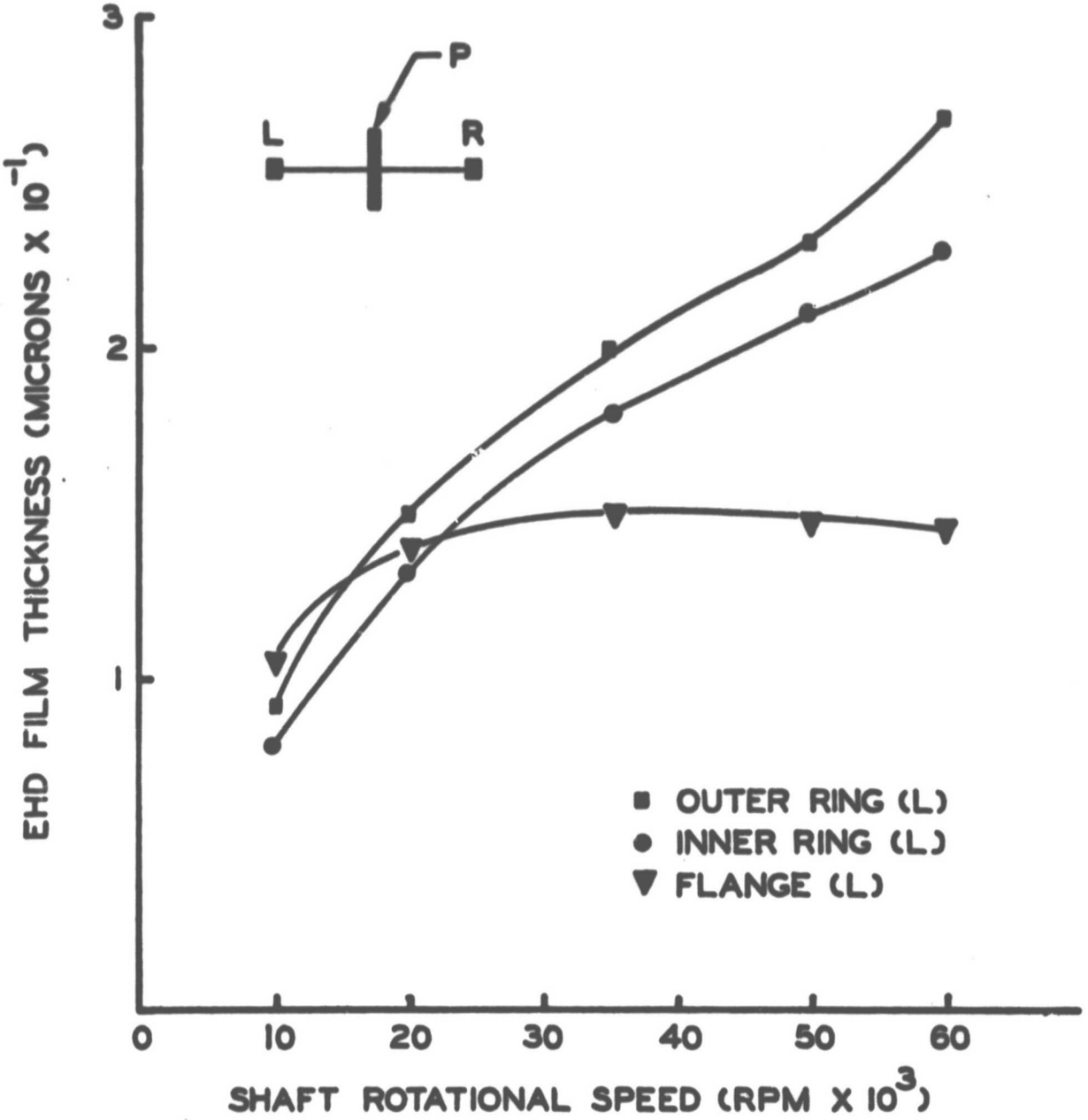

FIGURE NO. 18 EHD FILM THICKNESS AT INNER RING, OUTER RING AND FLANGE CONTACTS VERSUS SHAFT ROTATIONAL SPEED - ORIGINAL STRADDLE

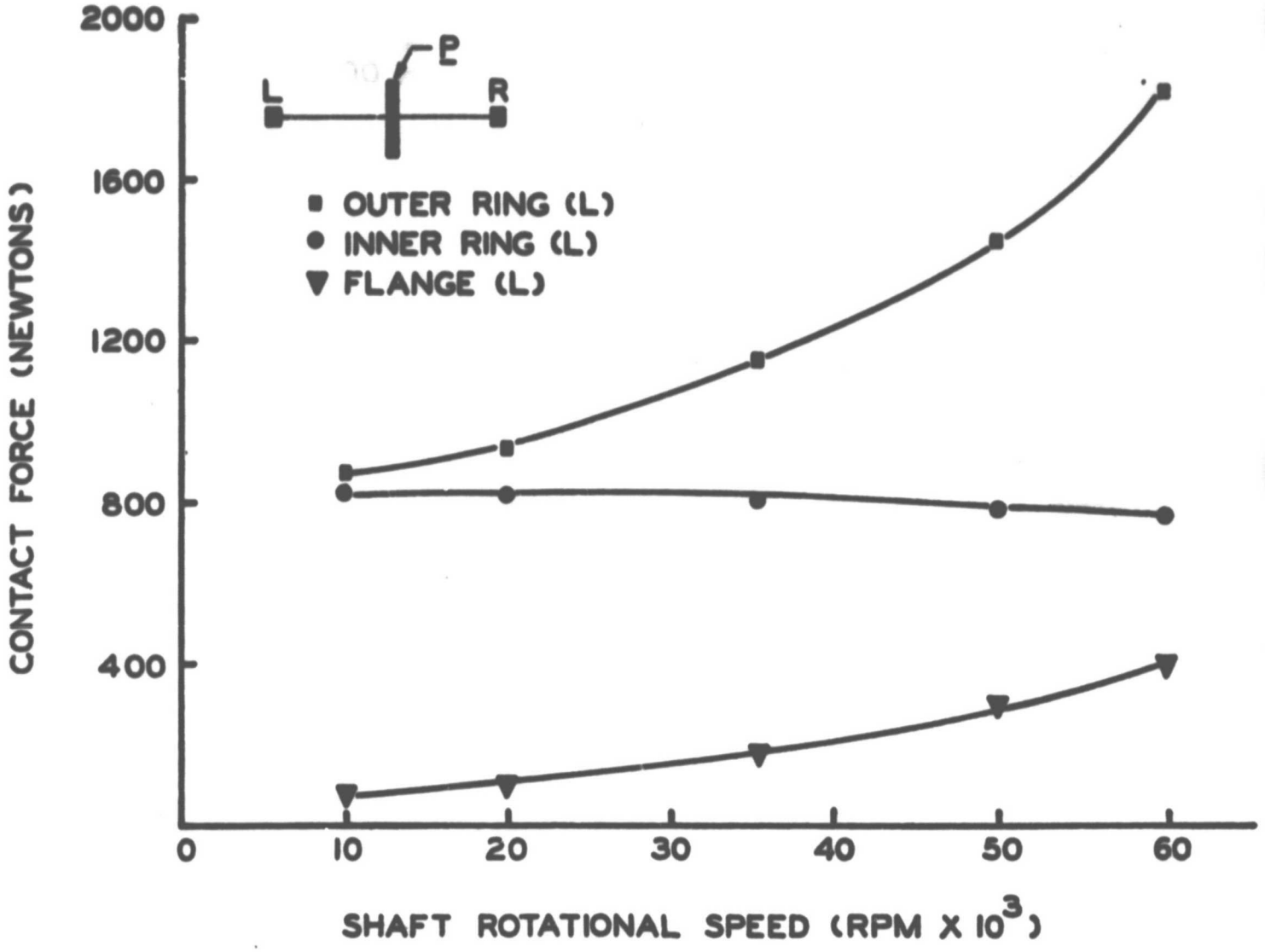

FIGURE NO. 19 MAXIMUM ROLLER NORMAL CONTACT FORCE AT INNER RING, OUTER RING AND FLANGE VERSUS SHAFT ROTATIONAL SPEED - ORIGINAL STRADDLE

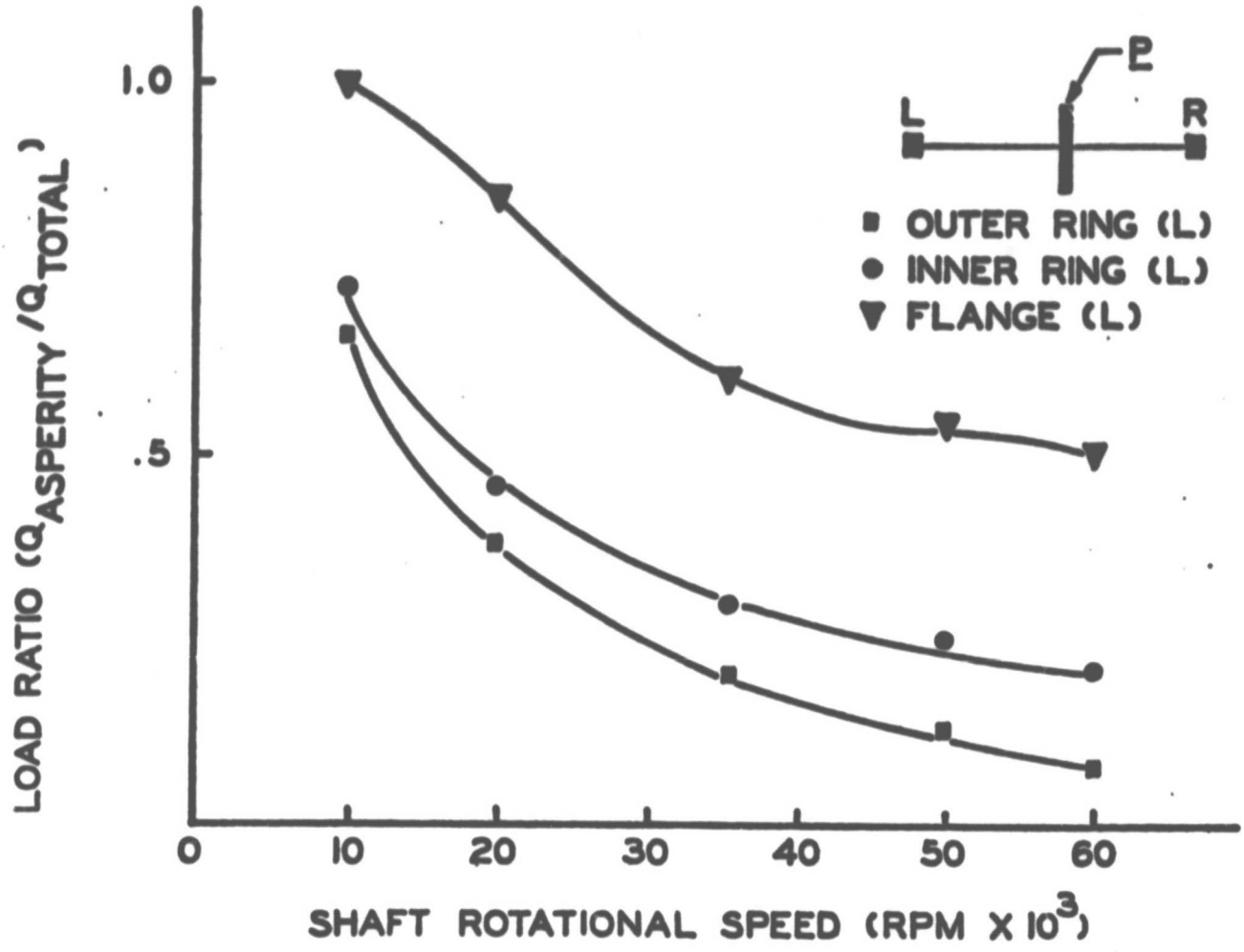

FIGURE NO. 20 CONTRACT LOAD RATIOS $Q_{ASPERITY}/Q_{TOTAL}$ AT OUTER RING, INNER RING AND FLANGE CONTACTS VERSUS SHAFT ROTATIONAL SPEED - ORIGINAL STRADDLE

APPENDIX 3
OPTIMIZATION OF TAPER SHAFT SUPPORT STRADDLE DESIGN

LETTER REPORT

TO: F. R. Morrison

REPORT NO: AT81D017L
PROJECT CODE: LC135
DATE: 28 April 1981
FROM: S. S. Gassel
COPIES TO: T. J. Deromedi
R. Avanzato

TITLE: Optimization of Taper Supported High Speed Input Pinion

REFERENCE:

I. INTRODUCTION

This analytic portion of the program provides a preliminary design of a support system for the high speed (36K rpm) input pinion. Previous analytic work [1] to define taper configurations using a pair of M88000 series bearings revealed that

- straddle arrangements are preferable to cantilever arrangements since they provided larger minimum L_{10} life for the same system mass.
- the capacity, and therefore size, of the bearing not opposing the applied thrust load could be reduced since its L_{10} life could be pushed well above the accepted value (2500 hrs at 60% nominal gear load (NGL)) by adjusting the preload.

This current effort was directed at selecting an optimum straddle design using an M88000 bearing to carry the applied thrust load and a smaller taper to oppose it. Initially, two (2) system configurations were considered. The opposing bearing was selected through parametric studies. Preloads and fits were selected and the effects of lubrication, friction and thermal interactions were evaluated by exercising SHABERTH [2] at level zero (0) and one (1), respectively.

An optimal design configuration, selected on the basis of weight, for allowable L_{10} life ($\geq$2500 hrs at 60% (NGL)) and pinion deformations (displacements <.001 in. and rotation <.1° at 100% NGL), were obtained through parametric studies at level zero. Parameter variations included: fits (O.D., I.D.), preload, and size (type) of bearings, not opposing the thrust load. The 2 new designs were compared to the dual M88000 design performance, used here as a baseline.

Subsequently, a steady-state thermal analysis of the optimum arrangement was performed using the SHABERTH code at level (one) with the thermal analysis option activated. This thermo-mechanical analysis enables final selection of fits, preloads, and lubricant flow rates, and confirms the acceptability of the selected pinion designed.

A description of the analysis to select the small bearing is presented in Section II. The thermomechanical analysis is described in Section III, followed by a summary (Section IV).

II. DEFINITION OF PINION DESIGN - ANALYSIS AT LEVEL = 0

II.1 Analytic Procedure

The strategy employed to determine the optimum bearing pair in a straddle configuration is defined in Figure 1.

A taper bearing series for the number II position, and minimum values for percent gear load and preload are selected. The test case is executed and the bearing fatigue lives are evaluated. If the minimum L_{10} life is less than 2500 hours under these conditions, the design will not satisfy the life constraint and a new bearing type is selected. If the fatigue life is acceptable, preloads are varied and the gear load increased to its nominal value to check the deflection constraint. Results are stored and ranked with respect to fatigue life. The next bearing type is then introduced for a similar analysis. The alternate taper bearings selected are from the LM67000 and LM11700 series. They are described in detail in Appendix A. The M88000 series bearing, used to establish a performance baseline, is described there as well.

The shaft support system designs are given by Figure 2 and Table 1. Computational details for bearing preload calibration and gear loads are provided in Appendices B and C, respectively. All analyses were performed at a shaft speed of 36,000 rpm and at a temperature of 100°C. Additionally, the wall thickness was held fixed at 50%. Each bearing center, right and left positions, was located 38.4 mm from the point of load application on the pinion. This enabled consistent evaluation of the relative performance of each bearing series.

II.2 Results of Parametric Execution

Initial parametric studies of the two alternate design configurations for the pinion resulted in the selection of an LM11700 for the right bearing. This arrangement minimizes the weight, and offers sufficient fatigue life and stiffness to satisfy the design constraints. (L_{10} > 2500 hrs at 60% of the nominal gear load, gear deflections <0.001 in. (0.0254 mm), gear rotation $\leq$0.1° at 100% of the nominal gear load).

The results from the parametric studies are presented in Table 2. These SHABERTH executions were carried out at level zero under the following conditions; Shaft speed = 36,000 rpm, Shaft Wall thickness = 50%, Fits = line-line, Temperature = 100°C. Gear loads were specified at 60 or 100% of the nominal applied gear load. Preloads ranged from 0-222.4N (50 lbs). In each configuration, both bearing centers were held at 38.4 mm from the point of load application. The M88000 was employed to define a performance baseline for the right bearing since it was known to be adequate.

A comparison of fatigue lives at the 60% load levels shows that

- The limiting bearing switches from left to right.
- The limiting bearing life increases with the introduction of either the LM67000 or the LM11700.
- The effect of preload on L_{10} life of each bearing is reversed at 60% NGL when the LM11700 bearing is employed.

The explanation for the first two results is attributed to the improved load distribution. The reduced contact angles (from 20° in the M88000 to 15.37° and 10.8° in the LM67000 and LM11700, respectively) enables a substantial reduction in the axial load carried by the left bearing. The smaller load yields a larger L_{10} life. The reversal in the effect of preload comes about because the fully-loaded roller complement in the left bearing becomes partially unloaded when the LM11700 is employed.

The life increases with preload since increased preload forces more rollers to carry the load. The deflections/rotations at the gear mesh at 100% nominal gear load are within the allowable limits in all cases.

Parametric studies were completed on the pinion support system to assess the variation of bearing fatigue life over a range of bearing centerline-to-centerline distances. These evaluations were conducted using SHABERTH-Level 0, an elastic solution, and SHABERTH-Level 1, which includes friction and lubrication effects. Preloads were maintained at 222.4N (50 lbs), and the gear loads were 60% of the nominal value. Other operating conditions were fixed at their previous values. The results of these studies are plotted in Figure 3 and show that:

- The LM11700 bearing is the life limiting element in the proposed system.
- An increase in bearing separation increases the estimated fatigue lives of both bearings. For the critical LM11700 bearing, the life varies from 1200 hours at a distance of 38.4 mm to 7200 hours at 76.8 mm, calculated at Level 1.
- The addition of lubrication and friction effects to the analysis produces a decrease in the lives of both bearings, i.e. equal to a loss of 600 hours in the critical LM11700 bearing.

The losses demonstrated at Level 1 were attributed to starvation effects at the minimal lubricant flow rate assumed for these test cases. It was anticipated that the trend would reverse in future thermal evaluations conducted with larger lubricant flow rates, given that the bearing temperatures would remain close to the current operating values of 100°C.

The design constraint that the bearings have a 2500 hour L_{10} life at 60% nominal applied gear load dictated a minimum bearing centerline-to-centerline distance of 45 mm (see Figure 2). Previous calculations established that gear deflections are maintained within the specified levels using separations as large as 76.8 mm. Therefore, for improved system performance, the bearing separation distances should be increased to the maximum allowable envelope, subject only to the weight/size limitations of the total system.

III. FURTHER EVALUATION OF THE SELECTED DESIGN - INTERACTING THERMAL ANALYSIS AT LEVEL=1

After finalizing the bearing separation parameter at 55 mm, a thermal analysis was performed on the selected straddle design. Preload, fits, and lubricant flow rates were varied, to assess their effect on system performance, and to optimize selection of these parameters.

III.1 General Description of Thermal Model

A SHABERTH steady-state thermal model was prepared for the selected straddle design, which consists of a magnesium alloy housing and a shaft with two tapered roller bearing supports of steel (see Figures 4, 5).

The mechanical structure to be analyzed is thought of as divided into a number of elements or nodes, each represented by a temperature. The net heat flow to node i from the surrounding nodes j, plus the heat generated at node i, must numerically equal zero. This is true for each node i, i going from 1 to n, n being the number of unknown temperatures.

After each calculation of bearing generated heat, which results from a solution of the shaft-bearing system portion of the program, a set of system temperatures is determined which satisfy the system of equations:

$$q_i = q_{oi} + q_{gi} = 0 \text{ for all temperature nodes } i$$

where

q_{oi} is the heat flow from all neighboring nodes to node i

q_{gi} is the heat generated at node i. These values may be input or calculated by the shaft bearing program as bearing frictional heat.

The transfer of heat within a medium or between two media can occur by conduction, convection, radiation and fluid flow (mass transport).

All these types of heat transfers occur in a bearing application as the following examples show.

1) Heat is transferred by conduction between inner ring and shaft and between outer ring and housing.

2) Heat is transferred by convection between the surface of the housing and the surrounding air.

3) Heat is transferred by radiation between the shaft and the housing (considered negligible for current analysis).

4) When the bearing is lubricated and cooled by circulating oil, heat is transferred by fluid flow.

Therefore, in calculating the net flow to a node all the above mentioned modes of heat transfer, except radiation were considered.

III.2 Tapered Bearing Straddle Design Thermal Model

Figure 4 shows the geometric model and the nodal system for the metal components and surrounding fluid media. The housing was taken to be magnesium while other metal nodes were considered to be steel for the purpose of obtaining heat conduction coefficients. There are five nodes for each tapered roller bearing, seven shaft nodes (including the gears) and five housing nodes. In addition, there are two air nodes. This nodal network provides for accurate local as well as global monitoring of component temperatures.

The lubricant flow paths and nodes are shown in Figure 5. It was assumed that oil from the chiller (node No. 30) exited at constant temperature (83°C). The oil flow is separated into four paths, two for the bearings and two for the gears. The calculation for the heat convection includes interactions between the

1) fluid and bearing rolling element, race and cages
2) fluid and gear surface
3) shaft and housing surface and surrounding air
4) oil and housing surface
5) housing external surface and the ambient air which is assumed to be at a constant temperature (21°C).

Appendix D details the calculations used to define conduction, convection and mass transport heat transfer coefficients for this tapered bearing straddle arrangement.

III.3 Parameter Specifications

Input pinion operating parameters that were held constant throughout the analysis include the following:

- Shaft Speed - 36,000 rpm
- % Shaft Wall Thickness - 50%
- Lubricant - Santotrac 50

The project definition required simulation at both 60% NGL, where fatigue life assessments of the proposed system were made, and at 100% NGL, where pinion deformations were evaluated.

Input variables associated with each of these loading conditions are as follows:

- Gear load vector (F_x,F_y,F_z):(-3578, 1084,-4509) N at 100% NGL

  (-2147, 650,-2705) N at 60% NGL

- Power losses at the bevel and tail rotor drive gear, respectively:

  (5600, 616) watts at 100% NGL

  (3360, 320) watts at 60% NGL

The purpose of this thermal analysis was final selection of preloads, fits, lubricant flow rates and verification of the resultant taper straddle design. This required evaluation of the coupled thermal and mechanical interactions of the proposed hardware and its environment. Accordingly, parameters that were selected to be varied included:

- Lubricant flow rate to bearings ($0.528\text{-}2.38\times10^{-1}$ lpm (0.2-0.9 gpm))
- Preload applied to each bearing (0-222 N)
- Shaft and housing fits (0.0-0.01 mm)

Also, the selection of bearing centerline-to-centerline distance was reevaluated. This was originally set at 55 mm (Figure 1; L_1=30 mm, L_2= 25 mm), where adequate system life had

been achieved in the previous analyses. These values remained constant throughout the initial thermal parametric studies, where optimal system operating conditions were found by varying the above parameters. However, these analyses indicated marginally acceptable system life at this separation, so that larger separations were considered.

III.4 Summary of Thermomechanical Analysis

Preliminary analyses had shown that the LM11700 (Figure 1 - Bearing II) is the system life limiting bearing. Therefore, studies evaluating system life focused on the operating conditions necessary to achieve the required 2500 hours life in that bearing.

The results of a study examining the relationship between lubricant flow rate to the bearings and system life is shown in Figure 6. For this study, the maximum preload (222N) was applied to both bearings, and the flow rate varied from $0.528\text{-}2.38 \times 10^{-1}$ lpm (0.2 to 0.9 gpm). The fit analysis option was not activated.

At the specified maximum flow rate of 0.106 lpm (0.4 gpm), an L_{10} life of 1714 hours was predicted for the life limiting (LM11700) bearing. This low life is directly attributable to the small film thickness generated within the LM11700, despite simulation of fully flooded (i.e. no starvation) conditions.

Film thickness (h) is a function of bearing geometry, lubricant and temperature. Since the former two are constants in this analysis, increased film thickness (and therefore, increased life) could only be achieved by decreasing bearing operating temperatures. This was done by increasing the flow rate (heat removal through mass transfer) to the bearings. As Figure 6 shows, the LM11700 life increases to 2159 hours at 0.158 lpm (0.6 gpm) and to 2434 hours at 0.238 lpm (0.9 gpm), just slightly under the required 2500 hours life.

The study was repeated with the fit analysis option activated (line-on-line) for preloads of 44.48, 133.45 and 222.0 Newtons. This couples the bearing clearance and thermal analyses together. The results (Figure 7) at this minimum fit condition clearly show the need for a small (44.48 N) preload and large lubricant flow rate of 0.238 lpm (0.9 gpm). The life at these conditions was found to be 2300 hours, the best performance for this configuration. Diminishing the flow rate to the specified 0.106 lpm (0.4 gpm) decreases system life to 1588 hours, only 63% of that required at 60% NGL.

These studies indicate that the pinion design being investigated will not achieve 2500 hours life at 60% NGL, with flow rates of 0.106 lpm (0.4 gpm). For this reason, additional parametric studies were implemented.

Subsequent simulations, in which the bearing centerline-to-centerline distance was increased from 55 mm to 65 mm, show adequate life can be obtained (Table 3). The increase in life is caused by decreased reaction loads at the life limiting LM11700 bearing. Table 3 lists pertinent input parameters and bearing lives for six simulations. All simulations at 60% NGL and 0.238 lpm (0.9 gpm) flow rate achieved 2500 hours life, regardless of the fit. The preload was set at 44.48 N for all simulations. Also, note that when the L_1/L_2 ratio is reversed (Case 2) life increases from 3779 to 5192 hours. Case 6, a 100% NGL simulation shows a maximum gear deflection of 0.0084 mm and a maximum gear rotation of 0.164×10^{-3} radians, well within the prescribed constraints.

A detailed temperature map of the input pinion is provided in Table 4. The operating conditions associated with this map are those of Case No. 5, Table 3.

IV. SUMMARY AND CONCLUSIONS

Computerized simulation using program SHABERTH was implemented to define a straddle pinion design using "off-the-shelf" taper roller bearings. The analysis proceeded in two parts.

Initial evaluation was done using an elastic analysis (Level=0) to select a particular bearing series for the number II position (i.e. not opposing the applied thrust). The evaluation included M88000 (baseline), LM67000 and LM11700 series taper bearings. The LM11700 was selected since it gave acceptable performance with minimum mass. Further analysis was carried out at both level=0 (elastic) and level=1 (lubrication and friction effects, no thermal analysis) to select bearing spacing.

Subsequent analysis was then carried out on the selected design at level=1 with the thermal option activated. These results were used to select preloads, fits and lubricant flow rates. Bearing spacing and gear locations were also reevaluated. Results from these analysis indicate that the straddle pinion consisting of an M88000 (position I) and an LM11700 (position II) will perform within the design constraints provided that

- Higher then specified (>0.106 lpm (0.4 gpm)) lubricant flow rates are supplied to bearing II to enable heat removal. A value of 0.238 lpm (0.9 gpm) is recommended.

- Sufficient bearing spacing is maintained. A value of 65 mm (centerline-to-centerline) gives acceptable performance at a flow rate of 0.238 lpm (0.9 gpm), light fits (0.005 mm/line-line: shaft/housing) and light preload 44.8N (10 lbs.).

REFERENCES

1. Gassel, S. S., "Research Report on Development of Small Bore, High Speed Tapered Rolling Bearing - Task I Bearing-Shaft System Analysis," SKF Report No. AL79P001, January 1979.

2. Crecelius, W. J., "User's Manual for SKF Computer Program SHABERTH (AT77Y001). Steady State And Transient Thermal Analysis of a Shaft Bearing System Including Ball, Cylindrical and Tapered Roller Bearings," SKF Research Report No. AL77P015, 1977.

3. Ragen, M. A., "Final Report on Simulation of the Steady State and Time Transient Thermal Performance of the AH-1G/Q Input Pinion Module," SKF Report No. AL79P012, May 1979.

4. Ragen, M. A., "Final Report on Prediction of Time to Failure of the CH-53 Helicopter Power Input Module After Loss of Lubrication," SKF Report No. AL79P013, submitted under U.S. Army Contract No. DAAD05-75-C-0755, Ballistic Research Laboratories, Aberdeen Proving Ground, Maryland, 1979.

5. Loewenthal, S. H. and Parker, R. J., "Rolling Element Fatigue Life with Two Synthetic Cycloalipathic Traction Fluids," NASA TN D-8124, March 1976.

6. Kreith, F., Principles of Heat Transfer, 3rd Edition, Intext Educational Publishers, 1973.

7. Patir, N. and Cheng, H. S., "Prediction of the Bulk Temperature in Spur Gears Based on Finite Element Temperature Analysis," ASLE Preprint No. 77-LC-3B-2, presented at ASLE/ASME Lubrication Conference in Kansas City, Missouri, October 3-5, 1977.

F-41954

FIGURE 1: ALGORITHM FOR BEARING PERFORMANCE EVALUATION

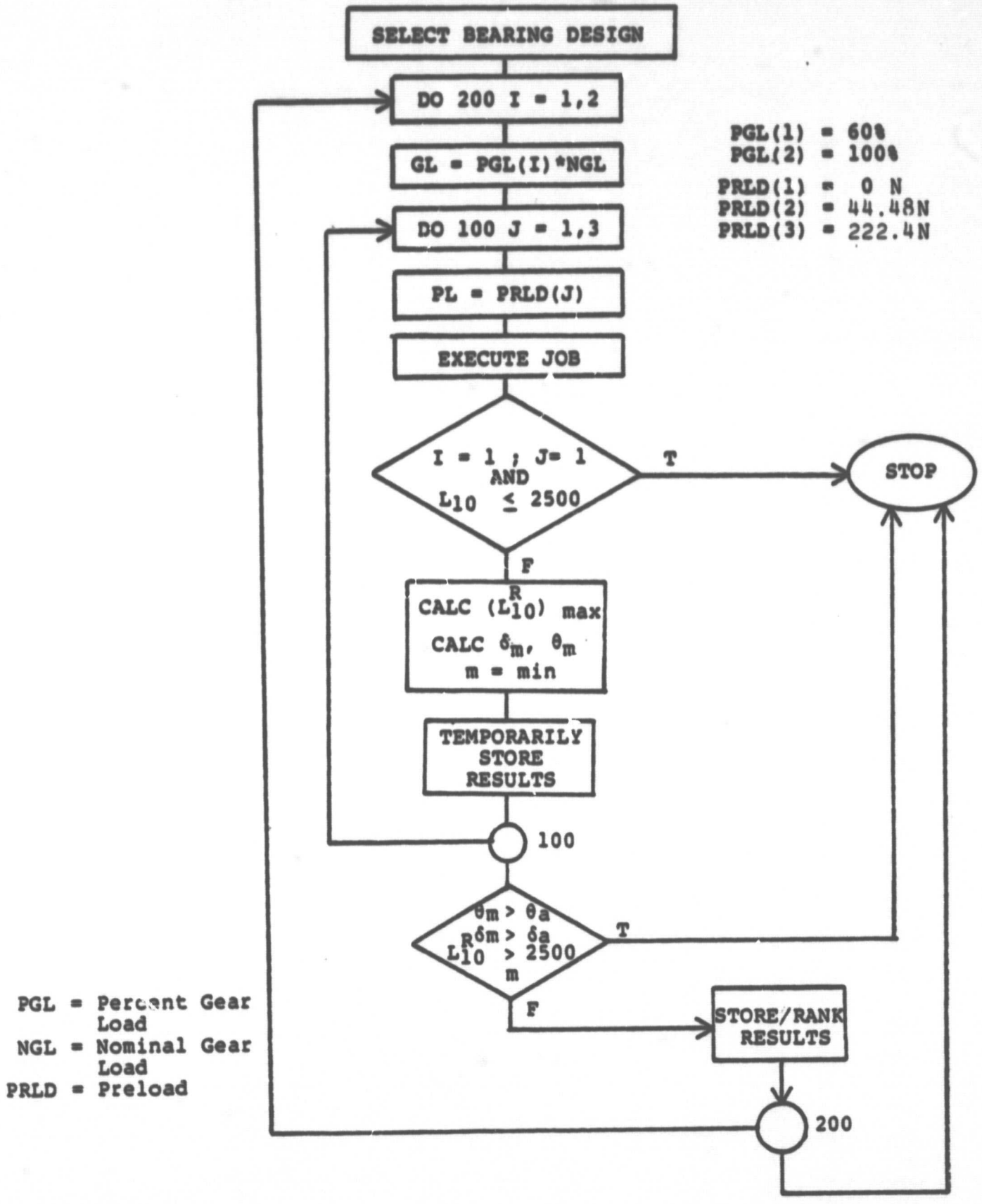

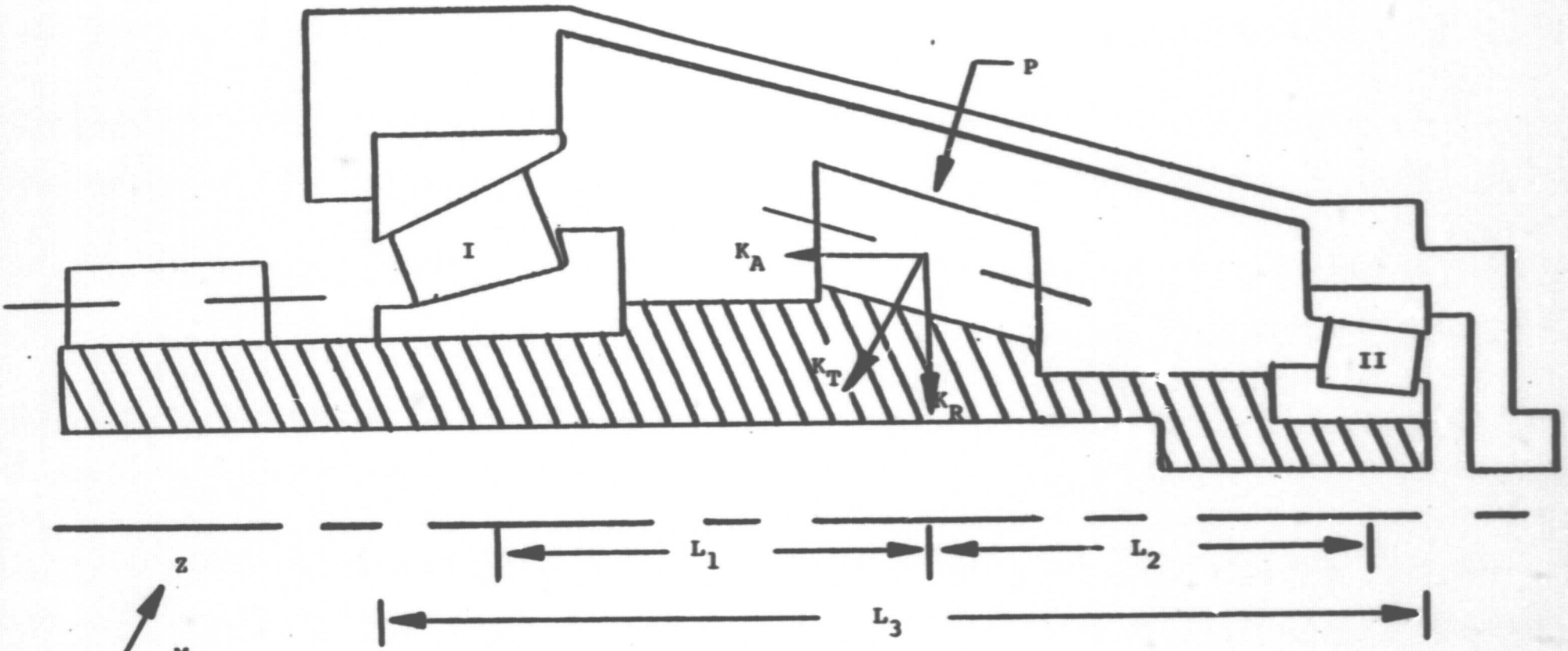

P - APPLIED GEAR LOAD
K_A - AXIAL FORCE
K_T - TANGENTIAL FORCE
K_R - RADIAL FORCE
L_1 - CENTERLINE-TO-CENTERLINE DISTANCE BETWEEN BEARING I AND GEAR
L_2 - CENTERLINE-TO-CENTERLINE DISTANCE BETWEEN BEARING II AND GEAR
L_3 - TOTAL ENVELOPE DISTANCE

FIGURE 2: STRADDLE DESIGN SYSTEM GEOMETRY

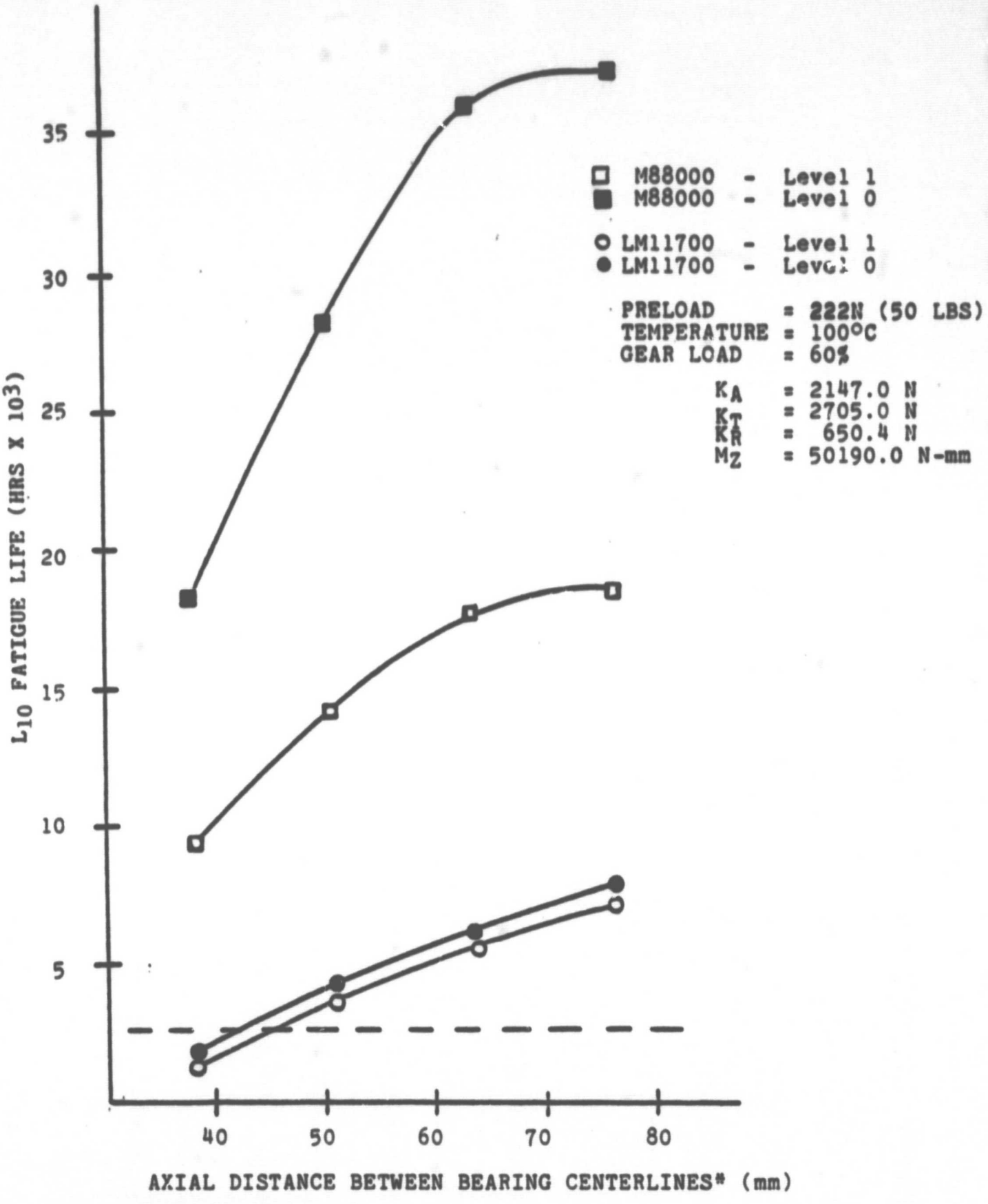

FIGURE 3. BEARINGS FATIGUE LIFE VS. AXIAL DISTANCE BETWEEN BEARINGS

* (L_1 + L_2 : Figure 1)

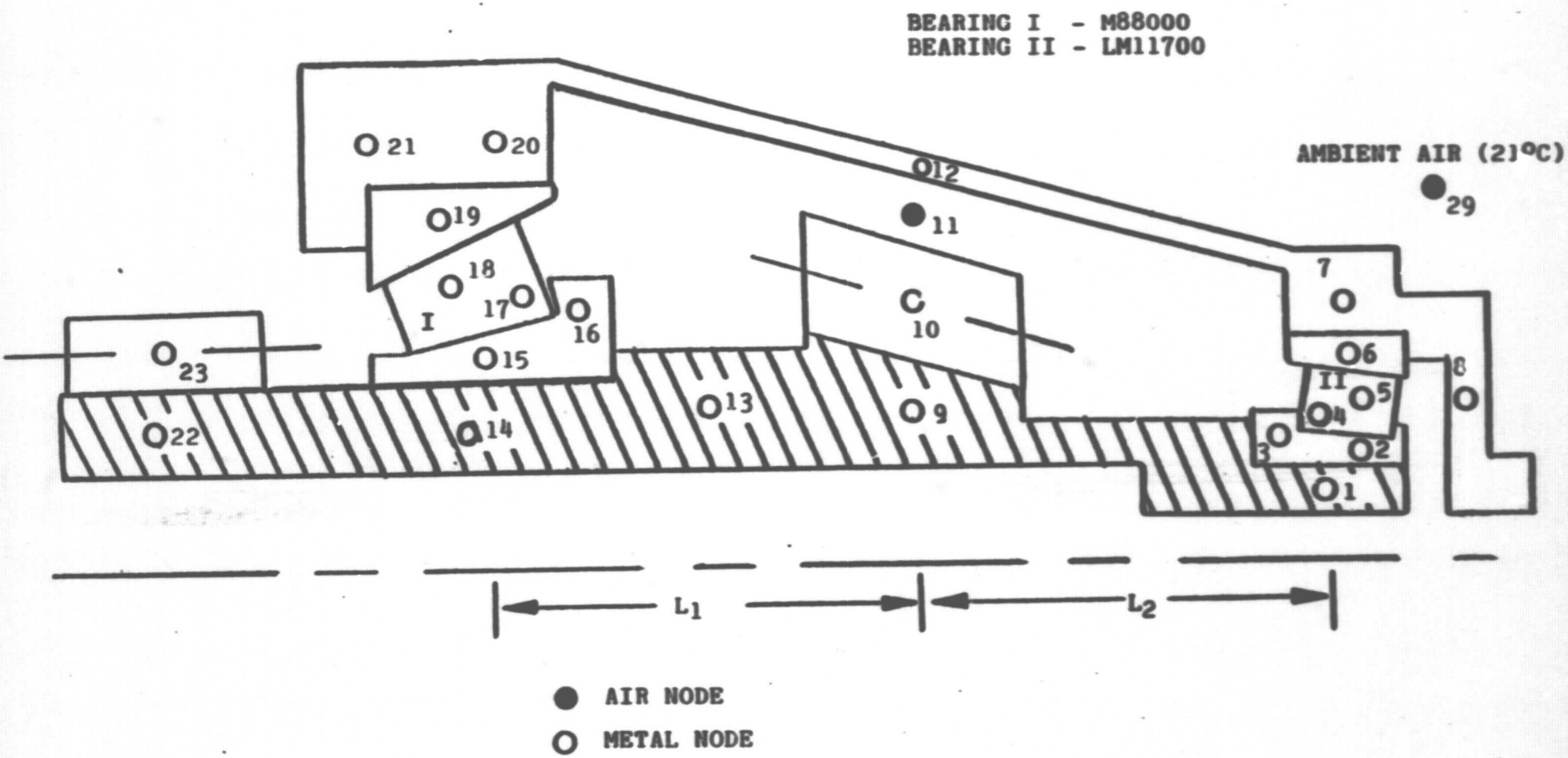

FIGURE 4: ANALYTICAL MODEL OF NASA INPUT PINION THERMAL SYSTEM

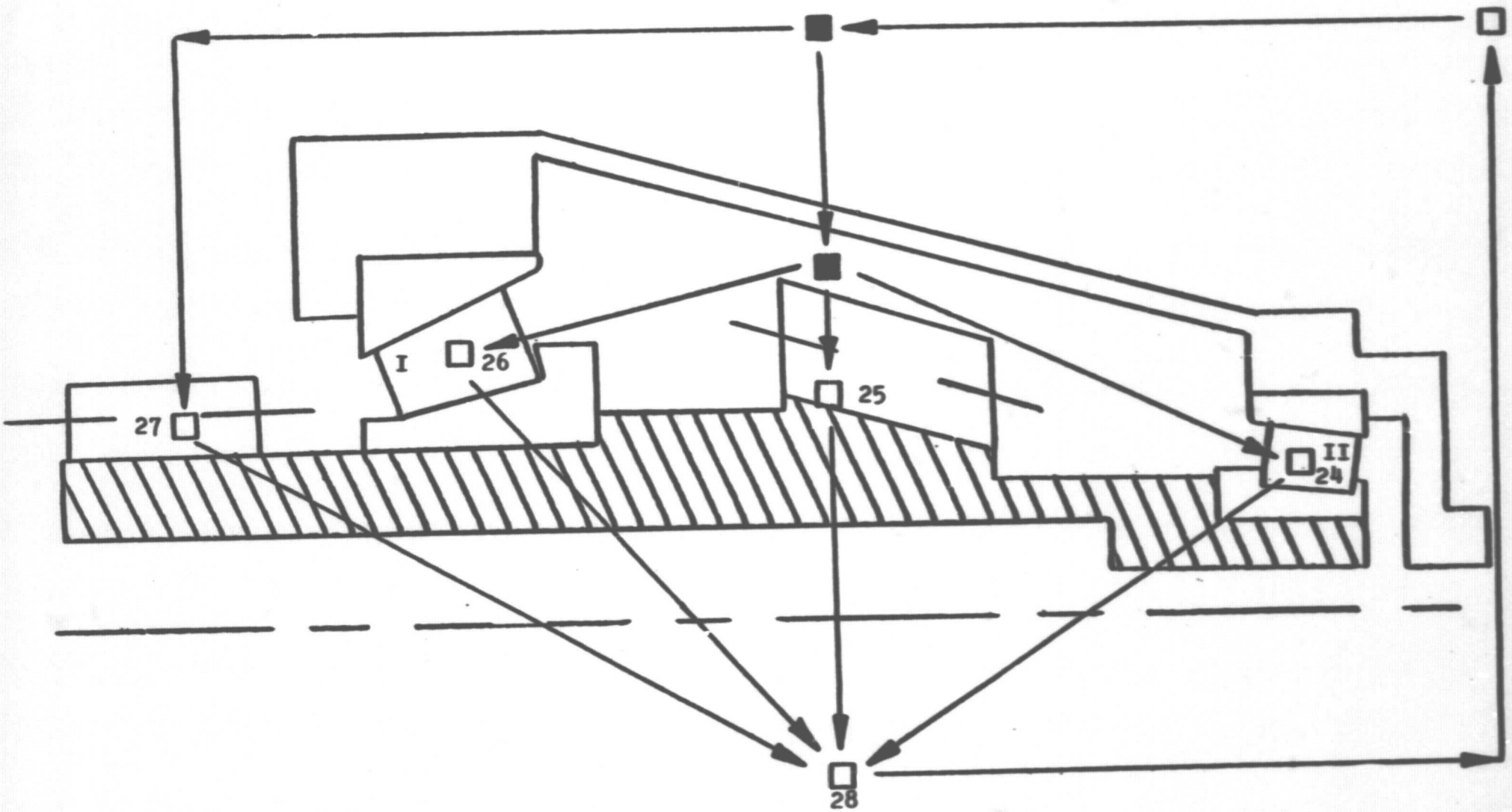

FLOW NODE

FLOW JUNCTURE

BEARING I - M88000

BEARING II - LM11700

FIGURE 5: ANALYTICAL MODEL OF NASA INPUT PINION LUBRICATION SYSTEM

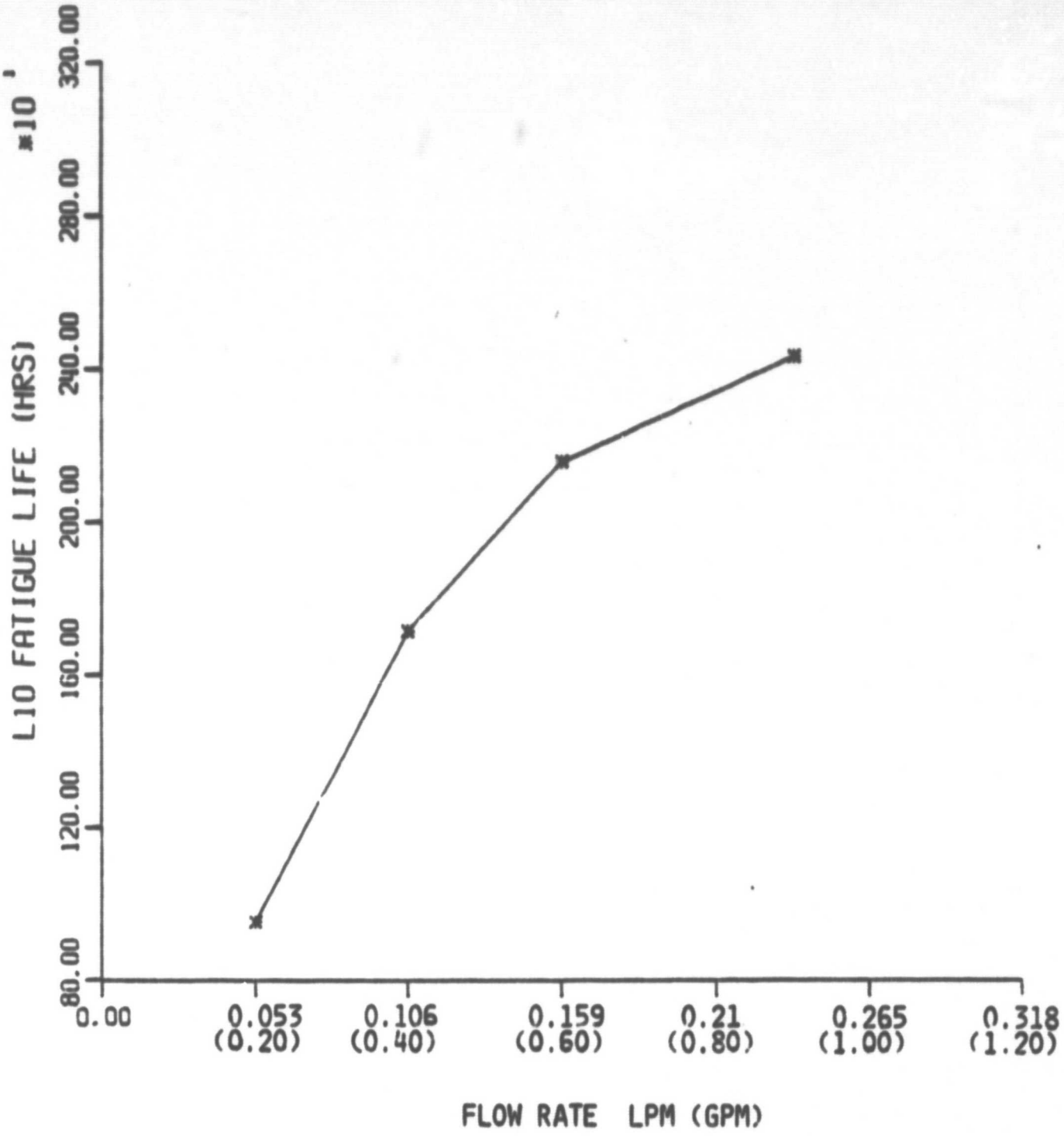

FIGURE 6:

FATIGUE LIFE VS. FLOW RATE
FOR THE LM11700 TAPERED ROLLER BEARING
WITHOUT FIT ANALYSIS

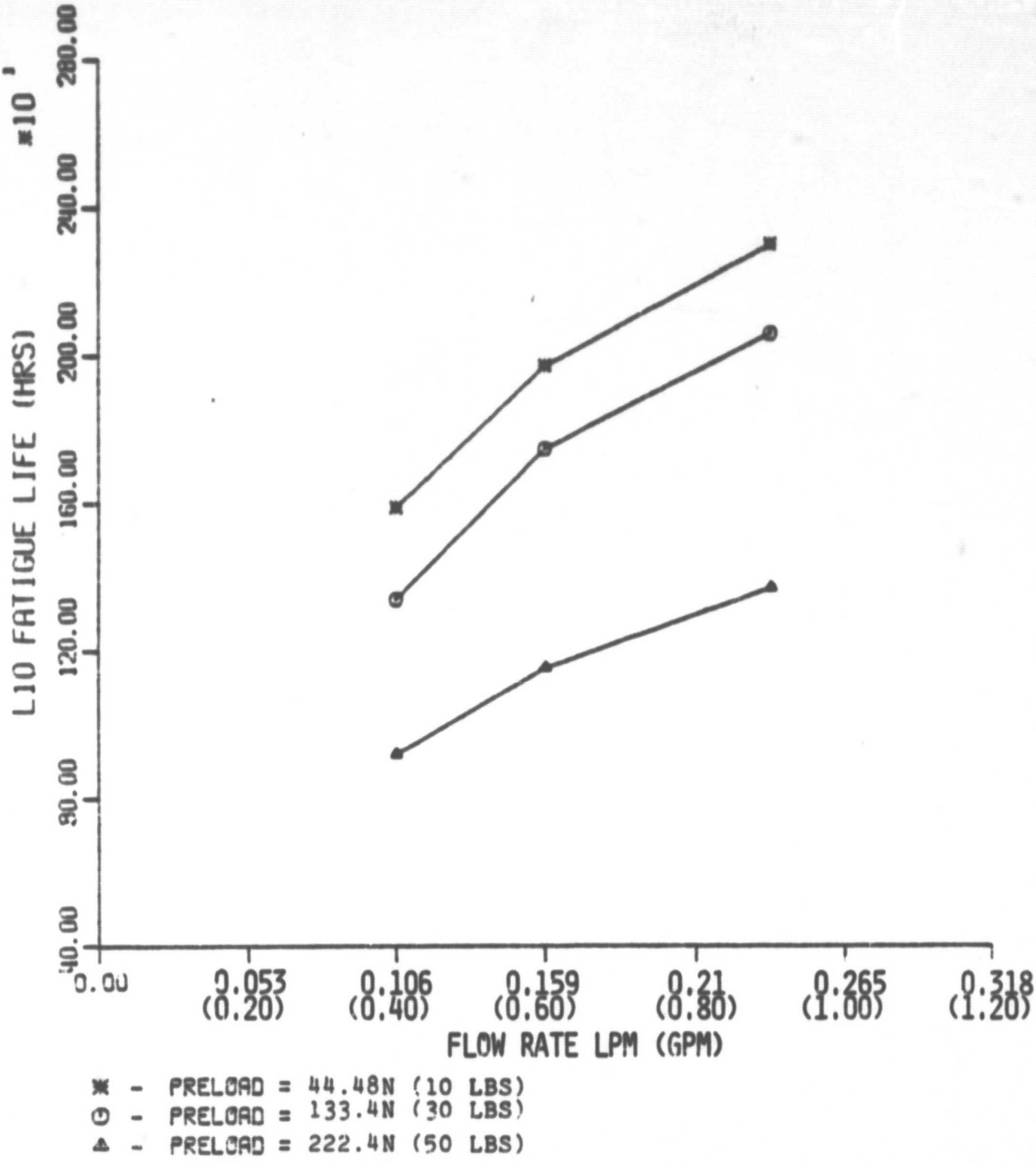

FIGURE 7:

FATIGUE LIFE VS. FLOW RATE
FOR THE LM11700 TAPERED ROLLER BEARING
WITH LINE-ON-LINE FITS

TABLE 1

PINION GEOMETRIES

STRADDLE DESIGN

(R)	(L)	L_b^L	L_1	L_2	L_b^R	L_3
			(MM)			
M88000	M88000	22.23	38.44	38.44	22.23	99.1
M88000	LM67000	22.23	38.44	38.44	15.88	95.9
M88000	LM11700	22.23	38.44	38.44	13.84	94.8

$L_b^{L,R}$ = Bearing Width (left, right)

Design L	Design R	% G.L.	Preload N	L_{10}^{L} (HRS)	L_{10}^{R} (HRS)	F_R^L/F_a^L (N/N)	F_R^R/F_a^R (N/N)	δ_r(mm)	δ_a(mm)	θ_{max} (DEG)
LM88000	LM88000	100	0	1511	9075.	3009/6696	2296/3114	4.47E-3	0.0221	4.70E-3
			40.5	1513	9204	3009/6694	2302/3121	4.43E-3	0.0211	4.63E-3
			222.4	1497	9675	3006/6715	2314/3132	4.36E-3	0.0188	4.46E-3
		60	0	5455	25700.	1800/4894	1384/2769	3.02E-3	0.0175	3.19E-3
			40.5	5434	26140.	1798/4907	1388/2762	3.00E-3	0.0165	3.14E-3
			222.4	5397	26930.	1793/4918	1404/2774	2.88E-3	0.0142	3.02E-3
LM88000	LM67000	100	0	3978	2964	3026/4953	2269/1363	5.17E-3	0.0172	4.88E-3
			40.5	3960	3065	3021/4952	2272/1372	5.16E-3	0.0163	4.87E-3
			222.4	3938	3291	3013/4962	2279/1383	5.06E-3	0.0140	4.68E-3
		60	0	21190.	11380.	1807/3246	1374/1092	3.84E-3	0.0112	3.36E-3
			40.5	21220.	11790.	1804/3248	1378/1089	3.77E-3	0.0103	3.27E-3
			222.4	20940.	13140.	1804/3254	1390/1112	3.73E-3	0.0080	3.12E-3
LM88000	LM11700	100	0	6224	1939	3043/4225	2216/758	5.70E-3	0.0148	4.75E-3
			40.5	6197	2069	3046/4229	2217/640	5.71E-3	0.0138	4.69E-3
			222.4	6178	2351	3049/4231	2217/652	5.72E-3	0.0115	4.67E-3
		60	0	16200	8026.	1802/2926	1353/781	4.00E-3	0.0155	3.43E-3
			222.4	18200	7887.	1809/2945	1350/797	3.79E-3	9.64E-3	3.22E-3

TABLE 2. TABULATION OF L_{10} LIVES, GEAR MESH DEFORMATIONS AND BEARING LOADS AS A FUNCTION OF PINION DESIGN, APPLIED LOAD AND PRELOAD

CASE	NGL (%)	BEARING DISTANCES*(MM) L1	L2	FLOW RATE LPM (GPM) I	II	FITS**(MM) I	II	L_{10} FATIGUE LIFE (HRS.) I	II
1	60	35	30	0.238 (.9)	0.238 (.9)	.000	.000	22,600	3,779
2	60	30	35	0.238 (.9)	0.238 (.9)	.000	.000	15,120	5,192
3	60	30	35	0.106 (.4)	0.106 (.4)	.000	.000	11,030	1,694
4	60	30	35	0.238 (.9)	0.238 (.9)	.010	.010	20,300	2,501
5	60	30	35	0.238 (.9)	0.238 (.9)	.010	.005	20,170	3,004
6	100	30	35	0.238 (.9)	0.238 (.9)	.010	.005	1,970	567

PRELOAD = 44.48N

TABLE 3 - RESULTS OF STUDY ON THE EFFECT OF VARIATION OF BEARING CENTERLINE-TO-CENTERLINE DISTANCE ON SYSTEM LIFE

* SEE FIGURE

** SHAFT FITS; HOUSING FITS HELD AT LINE-LINE

NODE	DESCRIPTION	TEMP (^{o}C)	NODE	DESCRIPTION	TEMP (^{o}C)
1	Shaft	112.2	16	Flange (I)	123.9
2	Inner Ring (II)	112.3	17	Cage (I)	98.9
3	Flange (II)	112.0	18	Roller (I)	151.7
4	Cage (II)	86.5	19	Outer Ring (I)	122.0
5	Roller (II)	109.8	20	Housing	116.6
6	Outer Rng (II)	108.2	21	Housing	115.8
7	Housing	109.9	22	Shaft	106.4
8	Housing	110.7	23	Rotor Drive Gear	93.2
9	Shaft	104.1	24	Oil Node (II)	85.4
10	Bevel Gear	92.7	25	Oil Node (Bevel Gear)	91.4
11	Internal Air	112.8	26	Oil Node (II)	96.6
12	Housing	112.0	27	Oil Node (Rotor Drive Gear)	92.5
13	Shaft	110.4	28	Collector	99.6
14	Shaft	116.4	29	Ambient Air	21.0*
15	Inner Ring (I)	119.7	30	Chiller	83.0*

TABLE 4

TEMPERATURE MAP OF INPUT PINION - TAPERED BEARING STRADDLE DESIGN

* KNOWN TEMPERATURE

APPENDIX A

BEARING GEOMETRIC PROPERTIES

The geometric properties for the bearings were computed from drawings of the assemblies, inner rings and rollers. The numerical values for the geometric parameters used in the analyses are tabulated below (Table A-1) while the nomenclature is defined with Figure A-1.

TABLE A-1

BEARING GEOMETRIC PARAMETERS

PARAMETER	M88000 SERIES	LM67000 SERIES	LM11700 SERIES
α	20°	15.37°	10.8°
β	15.05°	11.7°	7.367°
θ	15.55°	12.25°	7.796°
2ε	4.95°	3.67°	3.433°
R_s	87.38 mm	102.00 mm	95.39 mm
R_c	4500.88 mm	2049.78 mm	1270.00 mm
ℓ_w	16.32 mm	10.75 mm	9.220 mm
ℓ_a	15.80 mm	10.26 mm	7.635 mm
D_w	7.94 mm	6.53 mm	5.715 mm
D_o	33.34 mm	31.75 mm	17.46 mm
D_b	68.26 mm	59.13 mm	39.88 mm
B	22.23 mm	15.88 mm	13.84 mm
No. of Rollers	16	14	10
C = Capacity (N)	48,950	29,815	18,913

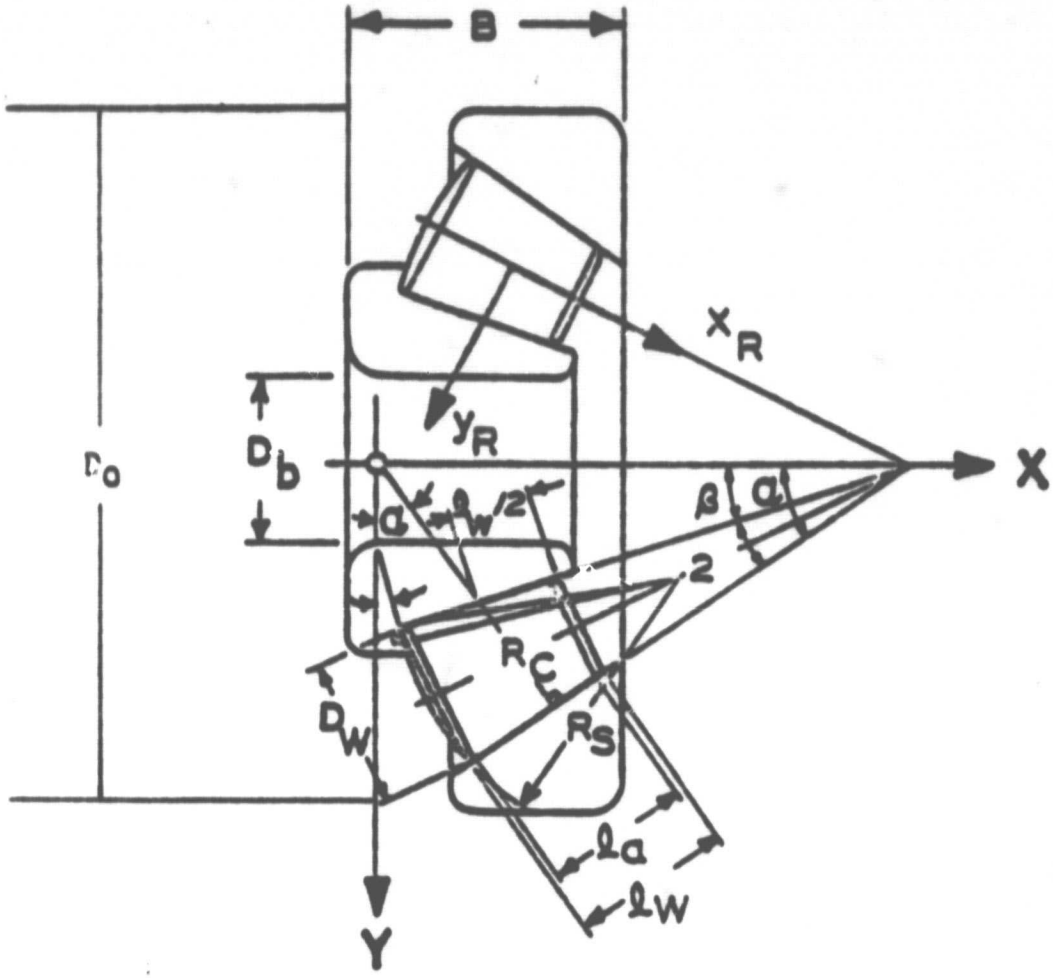

FIGURE A-1 TAPER BEARING GEOMETRY

APPENDIX B

PRELOAD CALIBRATION

In SHABERTH, axial preloads are imposed by selection of a negative initial deformation (axial play) parameter. An equivalent preload was computed using the procedure described below.

The system external loads were removed and the rotational speed set to 10 rpm. An axial play (compression) was selected and the support system analyzed to evaluate bearing axial loads on the inner rings. This provided a point on the load-deflection curve. The process was repeated until the entire calibration curve was obtained. At this point the displacement corresponding to a given preload could be extracted from the curve.

Calibration studies were performed for the M88000, LM67000 and LM11700 series. The results are tabulated below.

TABLE B-1

AXIAL PLAY VS. PRELOAD - CALIBRATION DATA

AXIAL COMPRESSION ($mm \times 10^4$)	M88000	LM67000	LM11700
0.000	0.000	0.0	0.0
10.000	43.199	16.2	13.3
20.000	125.999	44.6	35.5
30.000	219.002	77.2	63.7
40.000	333.000	113.0	101.0
50.000	-	169.0	144.0
60.000	-	235.0	192.0
80.000	-	-	294.0
100.000	-	-	-

TABLE B-2

PRELOAD VS. AXIAL PLAY

PRELOAD (N)	AXIAL PLAY (mm) $\times 10^{-3}$ M88000	LM67000	LM11700
44.48 (10 lb)	4.1	2.0	2.9
88.96 (20 lb)	1.8	3.3	4.6
133.44 (30 lb)	2.4	4.2	5.9
177.92 (40 lb)	2.9	5.1	7.1
222.4 (50 lb)	3.4	5.8	8.3

APPENDIX C

CALCULATION OF FORCE COMPONENTS ON SPIRAL BEVEL PINION GEAR

The procedure for computing the loads acting on the spiral bevel pinion gear was taken from Reference [1]. General expressions for the tangential, axial and radial load on the left hand gear driving clockwise are given below (see also Figure C-1).

$$K_t = \frac{T_p}{r_p}$$

$$K_a = \frac{K_t}{\cos\psi} (\tan\phi \sin\gamma_p + \sin\phi \cos\gamma_p)$$

$$K_r = \frac{K_t}{\cos\psi} (\tan\phi \cos\gamma_p - \sin\phi \sin\gamma_p)$$

$$M = K_a \cdot Pd/2$$

where

T_p = pinion torque = 105,410 N-mm

r_p = pitch radius = 23.38 mm

ϕ = pressure angle = 20°

ψ_p = spiral angle = 35°* (gives maximum loads)

γ = pitch angle = 15.33°

Substitution of these values gives

$$K_t = \frac{105,410}{23.38} = 4508.6 \text{ N}$$

$$K_a = \frac{4789.2}{20.8026} [(.364)(.268)+(.574)(.963)] = 3578. \text{ N}$$

$$K_r = \frac{4789.2}{20.8026} [(.364)(.9634)-(.574)(.268)] = 1084. \text{ N}$$

$$M = 3578 \cdot 46.76/2 = 83654 \text{ N-mm}$$

---

* The spiral angle ranges from 30° - 35°.

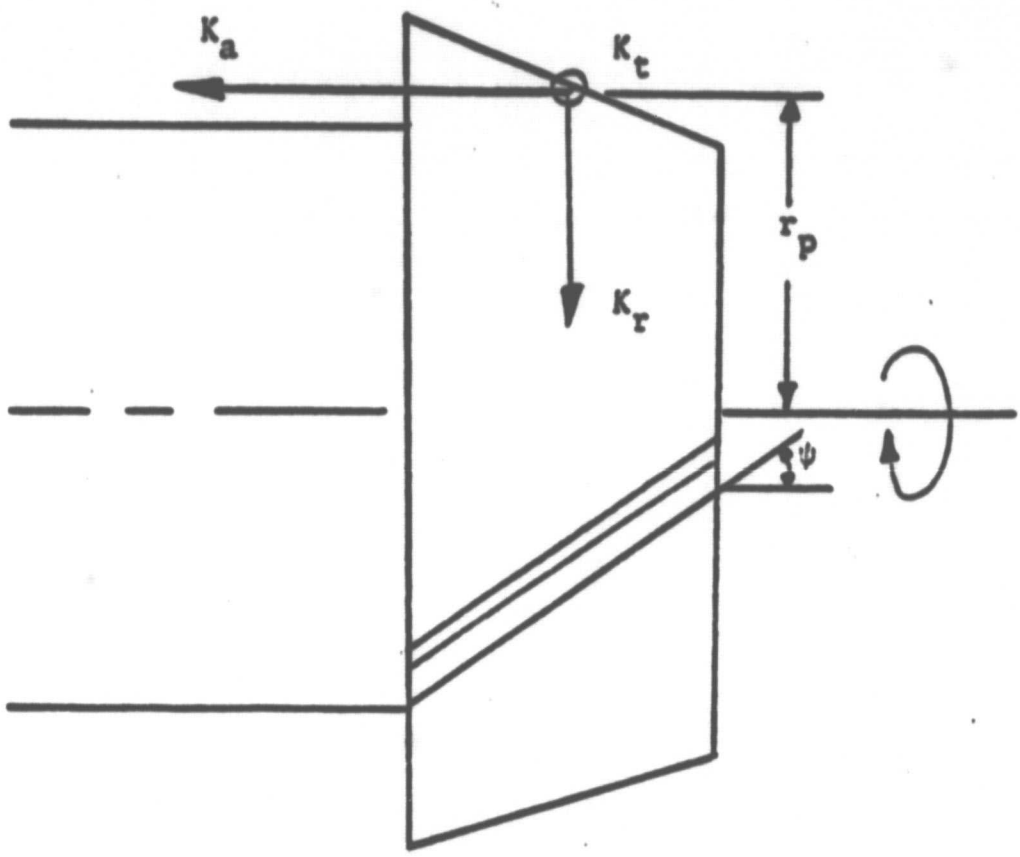

FIGURE C-1 TOOTH FORCES ON SPIRAL BEVEL GEAR

APPENDIX D

HEAT TRANSFER COEFFICIENTS FOR NASA HIGH SPEED INPUT PINION-TAPERED ROLLER BEARING STRADDLE DESIGN

1. Heat Conduction

This design of the NASA high speed input pinion module has a magnesium alloy housing and a shaft with two tapered roller bearing supports of steel. The model used to simulate the input pinion module is shown in Figure 2. Three conduction heat transfer coefficients (3) were used in the analysis:

1) Magnesium - 53.6517 watts/m-^{o}C
2) Steel - 46.7289 watts/m-^{o}C
3) Steel-Magnesium - 49.9516 watts/m-^{o}C

The third coefficient reflects conduction between a steel node and a magnesium node. The value was obtained using the following formula (4):

$$keqv = (0.5/K_S + 0.5/K_M)^{-1}$$

where K_S and K_M are the conductivities of the individual materials. Specifically:

$$K_3 = (0.5/53.6517 + 0.5/46.7289)^{-1} = 49.9516 \text{ watts/m-}^{o}\text{C}$$

The above calculation assumes a heat conduction path composed of 50% steel and 50% magnesium alloy. Since the magnitudes of the heat transfer coefficients for the two materials are very close, the error introduced is small, and the above assumption is justified.

Conduction between the bearing raceway and rolling element nodes is calculated internally by the program.

II. Forced Convection

The thermal properties of the lubricant, Santotrac 50, and air must be obtained to calculate the convection heat transfer coefficients. The values of the required thermal properties are summarized below:

Properties of Santotrac 50 Oil (5)

Thermal Conductivity	0.10 watts/m-^{o}C
Density at 100^{o}C	864 kg/m^{3}
Specific Heat	2130 watt-sec/kg-^{o}C
Kinematic Viscosity at 37.78^{o}C	33.6 X 10^{-6} m^{2}/sec
at 98.89^{o}C	5.61 X 10^{-6} m^{2}/sec

Properties of Air at 93^{o}C (6)

Thermal Conductivity	0.30 watts/m-^{o}C
Density	.96 kg/m^{3}
Specific Heat	1009 watts-sec/kg-^{o}C
Kinematic Viscosity	22.2 X 10^{-6} m^{2}/sec

(a) Convection between roller bearing components and lubricant

Using the equation on page B6 of Reference (2) for each of the two tapered roller bearings:

$$\alpha_i = 0.3047 \left\{ \frac{\omega}{\nu} \left[1 - \frac{D_i \cos \beta_i}{d_{m_i}} \right] \right\}^{1/2} K P_r^{1/3}$$

where ω = angular velocity of inner ring (rad/sec)
ν = kinematic viscosity of oil (m^{2}/sec)

β = 1/2 cup included angle (deg)
D = roller diameter (mm)
d_m = pitch diameter (mm)
K = thermal conductivity of oil (watts/m-^oC)
P_r = Prandtl number = $\rho\nu Cp/K$ = 103.24

with ρ = oil density
C_p = specific heat of oil
i = 1 ; BRG 1 (M88000)
2 ; BRG 2 (LM11700)

Substituting the appropriate values into the equation, one obtains:

$$\alpha_1 = 3337 \text{ watts/m}^2\text{-}^oC$$
$$\alpha_2 = 3446 \text{ watts/m}^2\text{-}^oC$$

(b) Convection between shaft and air inside input pinion module. The equation for forced convection from the outer surface of a rotating shaft on page B5 of Reference [2] was used to determine the Nusselt number.

$$Nu = 0.11\ [0.5\ Re^2\ Pr]^{0.35} = 4781$$

where $Re = \frac{\omega\pi L^2}{\nu_A} = 5.88 \times 10^5$

L = shaft mean diameter = .0333m
ν_A = kinematic viscosity of air (m^2/sec)

The convection coefficient, α, was then calculated by the equation below.

$$\alpha = Nu\ K_A/L = 4307 \text{ watts/m}^2\text{-}^oC$$

where K_A = thermal conductivity of air (watts/m-^oC)

(c) Convection heat transfer to ambient air outside transmission. A heat transfer coefficient of 37 watts/m^2-^oC was used as per per Reference [4].

(d) Convection heat transfer between gear surface and lubricant. Based on the formulation of Patir and Cheng [7], and assuming turbulent flow over the entire gear surface, the heat transfer coefficient was calculated by the equation given below.

$$\alpha_T = K \sqrt{\frac{\omega}{\nu}}\ 0.0197\ (m + 2.6)^{0.2}\ Re_r^{0.3}\ Pr^{0.6}$$

where Reynold's number at radius r =

$$Re_r = \frac{r^2 \omega}{\nu} = 3.65 \times 10^5$$

m - exponent of wall temperature distribution = 0

Interpolating from Table 1 of Reference [7] one obtains Nu 2.69. Then, for this 100% turbulent case, one obtains,

$$\alpha_T = (0.10)\ [3748/(5.61 \times 10^{-6})]^{0.5}\ (.0197)$$

$$(2.6)^{0.2}\ \ (3.65 \times 10^5)^{0.3} (103.24)^{0.6}$$

$$\alpha_T = 46{,}446 \text{ watts/m-}^{o}\text{C}$$

III. Mass Transport Heat Transfer

A lubricant flow model is included within the nodal network, thermally simulating the input pinion system. This model takes into account the heat transported by the flow of lubricant. Up to ten unique coefficients can be used to describe the flow network. The coefficients, c_i, are computed as follows:

$$c_i = \rho C_p \dot{V}_i \text{ (watt/}^{o}\text{C)}$$

where ρ = fluid density (kg/m^3)

C_p = fluid specific heat (watt-sec/kg-^{o}C)

$\dot{V}$ = volumetric flow rate (m^3/sec)

APPENDIX 4
ANALYSIS OF ALTERNATE SHAFT SUPPORT CONFIGURATIONS

LETTER REPORT

TO: F. R. Morrison

REPORT NO: AT81D031L
PROJECT CODE: C135
DATE: 27 April 1981
FROM: S. S. Gassel
T. J. Deromedi
COPIES TO:

TITLE: Design Analysis of Alternate Configurations for the High Speed Input Pinion

REFERENCE:

ABSTRACT

This effort constitutes an analysis of alternative design configurations for a high speed input pinion of an advanced helicopter transmission using SKF software SHABERTH. The objective is to select a design optimal with respect to weight, which provides sufficient bearing L_{10} life (> 2500 hrs) and controls gear deformations from exceeding specified magnitudes. (Deflections <.025 mm; Rotation < $1.75(10)^{-3}$ rad).

The work has been carried out in three phases. Phases one and two (elastic analysis at level 0 and level 1 - isothermal) yielded a specific design; a straddle arrangement consisting of a thrust carrying cylindrical bearing on one side of the bevel gear opposed by a pair of angular contact ball bearings mounted in tandem. In the final phase of the analysis, the computer simulations included a thermal analysis which accounted for thermal and mechanical interactions of the hardware and its environment.

The selected design was found to perform within the specified constraints over a broad range of operating conditions, and warrants consideration for use in helicopter transmissions under similar load and speed conditions.

I. INTRODUCTION

The need for helicopter transmissions which process increased power densities has led to the innovative design of various modules which compare the gear box assembly.

High speed spiral bevel input pinions are a case in point. Here the desire to reduce weight has led to designs which employ fewer supports through the use of tapered and thrust carrying cylindrical bearings [1-3]. These arrangements have been found to perform well at high speeds provided adequate attention is payed to lubrication of the flange contact.

Ir references [4,5], the performance of preliminary designs for a pinion support system consisting of a shaft and two tapered roller bearings was evaluated. SHABERTH [6] was used to explore competing straddle and cantilever design concepts with two off-the- shelf bearings. A sequence of parameter studies led ultimately to designs of minimum weight with adequate bearing L_{10} life and sufficiently small gear deformations.

This particular study, while including lubrication and friction effects, assumed isothermal conditions. Nevertheless, the simulation indicated a potential for smearing at the flange contact for the specified operating conditions. Subsequent testing at high speed (40,000 rpm) confirmed this result.

The current study was directed at alternate designs for the input pinion support system. The objective, as before, was to select a design that provided minimum weight with sufficient bearing fatigue life (2500 hrs at 60% nominal gear load (NGL)) and gear deformations within specified limits (deflections <.001 in., maximum rotation <0.1° at 100% NGL).

The selection process evolved in 3 steps. Various configurations, four in all, were evaluated at level 0 (elastic analysis) to obtain a preliminary assessment of their performance. Subsequent simulations at level 1 (isothermal analysis including fabrication and friction effects) enabled selection of a novel candidate; a thrust carrying cylindrical bearing opposed by a pair of angular contact ball bearings which straddle the bevel gear. This configuration was analyzed further at level 1 with the thermal option of SHABERTH activated to confirm the adequacy of this design.

A sequence of parameter studies were performed during this phase of the work to quantify the effects of preload, lube flow rate and distribution, interference fits and percent gear load on the bearing fatigue lives and gear deformations. It was concluded that for the prescribed load and speed conditions, wherein the thrust carrying capability of the cylindrical roller bearing is used primarily to carry preload, the selected design functions within the defined performance limits over a wide range of operational conditions.

The organizational structure of this report is as follows: Section II describes the results from the preliminary studies of the initial designs at level 0. In section III, the analysis at level 1 of these same designs is described. The thermo-mechanical analysis of the selected designs is presented in section IV. Section V provides a summary and cites specific conclusions and recommendations. Finally, a group of appendices follow the major sections to give additional technical detail on computations of model input parameters.

II. ANALYSIS OF ALTERNATE CONFIGURATIONS AT LEVEL 0

Results presented below correspond to analyses of the four pinion configurations (1A, 1B, 2A, 2B) (see Figures 1,2) consisting of cylindrical roller bearings (type 303 or 205) in the #1 position and a stack of angular contact ball bearings (type 205) in the #2, #3 and #4 positions. Designs 1A, 1B are straddle arrangements where the cylindrical carries only radial load. The ball bearings, preloaded against one another, provide axial restraint. Designs 2A, 2B are more novel in that thrust carrying cylindricals are employed. These are preloaded against a tandem of balls. In the former straddle arrangement the cylindrical carries only the preload axially. See Appendix A for a detailed description of each bearing type.

These SHABERTH runs peformed at level 0, do not include lubrication and friction effects. Shaft wall thickness was held at approximately 50% of the shaft diameter. Inner ring speed was fixed at 35,963 rpm. Preloads were applied as specified (Figures 1 & 2) and fits were modelled as line to line.

Design 1A offers slightly better minimum bearing fatigue life than design 1B. Minimum fatigue life for 1A was (3145 hrs) for the cylindrical roller bearing. The first ball bearing (#2) for design 1B showed the smallest life (2915 hrs). Corresponding minimum lives

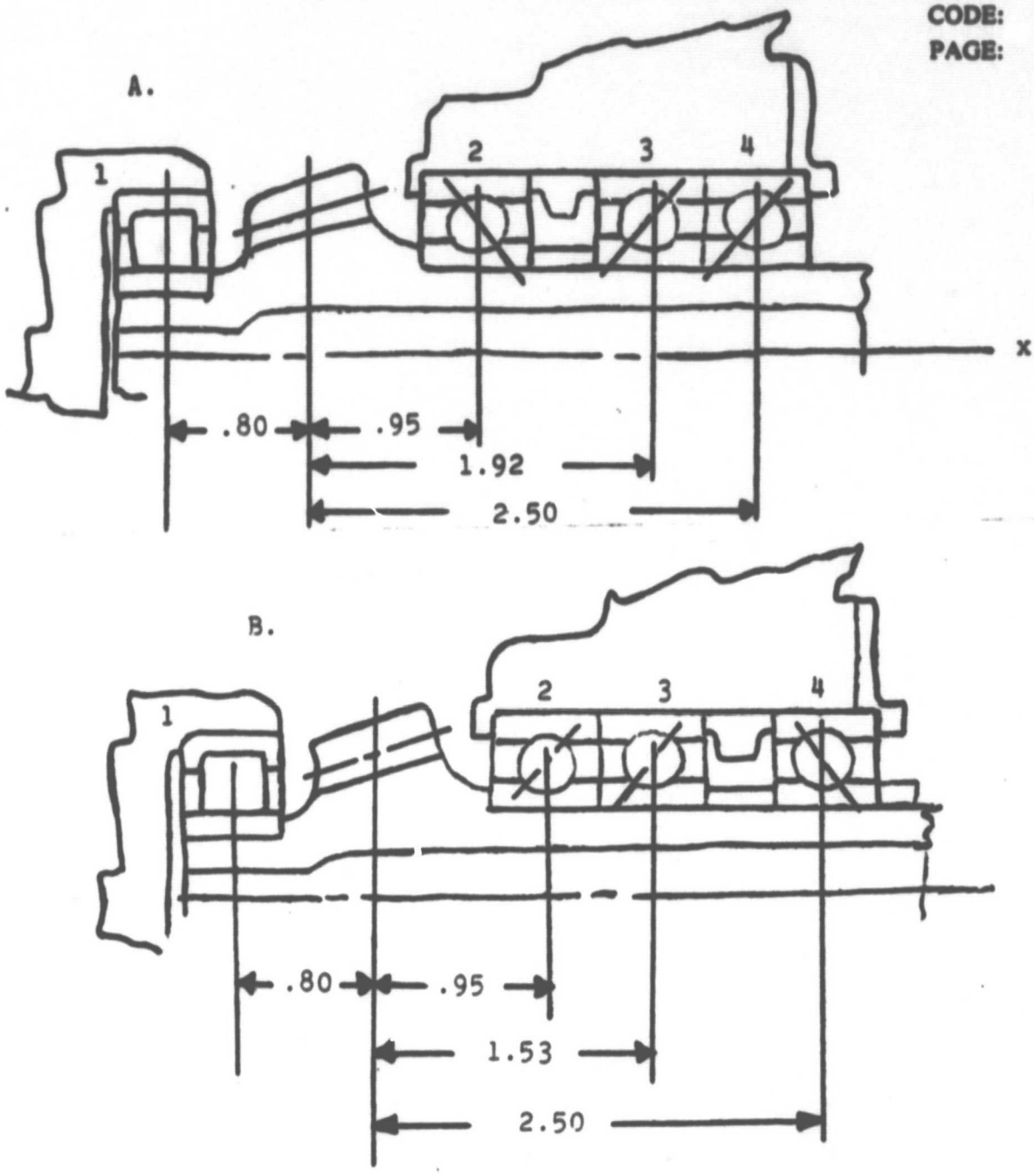

Notes: Bearing 1 - 303 Roller Bearing
Bearings 2,3,4 - 205 Ball Bearings

A. 2 Preloaded at 889.6N, shared equally by 3 & 4.
B. 4 Preloaded at 889.6N, shared equally by 2 & 3.

FIGURE 1. ALTERNATE PINION DESIGNS 1A AND 1B

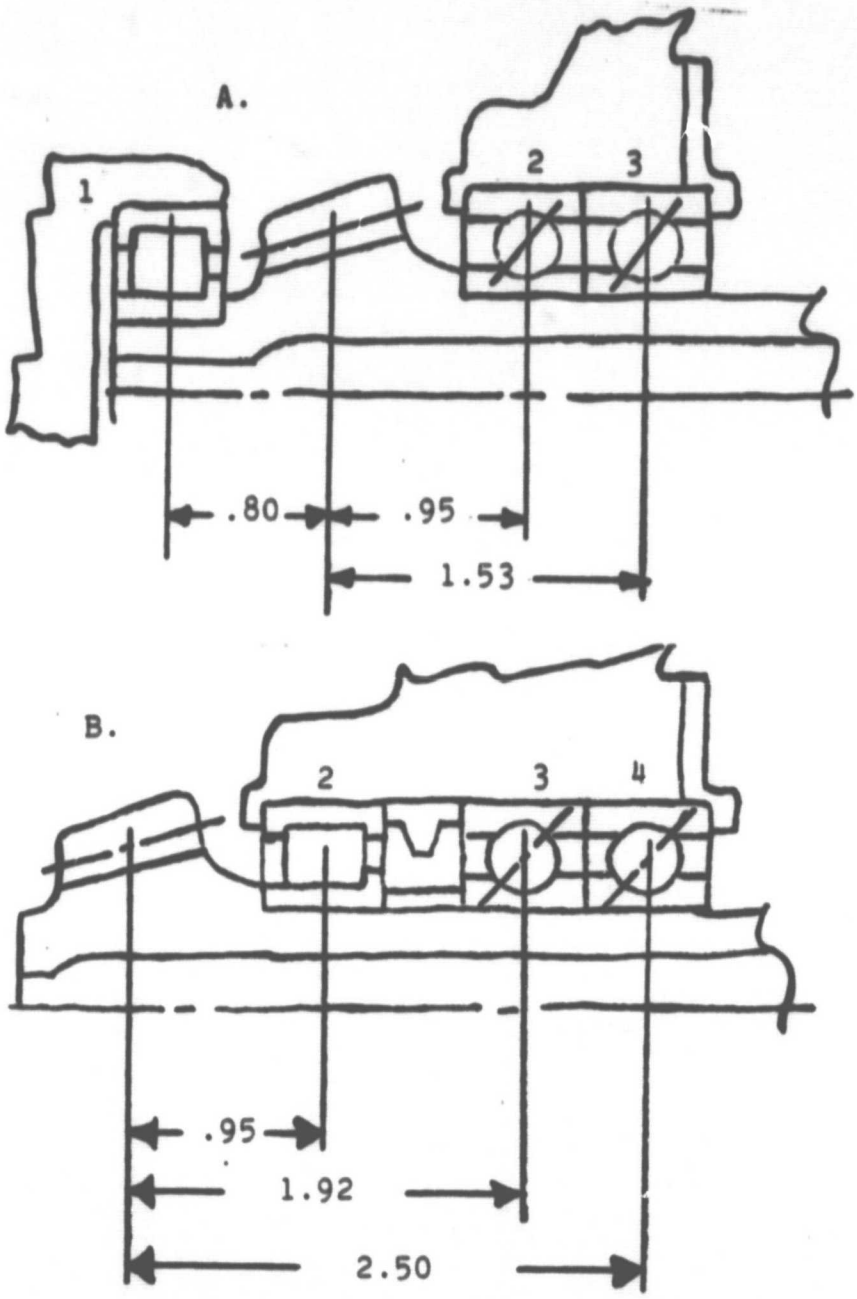

Notes:
A. Bearing 1 - 303 Roller with thrust capability, preloaded 444.8N, shared equally by 2 & 3. Bearings 2 & 3 - 205 ball bearings.
B. Bearing 2 - 205 Roller with thrust capability, preloaded at 444.8N shared equally by 3 & 4. Bearings 3 & 4 - 205 ball bearings.

FIGURE 2. ALTERNATE PINION DESIGNS 2A AND 2B

TABLE 1: COMPARISON OF FATIGUE LIFE FOR THE 4 DESIGNS AT 60% GEAR LOAD USING LIFE FACTOR = 5.

	Life in Hours			
Design	Bearing No. (1)	Bearing No. (2)	Bearing No. (3)	Bearing No. (4)
1A	3145	16300	5650	7600
1B	14300	2915	5595	19550
2A	5135	7450	5325	--
2B	70	16700	910	--

TABLE 2: GEAR DEFLECTIONS (mm/rotations(radians) AT 100% WGL AND 50% WALL THICKNESS

Design Type	δ Radial	δ Axial	θ Maximum
1A	1.00(-2) *	1.92(-2)	2.20(-4)
1B	0.94(-2)	1.81(-2)	2.46(-4)
2A	1.00(-2)	1.89(-2)	2.70(-4)
2B	5.56(-2)	4.41(-2)	15.30(-4)

* Notation number(-N) = number x 10^{-N}

for designs 2A and 2B were 5135 hours and 70 hours, respectively, for the thrust carrying cylindricals. The cylindrical bearing in the cantilever design (2B) is misaligned due to the large rotation at the gear end. This causes the extremely low fatigue life.

The gear deflections and rotations for designs 1A, 1B and 2A are within the prescribed limits (deflections < .001 in., rotations <.1°). The deflections, both axial and radial, for design 2B (cantilever) exceed the allowable limit. They are 4.41 (-2) and 5.59 (-2) mm, respectively.

It was clear that design 2A performs better than 2B. It was agreed to continue parameter studies for this design (2A). The choice between 1A and 1B was not obvious. The limiting bearing lives and peak gear deformations are close for both configurations. However, their system lives are considerably different. According to Harris [7],

$$L_{10}^{\text{systems}} = \left[\sum_{j=1}^{N_b} (L_{10,j})^{-1/8} \right]^{-8/9}$$

where N_b = number of bearings (4),

j = bearing index,

9/8 = Weibull slope (constant)

The system lives for designs 1A and 1B were computed to be, respectively, 1420 and 1815 hours. As such, it was agreed that design 1B be selected as a candidate for further studies at level 1 (i.e. including lubrication and traction effects).

III. ANALYSIS OF DESIGNS 1B AND 2A AT LEVEL 1

As reported, two of the proposed alternate designs (1B, 2A) were selected for further analytical study on the basis of the preliminary analytical investigation. In version 1B, the pinion shaft is supported by a cylindrical roller bearing on one end and a three bearing bidirectional, angular contact stack on the other, and for version 2A a thrust carrying cylindrical roller bearing is used on one end preloaded against two angular contact ball bearings

on the other. This analysis addressed the effects of lubrication and friction on the L_{10} life of the load support systems under isothermal conditions. Parametric studies of the effects of varying preload and interference fits on fatigue life and gear deformation were executed for an operating temperature of 150°C. These results provide a relative comparison between the two designs of interest. The initial results are shown below in Table 3,

TABLE 3: TABULATION OF L_{10} LIVES AT 60% NOMINAL GEAR LOAD FOR DESIGNS 1B AND 2A WITH (LEVEL 1) AND WITHOUT (LEVEL 0) LUBRICATION AND FRICTION EFFECTS

SHAFT = 50% WALL THICKNESS; FITS = 0.0 mm; PRELOADS = NOMINAL

	Bearing L_{10} Life (Hours)			
Design Type	No. 1	No. 2	No. 3	No. 4
1B (level 0)	14,300	2,915	5,595	19,550
1B (level 1)	6,006	1,632	3,133	10,950
2A (level 0)	5,135	7,450	5,325	---
2A (level 1)	2,157	3,874	2,769	---

A significant reduction in fatigue life, compared with the level 0 results (i.e. no lubrication and friction effects) is demonstrated in the table. This is attributed to the low lubrication life factors (0.56) associated with a small elastohydrodynamic film. The latter is due to low lubricant viscosity at the specified operating temperature of 150°C. Operational lubricant temperatures are expected to be significantly lower (100°C), so that the lubricant life factors will be large and will not reduce the life nearly as much as currently predicted.

Results from a series of computer runs performed at 60% nominal gear load, nominal preloads and a range of interference fits are given in Table 4.

TABLE 4: TABULATION OF L_{10} LIVES AT 60% NOMINAL GEAR LOAD FOR DESIGNS 1B AND 2A - LEVEL 1 - ISOTHERMAL

SHAFT = 50% WALL THICKNESS; FITS = .02 mm, .01 mm
NOMINAL PRELOADS (N)-1B: 0.0, 889.6, 444.8, 444.8
2A: 444.8, 222.4, 222.4

		Bearing L_{10} Life (Hours)			
Design Type	Fit (mm)	No. 1	No. 2	No. 3	No. 4
1B	0.02	4,230	2,290	2,395	8,135
1B	0.01	4,905	1,765	2,475	8,380
1B	0.00	6,006	1,632	3,133	10,950
2A	0.02	3,115	4,515	2,505	---
2A	0.01	2,370	4,140	2,585	---
2A	0.00	2,157	3,874	2,769	---

The presence of the fit induces axial preload in the ball bearings.* As such, the diametral clearance was adjusted for non-zero fits to obtain the nominal preload. In the case of the roller bearings, fits do not induce axial preload. However, they cause a redistribution of the load vector; hence the bearing fatigue lives are seen to vary with fits. The fits tend to stiffen the system by eliminating the operating clearance in the cylindrical bearings. As such, the deformations are smaller than previously computed in the level 0 runs.

The results, tabulated for 100% nominal gear load, are presented in Table 5.

* See Appendix B.

TABLE 5: TABULATION OF GEAR DEFORMATIONS (mm/radians) AT 100% NOMINAL GEAR LOAD FOR DESIGNS 1B AND 2A VS. INTERFERENCE FITS.

LEVEL 1 - ISOTHERMAL (FITS = 0.02 mm); LEVEL 0 - (FITS = 0.00 mm)

SHAFT = 50% WALL THICKNESS; NOMINAL PRELOAD

Design Type	Fit	Radial	Axial	Max.
1B (level 1)	0.02	0.84(-2)	1.47(-2)	1.85(-4)
1B (level 0)	0.00	0.94(-2)	1.81(-2)	2.46(-4)
2A (level 1)	0.02	0.9 (-2)	1.18(-2)	2.20(-4)
2A (level 0)	0.00	1.0 (-2)	1.89(-2)	2.70(-4)

The life performance of each design, as seen in Table 2, favors design 2A. Additionally, the life limiting bearing for design 1B (No. 2) is adjacent to the pinion gear. The large heat generation rate from the gear will detract from the anticipated fatigue life due to decreased lubricant film thickness produced at the higher temperatures. On the other hand, the limiting bearing in design 2A is remote from the gear and as such will not suffer such additional life reductions. Further, 2A is a more efficient design requiring 3 instead of 4 bearings. On this basis, it was decided that 2A be selected for further study with a coupled thermomechanical analysis.

IV. THERMAL ANALYSIS OF DESIGN 2A

A detailed thermal anlaysis of the pinion support design is required to more accurately quantify the performance of a load support configuration. The thermal option of SHABERTH was activated to study the final design configuration selected, 2A. This modelling improvement provided a more accurate simulation of the effects of preloads, fits and lubrication on bearing fatigue life and gear deformations.

IV.1 Description of Thermal Model

The SHABERTH steady-state thermal model was prepared for the straddle design which consists of a 303 cylindrical roller bearing with thrust carrying capability and a pair of 205 angular contact ball bearings.

The mechanical structure to be analyzed is thought of as divided into a number of elements or nodes, each represented by a temperature. The net heat flow to node i from the surrounding nodes j, plus the heat generated at node i, must numerically equal zero. This is true for each node i, i going from 1 to n, n being the number of unknown temperatures.

After each calculation of bearing generated heat, which results from a solution of the shaft-bearing system portion of the program, a set of system temperatures is determined which satisfy the system of equations:

$$q_i = q_{oi} + q_{gi} = 0 \text{ for all temperature nodes } i$$

where

q_{oi} is the heat flow from all neighboring nodes to node i

q_{gi} is the heat generated at node i. These values may be input or calculated by the shaft bearing program as bearing frictional heat.

The transfer of heat within a medium or between two media can occur by conduction, convection, radiation and fluid flow (mass transport).

All these types of heat transfers occur in a bearing application as the following examples show.

1) Heat is transferred by conduction between inner ring and shaft and between outer ring and housing.

2) Heat is transferred by convection between the surface of the housing and the surrounding air.

3) Heat is transferred by radiation between the shaft and the housing (considered negligible for current analysis).

4) When the bearing is lubricated and cooled by circulating oil, heat is transferred by fluid flow.

Therefore, in calculating the net flow to a node all the above mentioned modes of heat transfer, except radiation, were considered.

Figure 3 shows the geometric model and the nodal system for the metal components and surrounding fluid media. The housing was taken to be magnesium while other metal nodes were considered to be steel for the purpose of obtaining heat conduction coefficients. There are four nodes for each ball bearing, seven nodes for the roller bearing and thirteen nodes for the shaft (including the gears) and the housing. In addition, there are two air nodes. This nodal network provides for accurate local as well as global monitoring of component temperatures.

The lubricant flow paths and nodes are shown in Figure 4. It was assumed that oil from the chiller (node No. 40) exited at constant temperature (83°C). The oil flow is separated into five paths, three for the bearings and two for the gears. The calculation for the heat convection includes interactions between the

1) fluid and bearing rolling element, race and cages

2) fluid and gear surface

3) shaft and housing surface and surrounding air

4) oil and housing surface

5) housing external surface and the ambient air which is assumed to be at a constant temperature (21°C).

Other modeling assumptions as well as detailed description of program input are provided in Appendix C of this report. Pinion operating conditions are listed in the following:

- Shaft Speed = 36,000 rpm
- Gear Load Vector = (3578, 1084, 4509) N @ 100%
- Lubricant = Santotrac-50 [9]
- Bevel Gear and Tail Rotor Drive Gear Power Losses Equal 5600 and 616 watts, respectively.

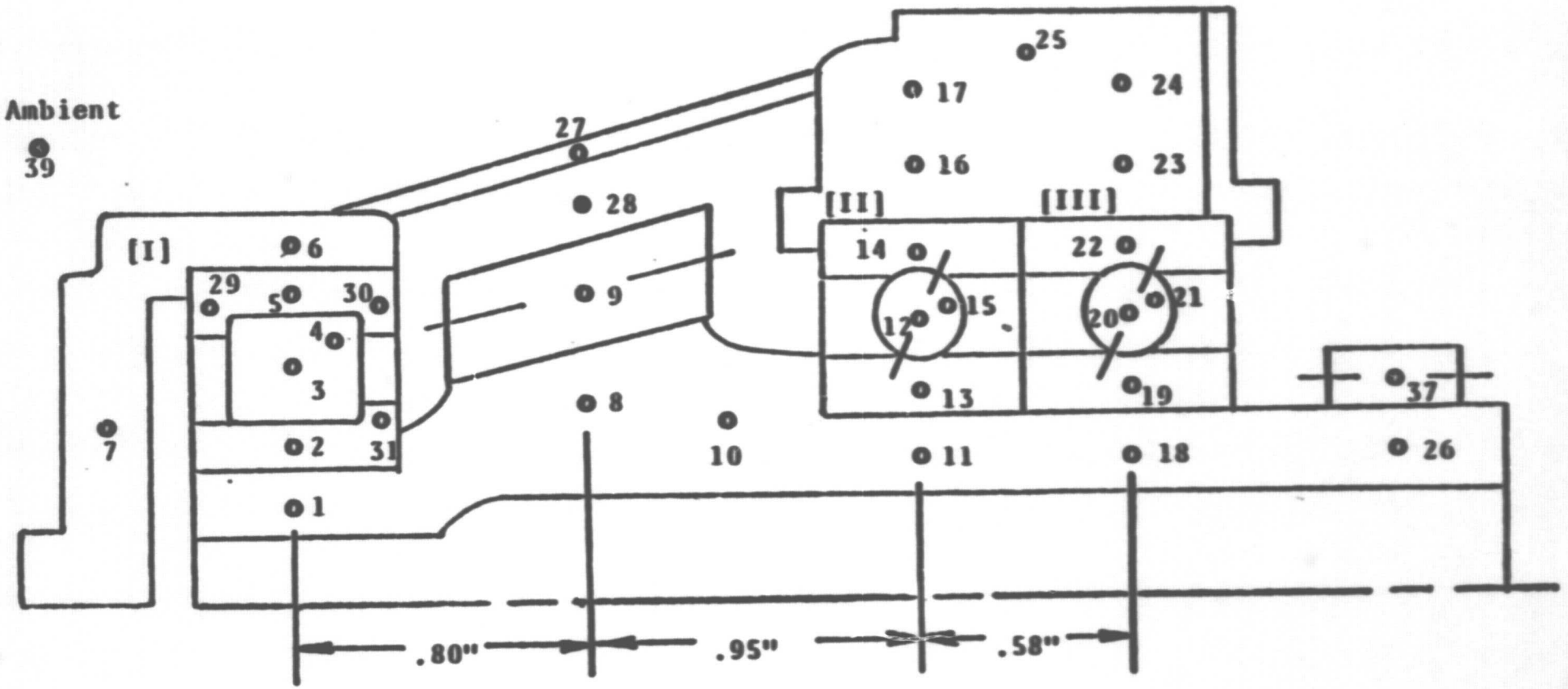

● Air Node

o Metal Node

I, II, III = Bearing Nos.

FIGURE 3. GEOMETRY MODEL & THERMAL NODES (AIR & METAL)

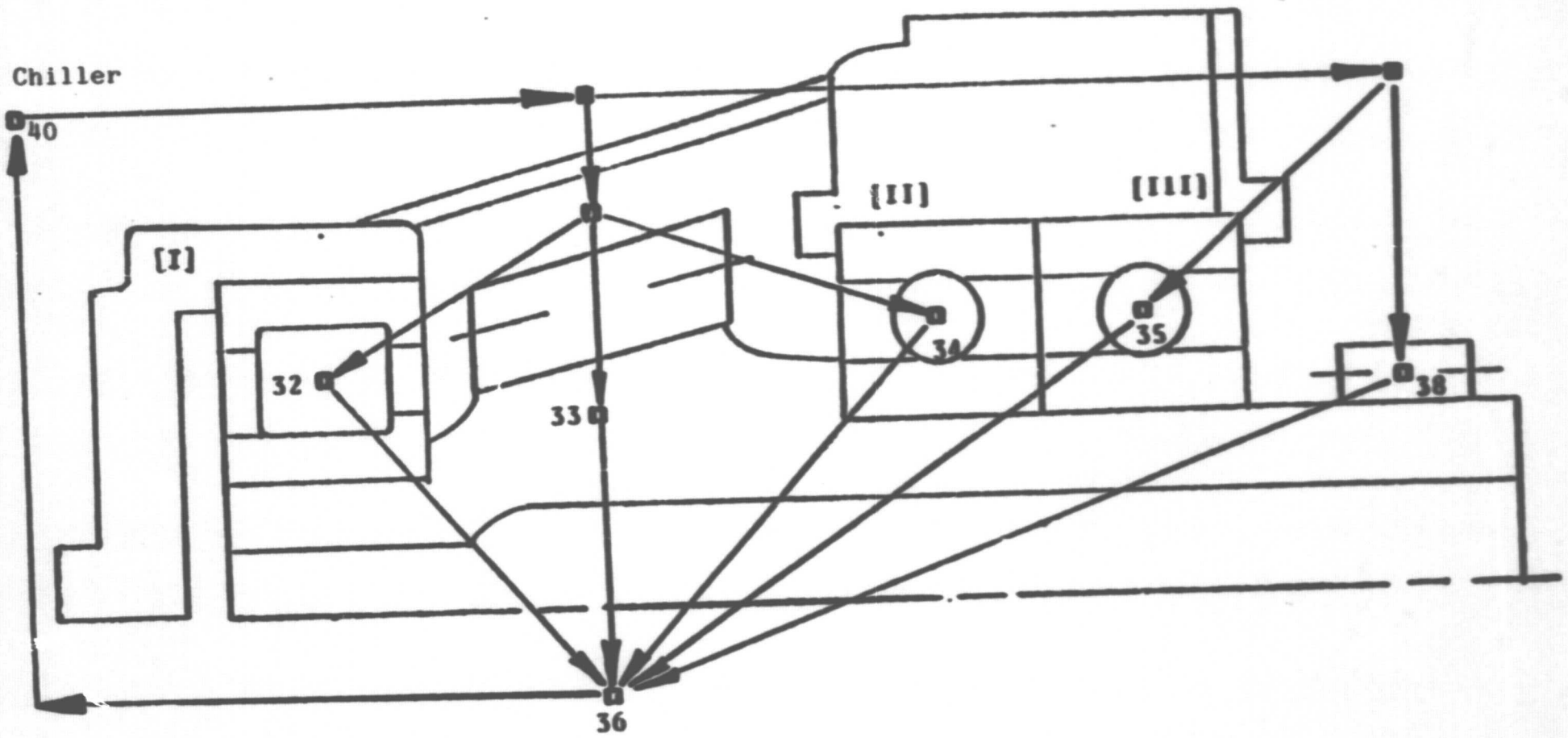

■ Flow Node

■ Flow Juncture

I, II, III = Bearing Nos.

FIGURE 4. OIL FLOW DIAGRAM & FLOW NODES

IV.2 Summary of Thermomechanical Analysis Results

A sequence of parameter studies were carried out on the selected pinion configuration. These included variation of fits, preload, lube flow rate, as well as applied bevel gear load.

Results which detail the effects of varying these parameters on the bearing fatigue lives and gear deformations are given in tabular form. Table 6 defines the values for small, nominal and large interference fits, preloads and lube flow rates. Table 7 shows the effect of varying these parameters on the bearing L_{10} lives at 60% nominal gear load. Table 8 provides the deformations at the gear mesh point at 100% nominal gear load.

The bearing fatigue lives are minimally affected by the specified changes in preload and lube flow rate. Companion results obtained from an isothermal (150°C) simulation (level 1 - lubrication and friction efforts included) are listed to establish a baseline. The dramatic increase in the lives of the ball bearings (more than triple) is attributed to enhanced film thickness at the newly predicted lower operating temperature. Such results highlight the need for a coupled analysis. The tight (large) fit does significantly reduce the life of the cylindrical roller bearing. This is attributed to the large radial preload as well as a decrease in film thickness associated with increased temperatures. In this case, as in all others, the diametral clearance in the ball bearings was adjusted to maintain the nominal preload, compensating for the tight fit. Deformations at the gear mesh point are well within allowable limits.

In addition to the global data described above, a detailed temperature map is available with each execution. An example is provided in Table 9 under operating conditions of nominal preload, fits and lube flow rate and 60% nominal gear load.

TABLE 6: VALUES FOR SMALL (S), NOMINAL (N) AND LARGE (L) INTERFERENCE FITS, PRELOADS AND LUBE FLOW RATES FOR BEARINGS 1, 2, 3.

Item	Small	Nominal	Large
Fits (mm) (Inner) (Outer)	0.01, 0.01, 0.01 0. , 0. , 0.	0.02, 0.02, 0.02 0. , 0. , 0.	0.04, 0.04, 0.04 0. , 0. , 0.
Preload (lbs)	50: 25/25	100: 50/50	200: 100/100
Lube Flow Rate lpm (gpm)	.025 .013 .013 (0.1) (0.05) (0.05)	.053 .025 .025 (0.2) (0.1) (0.1)	.106 .053 .053 (0.4) (0.2) (0.2)

TABLE 7: EFFECT OF FITS, PRELOAD AND LUBE FLOW RATE ON BEARING L_{10} LIVES AT 60% NOMINAL GEAR LOAD

			L_{10} Lives (Hrs)		
Fit	Preload	Flow Rate	Bearing 1	Bearing 2	Bearing 3
N	N	S	2923	14860	12510
N	N	L	3208	14710	11870
N	N	N	3117	14840	12810
N	S	N	3406	15490	12950
N	L	N	2913	13870	12530
L	N	N	760	14820	12040
S	N	N	2932	14880	12980
N	N	N	3117	14840	12810
	ISOTHERMAL		3115	4140	2585

TABLE 8: EFFECT OF VARYING PRELOAD ON THE DEFORMATIONS AT THE GEAR MESH POINT AT 100% NOMINAL GEAR LOAD

Preload	δ Axial (mm)	δ Radial (mm)	θ Max (rad)
L	0.009	0.0094	0.24 (-3)
N	0.010	0.0095	0.25 (-3)
S	0.011	0.0096	0.26 (-3)

NODE	DESCRIPTION	TEMP. (°C)	NODE	DESCRIPTION	TEMP. (°C)
1	Shaft	127.4	21	Cage (III)	96.1
2	Inner Ring	127.8	22	Outer Ring (III)	95.8
3	Roller (I)	124.8	23	Housing	95.7
4	Cage (I)	93.9	24	Housing	95.5
5	Outer Ring (I)	111.0	25	Housing	93.8
6	Housing	110.1	26	Shaft	99.7
7	Housing	109.8	27	Housing	97.2
8	Shaft	126.4	28	Internal Air	100.8
9	Bevel Gear	127.3	29	Flange (I)	113.8
10	Shaft	122.3	30	Flange (I)	141.1
11	Shaft	108.7	31	Flange (I)	111.7
12	Ball (II)	108.1	32	Oil Node (I)	91.2
13	Inner Ring (II)	103.7	33	Oil Node (Bevel Gear)	96.1
14	Outer Ring (II)	96.7	34	Oil Node (II)	91.1
15	Cage (II)	95.9	35	Oil Node (III)	90.6
16	Housing	95.8	36	Collector	107.8
17	Housing	95.4	37	Rotor Drive Gear	98.8
18	Shaft	103.5	38	Oil Node (Rotor Drive Gear)	96.3
19	Inner Ring (III)	103.4	39	Ambient	21.0*
20	Ball (III)	103.0	40	Chiller	83.0*

* Known Temperature

TABLE 9: TEMPERATURE MAP OF INPUT PINION

REFERENCES

1. Morrison, F. R. et al, "A Functional Evaluation of a Thrush Carrying Cylindrical Roller Bearing Design," ASME Paper No. 78-Lub-28.

2. Connors, T. F. and Morrison, F. R., "Feasibility of Tapered Roller Bearing for Main Shaft Engine Applications," USAAMRDL Technical Report 73-46, Eustis Directorate, U. S. Army Air Mobility Research and Development Laboratory, August 1973.

3. Lemanski, A. J., Lenski, J. W., Drago, R. J., "Design Fabrication Test and Evaluation of Spiral Bevel Support Bearings (Tapered Roller)," USAAMRDL Technical Report 73-16, Eustis Directorate, U. S. Army Air Mobility Research and Development Laboratory, June 1973, AD769064.

4. Gassel, S. S., "Development of a Small Bore, High Speed Tapered Roller Bearing, Task I Bearing Shaft Analysis," SKF Report No. AL79P004, January 1979.

5. Gassel, S. S., Deromedi, T. J. and Avanzato, R., "Optimization of Taper Supported High Speed Input Pinion," SKF Letter Report No. AT81D017L, April 1981.

6. Crecelius, W. J., Research Report User's Manual for SKF Computer Program, "SHABERTH, for the Steady State and Transient Thermal Analysis of Shaft Bearing Systems Including Ball, Cylindrical and Tapered Roller Bearings," SKF Report No. AL77P015, developed under U.S. Army Contract DAAD05-75-C-0747.

7. Harris, T., Roller Bearing Analysis, John Wiley and Sons, 1966.

8. Patir, N. and Cheng, H. S., "Prediction of Bulk Temperature in Spur Gears Based on Finite Element Temperature Analysis," ASLE Transactions, Vol. 22, 1, pp. 25-36.

9. Loewenthal, S. H. and Parker, R. J., "Rolling-Element Fatigue Life With Two Synthetic Cycloaliphatic Traction Fluids," NASA TND-8124, March 1976.

10. Kleckner, R. J. and Deromedi, T. J., "Curve Fit for ASME's Lubrication Life Factor vs. Lamda (Λ) Chart," SKF Letter Report No. AL79P007L, 27 September 1979.

11. Ragen, M. A., "Final Report on Simulation of the Steady State and Time Transient Thermal Performance of the AH-1G/Q Input Pinion Module," SKF Report No. AL79P012, May 1979.

12. Ragen, M. A., "Final Report on Prediction of Time to Failure of the CH-53 Helicopter Power Input Module After Loss of the Lubrication," SKF Report No. AL79P013, submitted under U. S. Army Contract No. DAAD05-75-C-0755, Ballistic Research Laboratories, Aberdeen Proving Ground, Maryland, 1979.

13. Kreith, F., Principles of Heat Transfer, 3rd Edition, Intext Educational Publishers, 1973.

APPENDIX A

BEARING DIMENSIONS

205/303 Roller Bearings

Roller Bearing No.	205	303
Bearing Width (mm)	15.0	14.0
Bore Diameter (mm)	25.0	17.0
Outer Diameter (mm)	52.0	47.0
Pitch Diameter (mm)	38.5	32.1
No. of Rollers	12	10
Roller Diameter (mm)	6.5	7.0
Roller Length (mm)	6.5	7.0
Roller Crown Radius (mm)	622.3	670.0
Roller Flat Length (mm)	2.1	4.5

205 Ball Bearing

Bearing Width (mm)	15.0
Bore Diameter (mm)	25.0
Outer Diameter (mm)	52.0
Pitch Diameter (mm)	38.5
Outer Ring Groove Radius (mm)	4.930
Inner Ring Groove Radius (mm)	4.917
Ball Diameter	9.525
No. of Balls	11
Nominal Contact Angle	25°

APPENDIX B

PRELOAD CALIBRATION

In SHABERTH, axial preloads are imposed by selection of a negative initial deformation (diametral clearance) parameter. An equivalent preload was computed for the 205 ball bearing using the procedure described below.

The system external loads were removed and the rotational speed set to 10 rpm. A negative diametral clearance was selected and the support system analyzed to evaluate bearing axial loads on the inner rings. This provided a point on the load-deflection curve. The process was repeated until the entire calibration curve was obtained. At this point the displacement corresponding to a given preload could be extracted from the curve. Since the shaft interference fit induces a preload for angular contact ball bearings, these curves were generated for fits of 0.0, 0.1, 0.2 mm as shown in Figure B-1.

The axial preload for the thrust carrying cylindrical bearings (No. 205, 303) was calibrated using the contact theory presented in Harris [7]. We have for the flange

$$\delta = 2.57 \times 10^{-4}\, \delta^{*}\, Q_f^{2/3}\, (\Sigma\rho)^{1/3} \text{ (mm)} \quad \text{(flange deflection)}$$

where

$\Sigma\rho = 1/R_1 + 1/R_2$ (R_1, R_2 = prinicpal radii of curvature at roller end-flange contact)

$$\delta^{*} = \frac{1/R_2 - 1/R_s}{\Sigma\rho}$$ (R_s = sphere end radius)

$Q_f = P/z$ (P = preload (N), z = no. of rollers)

The load-deflection curves are given in Figure B-2.

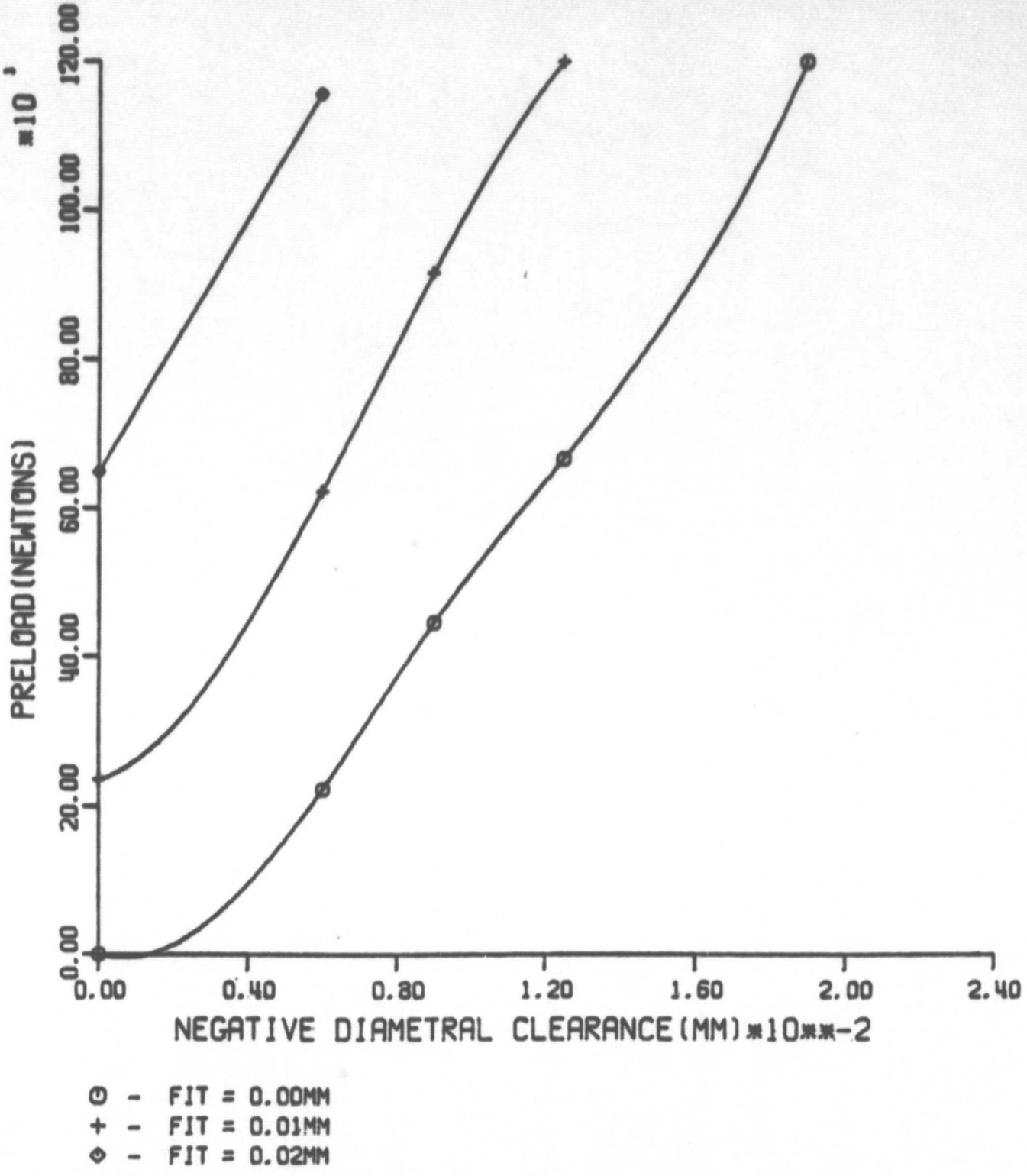

FIGURE B-1 PRELOAD CALIBRATION FOR 205 ANGULAR CONTACT BALL BEARING

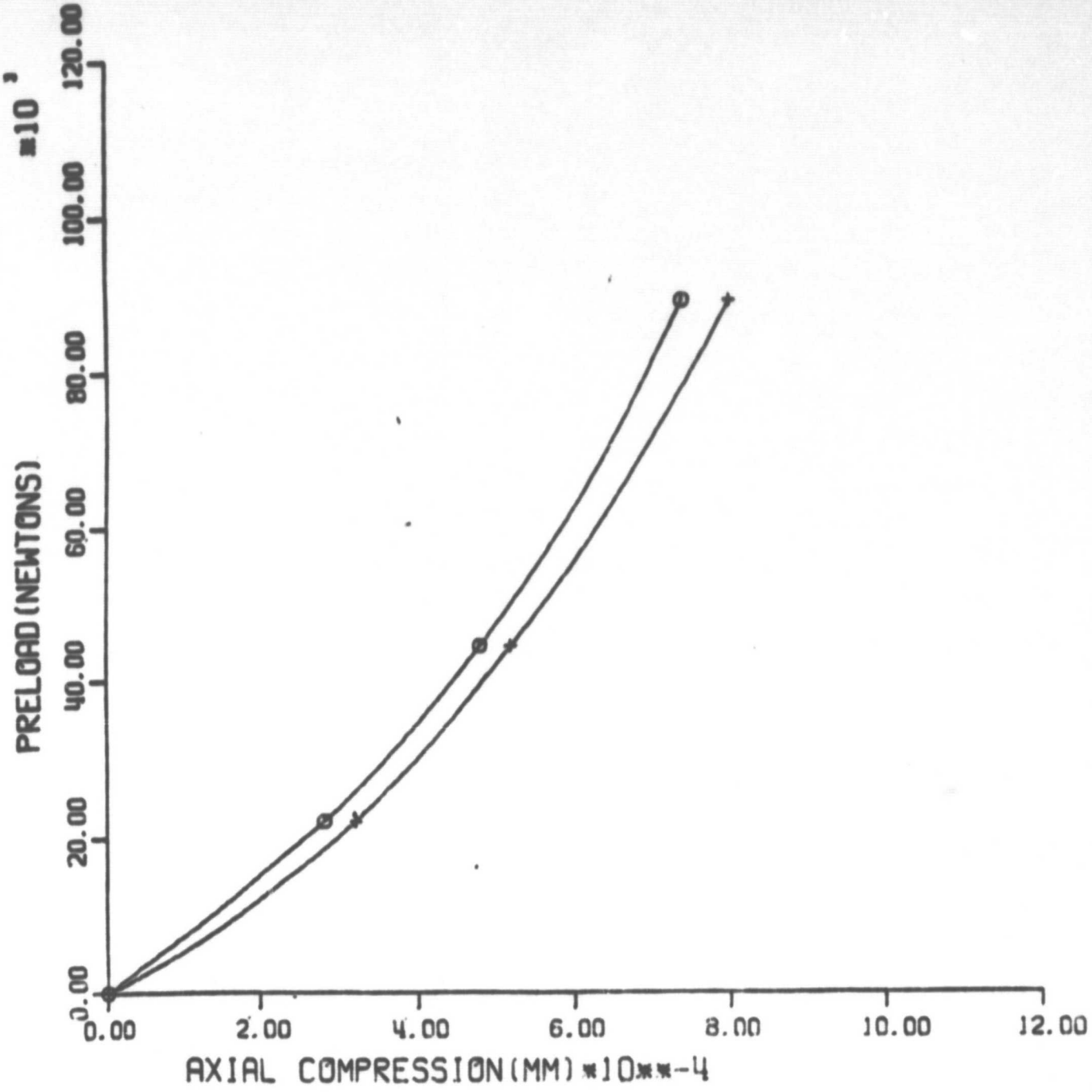

FIGURE B-2 PRELOAD CALIBRATION FOR 205/303 ROLLER BEARINGS

APPENDIX C

HEAT TRANSFER COEFFICIENTS FOR NASA HIGH SPEED INPUT PINION - CYLINDRICAL AND BALL BEARING TANDEM STRADDLE DESIGN

I. Heat Conduction

This design of the NASA high speed input pinion module has a magnesium alloy housing and a shaft supported by a thrust carrying cylindrical bearing on one side of the bevel gear opposed by a pair of angular contact ball bearings mounted in tandem. The model used to simulate the input pinion module is shown in Figure 3 . Two conduction heat transfer coefficients (11) were used in the analysis.

(1) Magnesium - 53.6517 watts/m-^{o}C

(2) Steel - 46.7289 watts/m-^{o}C

Since the magnitudes of the heat transfer coefficients for the two materials are very close, any variation in the coefficients due to steel-magnesium conduction paths is very small, and use of the coefficient acting over the majority of the conduction path is justified.

Conduction between the bearing raceway and rolling element nodes is calculated internally by the program.

II. Forced Convection

The thermal properties of the lubricant, Santotrac 50, and air must be obtained to calculate the convection heat transfer coefficients. The values of the required thermal properties are summarized below.

Properties of Santotrac 50 Oil (9)

Thermal Conductivity	0.10 watts/m-^{o}C
Density at 37.78^{o}C	886 kg/m^{3}
Specific Heat	2130 watt-sec/kg-^{o}C
Kinematic Viscosity at 37.78^{o}C	33.6 x 10^{-6} m^{2}/sec
at 98.89^{o}C	5.61 x 10^{-6} m^{2}/sec

Properties of Air at 50^{o}C (13)

Thermal Conductivity	0.0278 watts/m-^{o}C
Density	1.09 kg/m^{3}
Specific Heat	1000 watts-sec/kg-^{o}C
Kinematic Viscosity	17.8 x 10^{-6}m^{2}/sec

A. Forced Convection Between Roller Bearing Components and Lubricant

A program option was activated which allows the heat transfer coefficient (α) to be calculated internally, with α being a function of the Nusselt, Reynolds and Prandtl numbers and the viscosity being temperature dependent, specifically,

$$Nu = K\, Re^{a} Pr^{b}$$

$$\alpha = \lambda\, Nu/L$$

where

Re = Reynolds Number = $UL/\nu(t)$

Pr = Prandtl Number = $\frac{\rho\nu(t)C_p}{\lambda}$

K = 0.3

a = 0.57

b = 0.0

λ = thermal conductivity (watts/m-^oC)

L = characteristic length (m)

= .0070 m for roller bearing

= .00953 m for ball bearing

U = characteristic velocity (m/s)

= 38 m/s for roller bearing

= 43 m/s for ball bearing

$\nu(t)$ = temperature dependent kinematic viscosity (m^2/s)

ρ = density (kg/m^3)

C_p = specific heat (watts-sec/kg-^oC)

B. <u>Convection Between Shaft and Air Inside Input Pinion Module</u>

The heat transfer coefficient was calculated in the same manner as above, with the following substitutions:

L = .0468 m

U = 88.1 m/s

Also note that the properties of air replaced the properties of oil in this calculation.

C. Convection Heat Transfer to Ambient Air Outside Transmission

A heat transfer coefficient of 37 watts/m^2-^oC was used as per References [11,12].

D. Convection Heat Transfer Between Gear Surface and Lubricant

Based on the formulation of Patir & Cheng [8], the heat transfer coefficient was calculated by the equations given below.

For Laminar Flow:

$$\alpha_L = Nu\ K \sqrt{\frac{\omega}{\nu}}$$

For Turbulent Flow:

$$\alpha_T = K \sqrt{\frac{\omega}{\nu}}\ \ 0.0197(m+2.6)^{0.2}\ Re_r^{0.3}\ Pr^{0.6}$$

where

Re_r = Reynold's number at radius r = $\frac{r^2\omega}{\nu}$ = 3.65×10^5

m = exponent of wall temperature distribution = 0

Interpolating from Table 1 of Reference [8] one obtains Nu = 2.69. Then, for the laminar case,

$$\alpha_L = 2.69\ (0.10)\ [3748/5.61 \times 10^{-6}]^{0.5}$$

$$= 6952 \text{ watts/m-}^oC$$

For the turbulent case one obtains,

$$\alpha_T = (0.10)\ [3748/5.61 \times 10^{-6}]^{0.5}(.0197)(2.6)^{0.2}\ (3.65 \times 10^5)^{0.3}\ (103.24)^{.6}$$

$$\alpha_T = 46{,}446 \text{ watts/m-}^oC$$

It has been shown [8] that, in industrial applications, a large portion of the gear surface area is in the laminar regime, and a constant weighted average heat transfer coefficient reflecting that result is sufficiently accurate for our purposes:

$$\alpha = .9\ \alpha_L + .1\ \alpha_T$$

$$\alpha = 10{,}901 \text{ watts/m-}^{o}\text{C}$$

III. Mass Transport Heat Transfer

A lubricant flow model is included within the nodal network thermally simulating the input pinion system. This model takes into account the heat transported by the flow of lubricant. Up to ten unique coefficients can be used to describe the flow network. The coefficients, C_i, are computed as follows:

$$C_i = \rho C_p \dot{V}_i \text{ (watt/}^{o}\text{C)}$$

where

ρ = fluid density (kg/m^3)

C_p = fluid specific heat (watt-sec/kg-^{o}C)

$\dot{V}$ = volumetric flow rate (m^3/sec)

APPENDIX 5
EXPERIMENTAL DATA COLLECTED FROM INDIVIDUAL TEST SERIES

TABLE 1

DATA SHEET FUNCTIONAL TEST OF DOMESTIC M88000 SERIES BEARINGS UNDER 60%

Bearing Numbers: Inboard #2
Outboard #1

Lubricant: MIL-L-23699

Speed (Rad/S)	Time at Speed (Minutes)	Applied Load Per Bearing (N) Radial	Axial	Lubricant Flow Rate Per Brg. (L/Min.) Jets	Thru the Shaft	Operating Temperatures K Lubricant Supply	Inboard Bearing	Outboard Bearing	Lubricant Inboard Side	Scavenge Outboard Side
1047	55	1912	4715	.34	.28	316	305	316	316	316
1570	52	1912	5337	.21	.15	363	380	383	377	377
2094	50	1912	6005	.21	.15	363	394	400	386	386

TABLE 2

DATA SHEET FUNCTIONAL TEST OF DOMESTIC M88000
SERIES BEARINGS UNDER 60% LOAD

Bearing Numbers: Inboard #4
Outboard #3

Lubricant: MIL-L-23699

Speed (Rad/S)	Time at Speed (Minutes)	Applied Load Per Bearing (N) Radial	Axial	Lubricant Flow Rate Per Brg. (L/Min.) Jets	Thru the Shaft	Operating Temperatures K Lubricant Supply	Inboard Bearing	Outboard Bearing	Lubricant Inboard Side	Scavenge Outboard Side
1047	45	1912	1557	.35	.36	327	341	338	338	338
2094	45	1912	2135	.28	.34	352	375	369	375	377

TABLE 3

DATA SHEET FUNCTIONAL TEST OF DOMESTIC M88000
SERIES BEARINGS UNDER 60%

Bearing Numbers: Inboard #4
Outboard #3

Lubricant: MIL-L-23699

Speed (Rad/S)	Time at Speed (Minutes)	Applied Load Per Bearing (N) Radial	Axial	Lubricant Flow Rate Per Brg. (L/Min.) Jets	Thru the Shaft	Operating Temperatures K Lubricant Supply	Inboard Bearing	Outboard Bearing	Lubricant Inboard Side	Scavenge Outboard Side
523	60	1912	2135	.23	.19	333	338	338	338	338
1047	30	1912	1557	.24	.19	347	350	347	347	350
1570	120	1912	1557	.20	.19	361	372	372	369	377
2094	30	1912	1779	.20	.19	361	383	383	380	391
2617	15	1912	2446	.20	.19	361	402	413	400	430

TABLE 4

DATA SHEET FUNCTIONAL TEST OF DOMESTIC M88000 SERIES BEARINGS UNDER LIGHT LOAD

Bearing Numbers: Inboard #4, Outboard #5

Lubricant: MIL-L-23699

Speed (Rad/S)	Time at Speed (Minutes)	Applied Load Per Bearing (N) Radial	Axial	Lubricant Flow Rate Per Brg. (L/Min.) Jets	Thru the Shaft	Lubricant Supply	Operating Temperatures K Inboard Bearing	Outboard Bearing	Lubricant Inboard Side	Scavenge Outboard Side
2617	25	887	3114	.26	.68	355	383	380	388	380
3141	20	887	3914	.22	.76	372	405	422	405	433
3403	40	887	3412	.23	.74	380	408	411	408	416

TABLE 5

DATA SHEET FUNCTIONAL TEST OF DOMESTIC M88000 SERIES BEARINGS UNDER 60%

Bearing Numbers: Inboard #4
Outboard #1

Lubricant: MIL-L-23699

Speed (Rad/S)	Time at Speed (Minutes)	Applied Load Per Bearing (N) Radial	Axial	Lubricant Flow Rate Per Brg. (L/Min.) Jets	Thru the Shaft	Operating Temperatures K Lubricant Supply	Inboard Bearing	Outboard Bearing	Lubricant Inboard Side	Scavenge Outboard Side
523	25	1912	4092	.34	.28	336	341	341	338	341
1047	30	1912	4448	.34	.28	341	358	361	355	361
1570	25	1912	5160	.34	.28	355	377	377	377	386
2094	30	1912	5160	.30	.34	363	391	391	394	402
2617	30	1912	5929	.26	.34	322	388	402	394	421

TABLE 6

Summary of Lubricant Distribution Modification

Shaft Speed (Rads/Sec.)	Lubricant Temp. (°K)	Lubricant Flow (ℓ/min) Outboard Bearing Large End	Outboard Bearing Small End	Inboard Bearing Small End	Inboard Bearing Large End
523	293	.064	.041	.026	.022
1570	294	.045	.038	.060	.030
2617	344	.062	.170	.230	.143

Original Hole Configuration	Outboard Bearing Large End	Outboard Bearing Small End	Inboard Bearing Small End	Inboard Bearing Large End
Lubricant Supply Tube	4 Holes 1.57mm	4 Holes 1.57mm	4 Holes 1.57mm	4 Holes 1.57mm
Shaft	--	4 Holes 2.38mm	4 Holes 2.38mm	4 Holes 2.38mm
Inner Race	9 Holes 1.57mm	9 Holes .89mm	9 Holes .89mm	9 Holes 1.57mm

TABLE 7

Summary of Lubricant Distribution Modification

Shaft Speed (Rads/Sec.)	Lubricant Temp. (°K)	Lubricant Flow (ℓ/min) Outboard Bearing Large End	Outboard Bearing Small End	Inboard Bearing Small End	Inboard Bearing Large End
2617	340	.003	.227	.087	.109

Hole Configuration	Outboard Bearing Large End	Outboard Bearing Small End	Inboard Bearing Small End	Inboard Bearing Large End
Lubricant Supply Tube	4 Holes 1.57mm	4 Holes 1.57mm	4 Holes 1.57mm	4 Holes 1.57mm
Shaft	4 Grooves in Cap*	4 Holes 2.38mm	4 Holes 2.38mm	4 Holes 2.38mm
Inner Race	9 Holes 1.57mm	9 Holes .89mm	9 Holes .89mm	9 Holes 1.57mm

*Change from previous data sheet

TABLE 8

Summary of Lubricant Distribution Modification

Shaft Speed (Rads/Sec.)	Lubricant Temp. (°K)	Lubricant Flow (ℓ/m'n) Outboard Bearing Large End	Outboard Bearing Small End	Inboard Bearing Small End	Inboard Bearing Large End
2617	344	.041	.109	.109	.163

Two "O" rings put on lubricant supply tube to retard axial flow of air and lubricant.*

Hole Configuration	Outboard Bearing Large End	Outboard Bearing Small End	Inboard Bearing Small End	Inboard Bearing Large End
Lubricant Supply Tube	4 Holes 1.57mm	4 Holes 1.57mm	4 Holes 1.57mm	4 Holes 1.57mm
Shaft	4 Grooves in Cap	4 Holes 2.38mm	4 Holes 2.38mm	4 Holes 2.38mm
Inner Race	9 Holes 1.57mm	9 Holes .89mm	9 Holes .89mm	9 Holes 1.57mm

*Change from previous data sheet

TABLE 9

Summary of Lubricant Distribution Modification

Shaft Speed (Rads/Sec.)	Lubricant Temp. (°K)	Lubricant Flow (ℓ/min) Outboard Bearing Large End	Outboard Bearing Small End	Inboard Bearing Small End	Inboard Bearing Large End
2617	344	.087	.034	.079	.038
3141	344	.087	.034	.204	.072

"0" rings removed.

Teflon flinder/baffle added to outside of lubricant supply tube to retard axial flow of air and lubricant*.

Hole Configuration	Outboard Bearing Large End	Outboard Bearing Small End	Inboard Bearing Small End	Inboard Bearing Large End
Lubricant Supply Tube	4 Holes 1.57mm	4 Holes 1.57mm	4 Holes 1.57mm	4 Holes 1.57mm
Shaft	4 Grooves in Cap	4 Holes 2.38mm	4 Holes 2.38mm	4 Holes 2.38mm
Inner Race	9 Holes 1.57mm	9 Holes .89mm	9 Holes .89mm	9 Holes 1.57mm

*Change from previous data sheet

TABLE 10

Summary of Lubricant Distribution Modification

Shaft Speed (Rads/Sec.)	Lubricant Temp. (°K)	Lubricant Flow (ℓ/min) Outboard Bearing Large End	Outboard Bearing Small End	Inboard Bearing Small End	Inboard Bearing Large End
2617	338	.310	.401	.556	.030

Teflon flinger/baffle on lubricant tube

Hole Configuration	Outboard Bearing Large End	Outboard Bearing Small End	Inboard Bearing Small End	Inboard Bearing Large End
Lubricant Supply Tube	2 Holes 2.26mm*	2 Holes 1.57mm*	2 Holes 1.57mm*	2 Holes 1.57mm*
Shaft	4 Grooves in Cap	4 Holes 2.38mm	4 Holes 2.38mm	4 Holes 2.38mm
Inner Race	9 Holes 1.57mm	9 Holes .89mm	9 Holes .89mm	9 Holes 1.57mm

*Change from previous data sheet

TABLE 11

Summary of Lubricant Distribution Modification

Shaft Speed (Rads/Sec.)	Lubricant Temp. (°K)	Lubricant Flow (ℓ/min) Outboard Bearing Large End	Outboard Bearing Small End	Inboard Bearing Small End	Inboard Bearing Large End
2617	338	.231	.394	.564	.113

Teflon flinger/baffle on lubricant tube

Hole Configuration	Outboard Bearing Large End	Outboard Bearing Small End	Inboard Bearing Small End	Inboard Bearing Large End
Lubricant Supply Tube	2 Holes 2.26mm	2 Holes 1.57mm*	2 Holes 1.57mm*	1 Hole 1.57mm 1 Hole 2.26*
Shaft	4 Grooves in Cap	4 Holes 2.38mm	4 Holes 2.38mm	4 Holes 2.38mm
Inner Race	9 Holes 1.57mm	9 Holes .89mm	9 Holes .89mm	9 Holes 1.57mm

*Change from previous data sheet

TABLE 12

Summary of Lubricant Distribution Modification

Shaft Speed (Rads/Sec.)	Lubricant Temp. (°K)	Lubricant Flow (ℓ/min) Outboard Bearing Large End	Outboard Bearing Small End	Inboard Bearing Small End	Inboard Bearing Large End
2617	338	.337	.450	.600	.075

Fluorcarbon flinger/baffle added to outside of lubricant supply tube to retard axial flow of air and lubricant.

Hole Configuration	Outboard Bearing Large End	Outboard Bearing Small End	Inboard Bearing Small End	Inboard Bearing Large End
Lubricant Supply Tube	2 Holes 2.26mm	1 Hole 1.57mm	1 Hole 1.57mm	2 Holes 2.26mm
Shaft	4 Grooves in Cap	4 Holes 2.38mm	4 Holes 2.38mm	4 Holes 2.38mm
Inner Race	9 Holes 1.57mm	9 Holes .89mm	9 Holes .89mm	9 Holes 1.57mm

*Change from previous data sheet

TABLE 13

DATA SHEET FUNCTIONAL TEST OF DOMESTIC M88000
SERIES BEARINGS UNDER LIGHT LOAD

Bearing Numbers: Inboard #6
Outboard #5

Lubricant: MIL-L-23699

Speed (Rad/S)	Time at Speed (Minutes)	Applied Load Per Bearing (N)		Lubricant Flow Rate Per Brg. (L/Min.)		Operating Temperatures K				
		Radial	Axial	Jets	Thru the Shaft	Lubricant Supply	Inboard Bearing	Outboard Bearing	Lubricant Inboard Side	Scavenge Outboard Side
2617	40	890	2967	.23	.81	366	386	386	391	386
3403	10	890	3260	.23	.76	363	397	397	400	400
3665	25	890	3959	.23	.68	347	397	397	397	400

TABLE 14

DATA SHEET FUNCTIONAL TEST OF DOMESTIC M88000 SERIES BEARINGS UNDER LIGHT LOAD

Bearing Numbers: Inboard 8
Outboard 7

Lubricant: MIL-L-23699

Speed (Rad/S)	Time at Speed (Minutes)	Applied Load Per Bearing (N)		Lubricant Flow Rate Per Brg. (L/Min.)		Operating Temperatures K				
		Radial	Axial	Jets	Thru the Shaft	Lubricant Supply	Inboard Bearing	Outboard Bearing	Lubricant Inboard Side	Scavenge Outboard Side
523	30	890	3558	.26	.76	319	336	336	333	330
1047	25	890	3914	.23	.87	336	350	347	350	347
1570	15	890	3558	.26	.92	344	363	363	363	361
2094	30	890	4270	.26	.94	350	372	372	372	383
2617	25	890	4448	.23	.94	352	383	383	383	388
3141	20	890	4626	.43	1.05	358	391	391	394	400
3665	30	890	4982	.43	1.14	372	405	405	408	422

Stop Inboard Bearing Failed

TABLE 15

Summary of Lubricant Distribution Modification

Shaft Speed (Rads/Sec.)	Lubricant Temp. (°K)	Lubricant Flow (ℓ/min) Outboard Bearing	Inboard Bearing
1570	330	1.42	.821
2199	330	1.21	.842
2617	338	1.20	.793
3141	338	1.11	.872
3403	341	1.030	.898

Fluorcarbon flinger/baffle added to outside of lubricant supply tube to retard axial flow of air and lubricant.

Hole Configuration	Outboard Bearing Large End	Outboard Bearing Small End	Inboard Bearing Small End	Inboard Bearing Large End
Lubricant Supply Tube	2 Holes 1.57mm*	0 Holes*	0 Holes*	1 Hole 1.57mm*
Shaft	4 Grooves in Cap	0 Holes*	0 Holes*	4 Holes ?.38mm
Inner Race	18 Holes 1.57mm*	0 Holes*	0 Holes*	18 Holes 1.57mm*

*Change from previous data sheet

TABLE 16

Data Sheet: Preliminary Test of Domestic MB8000 Series Bearings Under Light Load

Bearing Numbers 9 & 10
Lubricant: MIL-L-23699

Speed (Rad/S)	Time at Speed (Minutes)	Applied Load Per Bearing (N) Radial	Axial	Lubricant Flow Rate Per Brg. (L/Min.) Jets	Thru the Shaft	Operating Temperatures (K) Lubricant Supply	Inboard Bearing	Outboard Bearing	Lubricant Inboard Side	Scavenge Outboard Side
2617	90	436	3260	1.37	1.23	327	356	356	347	348
3141	50	436	4448	1.37	1.23	316	358	361	351	350
3403	20	436	4982	1.37	1.23	317	361	366	352	355

Outboatd Bearing (#10) Failed After 10 Minutes at 3665 Rad. Per Sec.

TABLE 17

Data Sheet: Functional Test of Domestic M88000 Series Bearings Under 60% Load

Bearing Numbers 9 & 7
Lubricant: MIL-L-23699

Speed (Rad/S)	Time at Speed (Minutes)	Applied Load Per Bearing (N)		Lubricant Flow Rate Per Brg. (L/Min.)		Operating Temperatures (K)				
		Radial	Axial	Jets	Thru the Shaft	Lubricant Supply	Inboard Bearing	Outboard Bearing	Lubricant Inboard Side	Scavenge Outboard Side
2617	50	1912	3780	0.81	1.05	391	403	410	408	423
3141	60	1912	4225	0.81	1.05	375	403	411	403	411

Inboard Bearing (#9) Failed After 1 Hour at 3141 Rad. Per Second

TABLE 18

Data Sheet: Functional Test of German M88000 Series Bearings Under 60% Load

Bearing Numbers 11 & 12
Lubricant: MIL-L-23699

Speed (Rad/S)	Time at Speed (Minutes)	Applied Load Per Bearing (N)		Lubricant Flow Rate Per Brg. (L/Min.)		Operating Temperatures (K)				
		Radial	Axial	Jets	Thru the Shaft	Lubricant Supply	Inboard Bearing	Outboard Bearing	Lubricant Inboard Side	Scavenge Outboard Side
523	25	1913	2669	1.12	1.05	322	331	330	325	325
1047	40	1913	2357	1.37	1.23	338	349	348	342	342
1570	75	1913	3558	1.12	1.23	356	369	370	362	364
2094	90	1913	4003	1.37	1.23	372	384	384	380	382
2617	75	1913	4003	1.37	1.23	358	381	380	388	388
3141	50	1913	4448	1.37	1.55	370	394	391	387	388
3665	30	1913	4448	1.37	1.55	372	397	395	390	392
3926	30	1913	4226	1.37	1.55	373	401	400	394	395
4188	30	1913	4448	1.37	1.55	378	403	406	397	405

Test Completed

TABLE 19

Data Sheet: Functional Test of German Made M88000 Series Bearings Under 100% Load

Bearing Numbers 13 & 14
Lubricant: MIL-L-23699

Speed (Rad/S)	Time at Speed (Minutes)	Applied Load Per Bearing (N)		Lubricant Flow Rate Per Brg. (L/Min.)		Operating Temperatures (K)				
		Radial	Axial	Jets	Thru the Shaft	Lubricant Supply	Inboard Bearing	Outboard Bearing	Lubricant Inboard Side	Scavenge Outboard Side
523	30	3216	6227	1.37	1.55	338	346	345	341	344
1047	20	3216	5337	1.37	1.55	350	361	360	350	355
1570	40	3216	5338	1.37	1.55	369	385	384	372	383
2094	40	3216	5782	1.37	1.55	354	378	377	366	366
2617	135	3216	4226	1.37	1.55	379	396	395	391	395
3141	5	3216	4448	1.37	1.55	380	395	394	386	398
3403	5	3216	4448	1.37	1.55	379	401	400	395	400
3665	10	3216	4448	1.37	1.55	380	402	402	398	400
4188	15	3216	4448	1.37	1.55	383	407	406	403	406

Test Suspended: End of Day

TABLE 20

Data Sheet: Functional Test of German Made MB8000 Series Bearings Under 100% Load

Bearing Numbers 13 & 14
Lubricant: MIL-L-23699

Speed (Rad/S)	Time at Speed (Minutes)	Applied Load Per Bearing (N)		Lubricant Flow Rate Per Brg. (L/Min.)		Operating Temperatures (K)				
		Radial	Axial	Jets	Thru the Shaft	Lubricant Supply	Inboard Bearing	Outboard Bearing	Lubricant Inboard Side	Scavenge Outboard Side
2094	25	3216	8896	1.37	1.55	377	395	392	387	398
2617	75	3216	8896	1.37	1.55	358	388	386	380	395
3141	25	3216	8896	1.37	1.55	371	403			
3665	25	3216	8894	1.62	1.55	375	403	400	417	
4188	60	3216	8894	1.62	1.55	371		403	371	

Test Completed

TABLE 21

Data Sheet: Functional Test of German Made MB8000 Series Bearings Under 150% Load

Bearing Numbers 15 & 16
Lubricant: MIL-L-23699

Speed (Rad/S)	Time at Speed (Minutes)	Applied Load Per Bearing (N)		Lubricant Flow Rate Per Brg. (L/Min.)		Operating Temperatures (K)				
		Radial	Axial	Jets	Thru the Shaft	Lubricant Supply	Inboard Bearing	Outboard Bearing	Lubricant Inboard Side	Scavenge Outboard Side
1570	30	4844	7117	1.37	1.55	357	377	373	373	-
2094	20	4844	7117	1.62	1.55	376	397	393	391	-
2617	60	4844	7117	1.62	1.55	361	388	393	390	-
3141	25	4844	10231	1.62	1.55	372	408	404	412	-
3403	15	4844	10676	1.62	1.55	371	409	406	410	-

Inboard Bearing (#16) Failed After 15 Minutes at 3403 Rad. Per Second

TABLE 22

Summary of Lubricant Distribution Modification

Shaft Speed (Rads/Sec.)	Lubricant Temp. (°K)	Lubricant Flow (ℓ/min) Outboard Bearing	Inboard Bearing
2617	373	4.16	1.47
3141	373	4.54	1.74

Fluorcarbon flinger/baffle added to outside of lubricant supply tube to retard axial flow of air and lubricant.

Hole Configuration	Outboard Bearing Large End	Outboard Bearing Small End	Inboard Bearing Small End	Inboard Bearing Large End
Lubricant Supply Tube	2 Holes 1.57mm	0 Holes*	0 Holes*	1 Hole 1.57mm
Shaft	4 Grooves in Cap	0 Holes*	0 Holes*	4 Holes 2.38mm
Inner Race	18 Holes 1.57mm	0 Holes*	0 Holes*	18 Holes 1.57mm

*Change from previous data sheet

TABLE 23

Data Sheet: Functional Test of German M88000 Series Bearings Under 100% Load

Bearing Numbers 15 & 17
Lubricant: Santotrac 50

Speed (Rad/S)	Time at Speed (Minutes)	Applied Load Per Bearing (N)		Lubricant Flow Rate Per Brg. (L/Min.)		Operating Temperatures (K)				
		Radial	Axial	Jets	Thru the Shaft	Lubricant Supply	Inboard Bearing	Outboard Bearing	Lubricant Inboard Side	Scavenge Outboard Side
1570	50	3215	6450	1.62	1.55	368	380	386	376	372
2094	35	3215	5783	1.62	1.55	385	399	395	394	390
2617	35	3215	5783	1.62	1.55	376	395	391	391	386
3141	60	3215	6227	1.62	1.55	373	399	394	394	388
3403	95	3215	6227	1.62	1.55	375	403	399	400	394
3665	60	3215	6227	1.62	1.55	375	407	403	400	394
3926	25	3215	6672	1.62	1.55	366	401	397	397	391
4188	60	3215	-	1.62	1.55	371	411	406	406	406

Test Complete

TABLE 24

Data Sheet: Extended Duration Functional Test of German M88000 Series Bearings Under 100% Load - Run 1

Bearing Numbers 15 & 17
Lubricant: Santotrac 50

Speed (Rad/S)	Time at Speed (Hours)	Applied Load Per Bearing (N)		Lubricant Flow Rate Per Brg. (L/Min.)		Operating Temperatures (K)				
		Radial	Axial	Jets	Thru the Shaft	Lubricant Supply	Inboard Bearing	Outboard Bearing	Lubricant Inboard Side	Scavenge Outboard Side
523	.4	3215	7117	1.26	1.60	297	310	310	306	300
1047	.2	3215	7117	1.26	1.60	321	336	335	333	332
1570	.3	3215	7562	1.26	1.60	339	353	352	352	349
2094	.3	3215	7562	1.26	1.60	361	374	374	375	373
2617	.5	3215	8007	1.26	1.60	368	384	385	387	383
3141	.3	3215	8652	1.26	1.60	370	394			
3403	-	-	-	-	-	-	-	-	-	-
3665	.2	3215	8896	1.26	1.60	372	399	398	400	397
3926	-	-	-	-	-	-	-	-	-	-
4188	4.9	3.2	8.8	1.26	1.60	*	*	*	*	*

Test Suspended

*Data Lost Due to Computer Malfunction

TABLE 25

Data Sheet: Extended Duration Functional Test of German MB8000 Series Bearings Under 100% Load - Run 2

Bearing Numbers 15 & 17
Lubricant: Santotrac 50

Speed (Rad/S)	Time at Speed (Hours)	Applied Load Per Bearing (N)		Lubricant Flow Rate Per Brg. (L/Min.)		Operating Temperatures (K)				
		Radial	Axial	Jets	Thru the Shaft	Lubricant Supply	Inboard Bearing	Outboard Bearing	Lubricant Inboard Side	Scavenge Outboard Side
3141	1	3215	5783	1.60	1.67	351	377	371	365	371
3665	.5	3215	6005	1.60	1.67	371	397	389	386	391
4188	5.5	3215	6138	1.60	1.67	371	405	395	391	398

Test Suspended End of Day

TABLE 26

Data Sheet: Extended Duration Functional Test of German M88000 Series Bearings Under 100% Load - Run 3

Bearing Numbers 15 & 17
Lubricant: Santotrac 50

Speed (Rad/S)	Time at Speed (Hours)	Applied Load Per Bearing (N) Radial	Axial	Lubricant Flow Rate Per Brg. (L/Min.) Jets	Thru the Shaft	Operating Temperatures (K) Lubricant Supply	Inboard Bearing	Outboard Bearing	Lubricant Inboard Side	Scavenge Outboard Side
3141	.3	3215	6138	1.60	1.67	337	373	367	348	362
3665	.3	3215	6272	1.60	1.67	341	387	379	357	370
4188	6	3215	6672	1.60	1.67	365	401	395	368	381

Test Suspended End of Day

TABLE 27

Data Sheet: Extended Duration Functional Test of German M88000 Series Bearings Under 100% Load - Run 4

Bearing Numbers 15 & 17
Lubricant: Santotrac 50

Speed (Rad/S)	Time at Speed (Hours)	Applied Load Per Bearing (N) Radial	Axial	Lubricant Flow Rate Per Brg. (L/Min.) Jets	Thru the Shaft	Operating Temperatures (K) Lubricant Supply	Inboard Bearing	Outboard Bearing	Lubricant Inboard Side	Scavenge Outboard Side
3141	.2	3215	6140	1.60	1.67	337	370	367	365	357
3665	.2	3215	6183	1.60	1.67	341	384	381	383	366
4188	5.5	3215	6717	1.60	1.67	359	398	394	398	390

Test Suspended End of Day

TABLE 28

Data Sheet: Extended Duration Functional Test of German M88000 Series Bearings Under 100% Load - Run 5

Bearing Numbers 15 & 17
Lubricant Santotrac 50

Speed (Rad/S)	Time at Speed (Hours)	Applied Load Per Bearing (N)		Lubricant Flow Rate Per Brg. (L/Min.)		Operating Temperatures (K)				
		Radial	Axial	Jets	Thru the Shaft	Lubricant Supply	Inboard Bearing	Outboard Bearing	Lubricant Inboard Side	Scavenge Outboard Side
3141	.8	3215	5738	1.60	1.67	367	389	376	391	359
3665	.2	3215	5827	1.60	1.67	353	388	372	392	365
4188	6.2	3215	6183	1.60	1.67	369	407	404	412	380

Test Suspended End of Day

TABLE 29

Data Sheet: Extended Duration Functional Test of German M88000 Series Bearing Under 100% Load - Run 6

Bearing Numbers 15 & 17
Lubricant Santotrac 50

Speed (Rad/S)	Time at Speed (Hours)	Applied Load Per Bearing (N) Radial	Axial	Lubricant Flow Rate Per Brg. (L/Min.) Jets	Thru the Shaft	Operating Temperatures (K) Lubricant Supply	Inboard Bearing	Outboard Bearing	Lubricant Inboard Side	Scavenge Outboard Side
3141	.3	3215	5115	1.60	1.67	333	364	364	365	354
3665	.2	3215	5338	1.60	1.67	337	378	377	380	369
4188	1.2	3215	5783	1.60	1.67	365	398	393	406	394

Test Terminated by Lubricant Line Failure: Outboard Bearing Seized